REPORT No.
CP/SEAM-2012/01 | STRUCTURAL ENGINEERING AND APPLIED MECHANICS

BRIDGE DESIGN FOR EARTHQUAKE FAULT CROSSINGS: SYNTHESIS OF DESIGN ISSUES AND STRATEGIES

By

RAKESH GOEL, BING QU, OSMAR RODRIGUEZ and JENNIFER TURES

FINAL REPORT

PREPERAED FOR

CALIFORNIA DEPARTMENT OF TRANSPORTATION

CONTRACT NO. 65A0379

December 27, 2012

DEPARTMENT OF CIVIL & ENVIRONMENTAL ENGINEERING
CALIFORNIA POLYTECHNIC STATE UNIVERSITY
SAN LUIS OBISPO, CA 93407

Bridge Design for Earthquake Fault Crossings: Synthesis of Design Issues and Strategies

by

Rakesh Goel[1]

Bing Qu[2]

Osmar Rodriguez[3]

Jennifer Tures[4]

December 27, 2012

Research Conducted for the

California Department of Transportation

Contract No. 65A0379

1 Associate Dean, Research, Graduate Programs, and Partnerships, College of Engineering, and Professor, Department of Civil and Environmental Engineering, California Polytechnic State University, San Luis Obispo, CA 93407. Email: rogel@calpoly.edu.

2 Assistant Professor, Department of Civil and Environmental Engineering, California Polytechnic State University, San Luis Obispo, CA 93407. Email: bqu@calpoly.edu.

3 Former Graduate Student Assistant, Department of Civil and Environmental Engineering, California Polytechnic State University, San Luis Obispo, CA 93407. Email: osrodrig@calpoly.edu.

4 Graduate Student Assistant, Department of Civil and Environmental Engineering, California Polytechnic State University, San Luis Obispo, CA 93407. Email: jtures@calpoly.edu.

STATE OF CALIFORNIA • DEPARTMENT OF TRANSPORTATION

TECHNICAL REPORT DOCUMENTATION PAGE

TR0003 (REV 10/98)

ADA Notice

For individuals with sensory disabilities, this document is available in alternate formats. For information call (916) 654-6410 or TDD (916) 654-3880 or write Records and Forms Management, 1120 N Street, MS-89, Sacramento, CA 95814.

1. REPORT NUMBER CA12-2177	2. GOVERNMENT ASSOCIATION NUMBER	3. RECIPIENT'S CATALOG NUMBER
4. TITLE AND SUBTITLE Bridge Design for Earthquake Fault Crossing: Synthesis of Design Issues and Strategies		5. REPORT DATE December 2012
		6. PERFORMING ORGANIZATION CODE
7. AUTHOR Rakesh Goel, Bing Qu, Osmar Rodriguez, Jennifer Tures		8. PERFORMING ORGANIZATION REPORT NO. CP/SEAM-2012/01
9. PERFORMING ORGANIZATION NAME AND ADDRESS Cal Poly Corporation Building 15 1 Grand Avenue San Luis Obispo, CA 93407		10. WORK UNIT NUMBER
		11. CONTRACT OR GRANT NUMBER 65A0379
12. SPONSORING AGENCY AND ADDRESS California Department of Transportation Division of Engineering Services 1801 30th St., MS #9-2/5I Sacramento, California 95816		13. TYPE OF REPORT AND PERIOD COVERED Final report
		14. SPONSORING AGENCY CODE

15. SUPPLEMENTARY NOTES

16. ABSTRACT

Two approximate procedures, namely, the Fault Rupture-Response Spectrum Analysis (FR-RSA) and Fault Rupture-Linear Static Analysis (FR-LSA) procedures, were recently developed as alternatives to the nonlinear response history analysis (RHA) for bridge crossing fault rupture zones. However, obstacles still exist limiting the widespread acceptance of the approximate procedures, particularly in analysis of curved bridge and in implementation of the procedures on existing bridge analysis and design platform. To address these issues, this report first analyzed two actual multi-span curved bridges, which are typical of many bridges in California, to examine the adequacy of the FR-RSA and FR-LSA procedures. It is shown that the FR-RSA procedure provides estimates of bridge response that are close enough to the "exact" RHA results in all considered cases and therefore it is recommended for future practical application. In addition, the FR-LSA procedure is found to provide reasonable results for one bridge with three spans but overly conservative results for the other one with four spans. Analysis results from the validation work also demonstrate that the quasi-static response alone (which is caused by ground displacement offset only) is inadequate in estimating the total bridge response although it may be a significant portion of the total bridge response and even dominate the response in some cases. Finally, the research team of this project assisted Computers & Structures, Inc. in implementing the FR-RSA procedure on CSiBridge. Taking one of the considered bridge as an example, the report describes the process of model development using the FR-RSA procedure on CSiBridge, followed by assessment of the adequacy of this implementation.

17. KEY WORDS Curved Bridge, Crossing Fault Ruptures, Response Spectrum Analysis	18. DISTRIBUTION STATEMENT No Restrictions	
19. SECURITY CLASSIFICATION *(of this report)* Unclassified	20. NUMBER OF PAGES 113	21. COST OF REPORT CHARGED $194.024

Reproduction of completed page authorized.

DISCLAIMER STATEMENT

This document is disseminated in the interest of information exchange. The contents of this report reflect the views of the authors who are responsible for the facts and accuracy of the data presented herein. The contents do not necessarily reflect the official views or policies of the State of California or the Federal Highway Administration. This publication does not constitute a standard, specification or regulation. This report does not constitute an endorsement by the Department of any product described herein.

For individuals with sensory disabilities, this document is available in Braille, large print, audiocassette, or compact disk. To obtain a copy of this document in one of these alternate formats, please contact: the Division of Research and Innovation, MS-83, California Department of Transportation, P.O. Box 942873, Sacramento, CA 94273-0001.

ASTRACT

As shown by the bridge damages observed from recent earthquakes, the bridges crossing earthquake faults can be more vulnerable compared with those lying on one side of the earthquake faults. Avoiding building bridges across earthquake fault zones might be the best design strategy; however, it is not always possible to do so in regions of high seismicity such as California. While rigorous nonlinear response history analysis (RHA) using the spatially-varying ground motions generated based on site-specific seismological studies can be conducted for bridges crossing fault ruptures; such a design and analysis process is too onerous, making it less practical for bridge engineers.

In response to the observed bridge damages and the absence of practical analysis methods, two approximate procedures, namely, the Fault Rupture-Response Spectrum Analysis (FR-RSA) and Fault Rupture-Linear Static Analysis (FR-LSA) procedures, were recently developed as alternatives to RHA for bridge across fault rupture zones. While there are many favorable features of the two approximate procedures (e.g., requiring significantly reduced modeling and computational efforts), obstacles still exist limiting their widespread acceptance and application. For example, the prior validation work for FR-RSA and FR-LSA procedures was limited to ideal straight ordinary bridges. It is uncertain whether the two procedures can provide the same adequate predictions for actual bridges, particularly curved bridges, crossing earthquake ruptures. Moreover, there is a need to integrate the approximate procedure into existing bridge design and analysis software packages that are directly available and more convenient for bridge engineers. The research reported here specifically addresses these issues.

This report first revisits the FR-RSA and FR-LSA procedures and presents a detailed guideline for implementation. Then, two actual multi-span curved bridges, which are typical of many bridges in California, were analyzed to examine the adequacy of the FR-RSA and FR-LSA procedures. Ground motions, abutment longitudinal stiffness, and bridge orientation relative to earthquake fault rupture were varied in the analysis to expand the validation work under a broad range of the parameters. It is shown that the FR-RSA procedure provides estimates of bridge response that are close enough to the

“exact” RHA results in all considered cases and therefore it is recommended for future practical application. In addition, the FR-LSA procedure is found to provide reasonable results for one bridge with three spans but overly conservative results for the other one with four spans. Therefore, it is recommended that the FR-LSA procedure be used with caution in bridges with more than three spans or non-negligible higher mode effect. Analysis results from the validation work further demonstrate that the quasi-static response alone (which is caused by ground displacement offset only) is inadequate in estimating the total bridge response although it may be a significant portion of the total bridge response and even dominate the response in some cases.

Finally, the research team of this project assisted Computers & Structures, Inc. in implementing the FR-RSA procedure on CSiBridge™. Taking one of the considered bridge as an example, the report describes the process of model development using the FR-RSA procedure on CSiBridge™, followed by assessment of the adequacy of this implementation.

ACKNOWLEDGEMENTS

The research presented in this report is supported by California Department of Transportation (CALTRANS) under Contract No. 65A0379 with Dr. Allaoua Kartoum as the project manager. This support is gratefully acknowledged. The authors acknowledge Drs. Tom Shantz and Brian Chiou from the Division of Research and Innovation of CALTRANS who simulated the ground motions used in this investigation, and Bob Morris from Computers & Structures, Inc., who implemented one of the the considered analysis procedures on CSiBridge™. The authors are also grateful to Mark Yashinsky, Foued Zayati, Mark Mahan, and Toorak Zokaie of CALTRANS for their useful feedback on this project. Moreover, original numerical models of the selected bridges were developed by Dr. Farzin Zareian from University of California, Irvine.

TABLE OF CONTENTS

SECTION	TITLE	PAGE
1	**INTRODUCTION**	**1**
2	**REVIEW OF EXISTING ANALYSIS PROCEDURES AND GUIDELINE FOR IMPLEMENTATION**	**3**
2.1	Theoretical Background	3
2.2	Implementation of FR-RSA	5
2.3	Implementation of FR-LSA	7
3	**CASE STUDY OF BRIDGE 55-0837S**	**10**
3.1	Basic Information of 55-0837S	10
3.2	Modeling of 55-0837S	11
3.3	Selected Ground Motions	15
3.4	Consideration of Bridge Orientations	17
3.5	Response Quantities of Interest	18
3.6	Result Discussions and Conclusions	18
4	**CASE STUDY OF BRIDGE 55-0939G**	**22**
4.1	Basic Information of 55-0939G	22
4.2	Modeling of 55-0939G	24
4.3	Fault Rupture Locations and Bridge Orientations	25
4.4	Ground Motions and Response Quantities of Interest	26
4.5	Result Discussions and Conclusions	27
5	**IMPLEMENTATION AND VERIFICATION OF FR-RSA**	**32**
5.1	Definition of Bridge 55-0837S in CSiBridge™	33
5.2	Automated Caltrans Fault Crossing Seismic Bridge Design	41
5.3	Response Quantities of Interest and Result Discussions	44
6	**CONCLUSIONS AND FUTURE WORK**	**47**
7	**REFERENCES**	**50**
APPENDIX A	**COMPLETE RESULT COMPARISONS OF BRIDGE 55-0837S**	**51**
APPENDIX B	**COMPLETE RESULT COMPARISONS OF BRIDGE 55-0939G**	**69**
APPENDIX C	**PERIODS AND MODE SHAPE COMPARISONS OF CSI-BRIDGETM AND OPENSEES BRIDGE MODELS**	**91**
APPENDIX D	**COMPLETE RESULT COMPARISON QUANTITIES FOR VALIDATION OF CSIBRIDGE™**	**93**
APPENDIX E	**BRIDGE 55-0837S CSIBRIDGE™ MODEL: DETAILED MODEL DEVELOPMENT PROCESS**	**94**

SECTION 1

INTRODUCTION

Although avoiding building bridges across earthquake fault zones might be the best design strategy, it is not always possible to do so in regions of high seismicity such as California. Bridges crossing fault-rupture zones will experience ground offset across the fault and hence spatially-varying ground motions. Compared with the bridges lying on one side of an earthquake fault, the bridges crossing fault ruptures can be more vulnerable. As shown by the bridge damages observed from the recent earthquakes including the 1999 Chi-Chi earthquake (EERI, 2001; Yen, 2002), 1999 Kocaeli earthquake (EERI, 2000), 1999 Duzce earthquake (Ghasemi *et al*., 2000), and 2008 Wenchuan earthquake (Kawashima *et al*., 2009), the bridges crossing earthquake faults can be severely damaged as a result of rupture of causative faults.

While a rigorous analysis can be conducted for bridges crossing earthquake faults based on the nonlinear response history analysis (RHA) approach using the spatially varying ground motions defined according to the site-specific seismological procedure, such an analysis typically requires extensive modeling and computational efforts, limiting it from practical application. In response to the observed earthquake-induced bridge damages and the absence of practical analysis methods for bridge across fault rupture zones, research efforts have been made to develop effective and more efficient and well-organized procedures to estimate the seismic demands for bridges crossing fault rupture zones. With the support from CALTRANS, Goel and Chopra (2008a, 2008b, 2009a, 2009b) developed and validated two simplified procedures, namely, the Fault Rupture-Response Spectrum Analysis (FR-RSA) and Fault Rupture-Linear Static Analysis (FR-LSA) procedures as alternatives of the onerous RHA analysis procedure. While development of the FR-RSA and FR-LSA procedures is a major stride made in analysis and design of bridges crossing fault rupture zones, the prior validation of these procedures was limited to ideal straight ordinary bridges. As one may notice from the bridge inventory in California, a significant number of actual bridges have some features different from those used in the prior validation work. As such, there is an urgent

research need to further evaluate the adequacy of the developed simplified analysis procedures in the context of representative actual bridges, particularly curved bridges. In addition, a critical knowledge gap exists in further implementing the approximate procedures in practical design. This report presents the analytical research conduced to address the abovementioned issues.

The report is organized as follows. Section 2 revisits the FR-RSA and FR-LSA procedures and presents a detailed guideline to incorporate them into the existing bridge simulation and design platform, specifically the CSiBridge™. Sections 3 and 4 examine the adequacy of the FR-RSA and FR-LSA procedures based on the analyses of two actual multi-span curved bridges representative of many bridges in California. Taking one of the considered bridge as an example, Section 5 describes the process of model development using the FR-RSA procedure implemented on CSiBridge™, followed by assessment of the adequacy of this implementation. Finally, Section 6 summarizes the conclusions from this research and some suggestions for further work.

SECTION 2

REVIEW OF EXISTING ANALYSIS PROCEDURES AND GUIDELINE FOR IMPLEMENTATION

In a prior project supported by CALTRANS, two approximate procedures -- FR-RSA and FR-LSA -- were developed and demonstrated to be adequate for ordinary straight bridges crossing fault-rupture zones by Goel and Chopra (2008a, 2008b, 2009a, 2009b). These two procedures estimate the seismic demands on a bridge crossing earthquake fault by superposing the peak values of quasi-static and dynamic bridge responses. The peak quasi-static response in both methods is computed by nonlinear static analysis of the bridge under ground displacement offset associated with fault rupture. In FR-RSA and FR-LSA, the peak dynamic responses are estimated from combination of the peak modal responses using the complete-quadratic-combination (CQC) rule and linear static analysis of the bridge under appropriate equivalent seismic forces, respectively. This section revisits the theoretical background of FR-RSA and FR-LSA and provides a step-by-step guideline to implement these procedures in existing computer programs for bridge analysis and design, particularly CSiBridge™. Detailed information about derivation of the FR-RSA and FR-LSA procedures is available in elsewhere (Goel and Chopra 2008a).

2.1 Theoretical Background

The displacement components at support l of a bridge due to fault rupture motion along the fault-parallel and fault-normal directions, $u_{gl}^{\mathrm{FP}}(t)$ and $u_{gl}^{\mathrm{FN}}(t)$, may be respectively approximated as:

$$u_{gl}^{\mathrm{FP}}(t) = \alpha_l^{\mathrm{FP}} u_g^{\mathrm{FP}}(t) \tag{2.1}$$

$$u_{gl}^{\mathrm{FN}}(t) = \alpha_l^{\mathrm{FN}} u_g^{\mathrm{FN}}(t) \tag{2.2}$$

where $u_g^{\mathrm{FP}}(t)$ and $u_g^{\mathrm{FN}}(t)$ are the fault-parallel and fault-normal displacement histories of motion at a reference location, and α_l^{FP} and α_l^{FN} are the proportionality constants for the lth support. For a bridge crossing a strike-slip fault, α_l^{FP} will be equal to +1 for supports

on left side of the fault and –1 for supports on right side of the fault, and α_l^{FN} will be equal to +1 for supports on both side of the fault. For bridges crossing other types of faults, i.e., faults with other dip and rake angles, values of α_l^{FP} and α_l^{FN} may differ from +1 or –1.

For ground excitations defined by Equations (2.1) and (2.2), the equations of motion are

$$\mathbf{m}\ddot{\mathbf{u}} + \mathbf{c}\dot{\mathbf{u}} + \mathbf{k}\mathbf{u} = -\mathbf{m}\boldsymbol{\iota}_{\mathrm{eff}}^{\mathrm{FP}}\ddot{u}_g^{\mathrm{FP}}(t) - \mathbf{m}\boldsymbol{\iota}_{\mathrm{eff}}^{\mathrm{FN}}\ddot{u}_g^{\mathrm{FN}}(t) \tag{2.3}$$

where $\mathbf{m}$, $\mathbf{c}$, and $\mathbf{k}$ respectively represent the mass, stiffness and damping matrices of the system; $\ddot{\mathbf{u}}$, $\dot{\mathbf{u}}$ and $\mathbf{u}$ respectively represent the acceleration, velocity, and displacement vectors of the bridge; $\boldsymbol{\iota}_{\mathrm{eff}}^{\mathrm{FP}}$, as shown in Figure 2.1a, is the "effective" influence vector for fault-parallel motion defined as the vector of displacements at all structural degrees of freedom due to simultaneous static application of all support displacements with value equal to α_l^{FP} at the lth support of the elastic bridge model, $\boldsymbol{\iota}_{\mathrm{eff}}^{\mathrm{FN}}$, as shown in Figure 2.1b, is the "effective" influence vector for fault-normal motion defined as the vector of displacements at all structural degrees of freedom due to simultaneous static application of all support displacements with value equal to α_l^{FN} at the lth support of the elastic bridge model, and $\ddot{u}_g^{\mathrm{FP}}(t)$ and $\ddot{u}_g^{\mathrm{FN}}(t)$ are the accelerations at the reference support in the fault-parallel and fault-normal directions, respectively. The total displacements of the linear-elastic bridge are then given by

$$\mathbf{u}^t(t) = \mathbf{u}^s(t) + \mathbf{u}(t) = \boldsymbol{\iota}_{\mathrm{eff}}^{\mathrm{FP}}u_g^{\mathrm{FP}}(t) + \boldsymbol{\iota}_{\mathrm{eff}}^{\mathrm{FN}}u_g^{\mathrm{FN}}(t) + \sum_{n=1}^{N}\Gamma_n^{\mathrm{FP}}\boldsymbol{\phi}_n D_n^{\mathrm{FP}}(t) + \sum_{n=1}^{N}\Gamma_n^{\mathrm{FN}}\boldsymbol{\phi}_n D_n^{\mathrm{FN}}(t) \tag{2.4}$$

in which

$$\Gamma_n^{\mathrm{FP}} = \frac{\boldsymbol{\phi}_n^T\mathbf{m}\boldsymbol{\iota}_{\mathrm{eff}}^{\mathrm{FP}}}{\boldsymbol{\phi}_n^T\mathbf{m}\boldsymbol{\phi}_n} \tag{2.5}$$

$$\Gamma_n^{\mathrm{FN}} = \frac{\boldsymbol{\phi}_n^T\mathbf{m}\boldsymbol{\iota}_{\mathrm{eff}}^{\mathrm{FN}}}{\boldsymbol{\phi}_n^T\mathbf{m}\boldsymbol{\phi}_n} \tag{2.6}$$

and $D_n^{\mathrm{FP}}(t)$ and $D_n^{\mathrm{FN}}(t)$ are the deformation response of the nth-mode Single Degree of Freedom (SDOF) system subjected to the reference ground motions $\ddot{u}_g^{\mathrm{FP}}(t)$ and $\ddot{u}_g^{\mathrm{FN}}(t)$ in the fault-parallel and fault-normal directions, respectively. The first two terms on right side of Equation (2.4) are the quasi-static responses and the last two terms are the dynamic responses due to fault-parallel and fault-normal support motions.

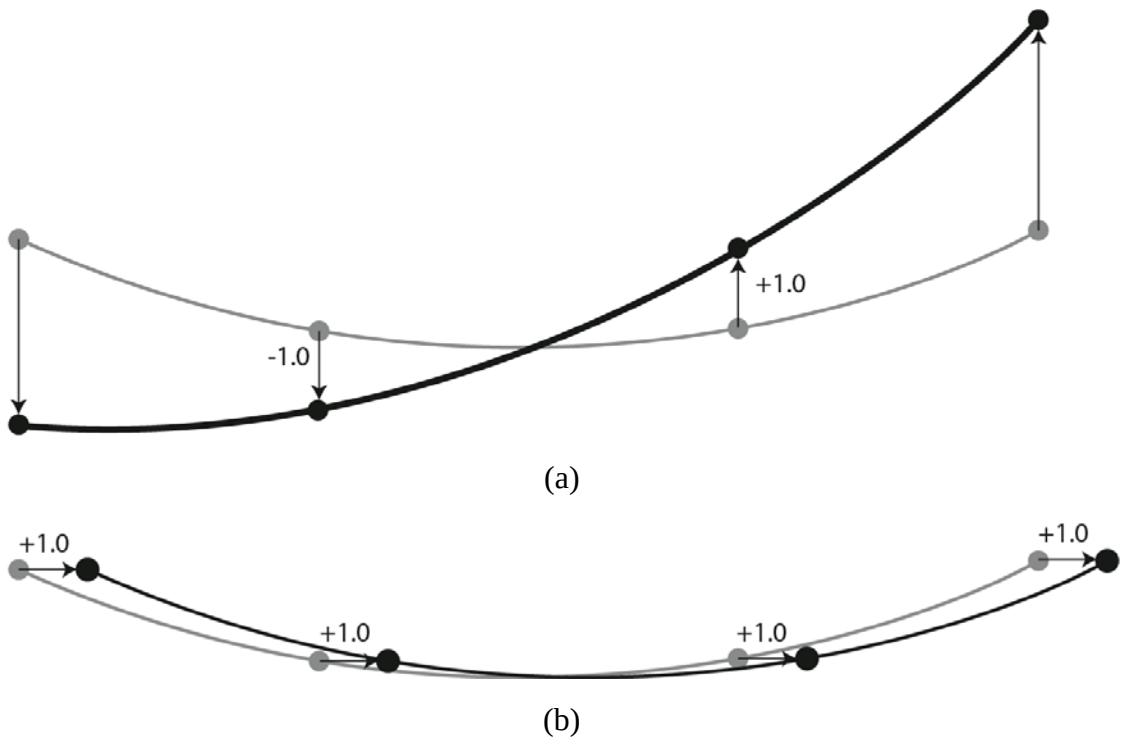

Figure 2.1 Illustration of "effective" influence vectors for an example three-span bridge (a) $\boldsymbol{\iota}_{\mathrm{eff}}^{\mathrm{FP}}$ for Fault-Parallel ground motion, (b) $\boldsymbol{\iota}_{\mathrm{eff}}^{\mathrm{FN}}$, for Fault-Normal ground motion

During strong ground shaking associated with rupture on a fault, the bridge is expected to respond beyond the linear elastic range. A previous study by Goel and Chopra (2008a), demonstrated that total response of such bridges can be estimated by superposing peak values of quasi-static and dynamic responses. The peak quasi-static demand is computed by nonlinear static analysis whereas the peak dynamic demand is estimated by linear analysis.

2.2 Implementation of FR-RSA

Presented below are the step-by-step descriptions to implement the FR-RSA procedure.

Step 1: Obtain the Design Fault Offset and Design Spectrum for the Bridge Site.

The location, amount, and direction of displacement at the structure due to the fault offset is provided by Geotechnical Services (GS) or by a geotechnical consultant with GS approval. When the deterministically derived predicted fault offset is much larger than the probabilistically derived predicted fault offset, a risk assessment study is recommended to justify the potentially large cost associated with designing for fault offset (CALTRANS 2012). The Ground Shaking Hazard in the form of Design Spectrum is also provided, as described in CALTRANS Seismic Design Criteria (SDC) Appendix B. This step will lead to identification of proportionality constants, α_l^{FP} and α_l^{FN}, and peak displacements at reference support location of the bridge, u_{go}^{FP} and u_{go}^{FN}. Additionally, this step will also lead to identification of the design spectra in the fault-parallel and fault-normal direction; the two design spectra may be identical if recommendations of the CALTRANS SDC Appendix B are used to define the Ground Shaking Hazard.

Step 2: Obtain the Quasi-Static Response of the Structure due to the Design Fault Offset

A nonlinear model of the bridge, including column plastic hinges (and possibly nonlinear springs for the shear keys and soil at the abutments based on the parameters provided in the SDC) is required to capture the behavior of the bridge for the Design Fault Offset. Gravity loads are applied to the bridge model followed by foundation offsets due to the fault movement. The analysis due to foundation offset involves application of all support displacements with values equal to $\alpha_l^{\mathrm{FP}} u_{go}^{\mathrm{FP}}$ and $\alpha_l^{\mathrm{FN}} u_{go}^{\mathrm{FN}}$ at support l in fault-parallel and fault-normal directions, respectively. Note that u_{go}^{FP} and u_{go}^{FN} may have both x- and y-components depending on the angle between the bridge primary axis and the fault. This analysis will lead to quasi-static responses $r_{\mathrm{QS}}^{\mathrm{FP}}$ and $r_{\mathrm{QS}}^{\mathrm{FN}}$, due to design fault offset in the fault-parallel and fault-normal directions, respectively.

Step 3: Obtain the Dynamic Response of the Structure

The peak dynamic responses, r_o^{FP} and r_o^{FN}, of the linear elastic bridge due to fault-parallel and fault-normal ground hazard are computed as follows:

- Compute the vibration periods (T_n) and mode shapes (ϕ_n) of the bridge. Compute as many modes as necessary to capture dynamic response of the bridge. In general, first 18 to 24 modes were found to be sufficient in the example structures considered in this study; however, more modes may be required for more complicated or larger structures.
- Compute the fault rupture effective influence vectors, $\boldsymbol{\iota}_{\mathrm{eff}}^{\mathrm{FP}}$ and $\boldsymbol{\iota}_{\mathrm{eff}}^{\mathrm{FN}}$, as vectors of displacements at all structural degrees of freedom due to simultaneous static application of all support displacements with values equal to α_l^{FP} and α_l^{FN} at the lth support.
- Compute the modal participation factors for fault-parallel and fault-normal analysis as $\Gamma_n^{\mathrm{FP}} = \boldsymbol{\phi}_n^T \mathbf{m} \boldsymbol{\iota}_{\mathrm{eff}}^{\mathrm{FP}} \big/ \boldsymbol{\phi}_n^T \mathbf{m} \boldsymbol{\phi}_n$ and $\Gamma_n^{\mathrm{FN}} = \boldsymbol{\phi}_n^T \mathbf{m} \boldsymbol{\iota}_{\mathrm{eff}}^{\mathrm{FN}} \big/ \boldsymbol{\phi}_n^T \mathbf{m} \boldsymbol{\phi}_n$. Note that these modal participation factors differ from those in standard modal analysis to uniform support excitation.
- Compute the response associated with the nth mode, r_n^{FP} and r_n^{FN}, due to fault-parallel and fault-normal ground hazards using modal analysis and modal participation factors computed in last step.
- Combine the modal responses, r_n^{FP} and r_n^{FN}, due to fault-parallel and fault-normal ground hazards using CQC procedure to obtain peak dynamic responses, r_o^{FP} and r_o^{FN}, due to fault-parallel and fault-normal ground hazards, respectively.

Step 4: Combine the Static and Dynamic Responses to Obtain the Seismic Demand.

The peak values of seismic demands are obtained by superposition of the peak values of the static and dynamic parts of the response as:

$$r_o^t = \left| r_{\mathrm{QS}}^{\mathrm{FP}} \right| + \left| r_{\mathrm{QS}}^{\mathrm{FN}} \right| + r_{\mathrm{o}}^{\mathrm{FP}} + r_{\mathrm{o}}^{\mathrm{FN}} \tag{2.7}$$

2.3 Implementation of FR-LSA

Presented below are the step-by-step descriptions to implement the FR-LSA procedure.

Step 1: Obtain the Design Fault Offset and Design Spectrum for the Bridge Site.

The location, amount, and direction of displacement at the structure due to the fault offset is provided by GS or by a geotechnical consultant with GS approval. When the deterministically derived predicted fault offset is much larger than the probabilistically derived predicted fault offset, a risk assessment study is recommended to justify the potentially large cost associated with designing for fault offset (CALTRANS 2012). The Ground Shaking Hazard (specified as either the Peak Ground Acceleration or the Design Spectrum) is also provided, as described in CALTRANS SDC Appendix B. This step will lead to identification of proportionality constants, α_l^{FP} and α_l^{FN}, peak displacements at reference support location of the bridge, u_{go}^{FP} and u_{go}^{FN}, and peak acceleration at reference support location of the bridge, $\ddot{u}_{go}^{\mathrm{FP}}$ and $\ddot{u}_{go}^{\mathrm{FN}}$, in fault-parallel and fault normal direction, respectively. Additionally, this step will also lead to identification of the design spectra in the fault-parallel and fault-normal directions; the two design spectra may be identical if recommendations of the CALTRANS SDC Appendix B are used to define the Ground Shaking Hazard.

Step 2: Obtain the Quasi-Static Response of the Structure due to the Design Fault Offset.

A nonlinear model of the bridge, including column plastic hinges (and possibly nonlinear springs for the shear keys and soil at the abutments based on the parameters provided in the SDC) is required to capture the behavior of the bridge for the Design Fault Offset. Gravity loads are applied to the bridge model followed by foundation offsets due to the fault movement. The analysis due to foundation offset involves application of all support displacements with values equal to $\alpha_l^{\mathrm{FP}} u_{go}^{\mathrm{FP}}$ and $\alpha_l^{\mathrm{FN}} u_{go}^{\mathrm{FN}}$ at support l in fault-parallel and fault-normal directions, respectively. Note that u_{go}^{FP} and u_{go}^{FN} may have both x- and y-components depending on the angle between the bridge primary axis and the fault. This analysis will lead to quasi-static responses, $r_{\mathrm{QS}}^{\mathrm{FP}}$ and $r_{\mathrm{QS}}^{\mathrm{FN}}$, due to design fault offset in the

fault-parallel and fault-normal directions, respectively. This step is similar to that in the FR-RSA procedure.

Step 3: Obtain the Dynamic Response of the Structure.

The dynamic responses, r_o^{FP} and r_o^{FN}, of the bridge due to fault-parallel and fault-normal ground hazards can be conservatively estimated by a static analysis of the linear structure due to the lateral forces, $\mathbf{m}\boldsymbol{\iota}_{\mathrm{eff}}^{\mathrm{FP}} A_{\max}^{\mathrm{FP}}$ in the fault-parallel direction, and $\mathbf{m}\boldsymbol{\iota}_{\mathrm{eff}}^{\mathrm{FN}} A_{\max}^{\mathrm{FN}}$, in the fault-normal direction, where $A_{\max}^{\mathrm{FP}}$ and $A_{\max}^{\mathrm{FN}}$ are peak value of the spectral acceleration for ground hazard in the fault-parallel and fault-normal directions, respectively and the other variables have been defined previously. It is important to note that fault rupture influence vectors $\boldsymbol{\iota}_{\mathrm{eff}}^{\mathrm{FP}}$ and $\boldsymbol{\iota}_{\mathrm{eff}}^{\mathrm{FN}}$ are computed from linear elastic analysis of the bridge. If $A_{\max}^{\mathrm{FP}}$ and $A_{\max}^{\mathrm{FN}}$ are not available readily, they can be approximated as $A_{\max}^{\mathrm{FP}} = 2.5\ddot{u}_{go}^{\mathrm{FP}}$ and $A_{\max}^{\mathrm{FN}} = 2.5\ddot{u}_{go}^{\mathrm{FN}}$.

Step 4: Combine the Static and Dynamic Responses to Obtain the Seismic Demand.

The total response is computed as

$$r_o^t = \max \begin{cases} \left| r_{\mathrm{QS}}^{\mathrm{FP}} + r_{\mathrm{QS}}^{\mathrm{FN}} + r_{\mathrm{o}}^{\mathrm{FP}} + r_{\mathrm{o}}^{\mathrm{FN}} \right| \\ \left| r_{\mathrm{QS}}^{\mathrm{FP}} + r_{\mathrm{QS}}^{\mathrm{FN}} + r_{\mathrm{o}}^{\mathrm{FP}} - r_{\mathrm{o}}^{\mathrm{FN}} \right| \\ \left| r_{\mathrm{QS}}^{\mathrm{FP}} + r_{\mathrm{QS}}^{\mathrm{FN}} - r_{\mathrm{o}}^{\mathrm{FP}} + r_{\mathrm{o}}^{\mathrm{FN}} \right| \\ \left| r_{\mathrm{QS}}^{\mathrm{FP}} + r_{\mathrm{QS}}^{\mathrm{FN}} - r_{\mathrm{o}}^{\mathrm{FP}} - r_{\mathrm{o}}^{\mathrm{FN}} \right| \end{cases} \tag{2.8}$$

SECTION 3

CASE STUDY OF BRIDGE 55-0837S

This section assesses the adequacy of the two approximate procedures (i.e., FR-RSA and FR-LSA) for analysis of bridges crossing fault rupture zones using a three-span curved bridge designated as Bridge 55-0837S. The following presents basic information of the bridge, development of linear and nonlinear models of the bridge, modeling consideration of abutments and bent bases, response quantities of interest, selection of ground motions, and result discussions and comparisons.

3.1 Basic Information of 55-0837S

As shown in Figure 3.1, Bridge 55-0837S is a three-span continuous curved bridge built in 2000, located in east Anaheim, California (District 12 – Orange County, Latitude: 33.821667, Longitude: -117.922222). The bridge serves as the West Street to North-bound-5 Interstate on-ramp for the large groups of vehicles leaving the Disneyland theme park.

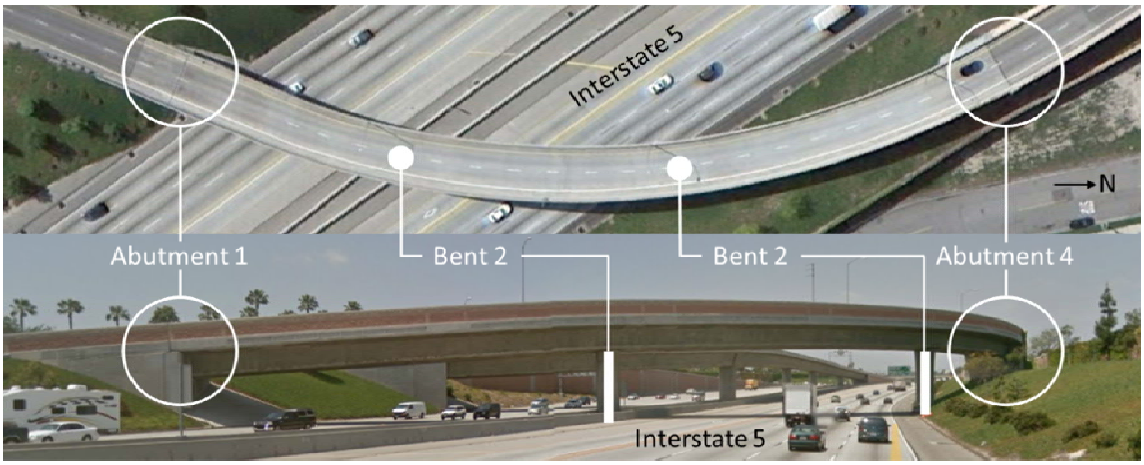

Figure 3.1 Plan view and elevation of Bridge 55-0837S
(Photos adapted from Google Street View)

General geometries of the bridge are schematically shown in Figure 3.2. More detailed information about bridge (including member size, reinforcement arrangement, and material properties) is available from the CALTRANS Bridge Inspection Records Information System (BIRIS). The bridge crosses over Interstate-5 with a minimum

vertical clearance of 5.63m. Structural length of the bridge is 151.3m and the length of its maximum span is 60.1m. The bridge consists of concrete box girders and spread single-column bents. According to the data collected in 2000, average daily traffic of Bridge 55-0837S is about 200,000 (city-data, 2010).

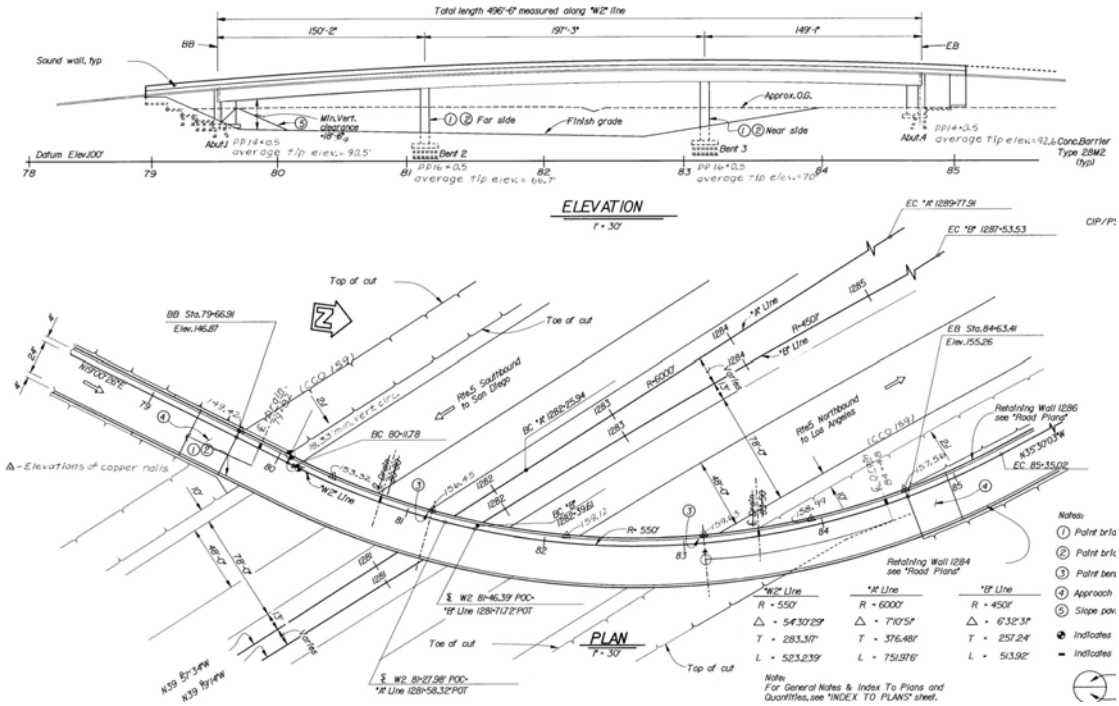

Figure 3.2 Schematic of Bridge 55-0837S
(drawings provided by CALTRANS BIRIS)

3.2 Modeling of 55-0837S

The finite element (FE) models of Bridge 55-0837S were originally developed using the Open System for Earthquake Engineering Simulation (OpenSees) (Mazzoni et al. 2006), by the researchers from University of California, Irvine (UCI) for other research purposes. The UCI models were modified to be linear and nonlinear models for use in the FR-RSA and FR-LSA procedures in this investigation. Consistent with the procedures described in Section 2, the linear model is used in the eigen-value analysis for extraction of modal information of the bridge that is required in the FR-RSA procedure to estimate the peak dynamic response of the bridge. Moreover, the linear model is used for the same purpose in the static analysis that is part of the FR-LSA procedure. The nonlinear model is used to determine the quasi-static response of the bridge in both the

FR-RSA and FR-LSA procedures. Moreover, the nonlinear model is used in the nonlinear RHA which provides the most rigorous results to assess the adequacy of the FR-RSA and FR-LSA procedures.

In the linear model, the bridge deck and each bent were respectively modeled using 30 and 5 elastic beam-column elements (i.e., elasticBeamColumn in OpenSees). The material properties and cross-section properties were assigned to these elements during analysis. The nonlinear model is identical to the linear model except that the bents were considered using the nonlinear displacement based beam-column elements with distributed plasticity and linear curvature distribution (i.e., dispBeamColumn in OpenSees). The following focuses on descriptions of other features of the bridge that were identically modeled in both the linear and nonlinear models. Figures 3(a) and (b) illustrate the nodes and elements assigned in the model.

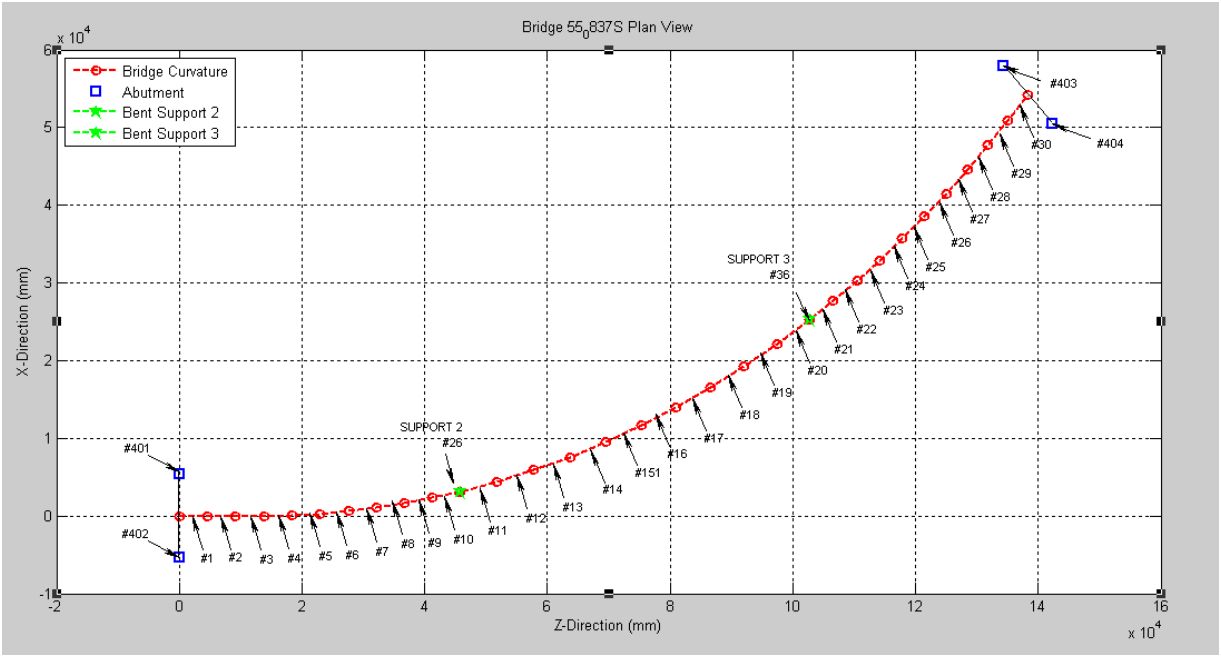

(a)

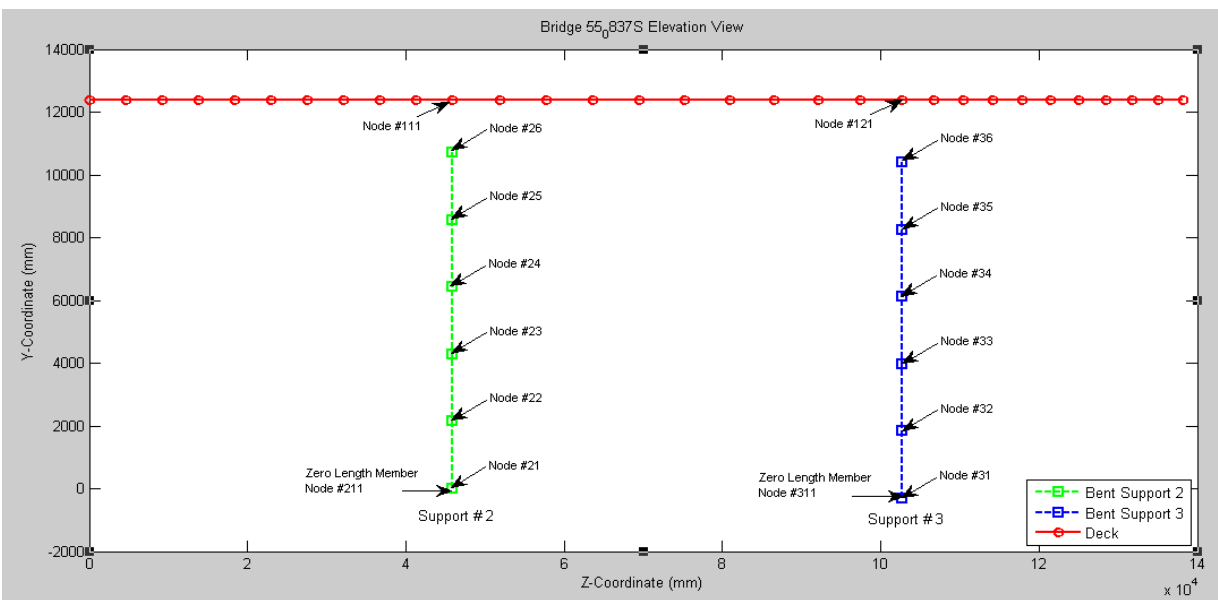

(b)

Figure 3.3 Assignments of nodes and elements in the FE model of Bridge 55-0837S

To consider the soil-structure interaction at the bent bases, soil springs were assigned in the FE model. The springs included elastic rotational springs with stiffness equal to 5.65×10^{10} kN-mm; elastic translational springs with stiffness equal to 145 kN/mm along

the longitudinal and transverse directions on the horizontal plane; and ideally rigid vertical and torsional springs.

In addition to the soil springs at the bent bases, spring elements were defined along the vertical, longitudinal and transverse directions of abutments to consider the soil-structure interaction and other restraining effects due to the presence of shear keys, wing walls, and back walls at the abutments. Along the vertical direction, the model included an elastic spring with stiffness equal to 49,380 kN/mm at each abutment, which is consistent with the original UCI model. In the transverse direction (i.e. bridge normal direction), the model included a linear elastic spring with stiffness equal to 50% of the elastic transverse stiffness of the adjacent bent with consideration of the soil springs at the bent base as recommended in the CALTRANS SDC (CALTRANS 2010). As a result, the spring stiffness along the transverse direction at each abutment is equal to 20.93 kN/mm. It is noted that degradation of the abutment transverse springs caused by the failure of shear keys was not considered in this investigation as the focus here is to evaluate adequacy of the approximate analysis procedures. Effect of shear keys on seismic performance of bridges crossing fault-rupture zones is discussed elsewhere (Goel and Chopra 2008b). In the longitudinal direction, the elastic-perfectly plastic gap spring specified in the original nonlinear model was converted to an elastic compression-only spring using the CALTRANS SDC recommendations (see Figure 3.4) where the equivalent effective stiffness, K_{eff}, can be determined as:

$$K_{eff} = \frac{P_{bw}}{\Delta_{eff}} = \frac{P_{bw}}{\Delta_{gap} + P_{bw} / K_{abut}} \tag{3.1}$$

where P_{bw} is the passive pressure force resisting movement at the abutment, and Δ_{gap} and K_{abut} are the coefficients determined from the elastic-perfectly plastic gap springs defined in the original UCI model. As a result, K_{eff} is determined to be 28.54 kN/mm.

Conceptually, the displacement restraining effect along the abutment longitudinal direction due to the presence of abutment components depends on the longitudinal displacement of the bridge. A larger longitudinal bridge displacement leads to more severe damages and thus less restraining effect. Therefore, a smaller stiffness should be

assigned to the abutment longitudinal springs to consider the less significant restraining action. The CALTRANS SDC suggests a stiffness varying from 0.1 to 1.0 K_{eff} for the longitudinal abutment springs, which can be further determined from an iterative process based on the longitudinal displacement of the bridge. To validate the FR-RSA and FR-LSA procedures under a broader range of the parameters, three stiffness values, $0.10K_{eff}$, $0.55K_{eff}$, and $1.00K_{eff}$, were considered in the investigation.

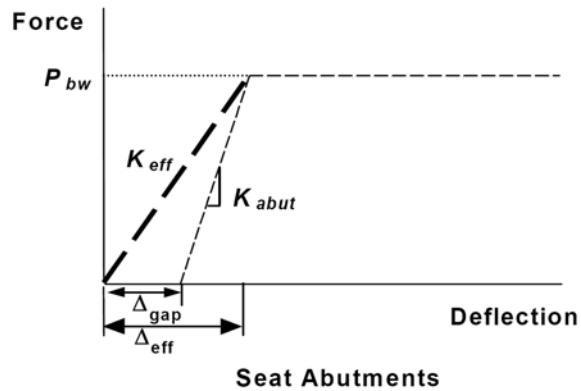

Figure 3.4 Simplification of longitudinal abutment springs
(Adapted from CALTRANS 2010)

3.3 Selected Ground Motions

Ground motion pairs were selected and modified to match the design spectrum provided by the CALTRANS SDC (CALTRANS 2010). Due to the limited number of actual ground motions recorded very close to actual ruptured faults (less than 100m), ground motion simulations are the only method to obtain time histories for this analysis. These simulated time histories were required to incorporate the near-fault source radiation pattern and to account for far- and near-field seismic radiations during rupture process as well as the sudden elastic rebound. A set of 10 ground motion records were provided by CALTRANS for this investigation (Shantz and Chiou, 2011). Table 3.1 lists the recorded ground motions that were used for generation of the fault rupture ground motions. The relative fault offset was determined to be 100 cm which would place bridge bents well into the inelastic range while not so large as to completely dominate the contribution of the dynamic response. Moreover, the S-wave arrival time and displacement offset rate were considered as random variables in the fault rupture ground motion generation.

Figure 3.5 compares the mean of the geometric means of the response spectra of the selected ground motions and the idealized CALTRANS SDC design spectrum.

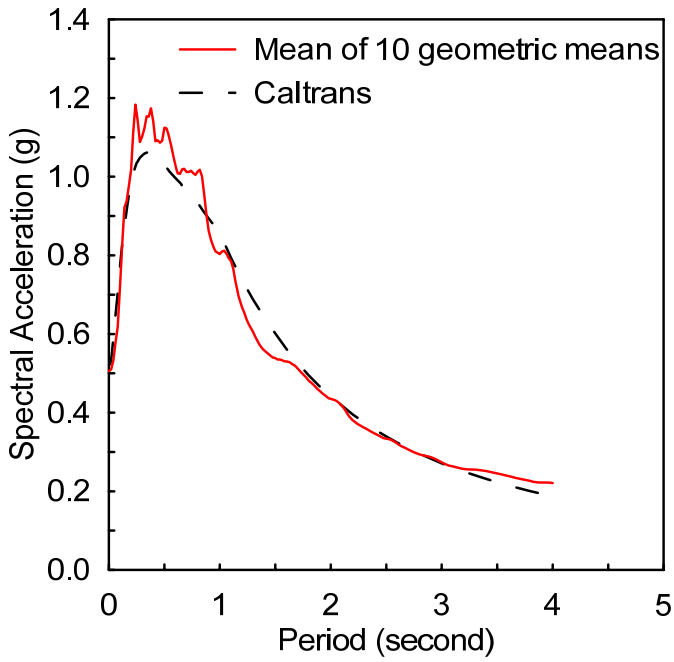

Figure 3.5 CALTRANS design spectrum and mean of geometric means of the elastic response spectra of the considered ground motions.

Table 3.1 Summary of considered base ground motion pairs*

Set No.	Component 1	Component 2	Time step (sec)	Number of Points
1	LOMAP-BVC220	LOMAP-BVC310	0.005	5918
2	LOMAP-HSP000	LOMAP-HSP090	0.005	11990
3	LOMAP-HDA165	LOMAP-HDA255	0.005	7928
4	KOBE-FUK000	KOBE-FUK090	0.02	3900
5	NORTHR-SAR000	NORTHR-SAR270	0.01	3600
6	NORTHR-NEE090	NORTHR-NEE180	0.01	4800
7	KOBE-OSA000	KOBE-OSA090	0.02	6000
8	KOBE-ABN000	KOBE-ABN090	0.01	14000
9	ITALY-A-TDG000	ITALY-A-TDG270	0.0029	18216
10	SFERN-WND143	SFERN-WND233	0.001	7997

*selected from the NGA database.

3.4 Consideration of Bridge Orientations

In fact, the fault rupture may not always orient perpendicular to the line connecting the two abutments of a bridge. It is necessary to evaluate adequacy of the approximate procedures over a broader ranges of the angles from the fault rupture to the line connecting the two abutments of a bridge. In this investigation the angle θ, which captures different bridge orientation angles from the fault rupture line as shown in Figure 3.6, was selected to be 53, 45, 30, 21, 15, 0, -15,-30 and -38 degrees. The angle is positive when it is counterclockwise. It is also noted that $\theta = 53$ or -38 degrees represent the extreme cases of bridge orientation as shown in Figure 3.7 for which the fault will remain between the two bents. Moreover, when $\theta = 0$ degree , the two bents are assumed to have the same distance to the fault line as shown in Figure 3.6.

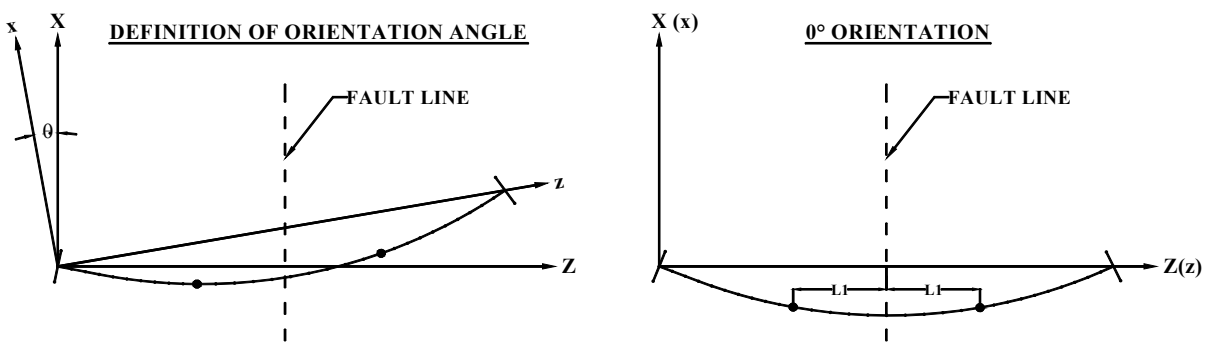

Figure 3.6 Definition of bridge orientation angle

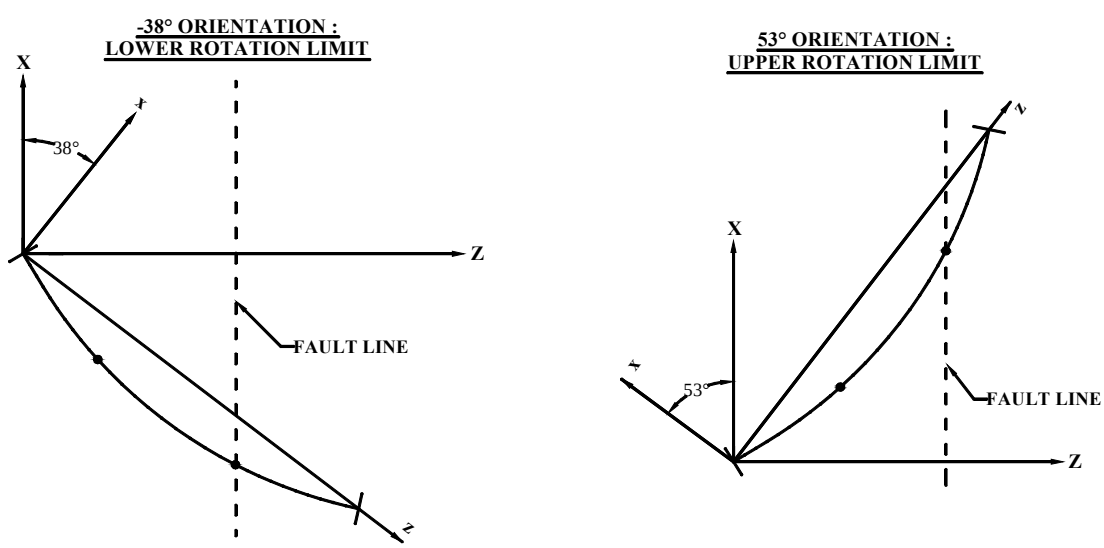

Figure 3.7 Bridge orientation limits

3.5 Response Quantities of Interest

The response quantities of interest include the displacement demands at the abutments and bents (see Abutments 1 and 4, and Bents 2 and 3 in Figure 3.1). The maximum absolute values of the abutment longitudinal and transverse displacement components were output for comparison purpose. In FR-RSA, the abutment longitudinal and transverse displacement components associated with each mode were combined using CQC as described in Section 2. Moreover, as required in the CALTRANS SDC (CALTRANS 2010), the bent rigid body movements caused by foundation deformations were taken into account when calculating the bent displacement demands. The maximum resultant bent displacements, which were obtained from the square root of the sum of squares of the maximum absolute values of the two horizontal bent displacement components, were compared in this investigation.

3.6 Result Summary and Discussions

As discussed in Sections 3.2 and 3.4, two parameters, including stiffness of the longitudinal abutment springs (selected to be $0.10K_{eff}$, $0.55K_{eff}$, and $1.00K_{eff}$) and the bridge orientation angle ($\theta = 53$, 45, 30, 21, 15, 0, -15,-30 and -38 degrees), were varied in the investigation to evaluate the robustness and adequacy of FR-RSA and FR-LSA under the practical ranges of the parameters. A total of 270 nonlinear RHA were conducted together with the corresponding analyses using FR-RSA and FR-LSA. Complete result comparisons of Bridge 55-0837S are provided in Appendix A. As consistent observations can be obtained from all considered cases, this section focuses on the results from the following selected cases, i.e., when $\theta = 53,\ 0,\ \text{and} - 38$ degrees and stiffness of longitudinal abutment springs is equal to $0.10K_{eff}$. The three selected angles correspond to the bridges perpendicular to the earthquake fault rupture (see Figure 3.6) and along the extreme orientations shown in Figure 3.7.

The response quantities of interest described in Section 3.5 obtained respectively from the approximate analysis procedures and the nonlinear RHA procedure are compared in Figures 3.8 to 3.10. The RHA results shown are essentially the average values of the bridge responses from the 10 ground motions pairs provided by CALTRANS. As part of

the responses predicted from the approximate procedures, the quasi-static responses of the bridge caused by the ground displacement offset (labeled “FR-RSA-QS” and “FR-LSA-QS”) are explicitly shown in the results FR-RSA and FR-LSA. The other portion of bridge response considered in FR-RSA and FR-LSA, i.e., the peak dynamic bridge responses (FR-RSA-DY and FR-LSA-DY) are assigned either GM or DS, to represent the results respectively predicted using the spectral accelerations from the elastic response spectra of ground motion pairs and the idealized CALTRANS SDC design spectrum. It is noted that the average values of the bridge responses from the 10 ground motions pairs are presented for the results from the GM category.

Comparing the quasi-static portion of the response (FR-RSA-QS and FR-LSA-QS) with the results from RHA, it is found in Bridge 55-0837S that 1) the bent resultant displacement caused by the quasi-static effect is not very sensitive to the bridge orientation angles and the quasi-static response remains around 50% of the total response in all considered cases; 2) the abutment displacements caused by the quasi-static effect is sensitive to the bridge orientation and it varies from “negligible” to “dominant” in the total response; to be specific, the quasi-static response tends to affect the abutment longitudinal displacement to a higher degree as the bridge orientation angle approaches the limiting values; moreover, the quasi-static responses of abutment transverse displacements are almost identical at each abutment when the bridge orientation angle is around 0 degree (see abutment transverse displacement results shown in Figure 3.8); but they will become significantly different when the angles approaches the limiting values (see abutment transverse displacement results shown in Figures 3.9 and 3.10); and 3) it is inadequate to only use the quasi-static response to approximate the bridge response.

Comparisons of the results from the approximate procedures to those from nonlinear RHA indicate that 1) the FR-RSA procedure consistently provides reasonable estimates for the seismic demands of both abutments and bents of the bridge; 2) the FR-LSA procedure also provides good estimates but it is slightly conservative in some cases due to the use of a conservative estimate of response spectral acceleration in the method; and 3) both the FR-RSA and FR-LSA procedures are valid for seismic analysis and design of Bridge 55-0837S.

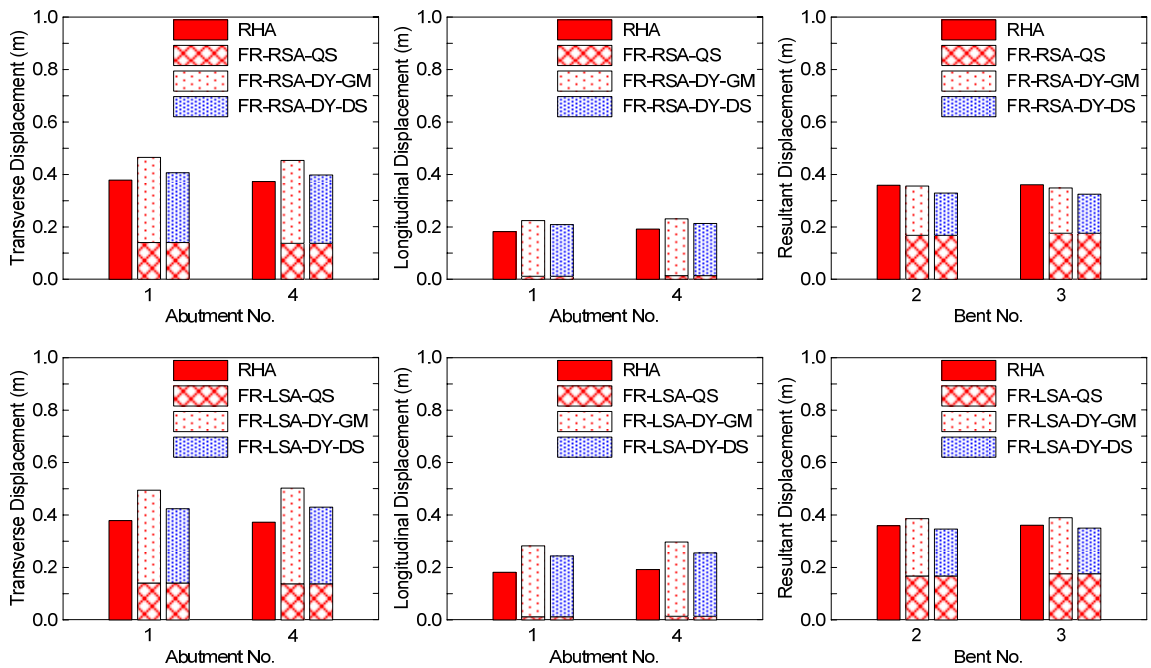

Figure 3.8 Bridge 55-0837S results when $\theta = 0^{o}$ and longitudinal abutment stiffness $= 0.10K_{eff}$.

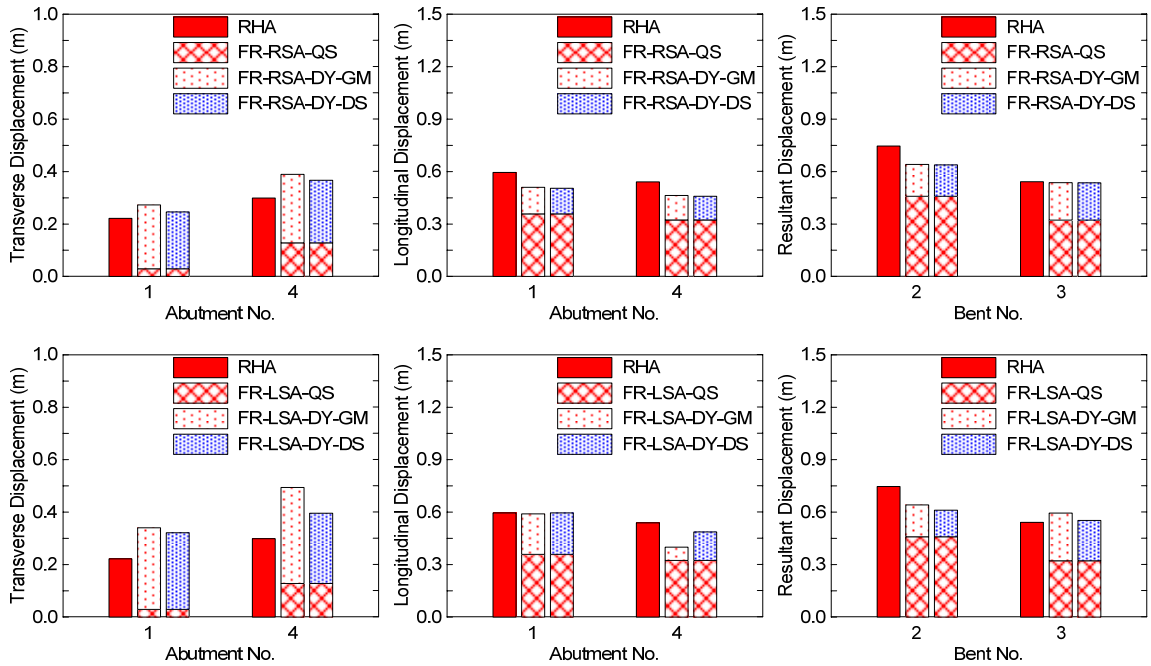

Figure 3.9 Bridge 55-0837S results when $\theta = 53^{o}$ and longitudinal abutment stiffness $= 0.10K_{eff}$

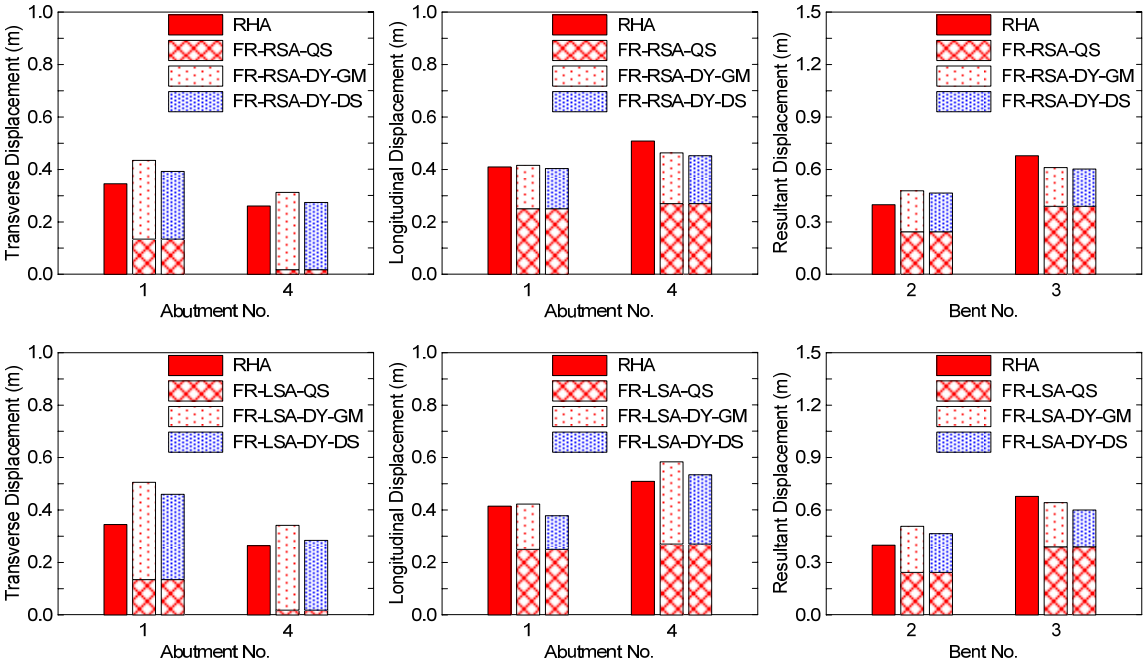

Figure 3.10 Bridge 55-0837S results when $\theta = -38^{\circ}$ and longitudinal abutment stiffness $= 0.10K_{eff}$

SECTION 4

CASE STUDY OF BRIDGE 55-0939G

Section 3 assessed the adequacy of FR-RSA and FR-LSA against results from the nonlinear RHA (which is the most rigorous analytical method) for a three-span curved bride denoted as Bridge 55-0837S. While result agreements have been consistently observed in all the considered scenarios (which take into consideration of various earthquake excitations, different longitudinal abutment stiffness values, and different bridge orientations), it should be noted that further verification work is needed since Bridge 55-0837S is relatively simple in terms of the numbers of spans, bents, and possible locations of crossing faults. As such, this section extends the validation work to a four-span bridge denoted as Bridge 55-0939G. The following presents basic information of the bridge, consideration of fault rupture locations and bridge orientations, and response quantities of interest followed by the result discussions and comparisons.

4.1 Basic Information of 55-0939G

As shown in Figure 4.1, Bridge 55-0939S is a four-span prestressed concrete continuous curved bridge built in 2001, located in southern California (District 12 – Orange County, Latitude: 33.776667, Longitude: -117.831667). General geometries of the bridge are schematically shown in Figure 4.2. Detailed information about bridge (including member size, reinforcement arrangement, and material properties) is available from the CALTRANS Bridge Inspection Records Information System (BIRIS). The bridge crosses over State highway 55 with a minimum vertical clearance of 5.62m. Structural length of the bridge is 190m and the length of its maximum span is 62m. The bridge consists of concrete box girders and single-column bents. According to the data collected in 1998, average daily traffic of Bridge 55-0939G is about 230,000 with truck traffic of 8% (city-data, 1998).

Figure 4.1 Plan view and elevation of Bridge 55-0939G

(Photos adapted from Google Street View)

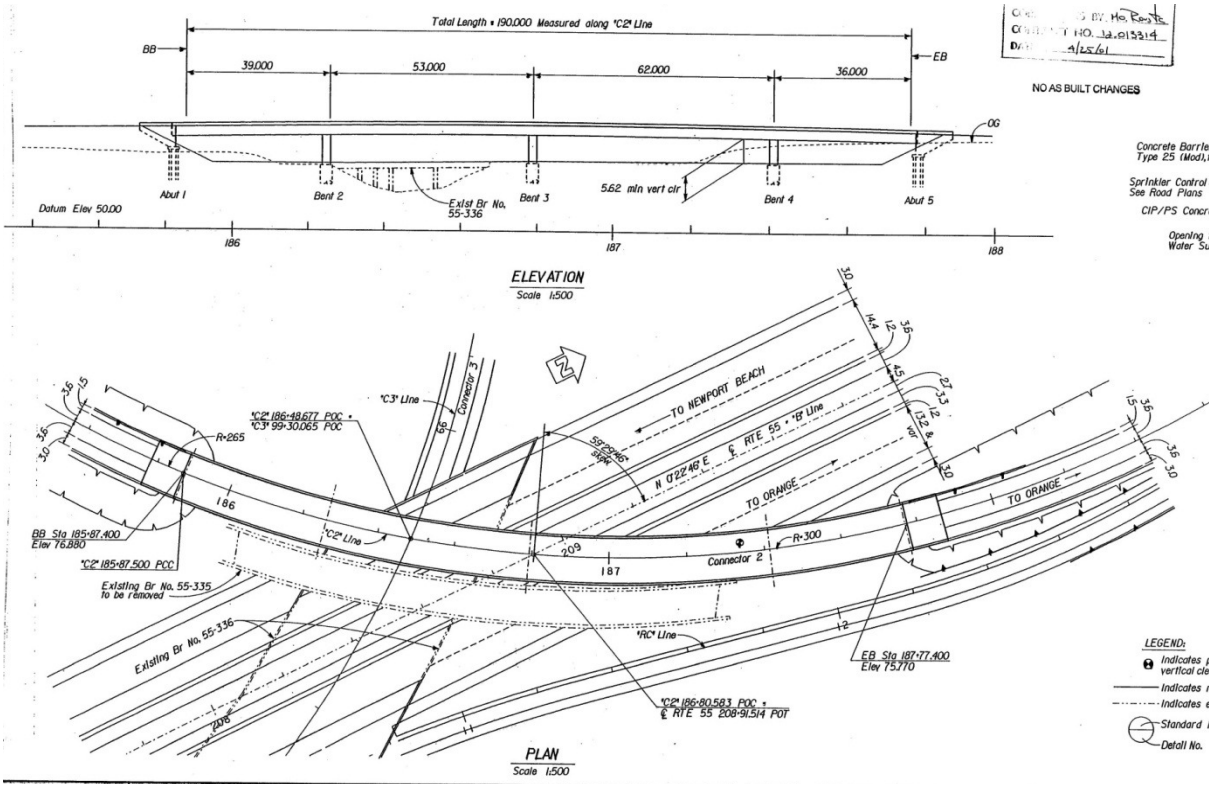

Figure 4.2 Schematic of Bridge 55-0939G

(drawings provided by CALTRANS BIRIS)

4.2 Modeling of 55-0939G

The FE model of Bridge 55-0939G was also originally developed using OpenSees by the researchers from UCI for other research purposes. Similar to Bridge 55-0837S, the original UCI model of Bridge 55-0939G was modified to be linear and nonlinear models for use in FR-RSA and FR-LSA in this investigation. Consistent with the procedures presented in Section 2, the eigen-value analysis was conducted on the linear model to obtain the bridge vibration periods and mode shapes that are necessary in the FR-RSA procedure for estimating the peak dynamic response of the bridge. Additionally, the linear model is used for the same purpose in the FR-LSA static analysis. The nonlinear model is used to determine the quasi-static response of the bridge in both the FR-RSA and FR-LSA procedures. Moreover, the nonlinear RHA that provides the benchmark reference results is also based on the nonlinear model.

In the linear model, the bridge deck and each bent were modeled using 40 and 5 elastic beam-column elements (i.e., elasticBeamColumn in OpenSees), respectively. The material properties and cross-section properties provided in the design documents were assigned to these elements during analysis. The nonlinear model is identical to the linear model except that the bents were considered using the nonlinear displacement based beam-column elements with distributed plasticity and linear curvature distribution (i.e., dispBeamColumn in OpenSees).

Consistent with the original UCI model, the bridge bents were fixed to ground. To consider the soil-structure interaction and other restraining effects due to the presence of shear keys, wing walls, and back walls, spring elements were assigned along the vertical, longitudinal, and transverse directions of the abutments. Along the vertical direction, each abutment included an elastic spring with stiffness equal to 63,475 kN/mm, which is consistent with the original UCI model. Moreover, along its transverse direction, each abutment had a linear elastic spring with stiffness equal to 50% of the transverse elastic stiffness of the adjacent bent as recommended in the CALTRANS SDC (CALTRANS 2010). Accordingly, stiffness values of the transverse springs are equal to 11.60 kN/mm and 27.58 kN/mm at Abutments 1 and 5, respectively. Following the CALTRANS SDC recommendations and the simplification procedures described in Section 3.2, the elastic-

perfectly plastic gap springs along the abutment longitudinal directions that were included in the original UCI model were converted to the corresponding elastic compression-only springs and the effective longitudinal abutment spring stiffness, K_{eff}, is determined to be 36.58 kN/mm. For the same reason described for Bridge 55-0837S, three stiffness values, $0.10K_{eff}$, $0.55K_{eff}$, and $1.00K_{eff}$, were considered for Bridge 55-0939G.

4.3 Fault Rupture Locations and Bridge Orientations

Different from Bridge 55-0837S, Bridge 55-0939G has two interior spans, which allows different placements of the fault ruptures crossing the bridge. As shown in Figure 4.3, two scenarios, denoted as Fault-a and Fault-b, which respectively represent the fault ruptures crossing the span between Bents 2 and 3 and the one between Bents 3 and 4, were considered in this research. Moreover, the angle θ defined in Figure 4.4 is used to capture bridge orientation angles. Same as Bridge 55-0837, the angle θ is positive when it is counterclockwise and the fault rupture line is perpendicular to the chord connecting the two abutments of the bridge when $\theta = 0$ degree. Figure 4.5 illustrates the limits of θ for Fault-a and Fault-b. These limits were identified by the extreme angles that place the two adjacent bents on different sides of the fault rupture. Within the identified angle limits, the bridge orientation angles was selected to be -36, -15, 0, 18, 41, and 55 degrees for Fault-a, and -34, -15, 0, 18, and 41 degrees for Fault-b.

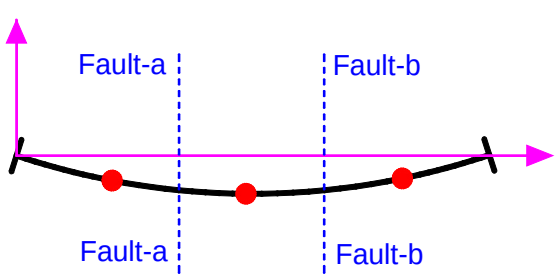

Figure 4.3 Considered fault ruptures

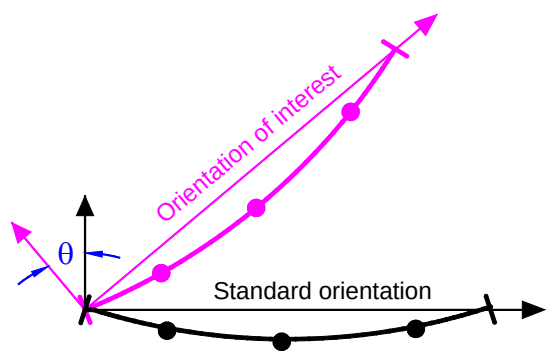

Figure 4.4 Bridge orientation angle θ

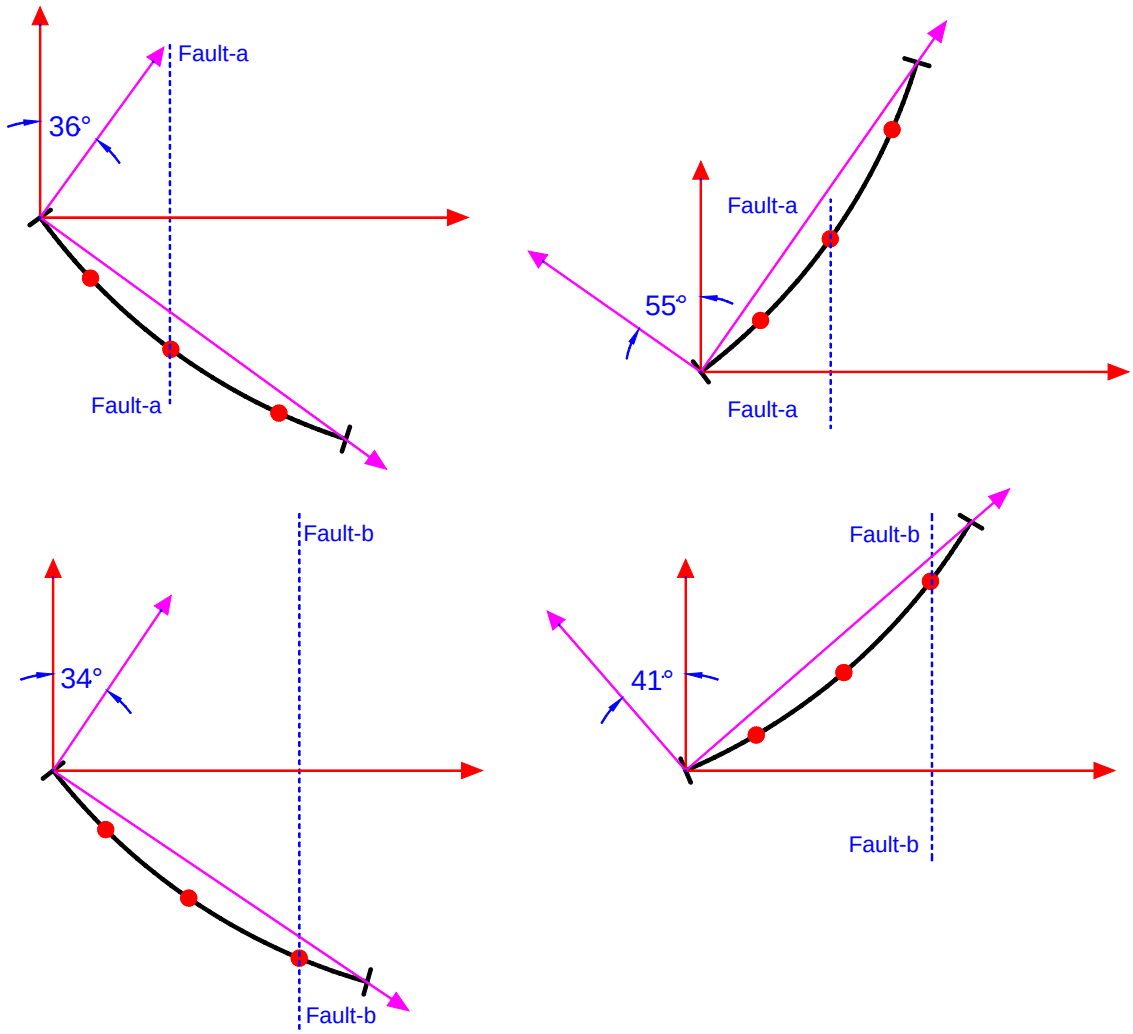

Figure 4.5 Limits of bridge orientation angle

4.4 Ground Motions and Response Quantities of Interest

The ground motions, which were provided by CALTRANS (Shantz and Chiou, 2011) and described in detail in Section 3.3, were used in analysis of Bridge 55-3909G. The response quantities of interest include the displacement demands at Abutments 1 and 4 and those at Bents 2, 3, and 4 (see Figure 4.1). The maximum absolute values of the abutment longitudinal and transverse displacement components were output for comparison purpose. In the FR-RSA, the abutment longitudinal and transverse displacement components associated with each mode were combined using CQC as described in Section 2. The maximum resultant bent displacements were obtained from the square root of sum of the squares of the maximum absolute values of the two

horizontal bent displacement components. The displacements of abutments and bents predicted from FR-RSA and FR-LSA were compared with those from nonlinear RHA for validation purpose.

4.5 Result Summary and Discussions

As discussed in Sections 4.2 and 4.3, two fault locations (respectively Fault-a and Fault-b), three stiffness values of the longitudinal abutment springs (selected to be $0.10K_{eff}$, $0.55K_{eff}$, and $1.00K_{eff}$), and different bridge orientation angles (6 and 5 angles for Fault-a and Fault-b, respectively), were considered in the investigation to evaluate the robustness and adequacy of FR-RSA and FR-LSA. As a result, a total of 330 nonlinear RHA were conducted together with the corresponding analyses using FR-RSA and FR-LSA. Appendix B provides complete result comparisons for Bridge 55-0939G. Since consistent observations can be obtained from all considered cases, this section only focuses on the results of some selected cases for each fault location, including the cases in which the bridge orientation angles equal to 0 degree and the two extreme values (-36 and 55 degrees for Fault-a ; and -34 and 41 degrees for Fault-b); and the stiffness of longitudinal abutment springs is equal to $0.10K_{eff}$.

Results of these selected cases are shown in Figures 4.6 to 4.11. The response quantities of interest obtained from nonlinear RHA were used as the reference values to evaluate adequacy of the approximate analysis procedures. The RHA results shown are essentially the average values of the bridge responses from the nonlinear time history analyses with the use of the 10 ground motions pairs provided by CALTRANS. Moreover, as shown, the total response of FR-RSA was separated into the quasi-static bridge response caused by the ground offset associated with fault rupture (which is represented by FR-RSA-QS) and the peak dynamic bridge response (which is represented by FR-RSA-DY). The FR-RSA-DY results were further differentiated into to two categories; FR-RSA-DY-GM and FR-RSA-DY-DS to represent the peak dynamic bridge responses respectively predicted using the spectral accelerations from the elastic response spectra of ground motion pairs and the idealized CALTRANS SDC design spectrum. The FR-LSA responses were also decomposed into FR-LSA-QS, FR-LSA-DY-GM, and

FR-LSA-DY-DS to represent the corresponding response components in the result comparisons. It is recognized that quasi-static responses (FR-RSA-QS and FR-LSA-QS) are the same in both approximate procedures.

Consistent with the observation from Bridge 55-0837S, comparison of the results respectively from RHA, FR-RSA-QS and FR-LSA-QS again indicate that the quasi-static response alone is inadequate in estimating the bridge displacement response while it is a significant portion of the total bridge response and even dominate the response in some cases (over 50% of the total response). Moreover, the FR-RSA procedure is found to consistently provide reasonable estimates for the seismic displacement demands of the bridge regardless the elastic response spectra of ground motion pairs (FR-LSA-DY-GM) or the idealized design spectrum (FR-LSA-DY-DS) are used in estimating the peak dynamic bridge response. Therefore, the FR-RSA is recommended for future analysis and design of bridges crossing earthquake fault ruptures. However, the FR-LSA is found to generally provide significantly conservative results except in a few cases in which it does underestimate the bridge responses. Compared with the result comparisons of Bridge 55-0537S (see Figures 3.8 to 3.10), it is found the FR-LSA becomes less accurate for Bridge 55-0939G. This is partially due to the fact that the higher mode effects, which can not be captured by FR-LSA, may be more important in Bridge 55-0939G which has more spans than Bridge 55-0537S. As such, the FR-LSA procedure, although provides estimates close enough to results of the “exact” nonlinear RHA for curved bridges with three spans (such as those like Bridge 55-0837S), should be used with caution in bridges with more than three spans (such those like Bridge 55-0939G) or non-negligible higher mode effect.

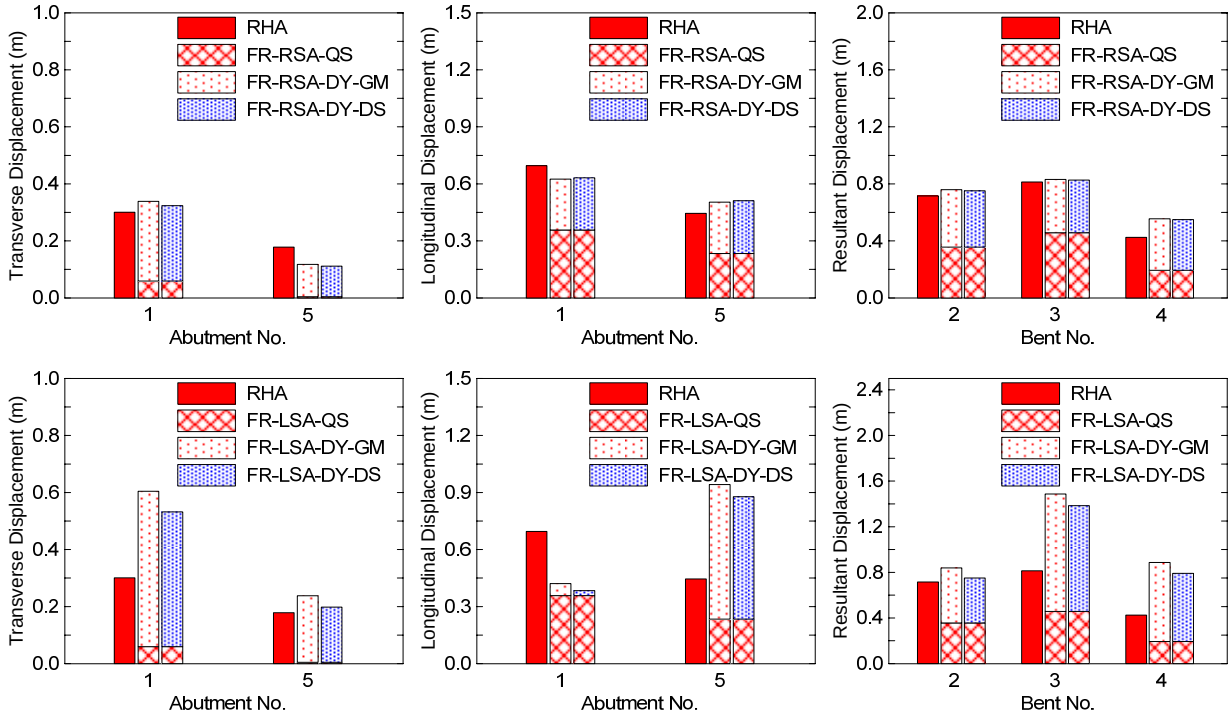

Figure 4.6 Bridge 55-0939G results when Fault-a applies $\theta = -36^{\circ}$ and longitudinal abutment stiffness $= 0.10K_{eff}$.

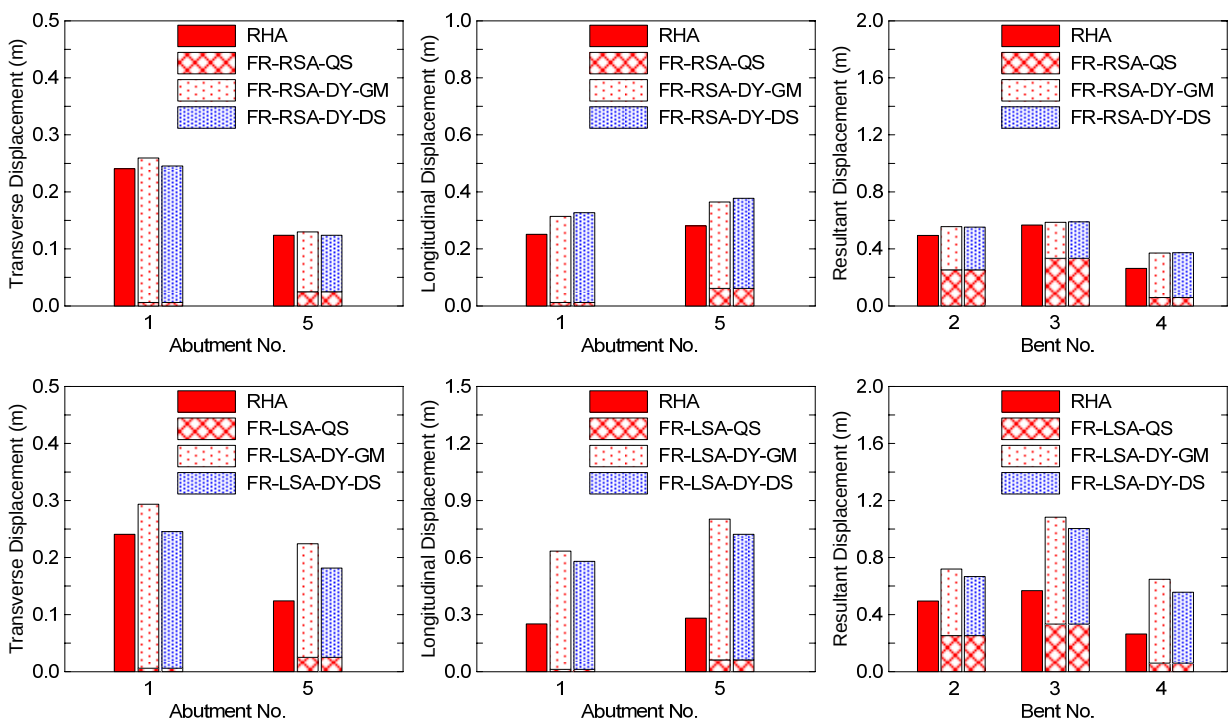

Figure 4.7 Bridge 55-0939G results when Fault-a applies $\theta = 0^{\circ}$ and longitudinal abutment stiffness $= 0.10K_{eff}$.

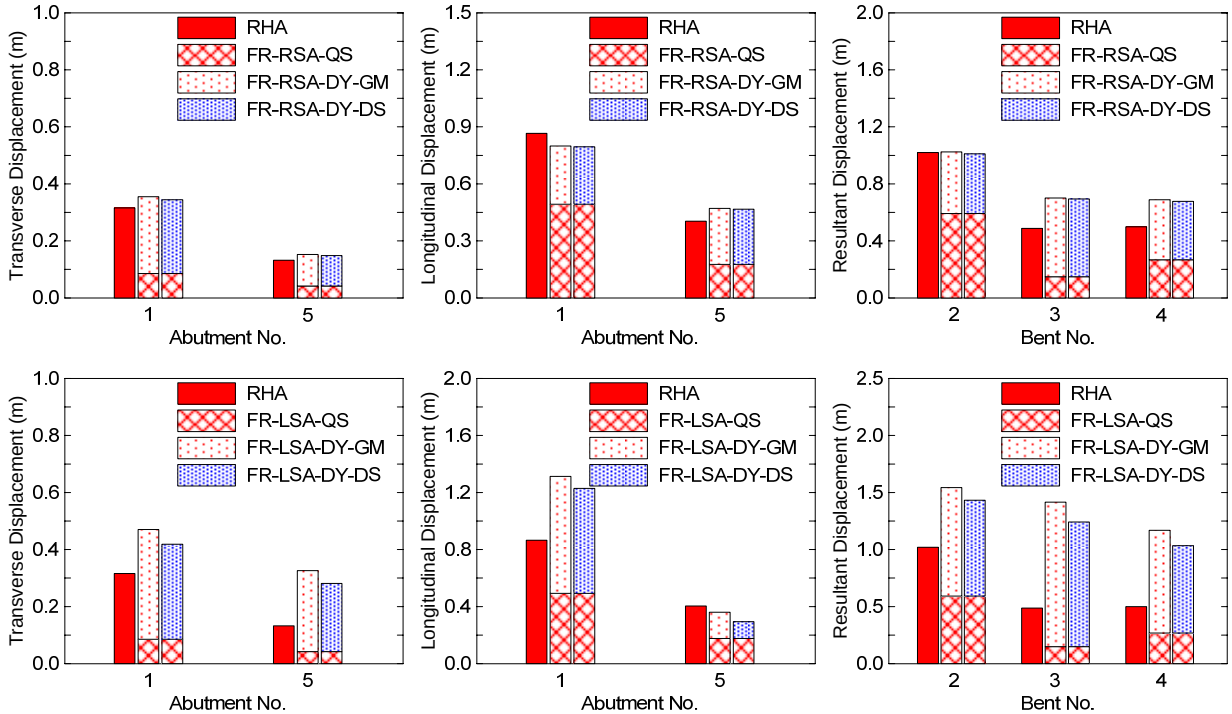

Figure 4.8 Bridge 55-0939G results when Fault-a applies $\theta = 55^{\circ}$ and longitudinal abutment stiffness $= 0.10K_{eff}$.

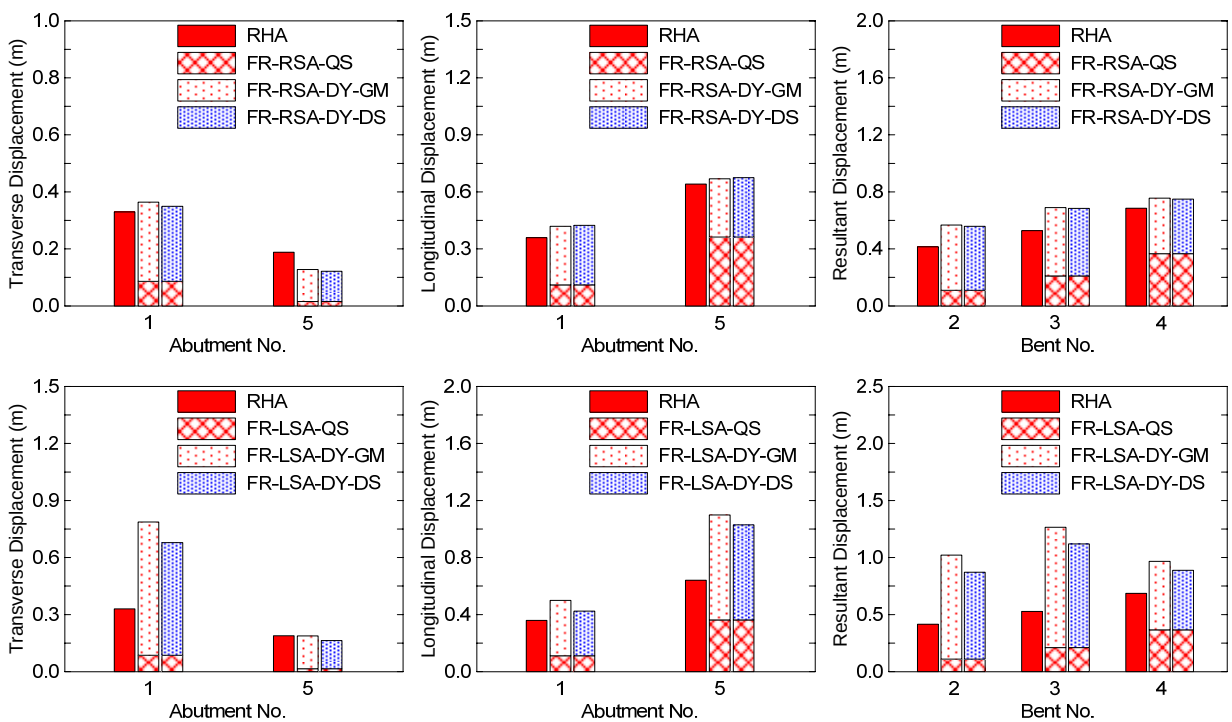

Figure 4.9 Bridge 55-0939G results when Fault-b applies $\theta = -34^{\circ}$ and longitudinal abutment stiffness $= 0.10K_{eff}$.

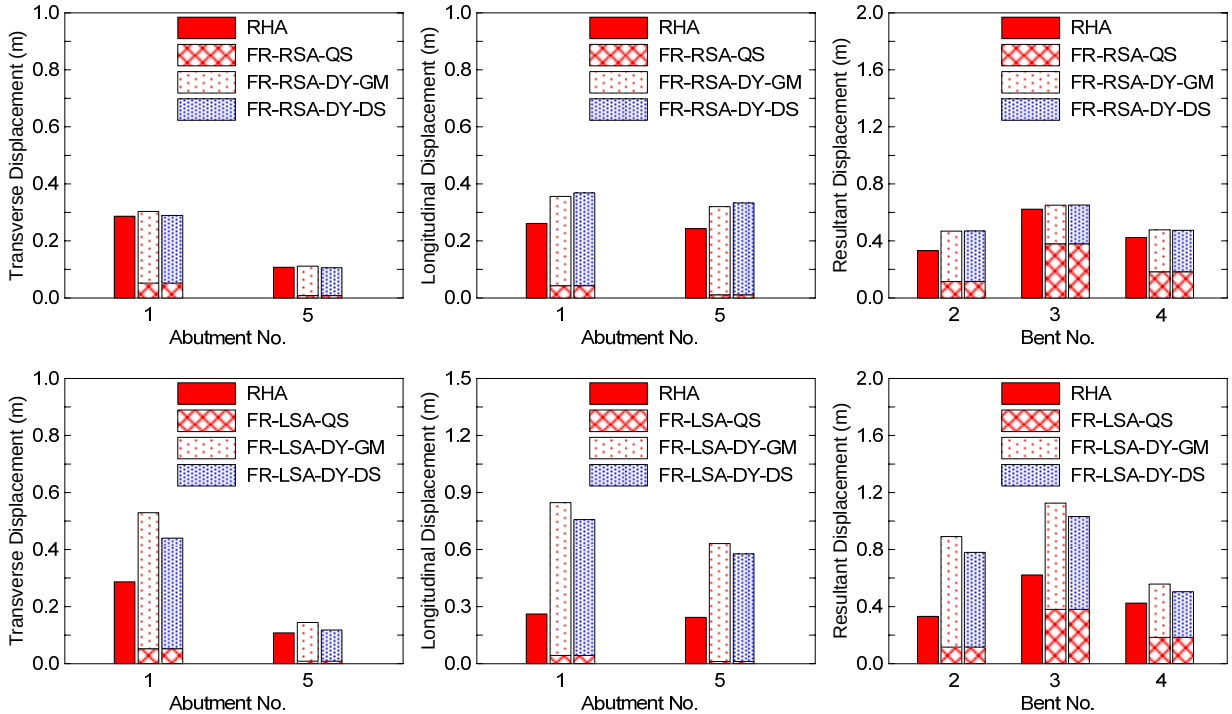

Figure 4.10 Bridge 55-0939G results when Fault-b applies $\theta = 0^{\circ}$ and longitudinal abutment stiffness $= 0.10K_{eff}$.

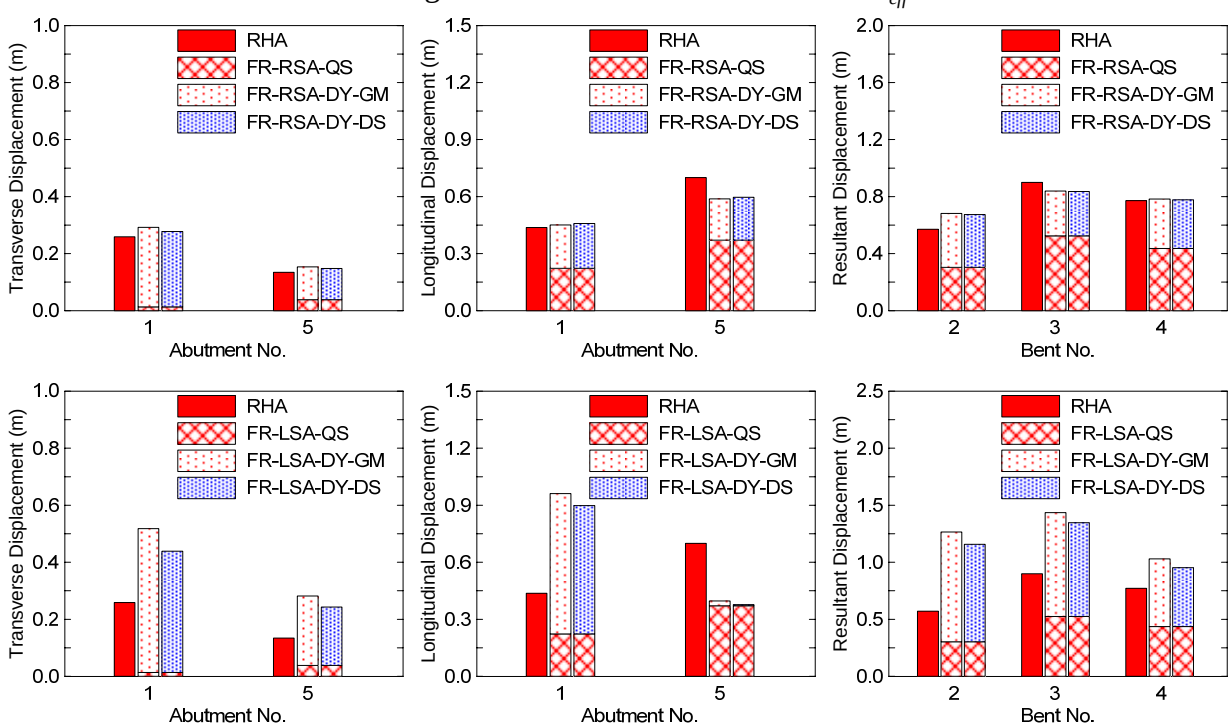

Figure 4.11 Bridge 55-0939G results when Fault-b applies $\theta = 41^{\circ}$ and longitudinal abutment stiffness $= 0.10K_{eff}$.

SECTION 5

IMPLEMENTATION AND VERIFICATION OF FR-RSA

As discussed in Sections 3 and 4, the FR-RSA procedure was confirmed to be adequate through analysis of two actual curved bridges representative in California and was recommended for future design. While the validation work of FR-RSA is a major stride made in analysis and design of bridges crossing fault rupture zones, it should be noted that the implementation and application of FR-RSA in OpenSees (which does not have a conventional graphic user interface) may be too onerous and complicated for practicing engineers, limiting the widespread acceptance of this analysis procedure. An urgent need exists in the bridge design community to incorporate FR-RSA into some existing bridge analysis and design platforms which the bridge engineers are familiar with. To this end, the research team collaborated with Computers and Structures, Inc. and embedded the FR-RSA method as a Caltrans Fault Crossing analysis component (see Figure 5.1) in the Automated Seismic Design function in CSiBridge™ version 16 beta build "W".

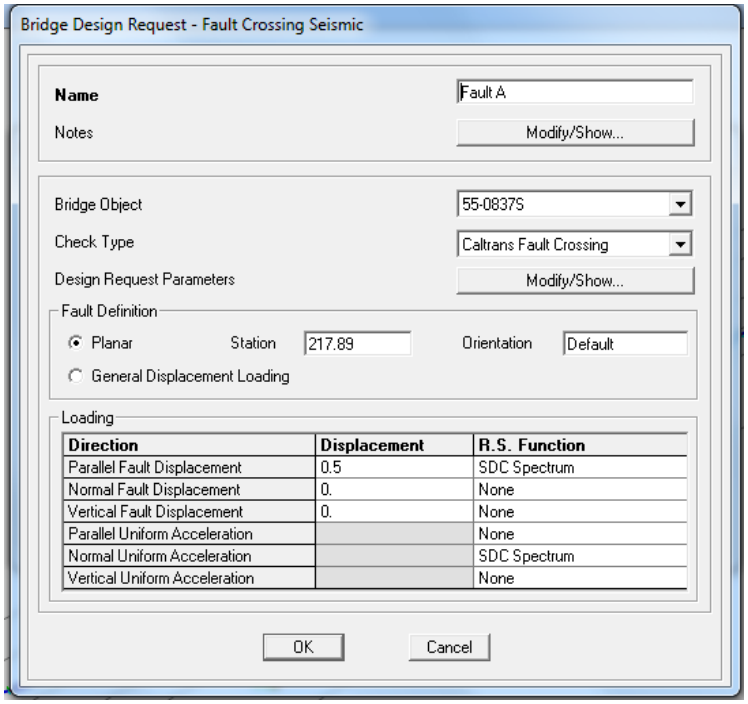

Figure 5.1 Added Caltrans Fault Crossing Automated Seismic Design Type presented as an option within Design Request parameters (see highlighted in dropdown window)

Taking Bridge 55-0537S as an example, this section briefly describes the key procedures to create the bridge model in CSiBridge™ along with validation of the automated Caltrans Fault Crossing Seismic Bridge Design. It is recognized that more detailed information about commands and step-by-step assistance in creating and analyzing the model of Bridge 55-0837S in CSiBridge™ is provided in Appendix E.

5.1 Definition of Bridge 55-0837S in CSiBridge™

For verification purpose, the CSiBridge™ model of Bridge 55-0837S was created to accurately resemble the OpenSees model. In order to achieve this, some of the automated bridge creation functions offered in CSiBridge™ were overridden to ensure consistency between models. The selected bridge, 55-0837S, was modeled in CSiBridge™ by implementing the following steps:

1. Creating a Bridge Object which includes defining the superstructure layout and identifying the location and orientation of bridge components
2. Defining and assigning frame section properties to both the bent columns and bridge deck
3. Overriding the applied mass at each node to set equal to the mass defined in the OpenSees model
4. Defining stiffness values for bent foundation and abutment soil springs

The Bridge Object is generated by assigning bridge components to stations along a Layout Line (a reference line at zero elevation coinciding with the deck). The Bridge Layout Line for bridge 55-037S was created by identifying the location and orientation of each deck segment between neighboring nodes as show in Figure 5.2. These parameters were extracted from the nodal information used in creating the OpenSees model. Thirty-one layout line nodes were specified, all located at zero vertical elevation.

Once the layout line is defined, the Bridge Object Data is specified; the deck is applied along the Bridge Layout Line, the bridge abutments are designated at the end of the layout line, and the bents are designated to the appropriate location along the deck as shown in Figure 5.3.

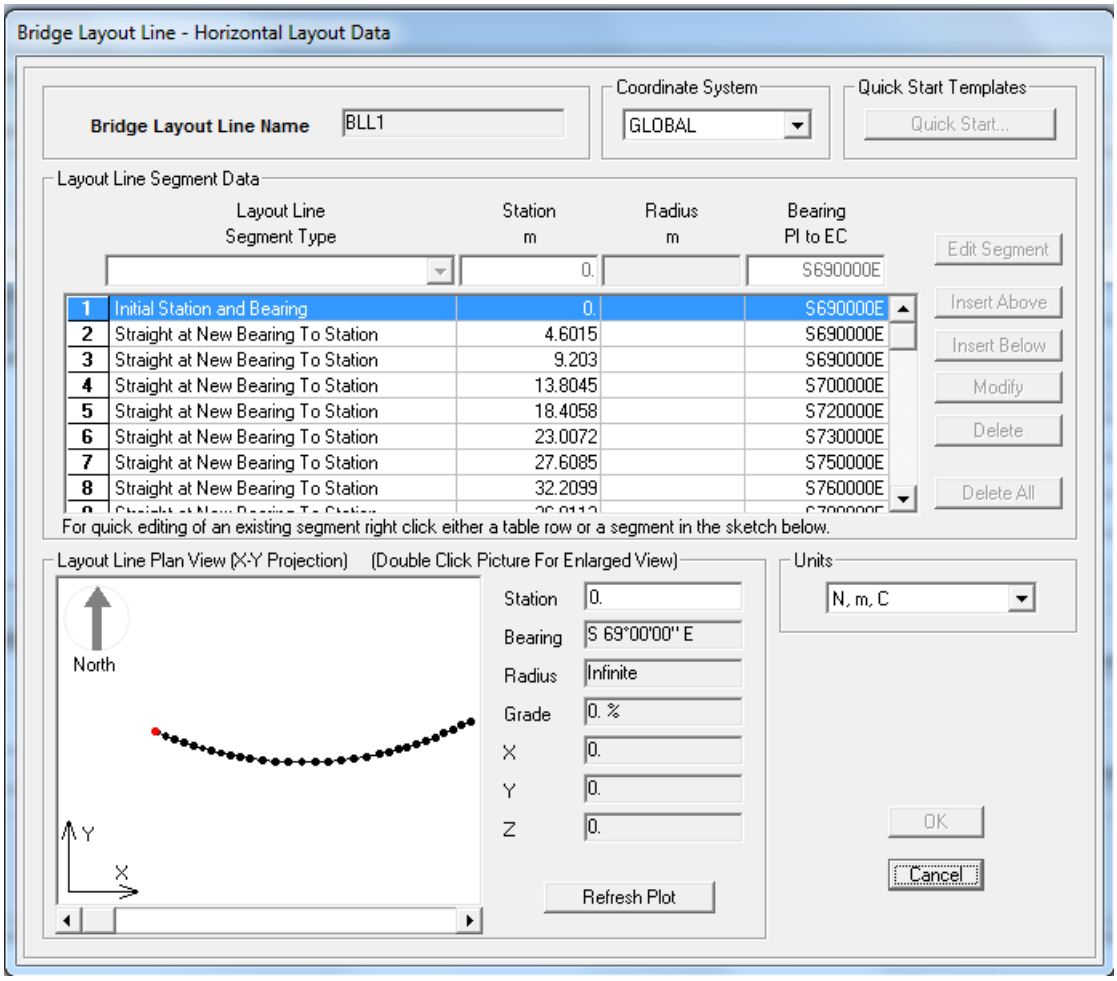

Figure 5.2 CSiBridge™ Bridge Horizontal Layout Line definition for Bridge 55-0837S

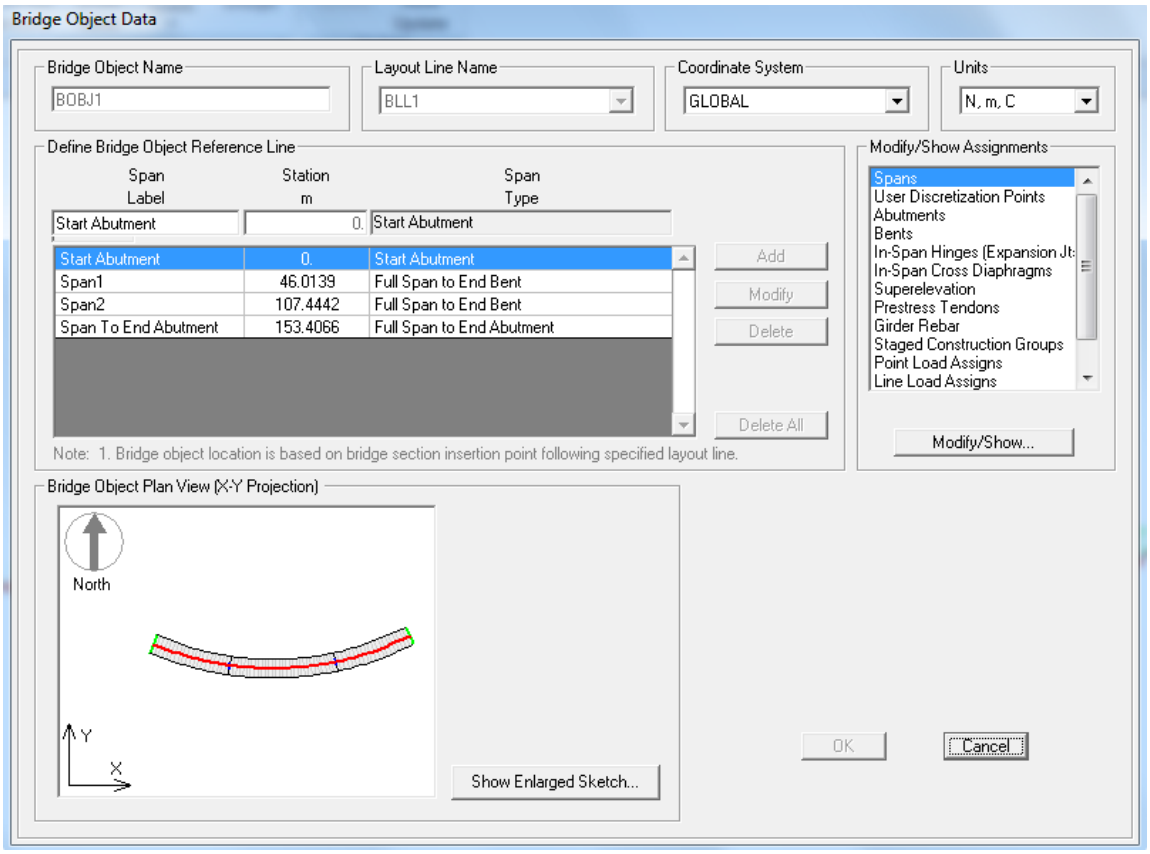

Figure 5.3 CSiBridge™ Bridge Object assignments for Bridge 55-0837S

Next, the cross-sectional properties are assigned to the objects identified. The bent properties assigned to this Bridge Object included the length of each bent (Bent 2 = 10.7 m, Bent 3 = 11 m), the column Frame Section and the distance from the top bent node to Layout Line (1.68 m). The bent column Frame Section was created using the Section Designer application to customize the column material properties, reinforcement, and confinement (see Figure 5.4 a). Instead of applying a General Frame Section to the bent columns, which assigns only the desired stiffness properties without need of further specifications, it was crucial to accurately model the bent reinforcement in order to achieve the expected value of moment of inertia taking into account concrete crack (i.e., I-cracked) and plastic hinge models that are automatically calculated by CSiBridge™. The bent cross-section used was specified in Bridge 55-0837S official plans provided by CALTRANS (see Figure 5.4 b). The material properties applied to the column section were defined in accordance to the properties used in the OpenSees model. Table 5.1

compares the cross-section geometry and stiffness properties defined in the OpenSees and CSiBridge™ models.

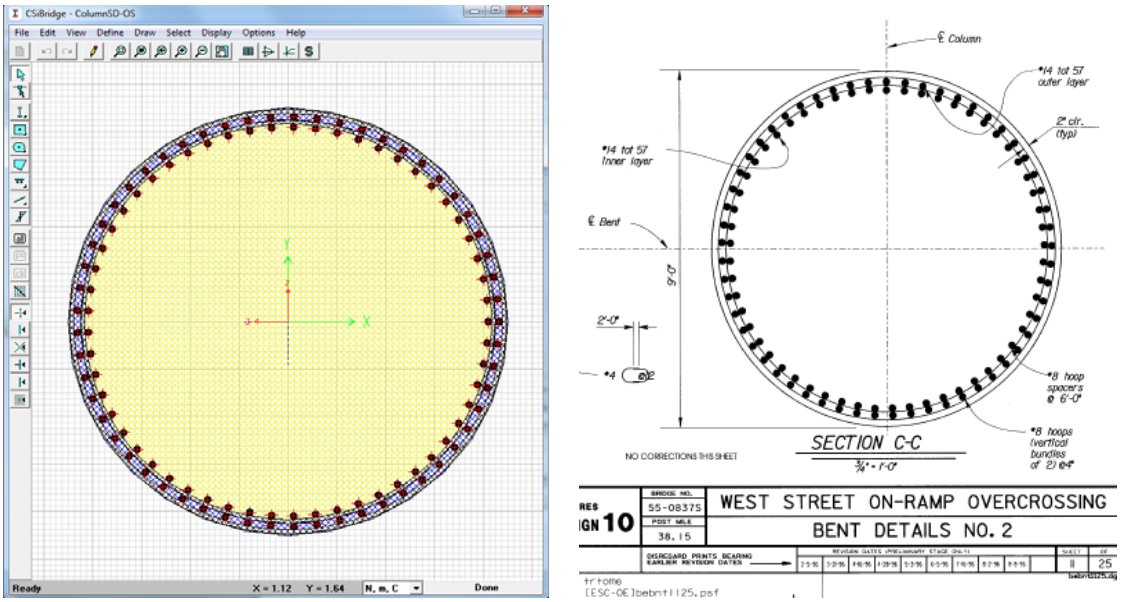

(a) **(b)**

Figure 5.4 Bent Column Section (a) CSiBridgeTM Section Designer

(b) Bent details of Bridge 55-0837S (provided by CALTRANS)

Table 5.1 Comparsion of Bent Frame Section properties

Section Property	**OpenSees Model**	**CSiBridge™ Model**
Cross-sectional Area (m^2)	5.8965	5.8723
Torsional Constant (m^4)	5.5335	5.4880
Moment of Inertia about U3 (m^4)	2.7668	2.7442
Moment of Inertia about U2 (m^4)	2.7668	2.7442

In assigning the Deck to the Bridge Object, the Deck Section design function can be used to automatically calculate deck stiffness properties given a user-defined geometry and material. When defining the deck section geometry as specified by Bridge 55-0837S official plans, the automatically calculated deck stiffness properties were not consistent with those assigned in the OpenSees model. To ensure congruency in deck properties among models, the deck section properties of the CSiBridge™ model (which are listed in Table 5.2) were manually defined using a General Frame Section.

Table 5.2 Comparsion of Deck Frame Section properties

Section Property	**OpenSees Model**	**CSiBridge™ Model**
Cross-sectional Area (m^2)	7.6293	7.6293
Torsional Constant (m^4)	0.2099	0.2099
Moment of Inertia about U3 (m^4)	5.95	5.95
Moment of Inertia about U2 (m^4)	47.16	47.16
Shear Area in 2 Direction (m^2)	7.6293	7.6293
Shear Area in 3 Direction (m^2)	7.6293	7.6293

Once a frame section has been created and applied to the model in CSiBridge™, mass will automatically be distributed along the member nodes based on cross-sectional area and defined material density. However, the mass distribution generated as such for Bridge 55-0837S did not match the distribution of masses applied to the OpenSees bridge model, which were a series of a lumped masses tributary to the corresponding node. Therefore, the masses in the CSiBridge™ model were overridden to ensure consistency between models. To override the masses assigned to the bridge model, a Property Modifier multiplier of 0 was applied to the Mass of all frame sections assigned to the Bridge Object. Each node along the deck and bent columns was selected and assigned mass in all three translational degrees of freedom with quantities equal to that applied to the corresponding node in OpenSees model. No rotational mass was assigned. Only mass, not weight, can be assigned manually to each node in CSiBridge™. Therefore, the weight Property Modifier was kept equal to 1 allowing CSiBridge™ to automatically assign weight based on material density and tributatry area. The diffence in total weight between models was negligible. It is noted that the mass of the structure is used in the

dynamic load case and eigenvalue analysis case, whereas the weight is only used in calculating the effects of dead load.

Lastly, the abutment and bent foundation soil springs were assigned to the Bridge Object consistent with the spring stiffness values and local axis orientations of the OpenSees model. Figure 5.5 shows the local axis orientations (i.e. longitudinal and transverse) at the abutment and bent locations. As shown, the u2 axis and the u1 axis respectively represent the transverse and longitudinal directions at each node in CSiBridge™. The soil spring stiffness values are discussed in Section 3 of this report. At the abutment locations, a series of soil spring restraint links were automatically assigned to the Bridge Object to take into account the interactions of deck, bearings, abutments, and foundations. The spring stiffness coefficients were user defined and each soil spring was oriented along the local axis of the respective node in which it was assigned. Properties of these multi-link springs were modified to replicate the soil springs defined in the OpenSees Model (which is discussed in detail in Section 3). Figure 5.6 illustrates the modified series of links located at the abutment. Although only vertical springs are portrayed, the links perform with defined stiffness along all six degrees of freedom. The Abutment Soil Spring, defined in Table 5.3, links the Bearing Spring, which is fixed in all six degrees of freedom, to the Ground Joint that is displaced a specified amount in a Caltrans Fault Crossing Design Request (as shown in Figure 5.1). The bent soil spring restraints were assigned at the bottom node of each bent column and are defined according to Table 5.3.

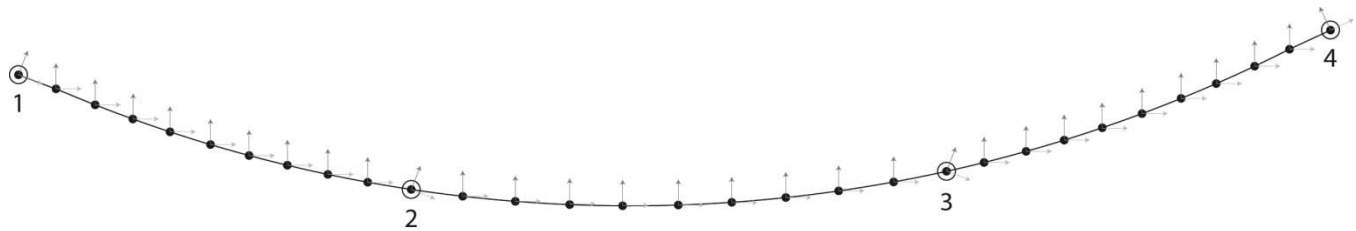

Plan View of Bridge 55-0837S

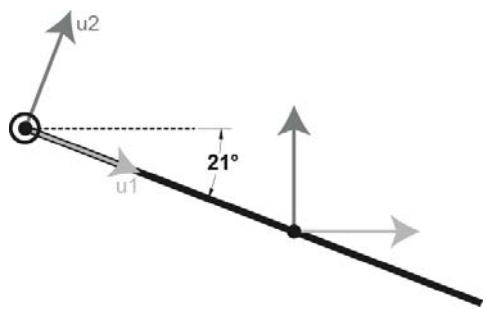

Abutment 1

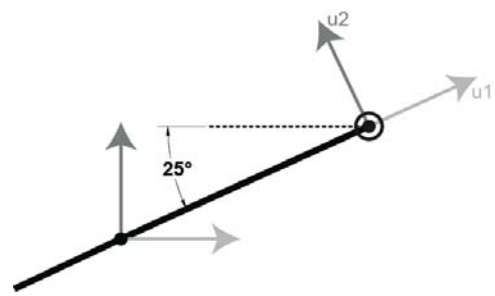

Abutment 4

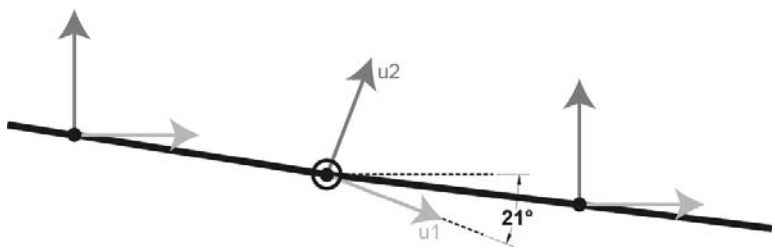

Bent 2

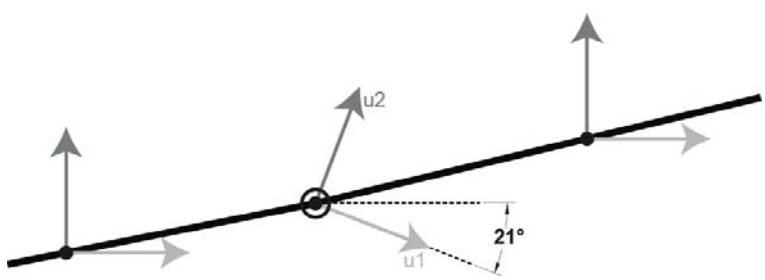

Bent 3

Figure 5.5 Local Axis orientations where u1 is the Local Longitudinal Axis and u2 is the Local Transverse Axis

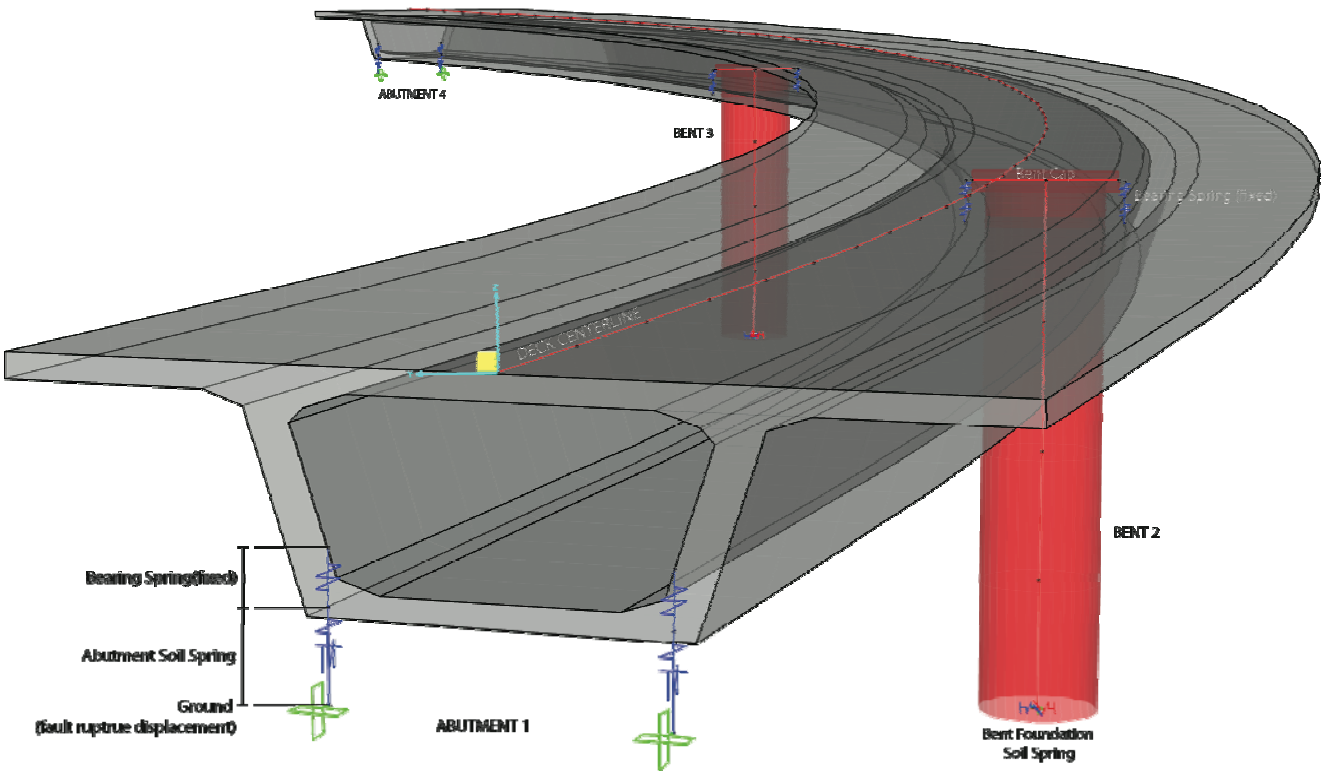

Figure 5.6 Assignments of Soil Springs in the CSiBridge™ model of Bridge 55-0837S

Table 5.3 Soil Spring stiffness assigned along the nodal Local Axis

Type	Direction	Abutment Soil Spring Stiffness		Bent Foundation Soil Spring	
		Release Type	Stiffness (kN/mm)	Release Type	Stiffness (kN/mm)
Translation	Vertical	Partial Fixity	49400	Fixed	5.65E+10
	Longitudinal	Partial Fixity	2.854	Partial Fixity	145
	Transverse	Partial Fixity	10.465	Partial Fixity	145
Rotation	Vertical	Free	0	Partial Fixity	56500
	Longitudinal	Free	0	Partial Fixity	56500
	Transverse	Free	0	Partial Fixity	56500

Figure 5.7 illustrates the plan view and elevation of the bridge model developed in CSiBridge™. As shown, node assignments, boundary conditions, and geometries of the model are the same as that developed in OpenSees (see Figure 3.3).

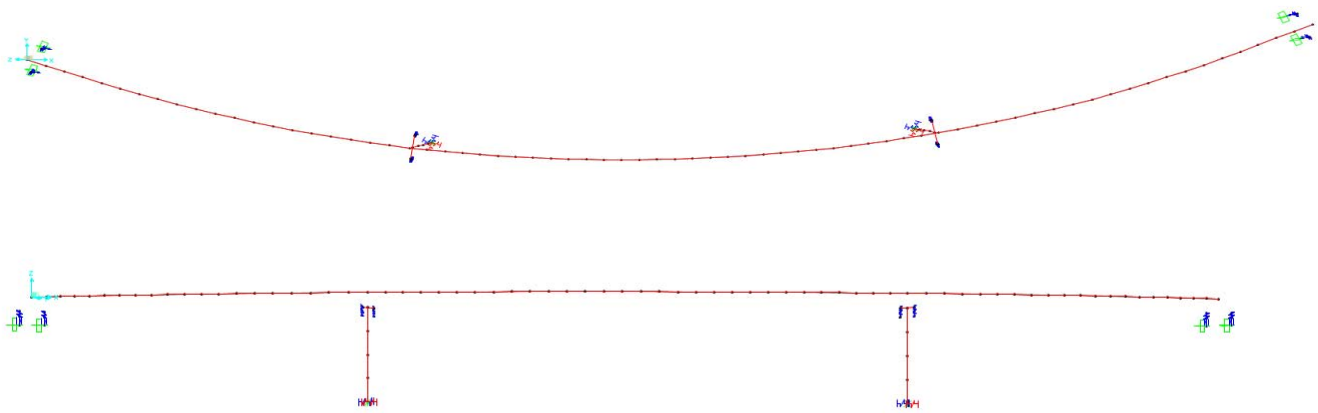

Figure 5.7 Plan and elevation of Bridge 55-0837S modeled in CSiBridge™

5.2 Automated Caltrans Fault Crossing Seismic Bridge Design

Previous versions of CSiBridge™ offer an Automated Seismic Bridge Design function which, once the bridge model is created, will run a series of load cases to automatically generate Demand/Capacity Ratios to aid in design of bridge components. This automated function follows the process presented in Figure 5.8. For more information on the features and methods used in the Automated Seismic Bridge Design see Computers and Structures, Inc. (2010). In CSiBridge™ version 16, the FR-RSA method described in Section 2 was implemented as an Automated Caltrans Fault Crossing Seismic Bridge Design function. When creating a Seismic Design Request, as shown in Figure 5.1, this Caltrans Fault Crossing seismic bridge design function can be selected and fault location, orientation, rupture displacement and response spectrum can be specified. For this study, the bridge object created in Section 5.1 was assumed to be on a fault running perpendicular to the line connecting the two abutments and located equidistant from each bent. As shown in Figure 5.9 and stated in Figure 5.1, the applied fault displacement was specified at 500 mm (0.5 m) on each side of the fault line allowing the total fault offset to be 1m. The design spectrum determined according to Caltrans SDC was specified as the

Response Spectrum for the Seismic Design Request and will be applied as such in both the fault-parallel and fault-normal orientations.

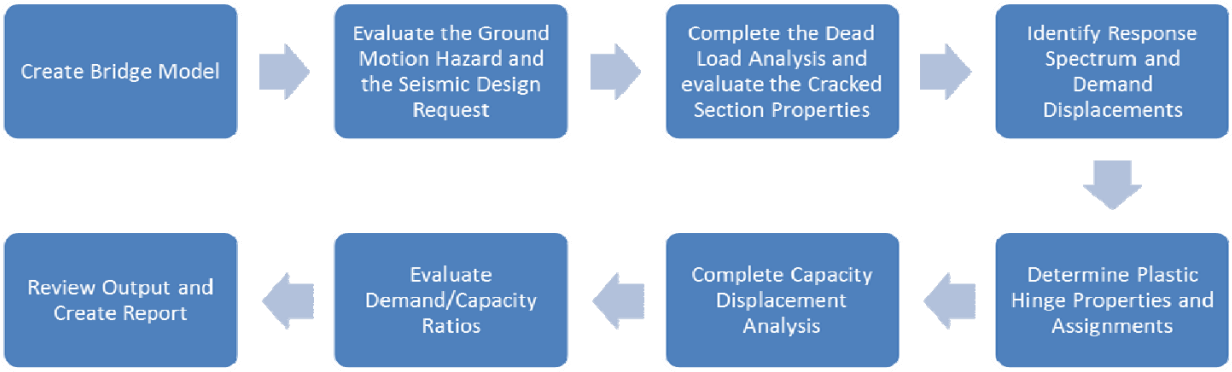

Figure 5.8 CSiBridge™ Automated Seismic Bridge Design Process

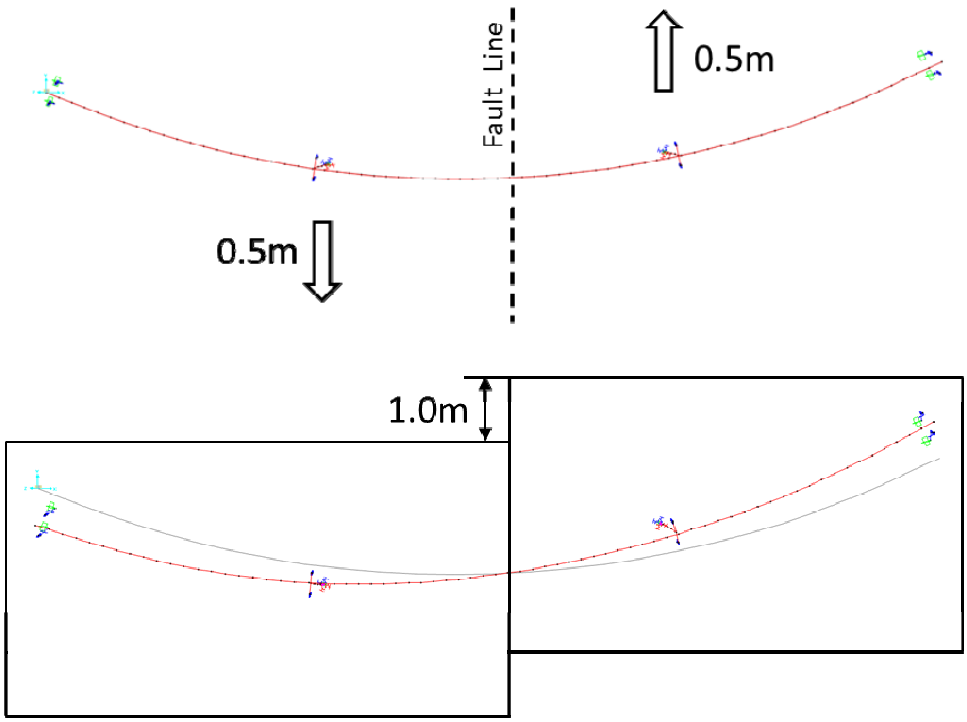

Figure 5.9 Plan view of Bridge 55-0837S Fault Rupture Displacement specified for CSiBridge™ Automated Fault Crossing Seismic Bridge Design

Consistent with FR-RSA, the Automated Fault Crossing Seismic Design function calculates the displacement demands on the bridge by combining the quasi-static

response caused by fault offset and the peak dynamic responses due to the fault-parallel and fault-normal ground motions through response spectrum analysis. Figure 5.10 shows the load cases created in CSiBridge™ to generate the Combined Response of a Bridge Object. Initially, a gravity loading case is performed to determine the cracked section properties for use in the load case analyses that determines the bridge responses caused by fault offset (i.e. Quasi-Static Load Case) and ground motions (i.e. Ritz Modal Load Case)..

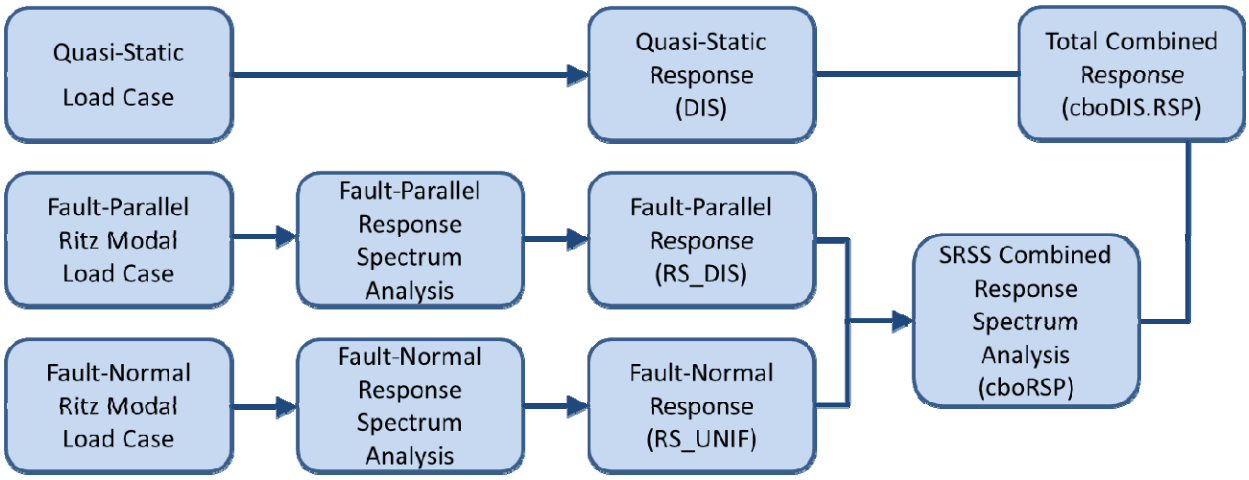

Figure 5.10 CSiBridge™ v.16 beta build "W" Response Combination as a product of the Automated Fault-Crossing Seismic Design command

As shown in Figure 5.10, a nonlinear Quasi-static Load Case first applies the fault rupture displacement to the nonlinear bridge model to produce the quasi-static results. The Ritz Model Load Cases, in both the fault-parallel and fault-normal orientations, approximate the periods of the bridge by assuming load-dependent Ritz vectors (Chopra, 2012). Response spectrum analysis is then used to estimate the bridge peak dynamic response caused by fault-parallel and fault-normal ground motions, respectively. For comparison with eigenvector mode shapes used in analysis in OpenSees, Appendix C provides the fundamental periods and the assumed Ritz vectors associated with both Fault-Parallel (Figure C.2) and Fault-Normal (Figure C.3) Ritz Modal Load Cases. Lastly, the Fault-Parallel Response and Fault-Normal Response, which are designated in CSiBridge™ as load cases RS_DIS and RS_UNIF respectively, are automatically combined and output as the dynamic bridge demand in both the transverse and longitudinal directions, which is defined as the cboRSP load combination. The total combined bridge response

considered, combines the cboRSP load combination with the quasi-static fault rupture displacement load case, output at DIS, to estimate the peak demands on the bridge.

5.3 Response Quantities of Interest and Result Discussions

To validate the CALTRANS Fault Crossing Seismic Design application added to CSiBridge™ v.16, this section compares the results obtained from the OpenSees and CSiBridge™ models. The response quantities of interest that were compared in this study as a means of validating the CALTRANS Fault Crossing Seismic Design Request added to CSiBridge™ v.16 were the displacements at the abutments and at the ends of each bent. Abutment displacements were measured as the change in length of the abutment soil springs in the local transverse and local longitudinal directions. Displacements at the bent ends were also compared in both the local transverse and local longitudinal directions. It is recognized that OpenSees uses fiber elements with distributed plasticity and CSiBridge™ uses beam-column elements with lumped plasticity (i.e., plastic hinges at the ends), each to capture the nonlinear bent behavior. While these two types of elements provide very similar results for translational displacement quantities as discussed in detail in the following, they produce disparities in angles of rotation at the ends of the bents resulting in less comparable values of bent drifts calculated according to the drift equation defined in CSiBridge™ which takes into account the angles of rotation at the ends of each bent. Therefore, comparisons of the bent drifts are not used for validation in this report.

As rooted in the FR-RSA procedure (which is reviewed in detail in Section 2), the total displacement demands on a bridge crossing fault ruptures combine the peak response values respectively caused by fault offset and both fault-parallel and fault-normal ground motions. Therefore, it is important and necessary to evaluate the adequacy of CSiBridge™ in predicting the total bridge response as well as each individual response component. To this end, the combined responses and the response quantity components summing to the combined responses shown in Figure 5.10 were compared. Accordingly, a total of 48 result comparisons are presented for this case study including displacements in both the transverse and longitudinal directions at the two abutments and each end of

the two bents due to fault offset, fault-parallel and fault-normal ground motions, and the combination of these three responses.

Figure 5.11 presents graphical comparisons of the results from CSiBridge™ (including bridge response components summing to the total bridge response) to those from OpenSees. In the figure, OpenSees-QS and CSiBridge™-QS represent the bridge quasi-static response components determined from the OpenSees and CSiBridge™ models, respectively; OpenSees-DY and CSiBridge™-DY represent the bridge peak dynamic response components determined from the OpenSees and CSiBridge™ models, respectively. It is noted that the detailed quantities of the bridge responses are provided in Appendix D. As shown in Figure 5.11, overall, the two models provide very similar results (particularly, the total bridge response), indicating the validity of the CSiBridge™ model. The slight differences observed in the result comparisons, which are acceptable for practical applications, are primarily due to the following effects:

1. The bridge vibration periods and mode shapes were determined from eigenvalue analysis in the OpenSees model, while in CSiBridge™, the bridge vibration periods were approximated through the use of Ritz vectors. See Appendix C for comparison of mode shapes and Ritz vectors.

2. The difference in quasi-static responses is due to discrepancy in nonlinear models for bents. The CSiBridge™ model used plastic hinges at the ends of the bents to take into account the nonlinear bent behavior, whereas the OpenSees model adopted fiber element with distributed plasticity for the bents.

It is useful to note that the version of CSiBridge™ used in this investigation models the box girder based on the recommendations from AASHTO. However, the AASHTO procedures cannot consider the box girder deck under push boundary conditions along the deck longitudinal direction (which may exist in some cases, e.g., a bridge crossing a reverse fault). There is a need to evaluate if the approximate procedures remain valid in these cases.

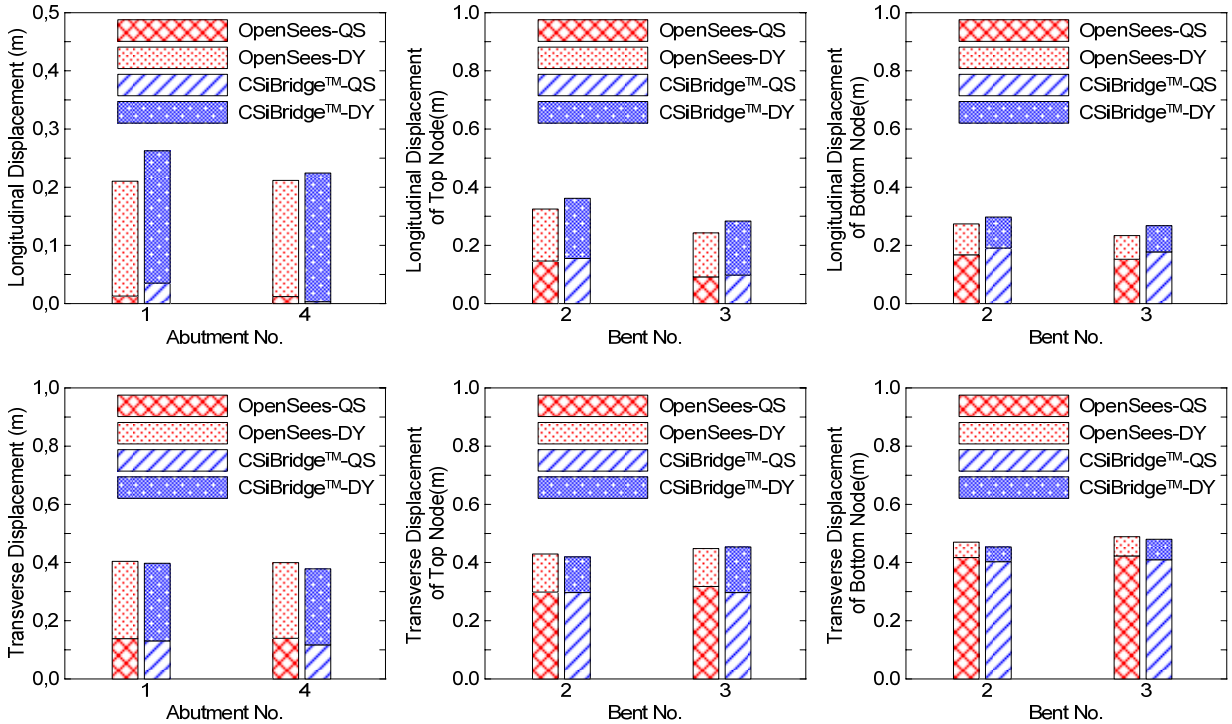

Figure 5.11 Result Comparison of Bridge 55-0537S: OpenSees vs. CSiBridge™

SECTION 6

CONCLUSIONS AND FUTURE WORK

This investigation was initiated to verify the adequacy of FR-RSA and FR-LSA for analysis of actual curved bridges crossing earthquake fault ruptures. To this end, two actual curved bridge, Bridge 55-0837S and Bridge 55-0939G, which respectively include three and four spans and represent the current bridge design and construction practice in California, were selected. The selected bridges were analyzed using the most rigorous method – nonlinear RHA, as well as FR-RSA and FR-LSA. Results from the approximate procedures including the combined bridge responses and each individual response component were compared with those from RHA for validation purpose. Throughout the analysis, ground motions, abutment longitudinal stiffness, and bridge orientation relative to earthquake fault rupture were varied to expand the validation work under a broad range of the parameters.

Comparisons of the results from RHA and FR-RSA show that FR-RSA consistently provides reasonable estimates for RHA in all considered cases. Therefore, FR-RSA, which requires significantly less amount of modeling and computational work, can be used as an alternative to RHA, and is recommended for future practical application.

Result comparisons of RHA and FR-LSA are not consistent for Bridge 55-0837S and Bridge 55-0939G. Based on the results from Bridge 55-0837S, it is found FR-LSA provides similar results to those from RHA. However, FR-LSA is found to generally provide overly conservative predictions based on the results from Bridge 55-0837S. It is noted that Bridge 55-0837S and Bridge 55-0939G respectively have three and four spans. The inconsistent observation is partially due to the fact that the higher mode effects, which cannot be captured by FR-LSA, may be more important in Bridge 55-0939G that has more spans than Bridge 55-0537S. Therefore, it is suggested that the FR-LSA procedure should be used with caution in bridges with more than three spans or non-negligible higher mode effect.

Moreover, analysis results from Bridge 55-0837S and Bridge 55-0939G both demonstrate that the quasi-static response alone (which is caused by ground displacement offset only)

is inadequate in estimating the bridge response under the ground motions considered (which include a ground offset of 100 cm). Although the quasi-static response may be more significant in an earthquake event associated with larger ground offset, it is recommended to use the combination of quasi-static and dynamic responses in analysis and design of bridges crossing fault-ruptures.

Furthermore, it is shown that the FR-RSA procedure can be implemented on CSiBridge™, an existing bridge analysis and design platform that is more convenient for bridge engineers. Based on the results of Bridge 55-0837, it is shown that the implementation on CSiBridge™ can provide adequate predictions for bridge responses and can be used in future practice.

While the current investigation led to significant progress in advancing the practice on seismic analysis of bridges crossing fault rupture zones, following issues need further investigation:

1. The validation of analytical procedures in this project was limited to ground motions associated with strike-slip earthquake fault ruptures. While the FR-RSA and FR-LSA were developed based on fundamental theories from structural dynamics and they are expected to work regardless the type of ground motion inputs, it would be useful to further verify their adequacy using the ground motions associated with other types of faults (e.g., normal or reverse normal faults with different dip and rake angles).
2. The bridges investigated in this project did not include seismic bearings/isolators which are being widely used in bridge engineering. Particularly, the displacement demand on bridges crossing fault ruptures can be significant and inclusion of seismic bearings/isolators can help the bridges accommodate the large displacement demands. Future work is needed to investigate if the approximate procedures are valid when seismic bearings/isolators are present in the bridges crossing fault rupture zones.
3. The bridges selected in this investigation included only single-column bents. It would be useful to verify the validity of FR-RSA and FR-LSA for bridges with multiple-column bents.

4. The bridges investigated in this project assumed elastic soil spring properties. It is not clear how the demands on critical elements will be affected by the nonlinear soil behavior. Therefore, there is a need to investigate the effects of soil nonlinearity on the bridge displacement demands.
5. Large tensile and/or compressive force may develop in bridge deck along the longitudinal direction, especially for normal or reverse normal faults. It is necessary to identify the key parameters and develop convenient analysis models for estimating the deck axial force to ensure desirable deck seismic performance.
6. Based on the validated analysis procedures, parametric analyses are necessary in the future to identify the critical/vulnerable components and develop the corresponding design implication for bridge crossing fault ruptures.
7. There is a need to evaluate and improve pushover analyses used to assess displacement capacities of components (e.g., bents) in bridges crossing fault rupture zones because of significantly different motions experienced by the bridge during fault rupture compared to the traditional uniform support excitation.

SECTION 7

REFERENCES

CALTRANS. (2010). Seismic Design Criteria (Version 1.6 ed.) California Dept. of Transportation, Sacramento, CA (http://ww.dot.ca.gov)

CALTRANS. (2012). Memo to Designers 20-10 California Dept. of Transportation, Sacramento, CA (http://www.dot.ca.gov/hq/esc/techpubs/updates/page/mtd-20-10.pdf)

City-Data, (1998). http://www.city-data.com/bridges/bridges-Orange-California2.html

City-Data, (2010). http://www.city-data.com/bridges/bridges-Anaheim-California4.html

Computers and Structures, Inc. (2010). "CSiBridgeTM Bridge Seismic Design." Automated Seismic Design of Bridges. AASHTO Guide Specifications for LRFD Seismic Bridge Design, Berkeley, CA, USA.

Earthquake Engineering Research Institute (EERI), (2000). Chapter 18: Impact on Highway Structures in Kocaeli, Turkey, Earthquake of August 17, 1999 Reconnaissance Report, Earthquake Spectra, Supplement A to Volume 16.

Earthquake Engineering Research Institute (EERI), (2001). Chapter 8: Highway Bridges in Chi-Chi, Taiwan, Earthquake of September 21, 1999 Reconnaissance Report, Earthquake Spectra, Supplement A to Volume 17.

Goel, R.K. and Chopra, A.K. (2008a). Analysis of Ordinary Bridges Crossing Fault-Rupture Zones. Report No. UCB/EERC-2008/01, Earthquake Engineering Research Center, University of California, Berkeley, CA.

Goel, R.K. and Chopra, A.K. (2008b). "Role of Shear Keys in Seismic Behavior of Bridges Crossing Fault-Rupture Zones." Journal of Bridge Engineering, 13(4):398-408.

Goel, R.K. and Chopra, A.K. (2009a). "Linear Analysis of Ordinary Bridges Crossing Fault-Rupture Zones." Journal of Bridge Engineering, 14(3): 203-215.

Goel, R.K. and Chopra, A.K. (2009b). "Nonlinear Analysis of Ordinary Bridges Crossing Fault-Rupture Zones." Journal of Bridge Engineering, 14(3): 216-224.

Ghasemi, H., Cooper, J.D., Imbsen, R., Piskin, H., Inal, F., and Tiras, A. (2000). The November 1999 Duzce Earthquake: Post-Earthquake Investigation of the Structures in the TEM. Publication No. FHWA-RD-00-146, U.S. Department of Transportation, Federal Highway Administration.

Kawashima, K., Takahashi, Y., Ge, H., Wu, Z., Zhang, J. (2009). Damage of Bridges in 2008 Wenchuan, China Earthquake. Journal of Earthquake Engineering, Vol.13, pp956-998.

Mazzoni, S., McKenna, F., Scott, M. H., and Fenves, G. L. (2006). OpenSees Command Language Manual.

Shantz, T., and Chiou, B. (2011). Creation of Record Set for Use in Fault Crossing Study. Division of Research and Innovation. California Department of Transportation.

Yen, W.-H. (2002). Lessons Learned about Bridges from Earthquake in Taiwan. Public Roads, U.S. Department of Transportation, Federal Highway Administration, Volume 65, No. 4.

APPENDIX A

COMPLETE RESULT COMPARISONS OF BRIDGE 55-0837S

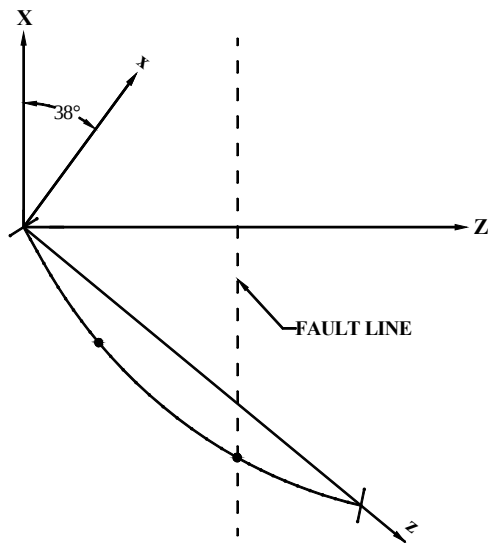

Figure A.1 Sketch of Bridge 55-0837S when $\theta = -38^{o}$.

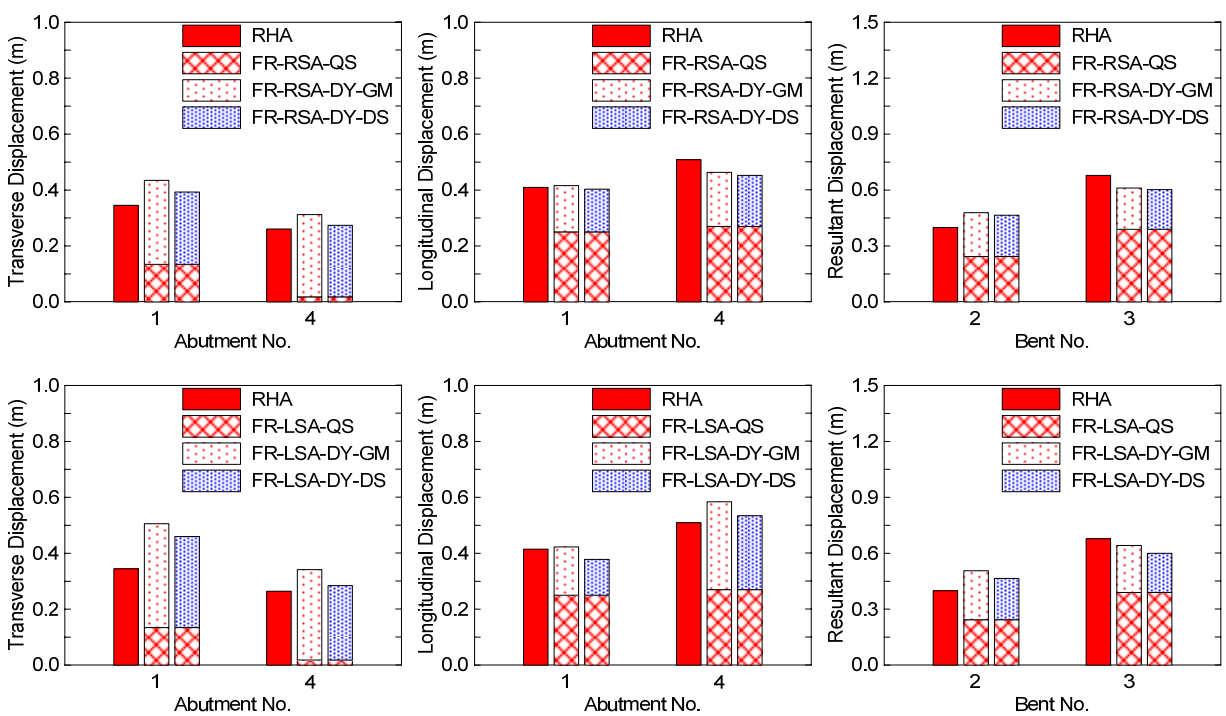

Figure A.2 Results of Bridge 55-0837S when $\theta = -38^{o}$ and longitudinal abutment stiffness $= 0.10K_{eff}$.

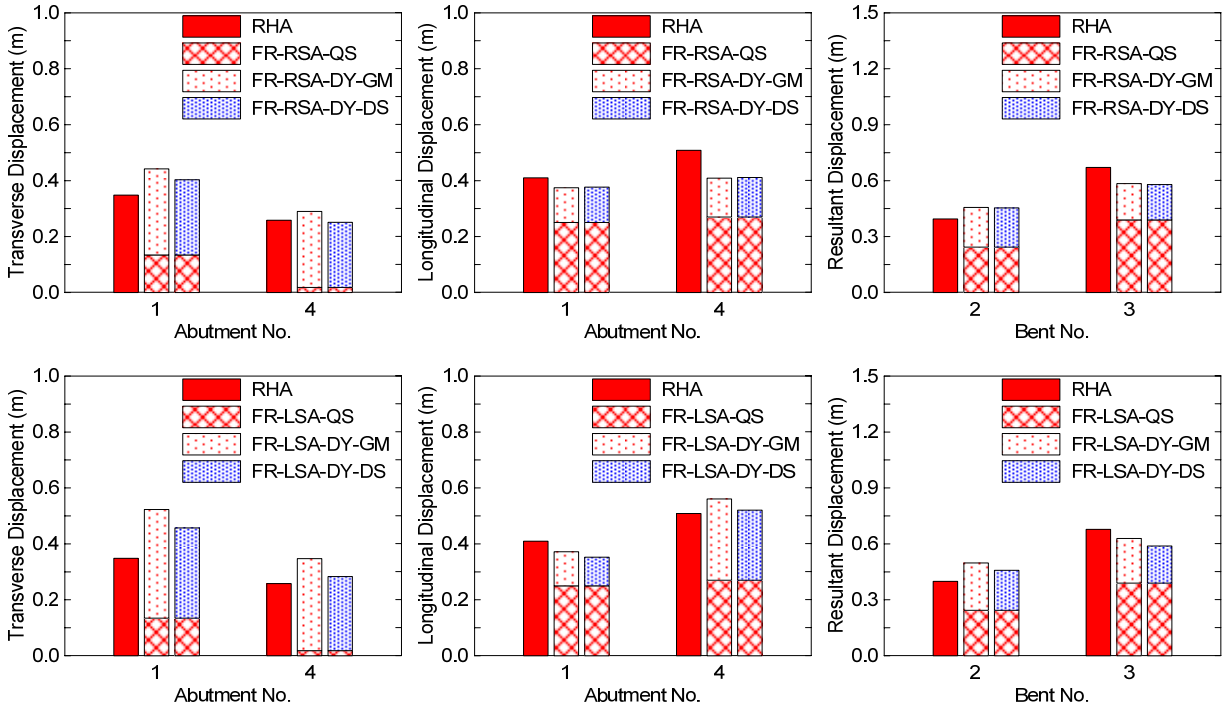

Figure A.3 Results of Bridge 55-0837S when $\theta = -38^{\circ}$ and longitudinal abutment stiffness $= 0.55K_{eff}$.

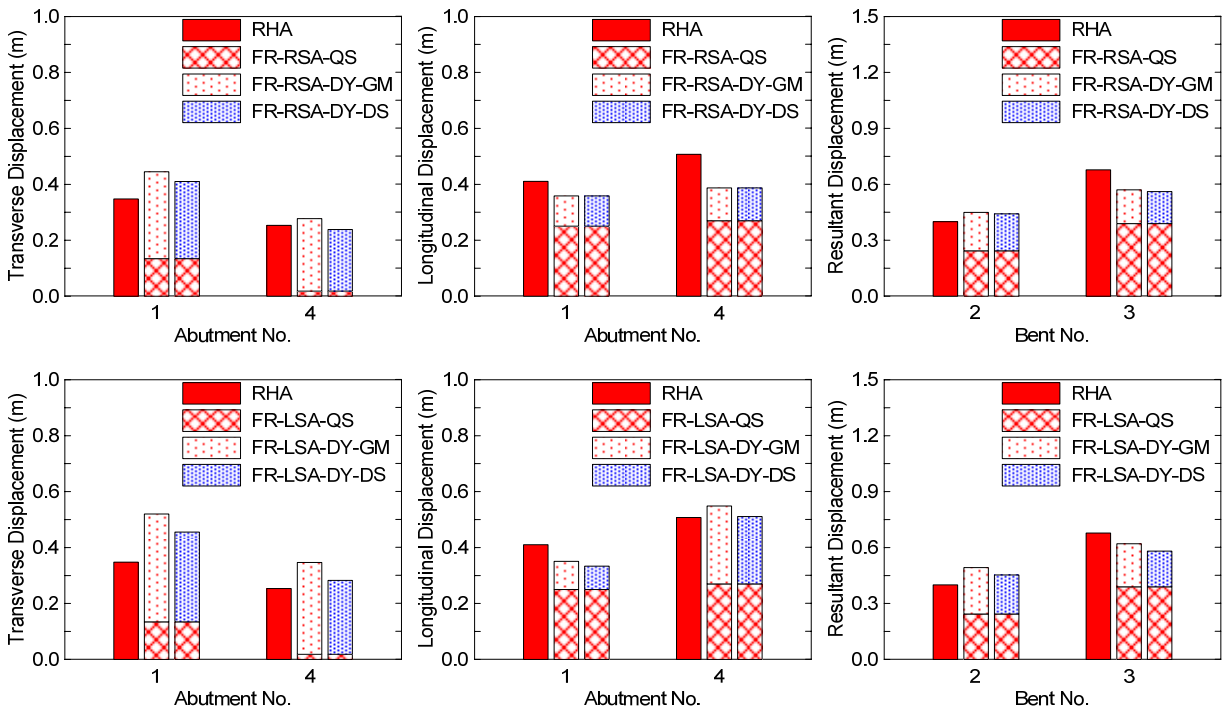

Figure A.4 Results of Bridge 55-0837S when $\theta = -38^{\circ}$ and longitudinal abutment stiffness $= 1.00K_{eff}$.

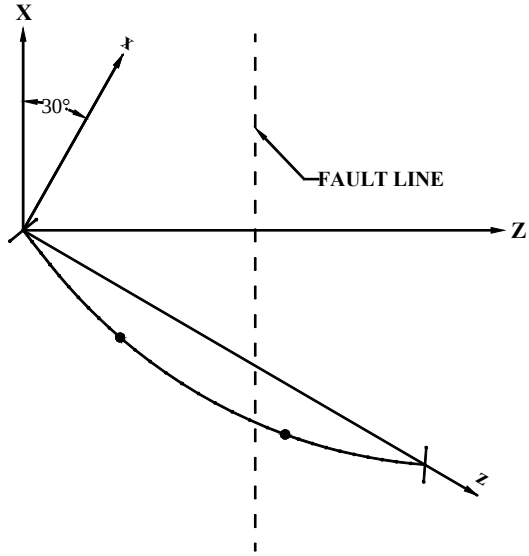

Figure A.5 Sketch of Bridge 55-0837S when $\theta = -30^{o}$.

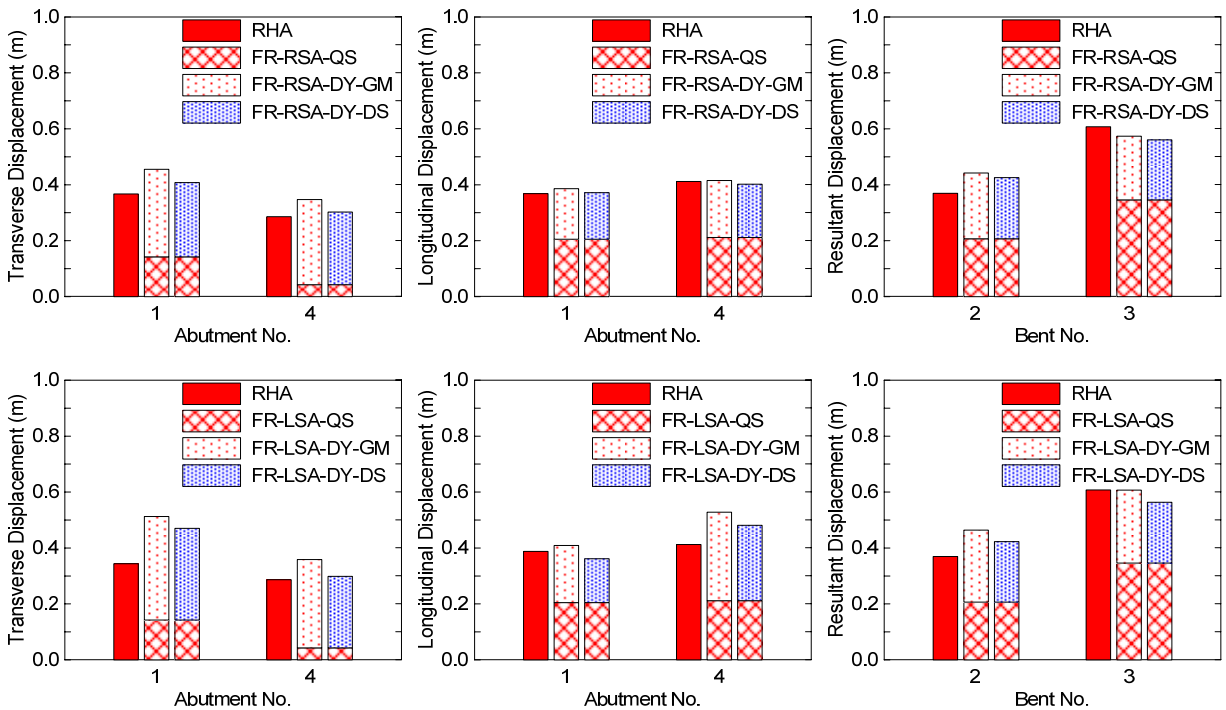

Figure A.6 Results of Bridge 55-0837S when $\theta = -30^{o}$ and longitudinal abutment stiffness $= 0.10K_{eff}$.

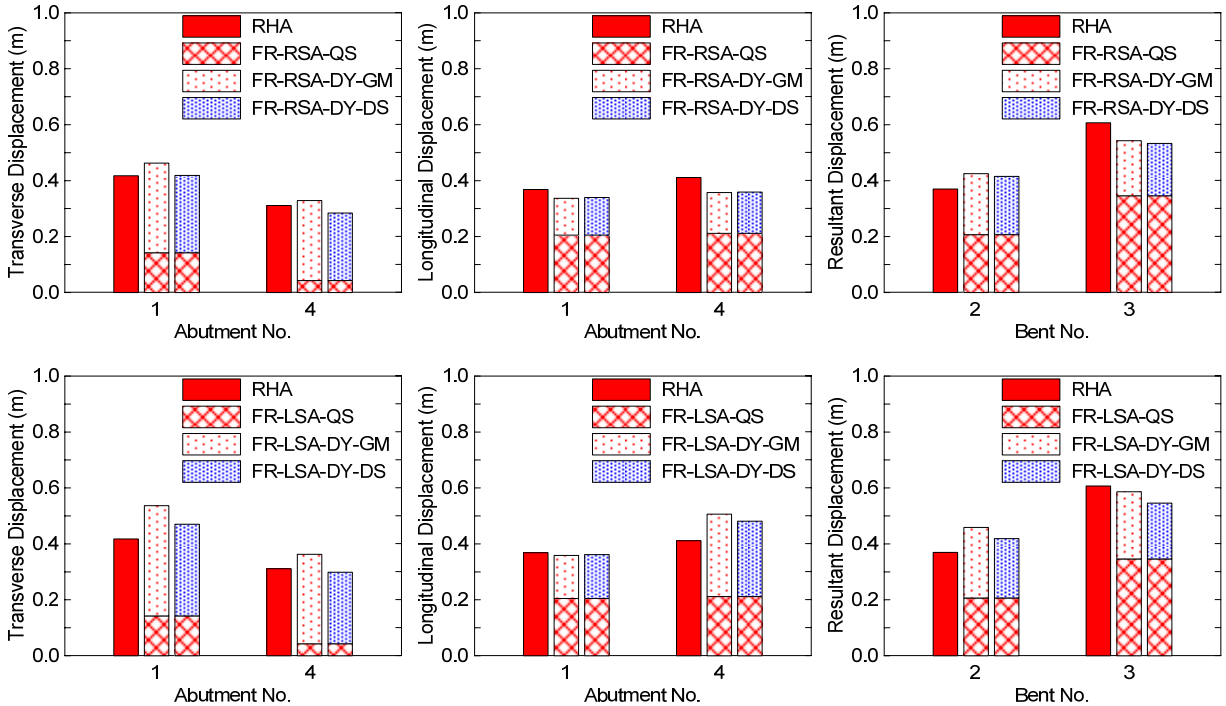

Figure A.7 Results of Bridge 55-0837S when $\theta = -30^{o}$ and longitudinal abutment stiffness $= 0.55K_{eff}$.

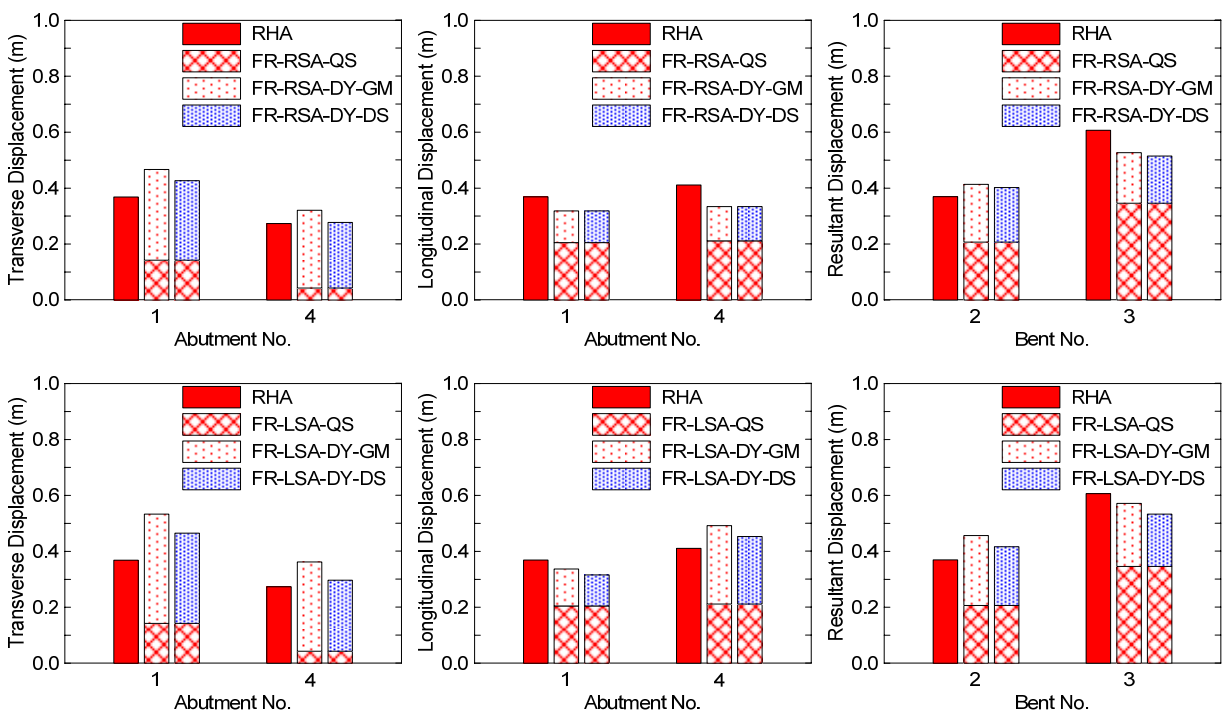

Figure A.8 Results of Bridge 55-0837S when $\theta = -30^{o}$ and longitudinal abutment stiffness $= 1.00K_{eff}$.

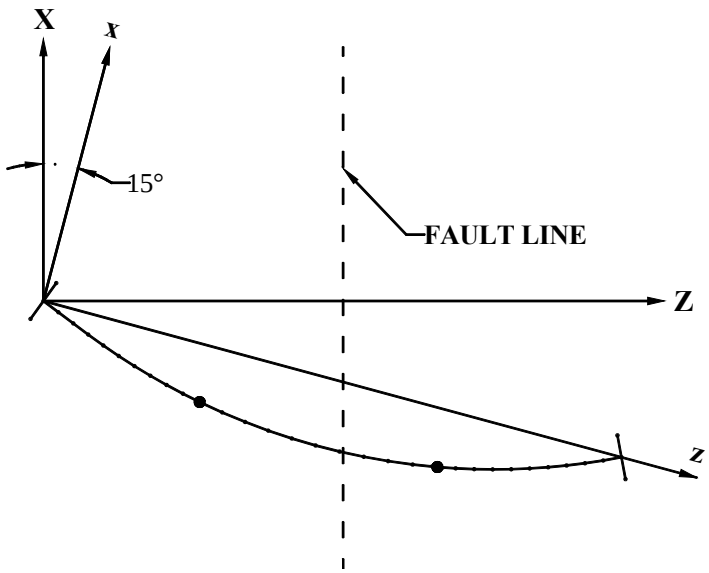

Figure A.9 Sketch of Bridge 55-0837S when $\theta = -15^{o}$.

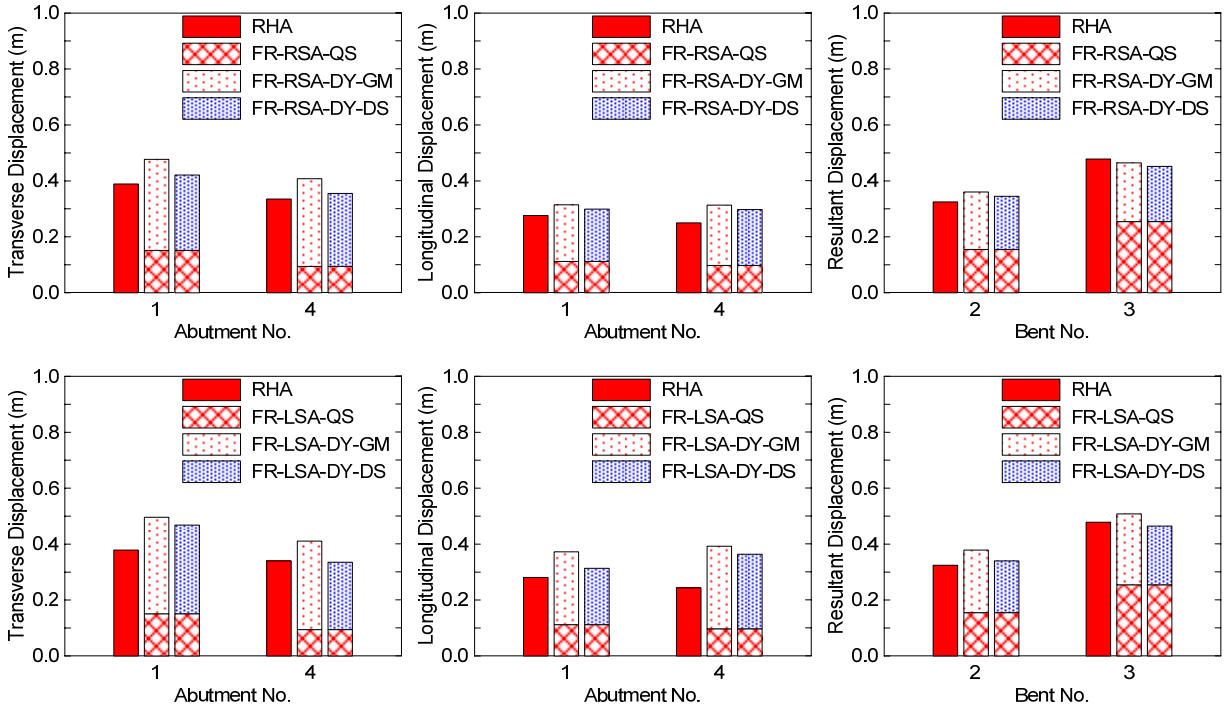

Figure A.10 Results of Bridge 55-0837S when $\theta = -15^{o}$ and longitudinal abutment stiffness $= 0.10K_{eff}$.

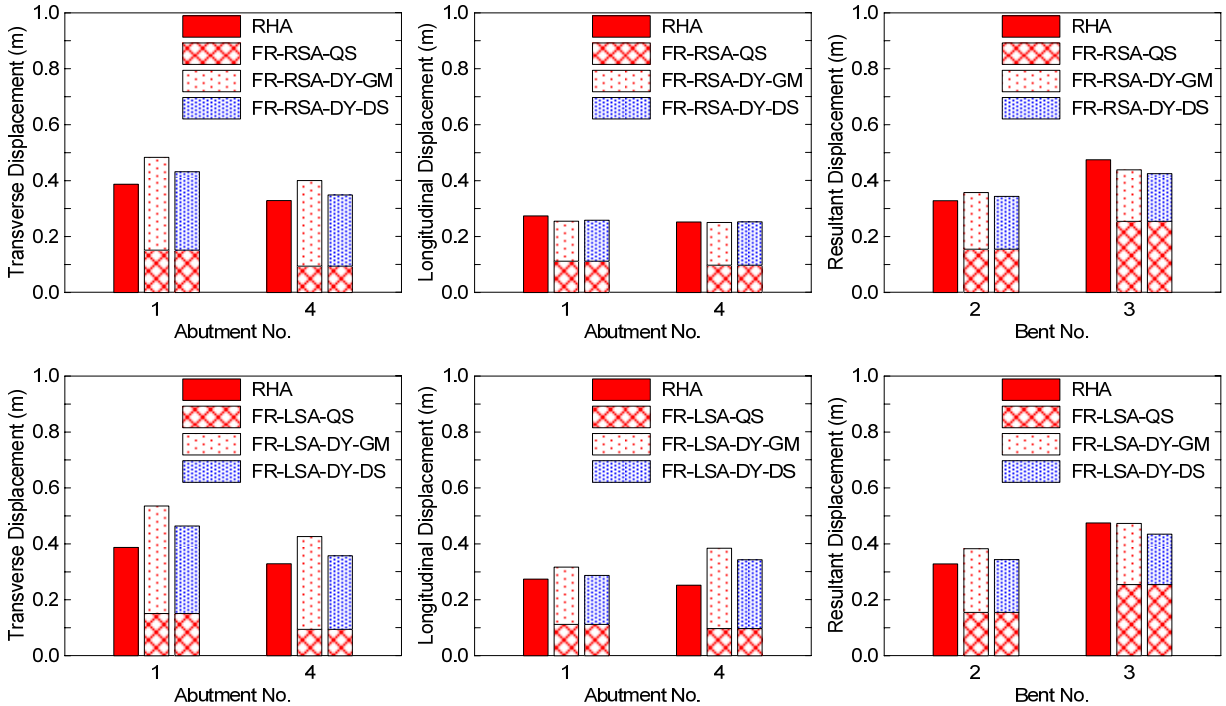

Figure A.11 Results of Bridge 55-0837S when $\theta = -15^{\circ}$ and longitudinal abutment stiffness $= 0.55K_{eff}$.

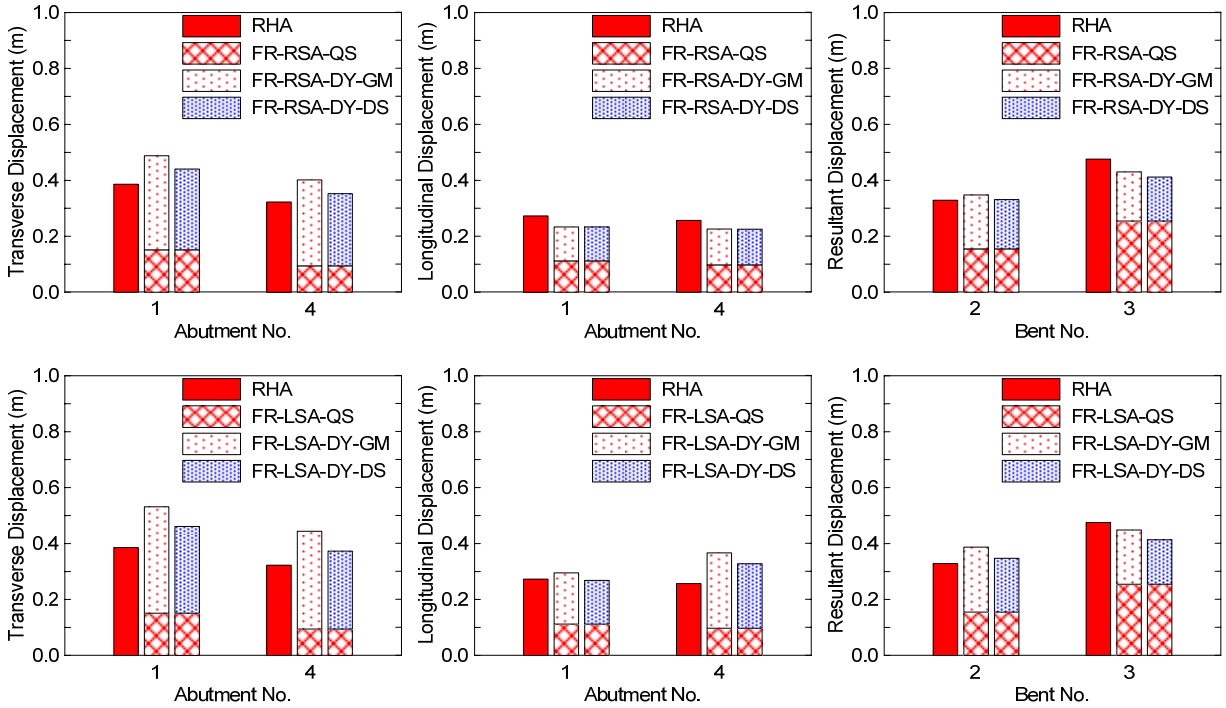

Figure A.12 Results of Bridge 55-0837S when $\theta = -15^{\circ}$ and longitudinal abutment stiffness $= 1.00K_{eff}$.

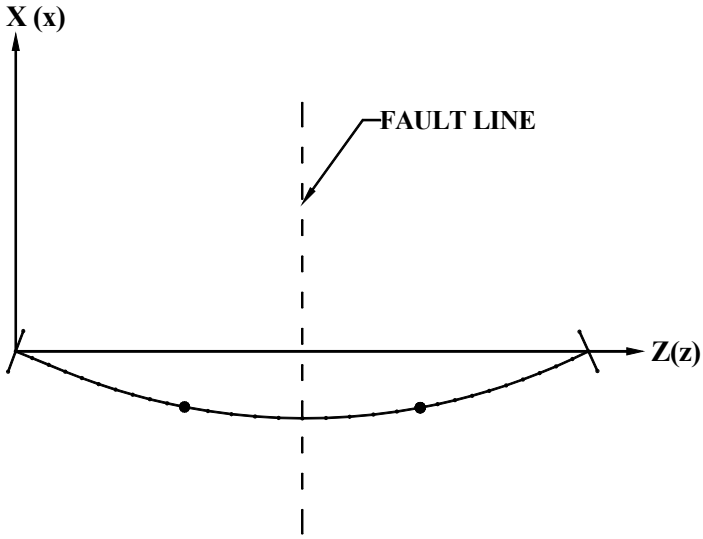

Figure A.13 Sketch of Bridge 55-0837S when $\theta = 0^{o}$.

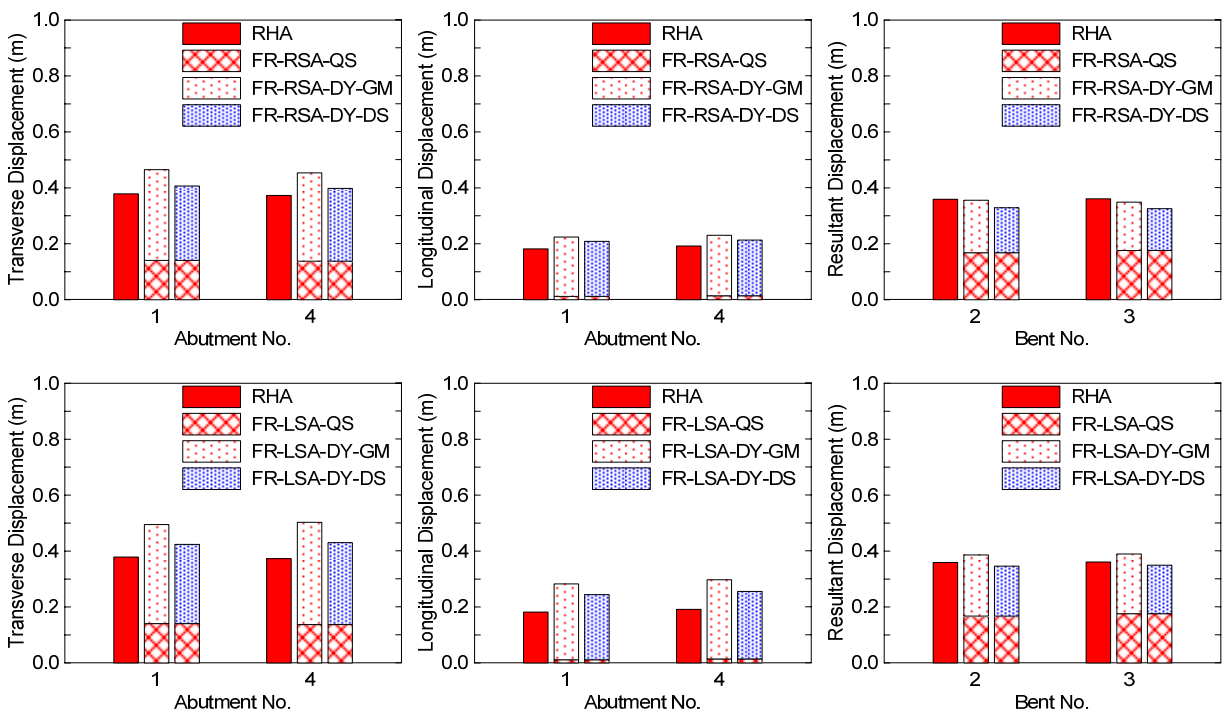

Figure A.14 Results of Bridge 55-0837S when $\theta = 0^{o}$ and longitudinal abutment stiffness $= 0.10K_{eff}$.

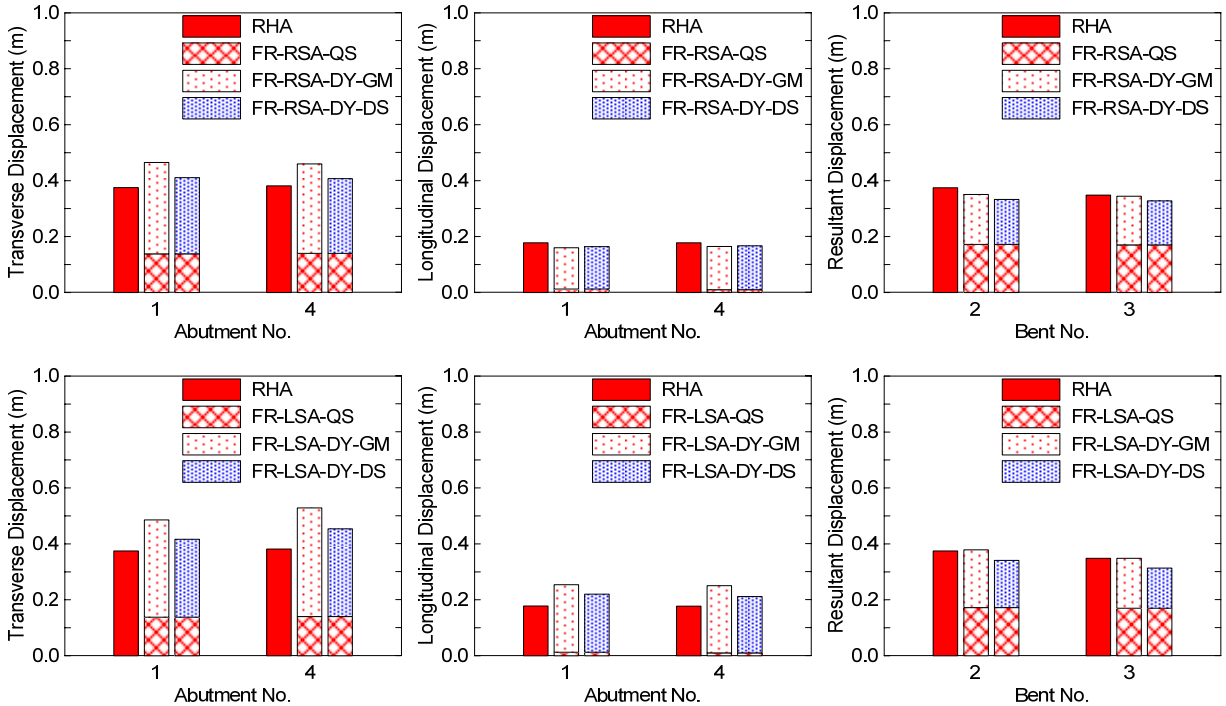

Figure A.15 Results of Bridge 55-0837S when $\theta = 0^{o}$ and longitudinal abutment stiffness $= 0.55K_{eff}$.

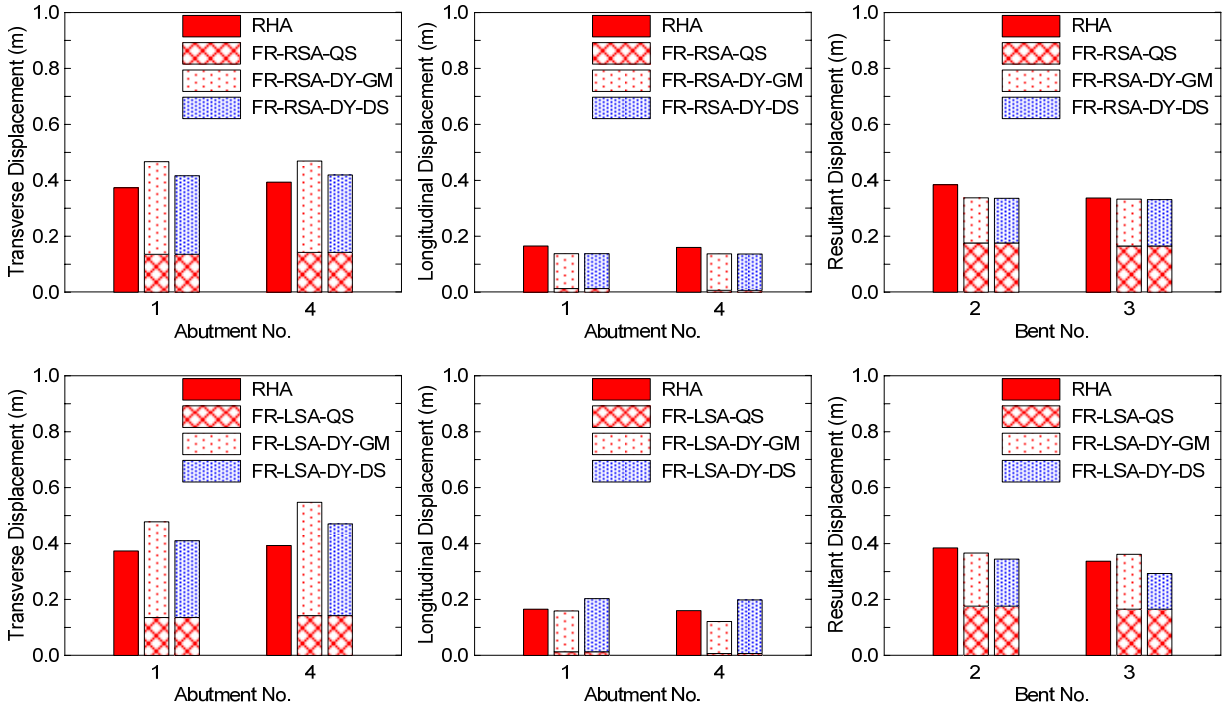

Figure A.16 Results of Bridge 55-0837S when $\theta = 0^{o}$ and longitudinal abutment stiffness $= 1.00K_{eff}$.

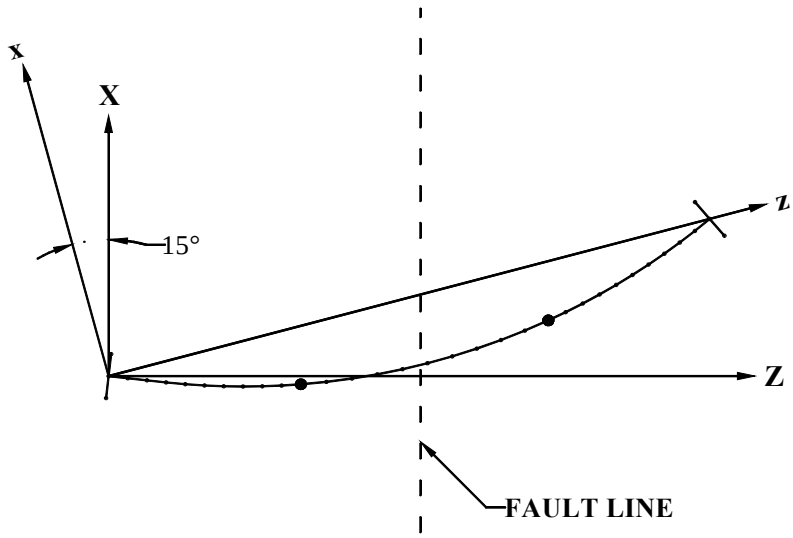

Figure A.17 Sketch of Bridge 55-0837S when $\theta = 15^{o}$.

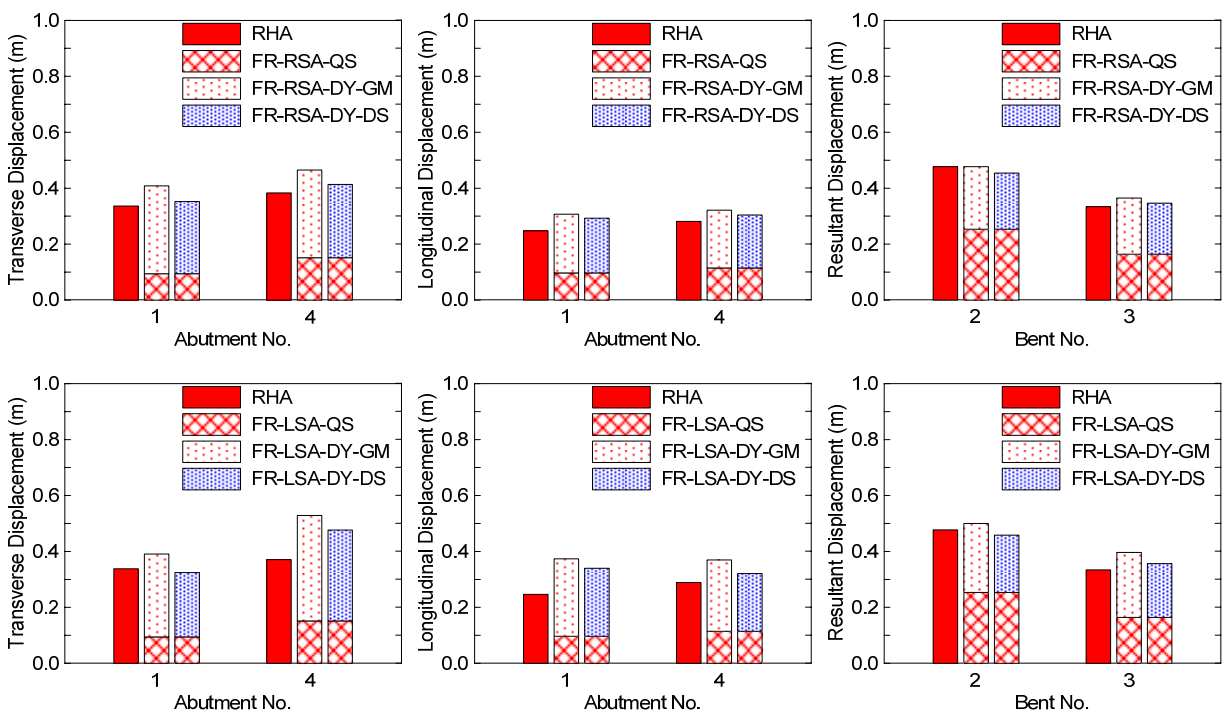

Figure A.18 Results of Bridge 55-0837S when $\theta = 15^{o}$ and longitudinal abutment stiffness $= 0.10K_{eff}$.

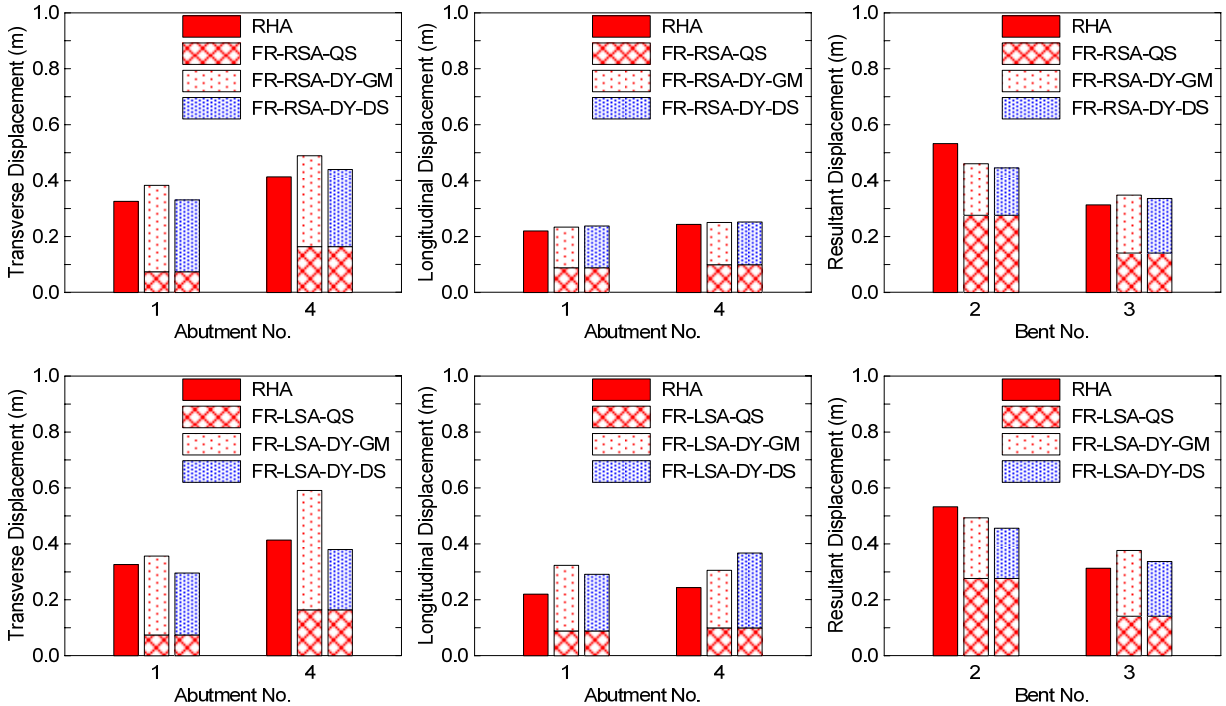

Figure A.19 Results of Bridge 55-0837S when $\theta = 15^{o}$ and longitudinal abutment stiffness $= 0.55K_{eff}$.

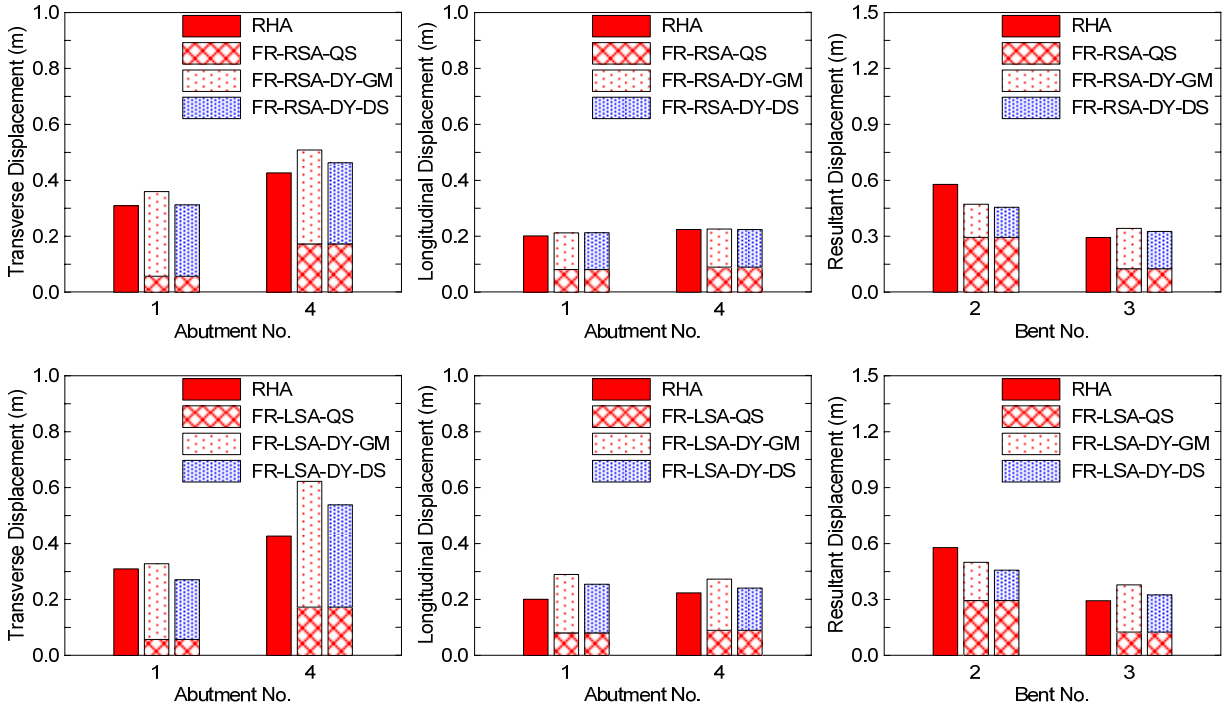

Figure A.20 Results of Bridge 55-0837S when $\theta = 15^{o}$ and longitudinal abutment stiffness $= 1.00K_{eff}$.

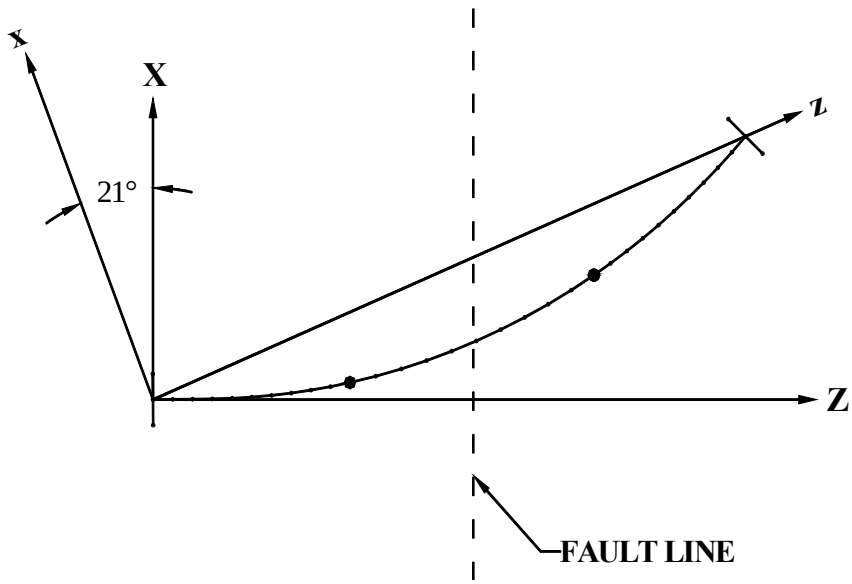

Figure A.21 Sketch of Bridge 55-0837S when $\theta = 21^{o}$.

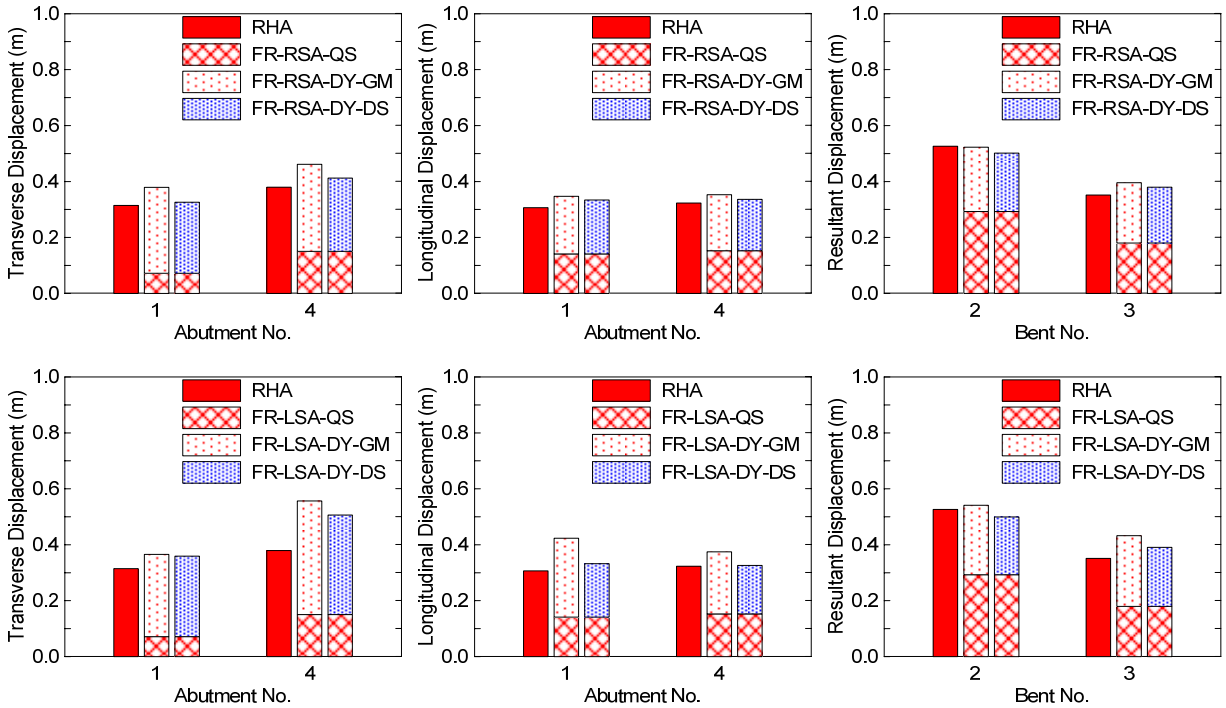

Figure A.22 Results of Bridge 55-0837S when $\theta = 21^{o}$ and longitudinal abutment stiffness $= 0.10K_{eff}$.

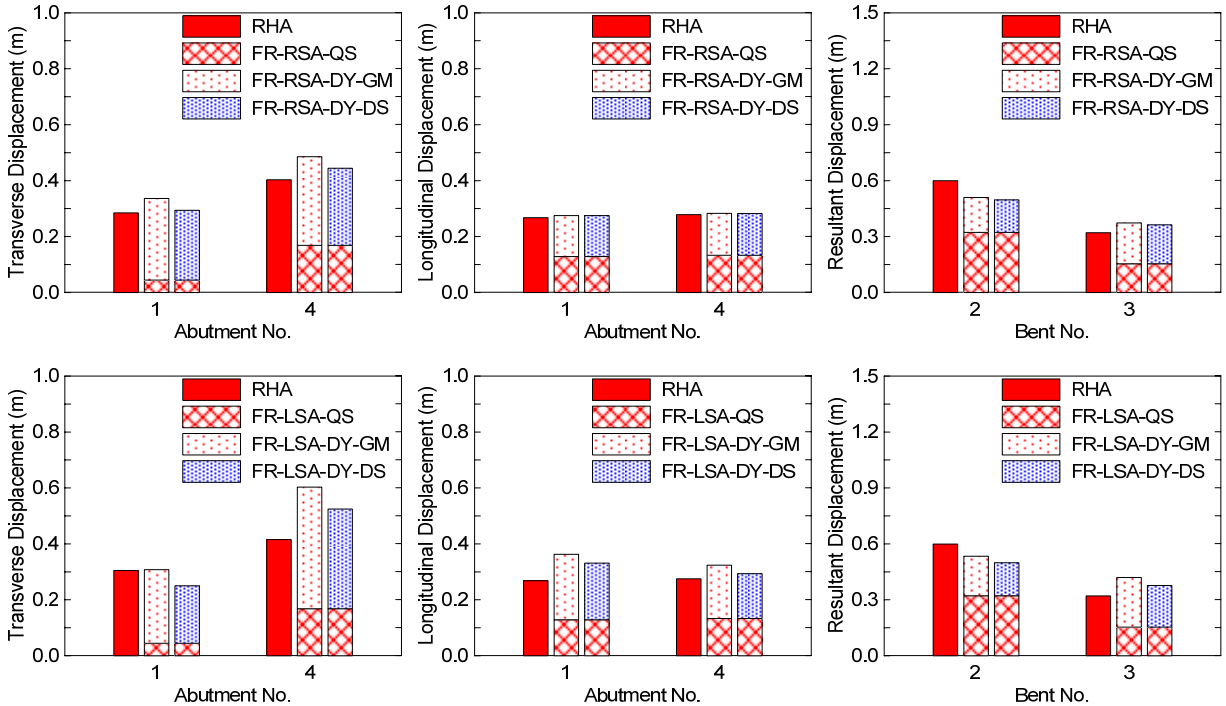

Figure A.23 Results of Bridge 55-0837S when $\theta = 21^{o}$ and longitudinal abutment stiffness $= 0.55K_{eff}$.

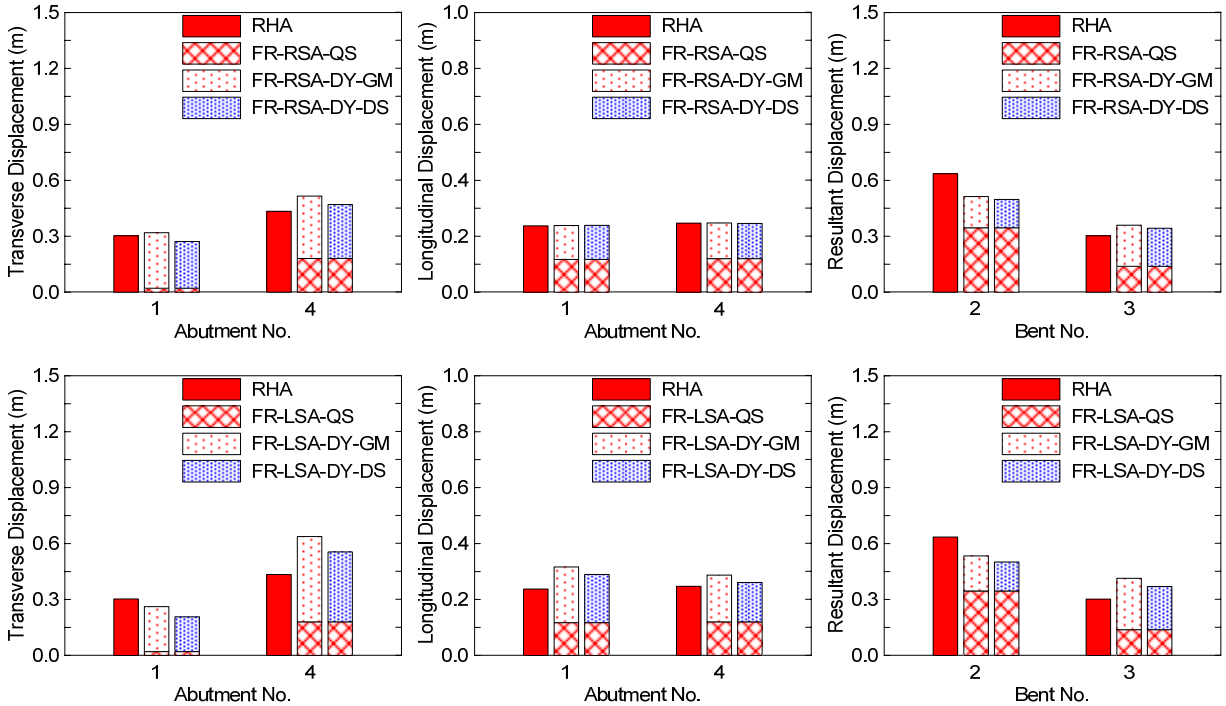

Figure A.24 Results of Bridge 55-0837S when $\theta = 21^{o}$ and longitudinal abutment stiffness $= 1.00K_{eff}$.

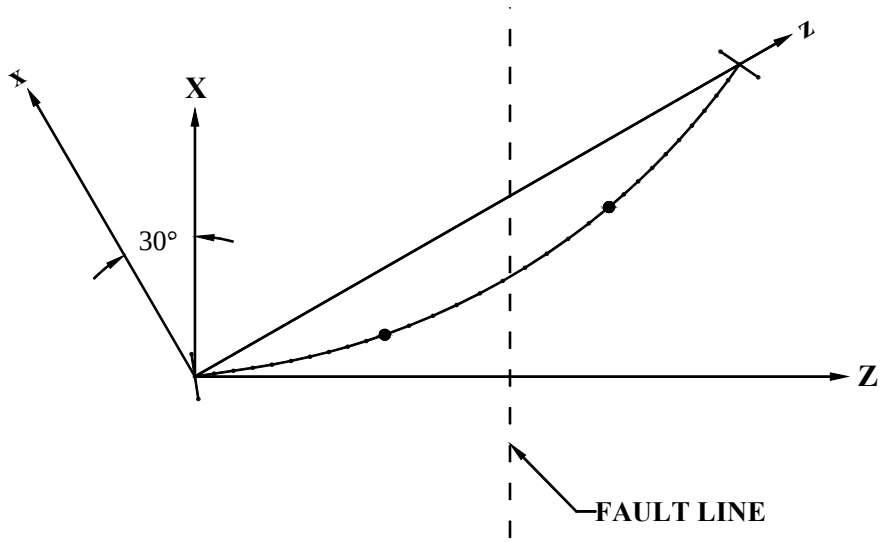

Figure A.25 Sketch of Bridge 55-0837S when $\theta = 30^{o}$.

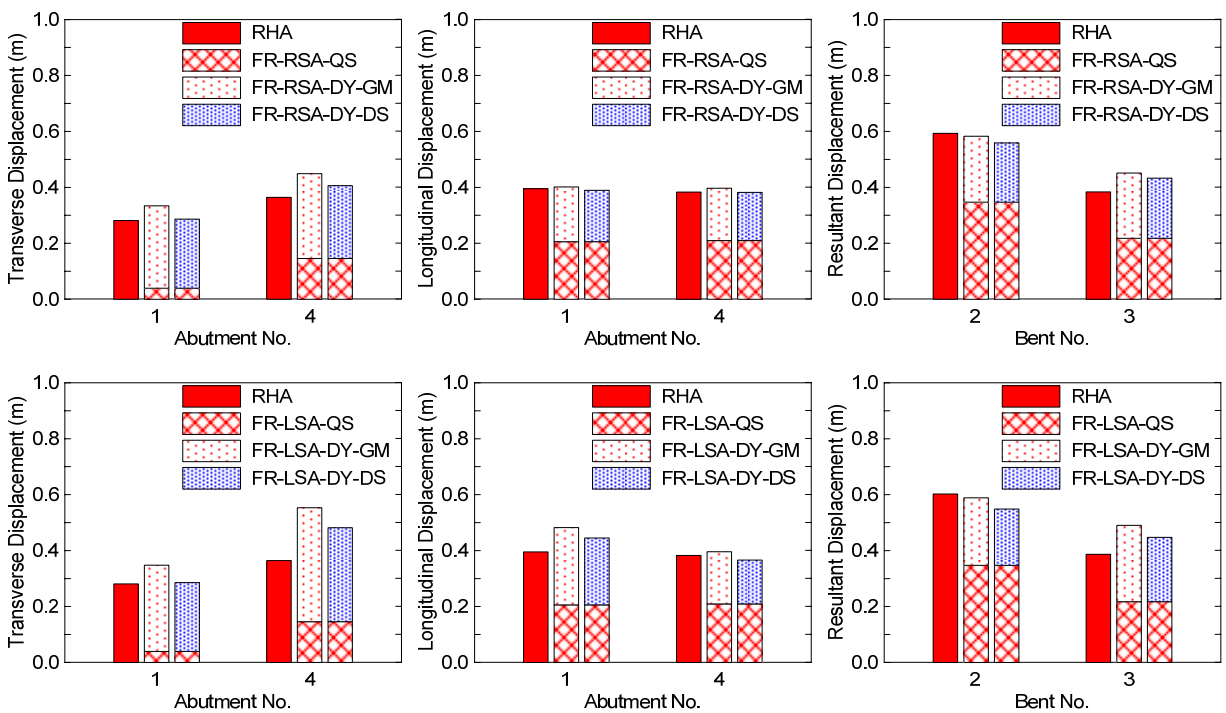

Figure A.26 Results of Bridge 55-0837S when $\theta = 30^{o}$ and longitudinal abutment stiffness $= 0.10K_{eff}$.

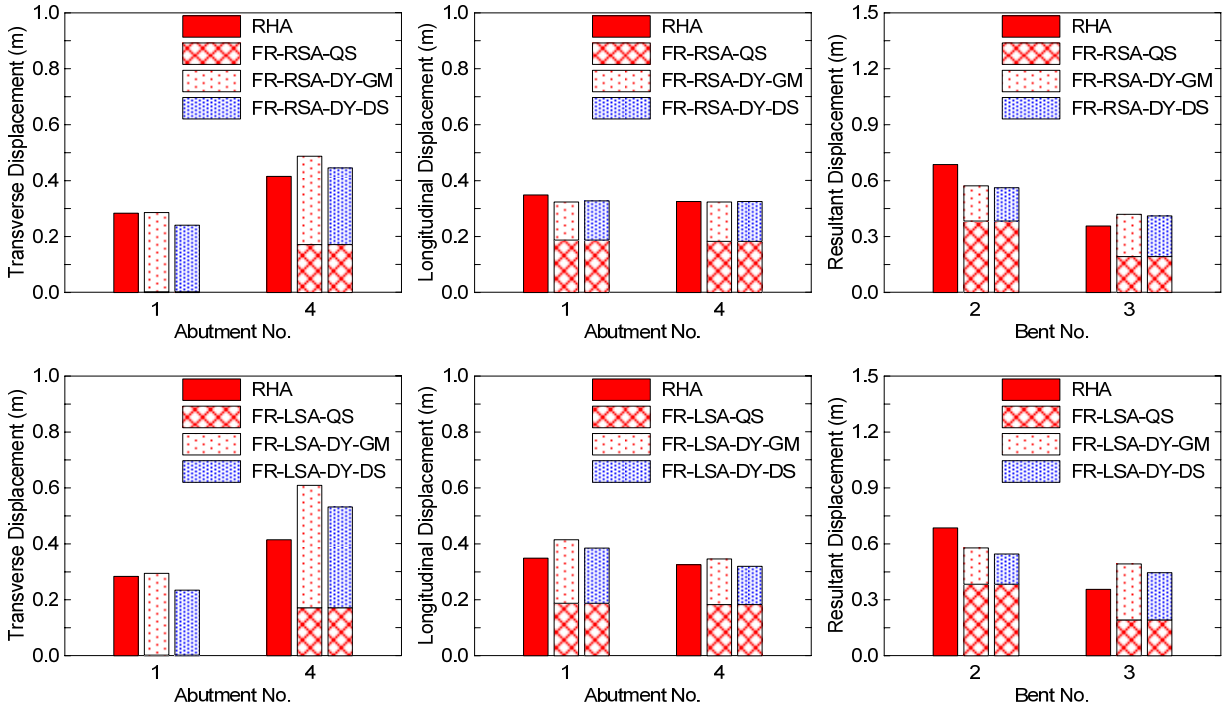

Figure A.27 Results of Bridge 55-0837S when $\theta = 30^{o}$ and longitudinal abutment stiffness $= 0.55K_{eff}$.

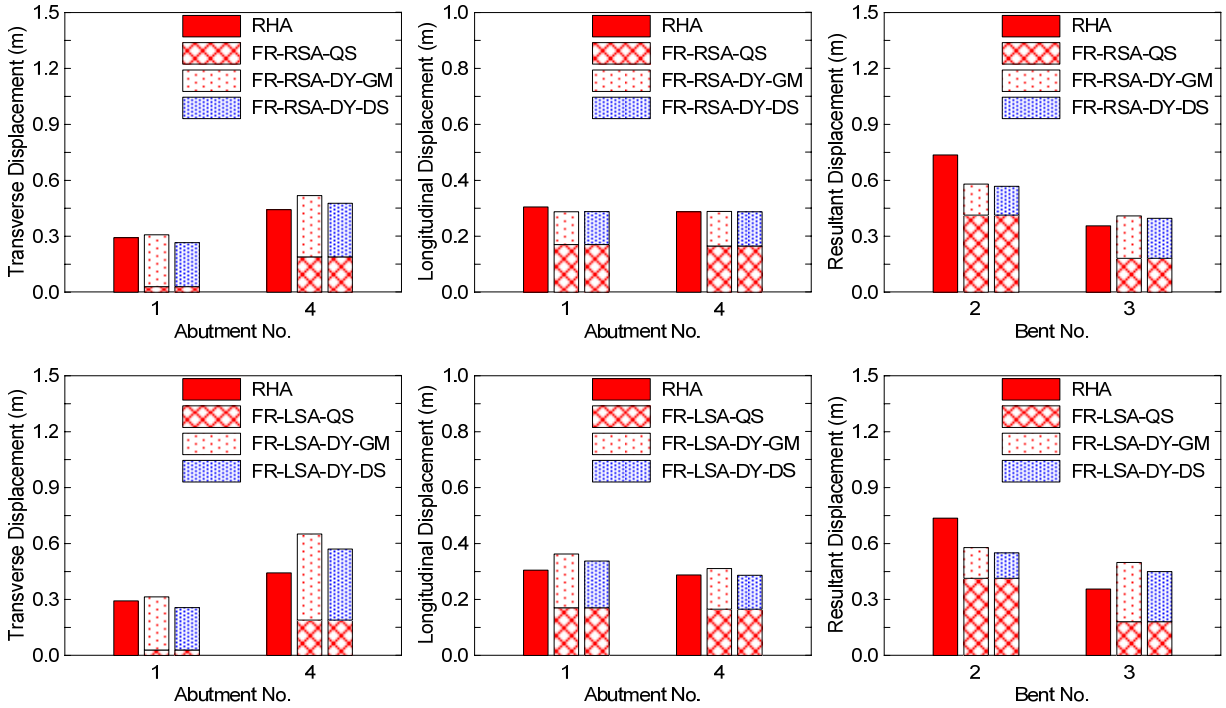

Figure A.28 Results of Bridge 55-0837S when $\theta = 30^{o}$ and longitudinal abutment stiffness $= 1.00K_{eff}$.

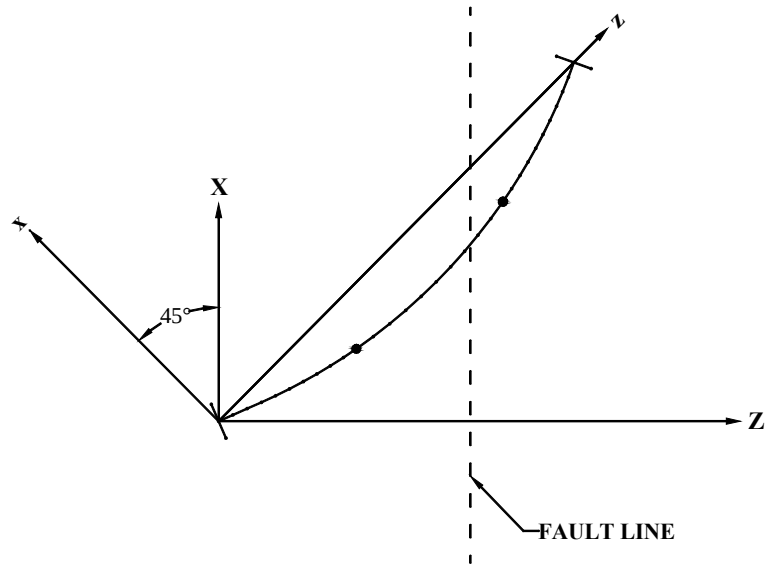

Figure A.29 Sketch of Bridge 55-0837S when $\theta = 45^{o}$.

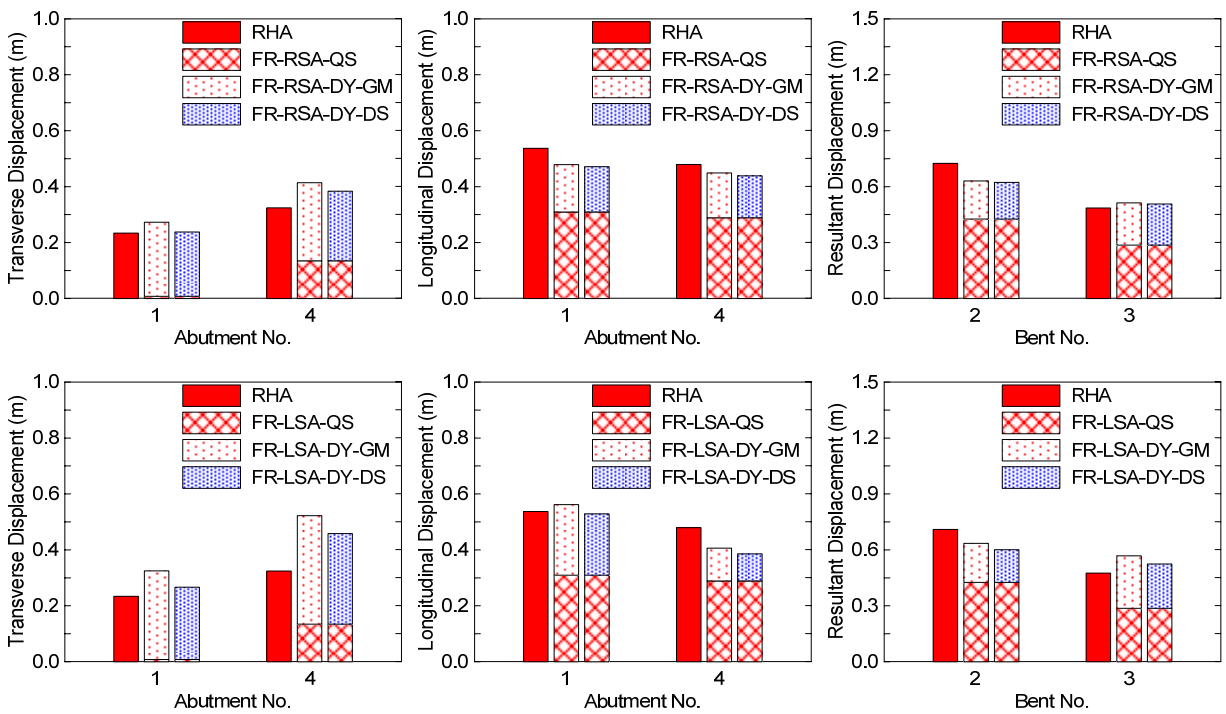

Figure A.30 Results of Bridge 55-0837S when $\theta = 45^{o}$ and longitudinal abutment stiffness $= 0.10K_{eff}$.

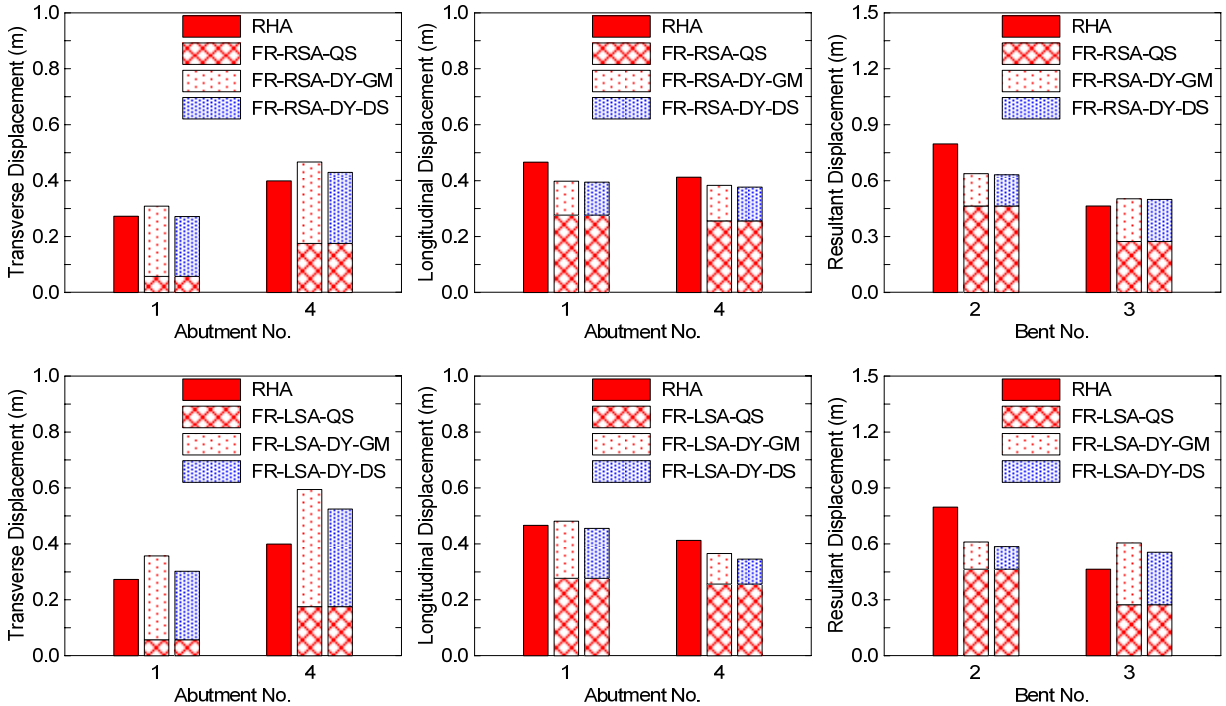

Figure A.31 Results of Bridge 55-0837S when $\theta = 45^{o}$ and longitudinal abutment stiffness $= 0.55K_{eff}$.

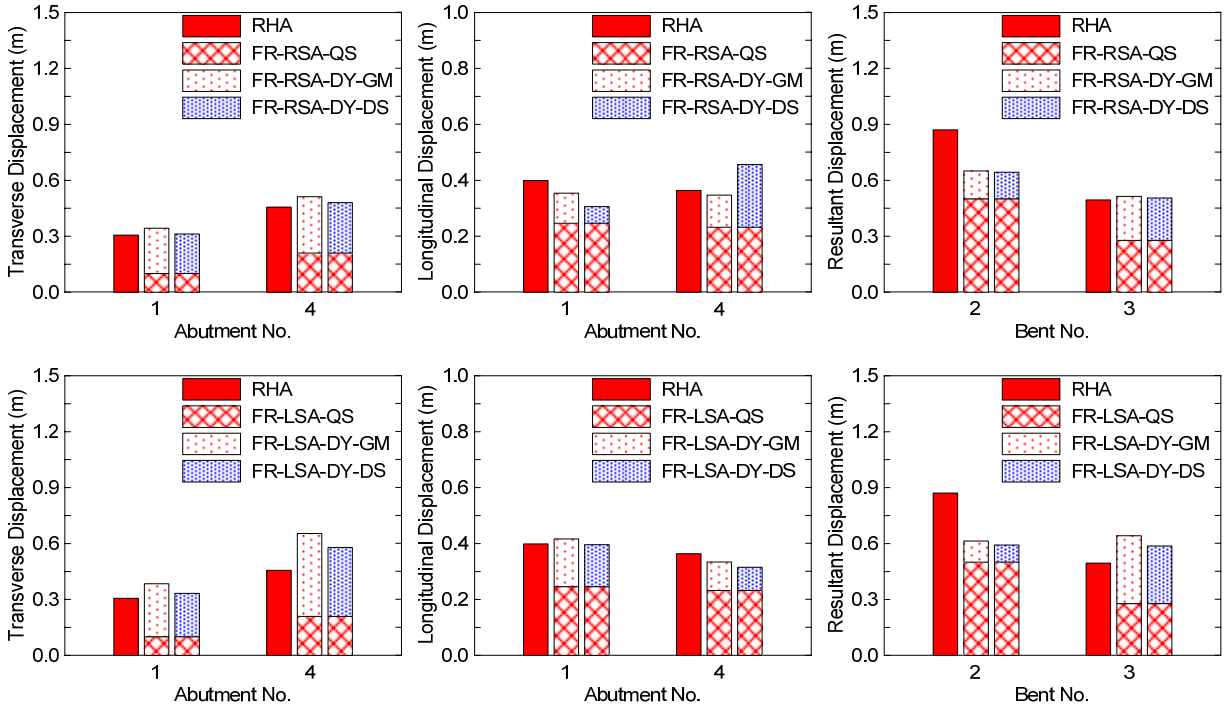

Figure A.32 Results of Bridge 55-0837S when $\theta = 45^{o}$ and longitudinal abutment stiffness $= 1.00K_{eff}$.

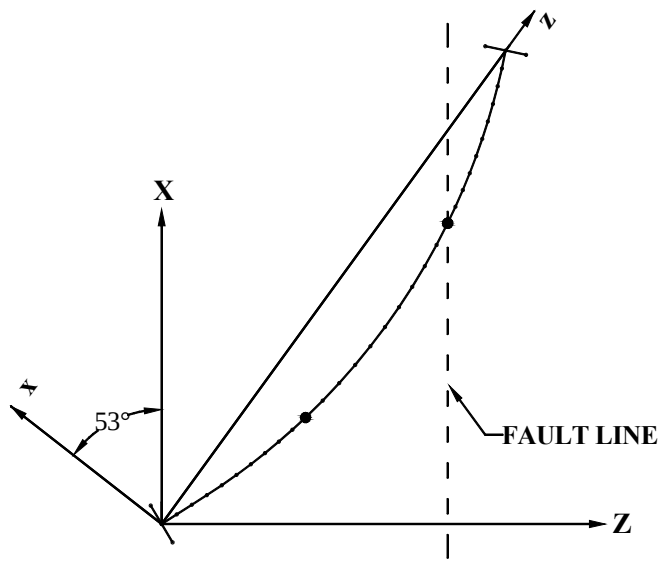

Figure A.33 Sketch of Bridge 55-0837S when $\theta = 53^{o}$.

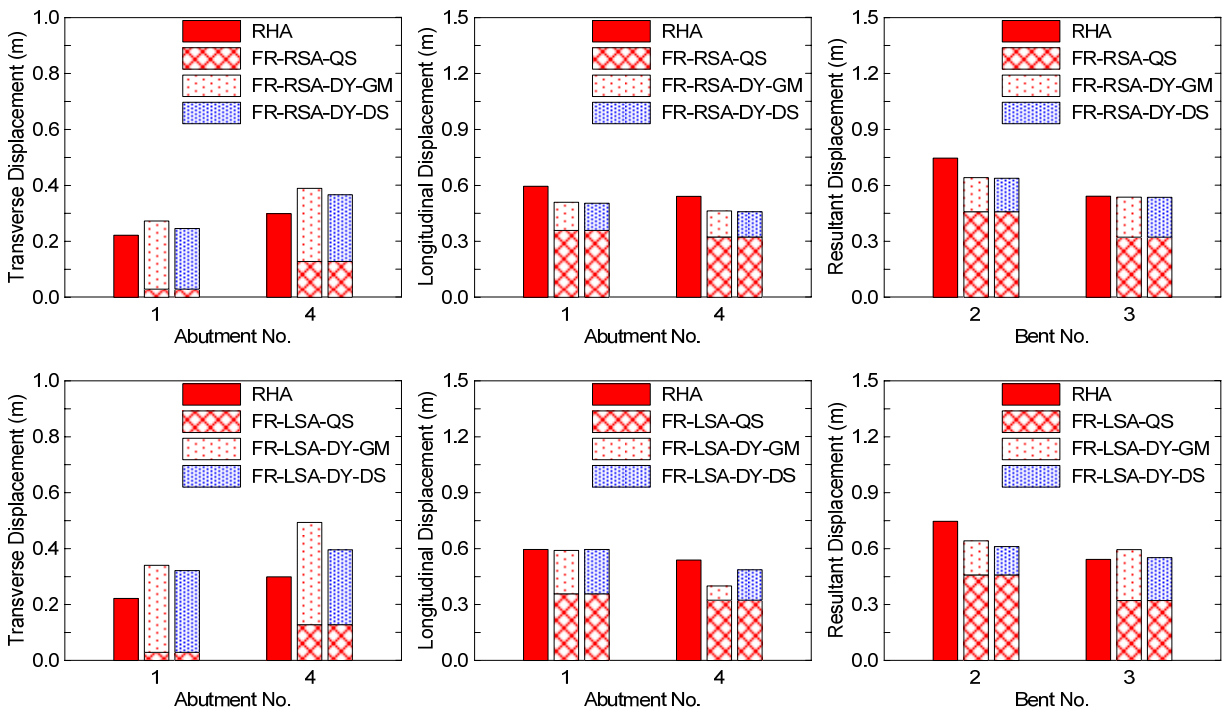

Figure A.34 Results of Bridge 55-0837S when $\theta = 53^{o}$ and longitudinal abutment stiffness $= 0.10K_{eff}$.

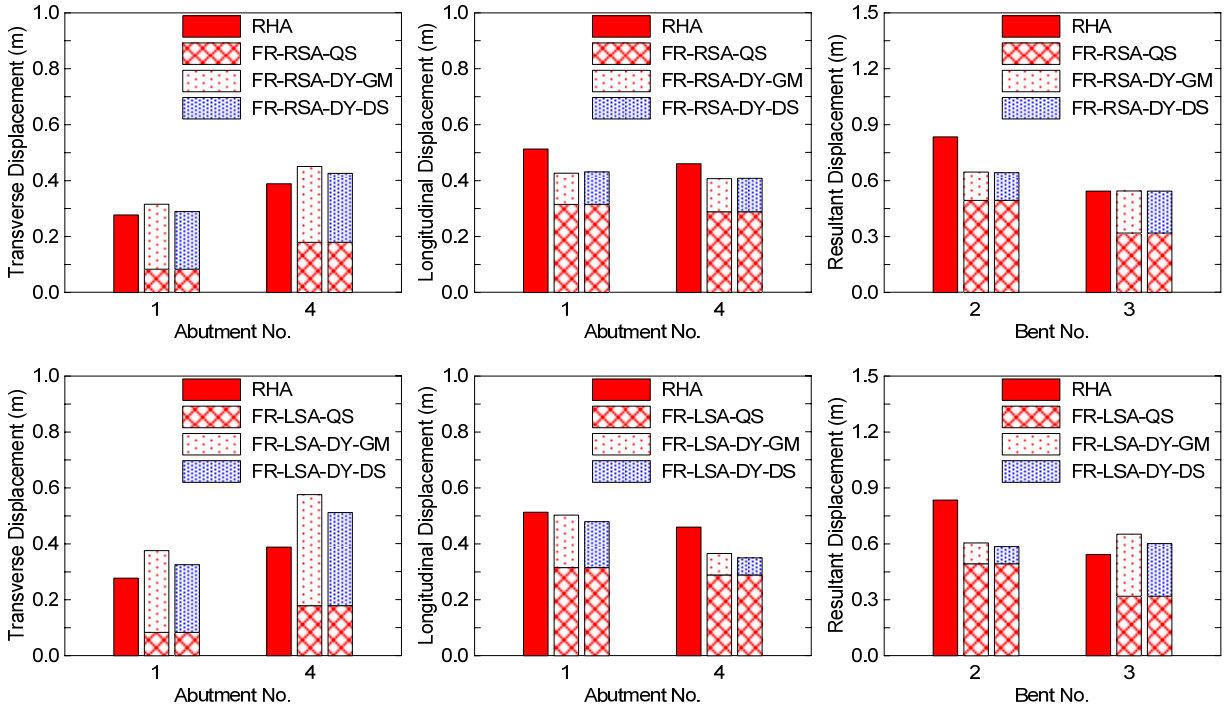

Figure A.35 Results of Bridge 55-0837S when $\theta = 53^{o}$ and longitudinal abutment stiffness $= 0.55K_{eff}$.

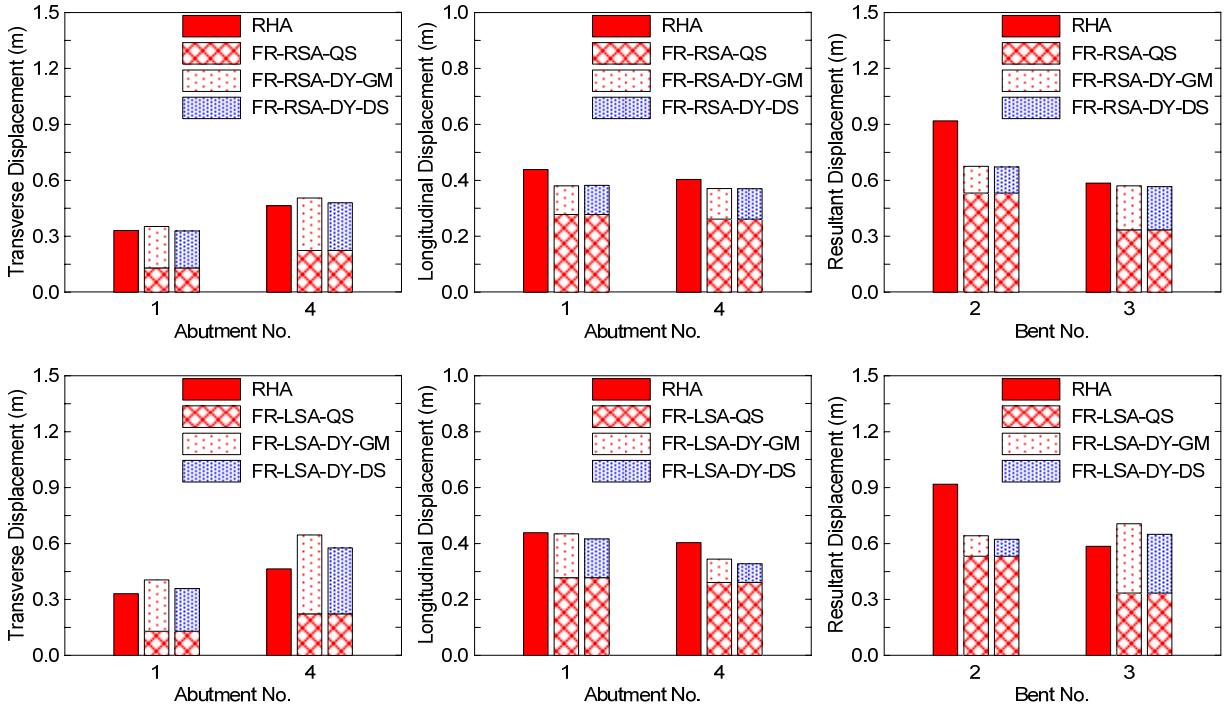

Figure A.36 Results of Bridge 55-0837S when $\theta = 53^{o}$ and longitudinal abutment stiffness $= 1.00K_{eff}$.

APPENDIX B

COMPLETE RESULT COMPARISONS OF BRIDGE 55-0939G

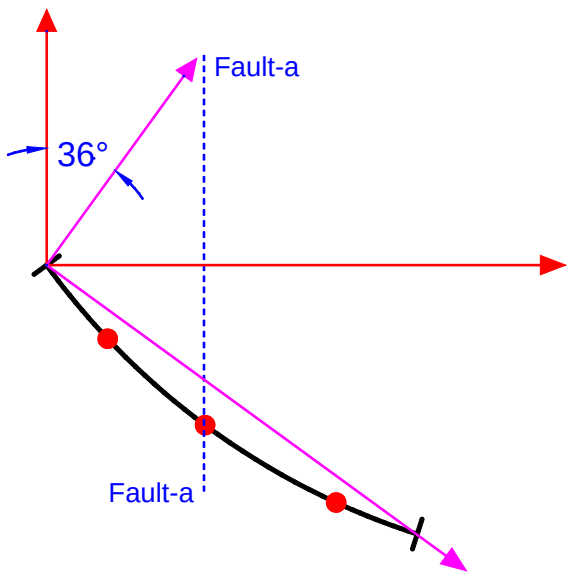

Figure B.1 Sketch of Bridge 55-0939G under Fault-a when $\theta = -36^{o}$.

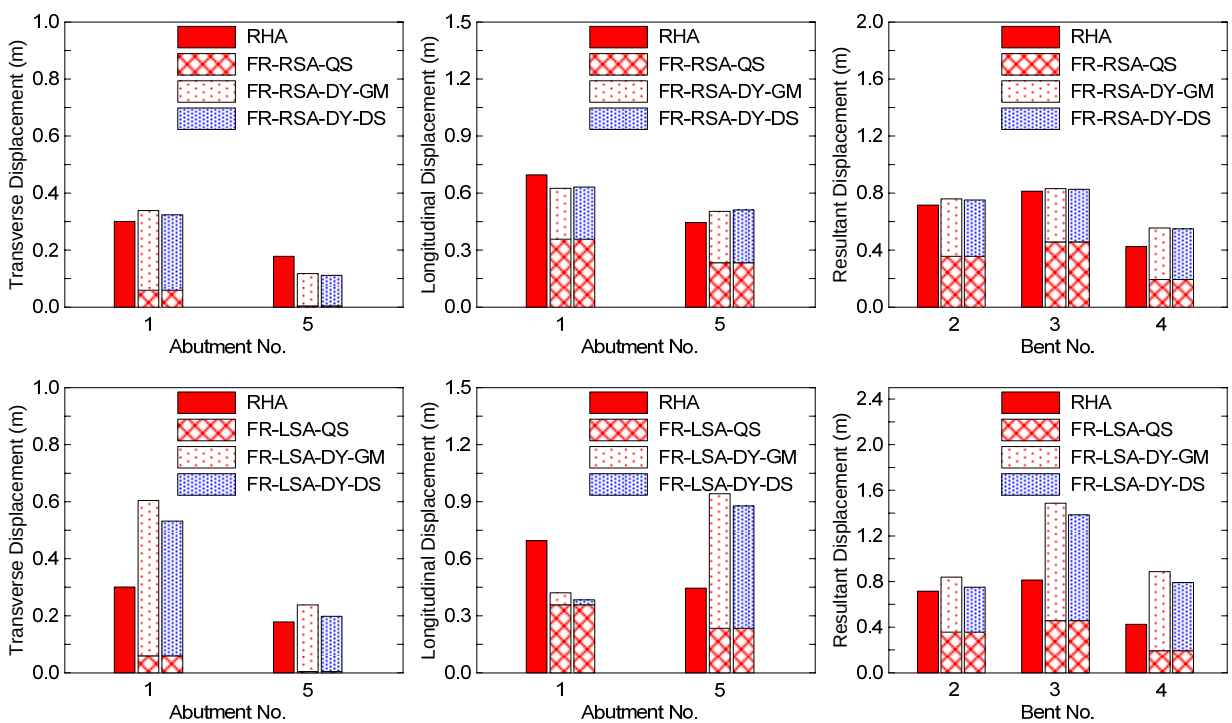

Figure B.2 Results of Bridge 55-0939G under Fault-a
when $\theta = -36^{o}$ and longitudinal abutment stiffness $= 0.10K_{eff}$.

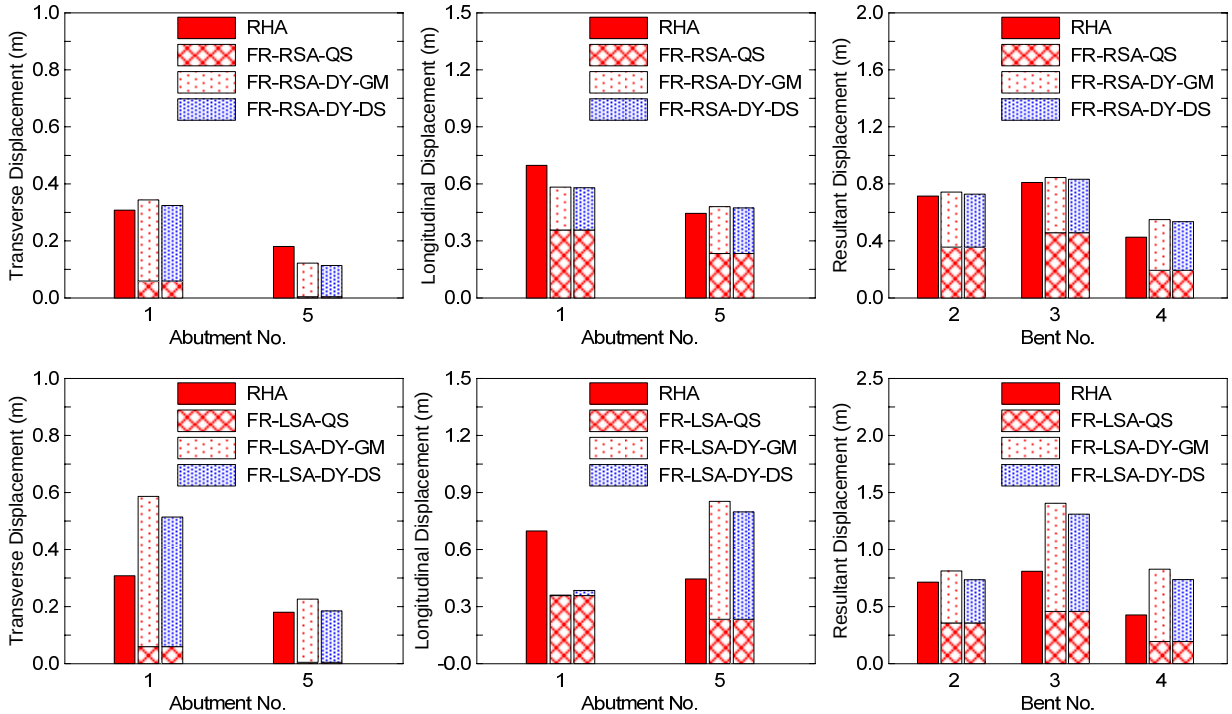

Figure B.3 Results of Bridge 55-0939G under Fault-a
when $\theta = -36^{\circ}$ and longitudinal abutment stiffness $= 0.55K_{eff}$.

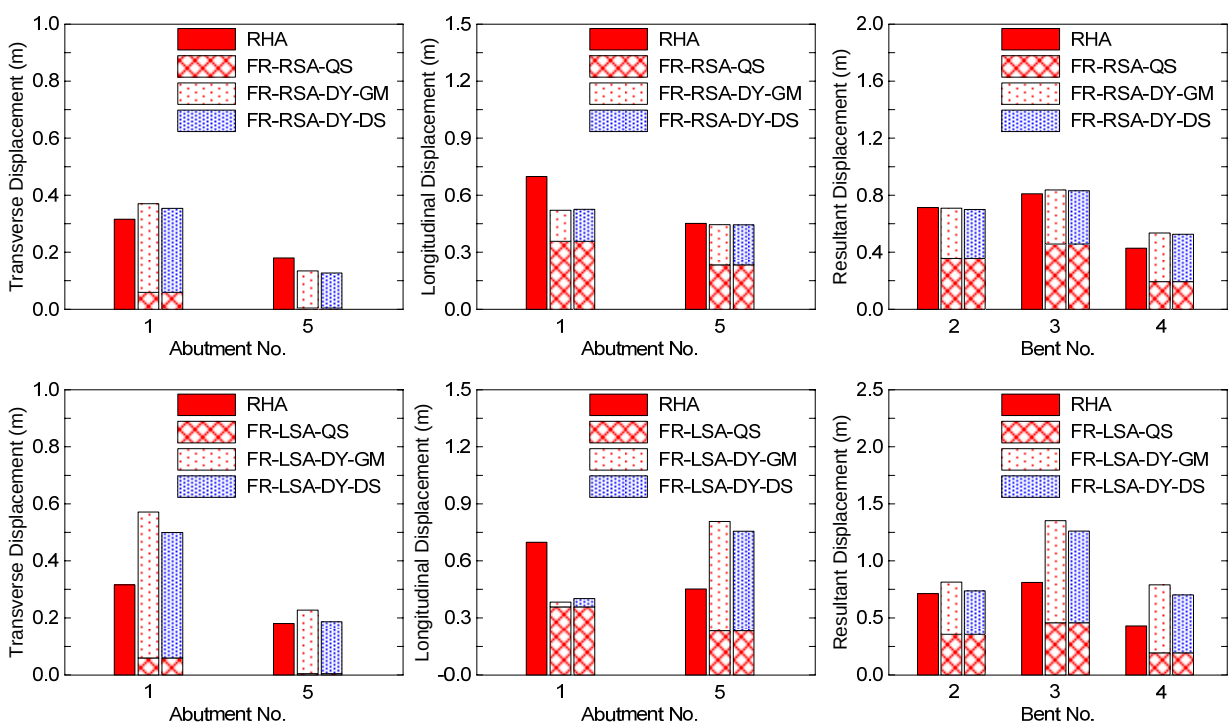

Figure B.4 Results of Bridge 55-0939G under Fault-a
when $\theta = -36^{\circ}$ and longitudinal abutment stiffness $= 1.0K_{eff}$.

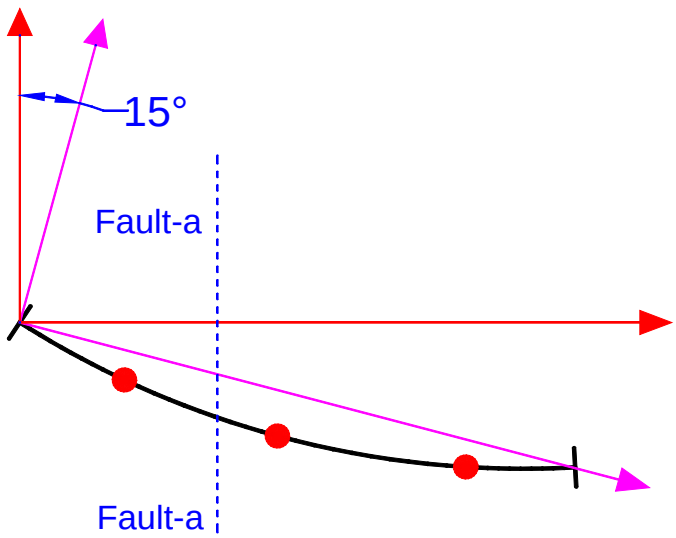

Figure B.5 Sketch of Bridge 55-0939G under Fault-a when $\theta = -15^{\circ}$.

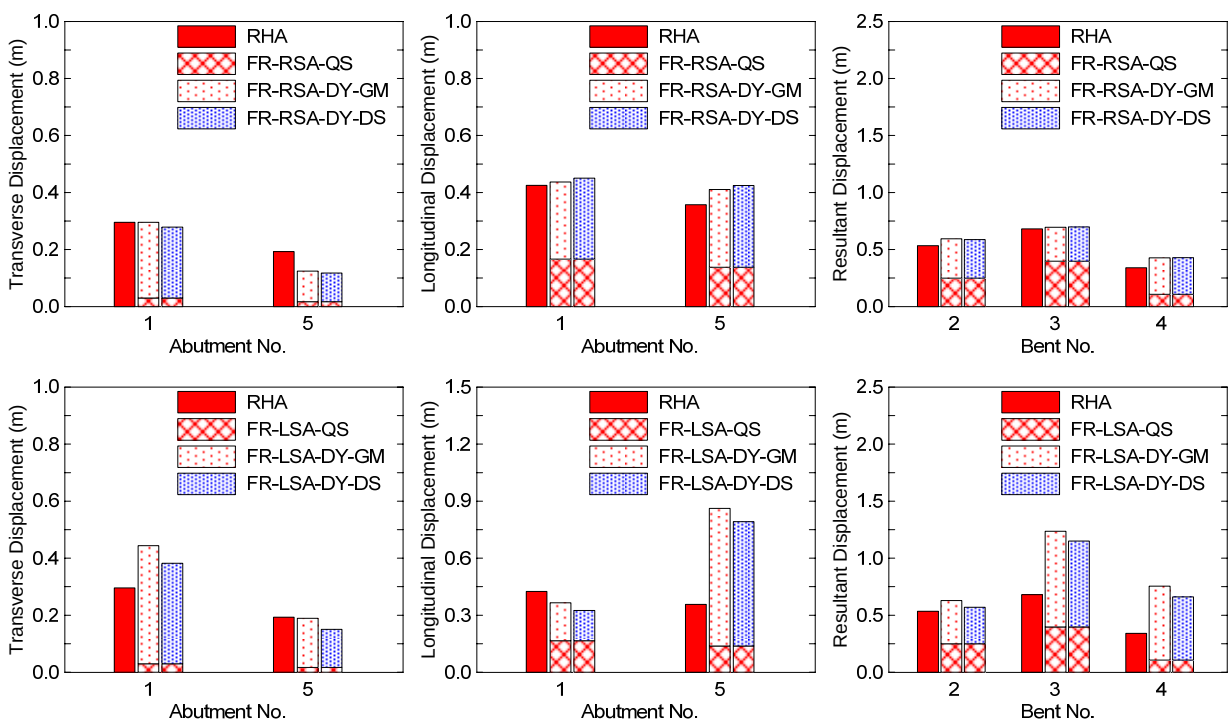

Figure B.6 Results of Bridge 55-0939G under Fault-a when $\theta = -15^{\circ}$ and longitudinal abutment stiffness $= 0.10K_{eff}$.

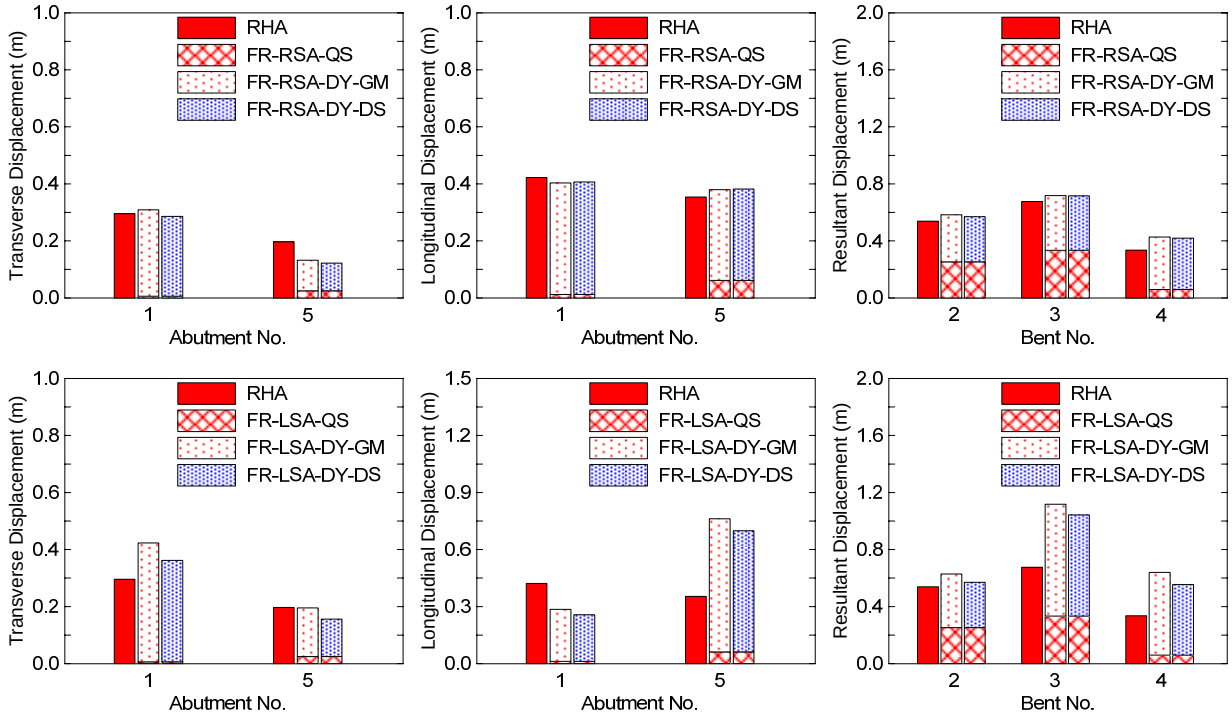

Figure B.7 Results of Bridge 55-0939G under Fault-a
when $\theta = -15^{\circ}$ and longitudinal abutment stiffness $= 0.55K_{eff}$.

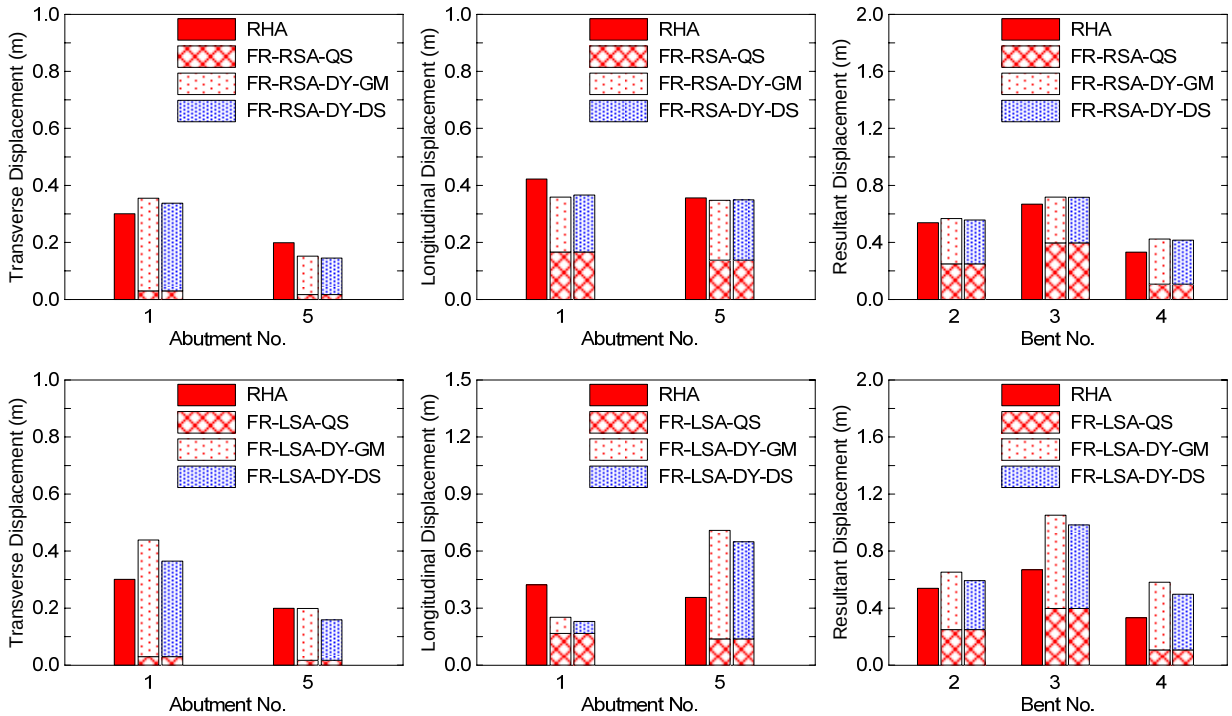

Figure B.8 Results of Bridge 55-0939G under Fault-a
when $\theta = -15^{\circ}$ and longitudinal abutment stiffness $= 1.0K_{eff}$.

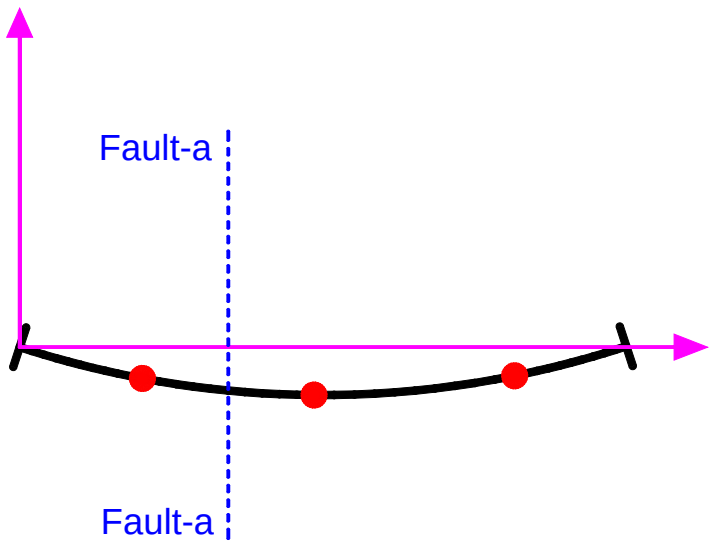

Figure B.9 Sketch of Bridge 55-0939G under Fault-a when $\theta = 0^{o}$.

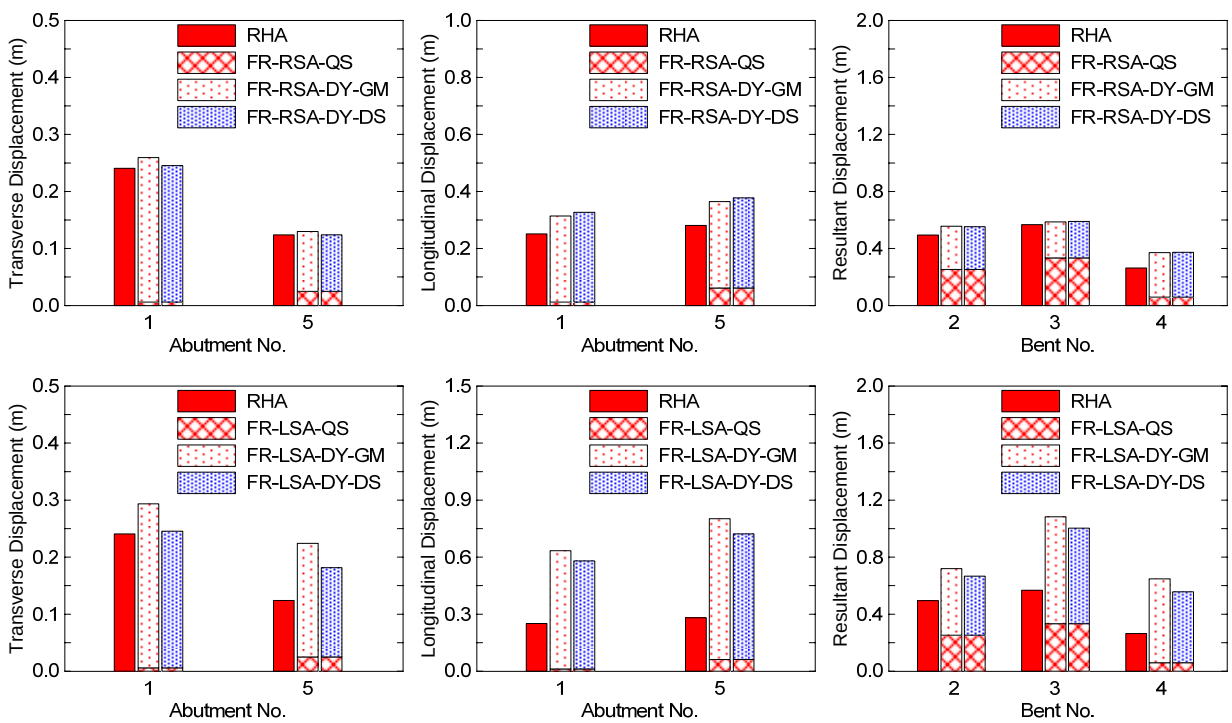

Figure B.10 Results of Bridge 55-0939G under Fault-a when $\theta = 0^{o}$ and longitudinal abutment stiffness $= 0.10K_{eff}$.

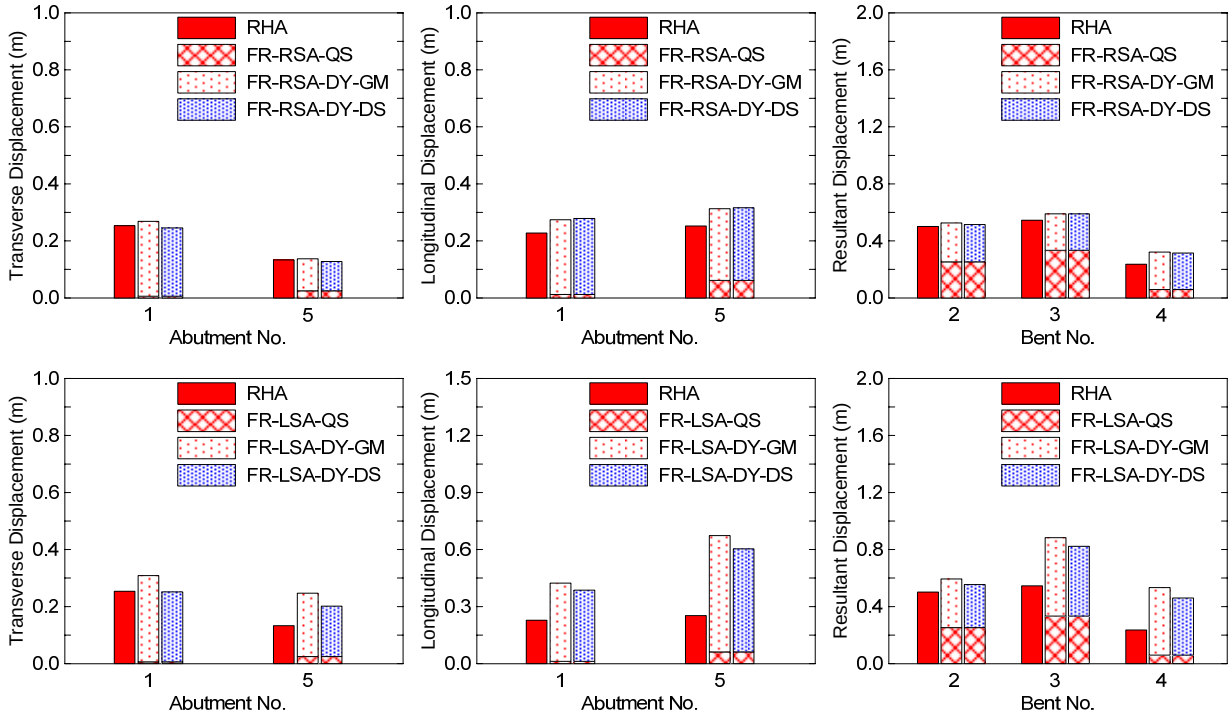

Figure B.11 Results of Bridge 55-0939G under Fault-a when $\theta = 0^{o}$ and longitudinal abutment stiffness $= 0.55K_{eff}$.

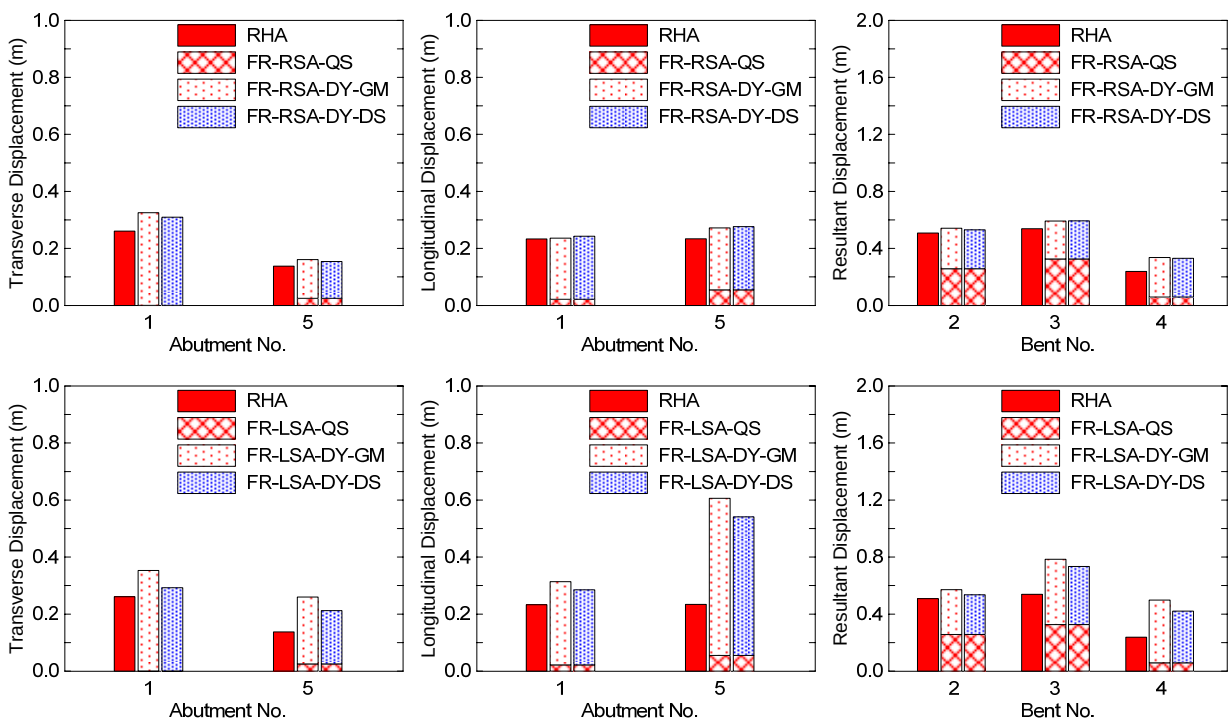

Figure B.12 Results of Bridge 55-0939G under Fault-a when $\theta = 0^{o}$ and longitudinal abutment stiffness $= 1.0K_{eff}$.

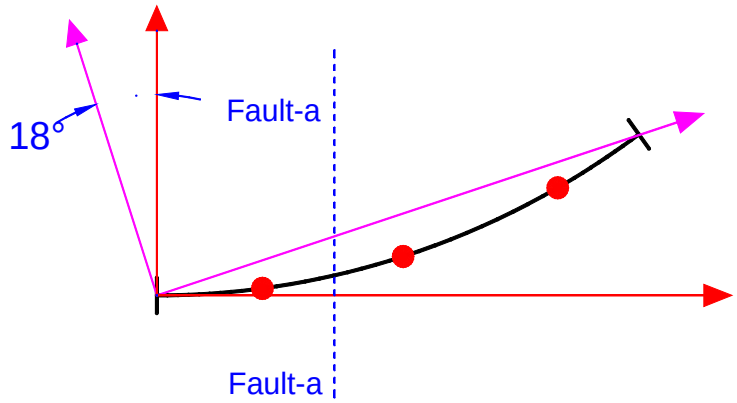

Figure B.13 Sketch of Bridge 55-0939G under Fault-a when $\theta = 18^{o}$.

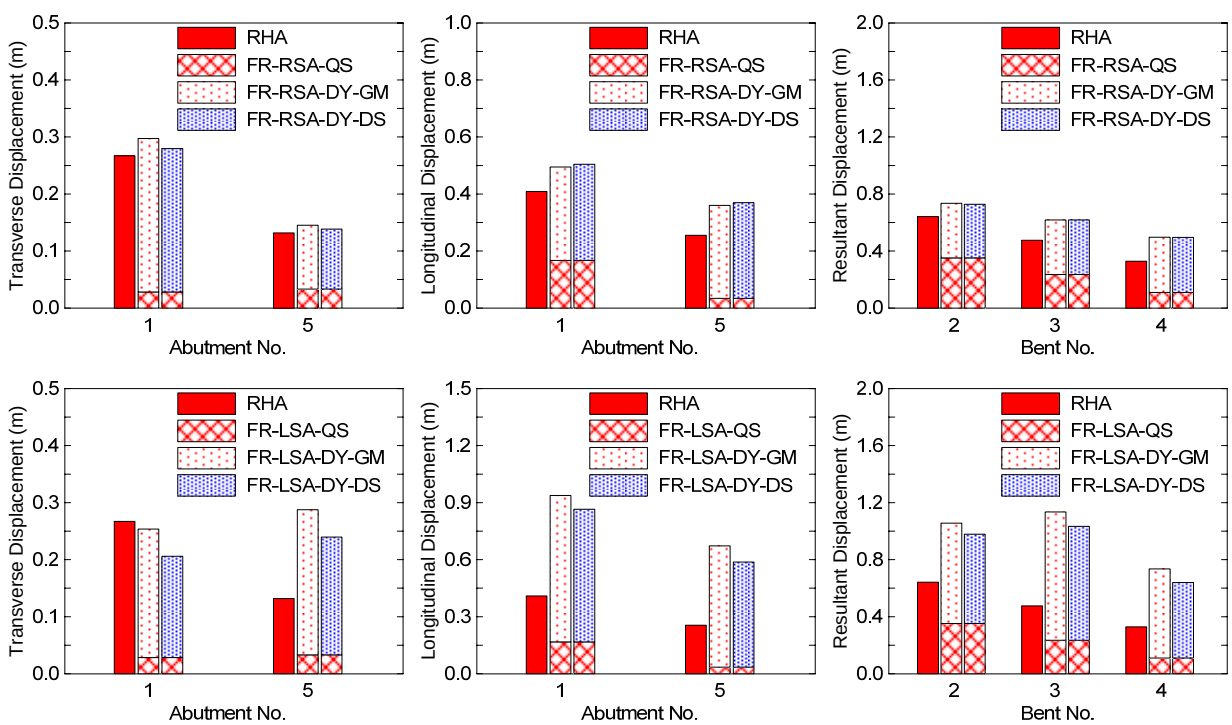

Figure B.14 Results of Bridge 55-0939G under Fault-a when $\theta = 18^{o}$ and longitudinal abutment stiffness $= 0.10K_{eff}$.

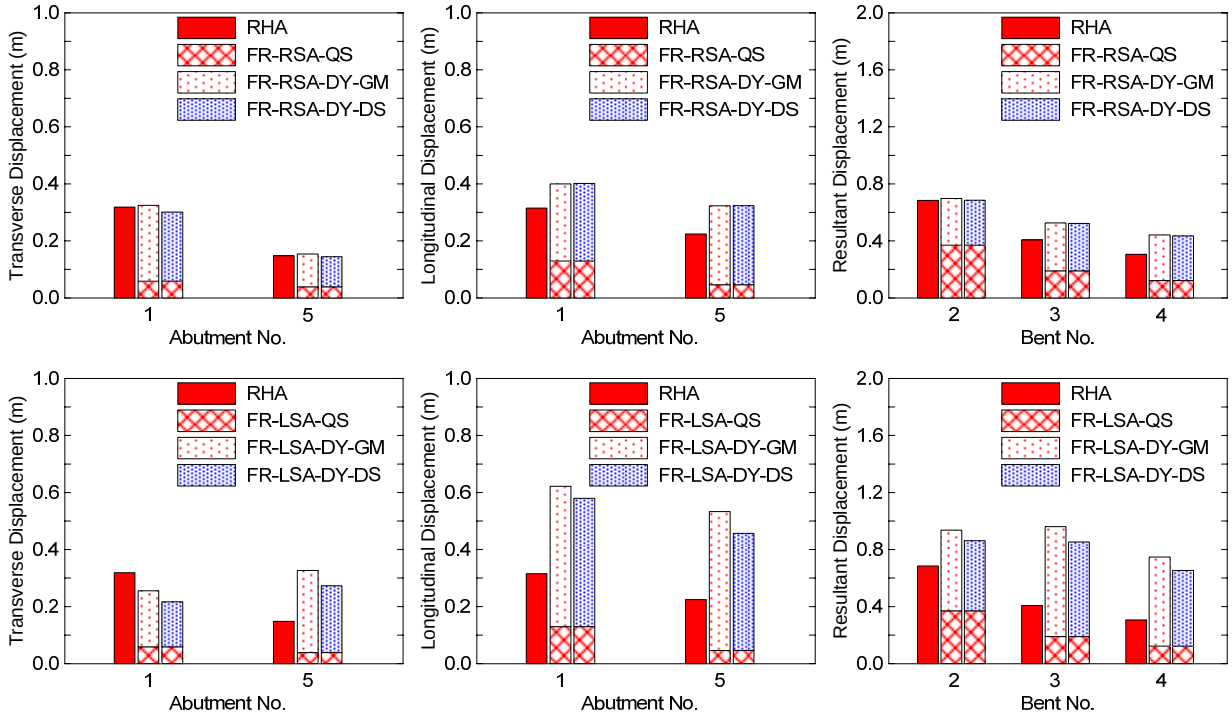

Figure B.15 Results of Bridge 55-0939G under Fault-a when $\theta = 18^{o}$ and longitudinal abutment stiffness $= 0.55K_{eff}$.

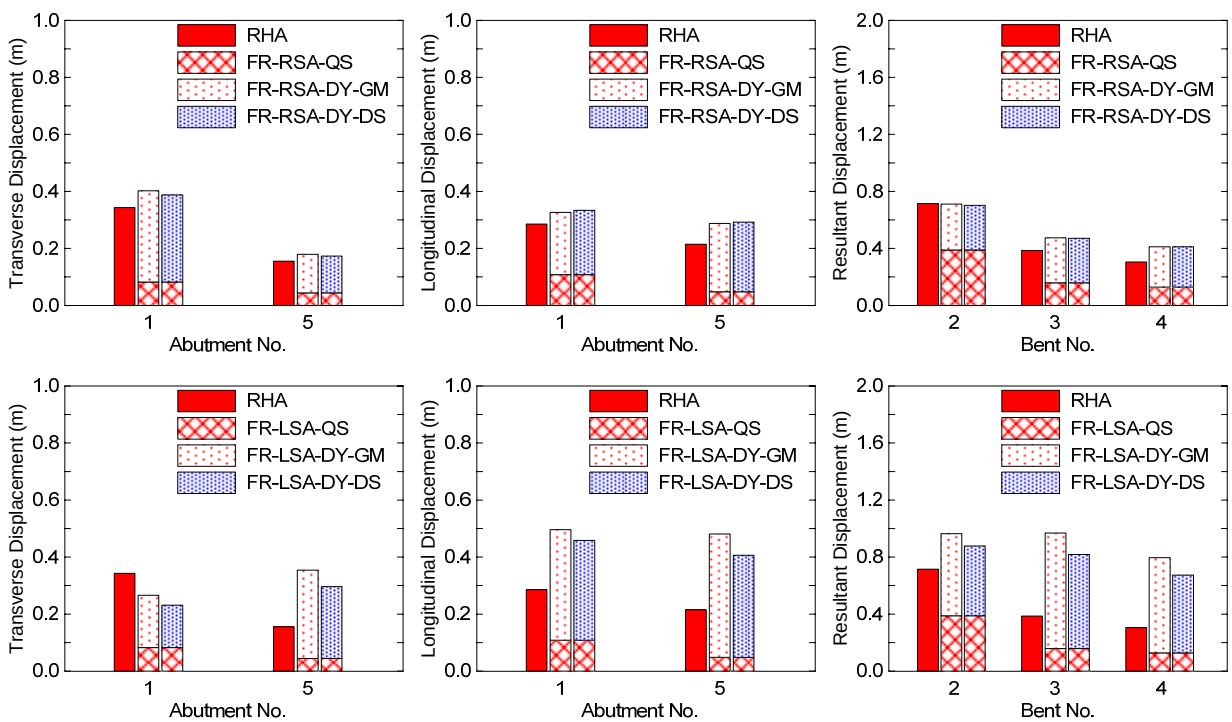

Figure B.16 Results of Bridge 55-0939G under Fault-a when $\theta = 18^{o}$ and longitudinal abutment stiffness $= 1.0K_{eff}$.

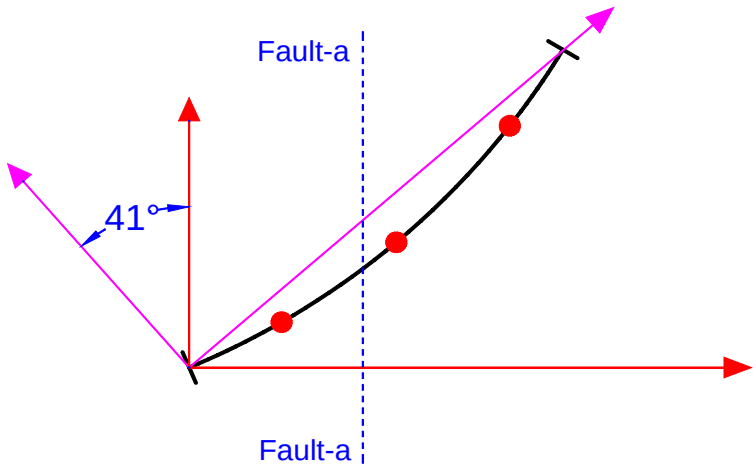

Figure B.17 Sketch of Bridge 55-0939G under Fault-a when $\theta = 41^{o}$.

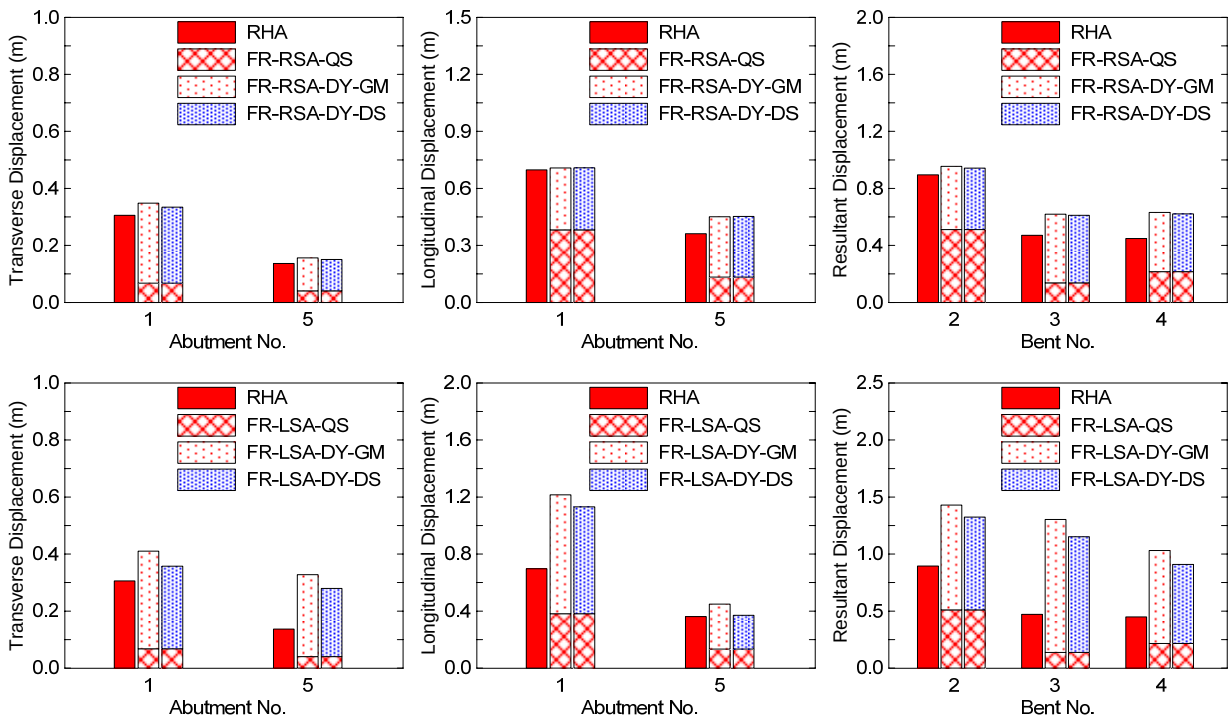

Figure B.18 Results of Bridge 55-0939G under Fault-a when $\theta = 41^{o}$ and longitudinal abutment stiffness $= 0.10K_{eff}$.

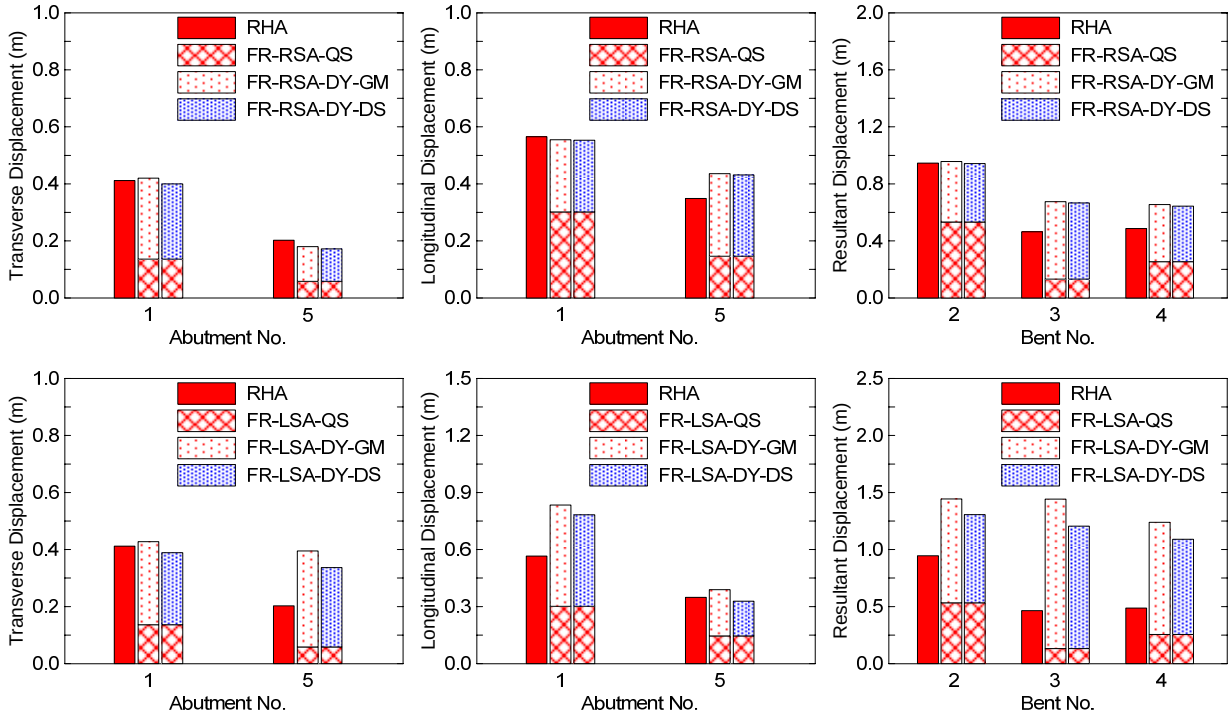

Figure B.19 Results of Bridge 55-0939G under Fault-a
when $\theta = 41^{o}$ and longitudinal abutment stiffness $= 0.55K_{eff}$.

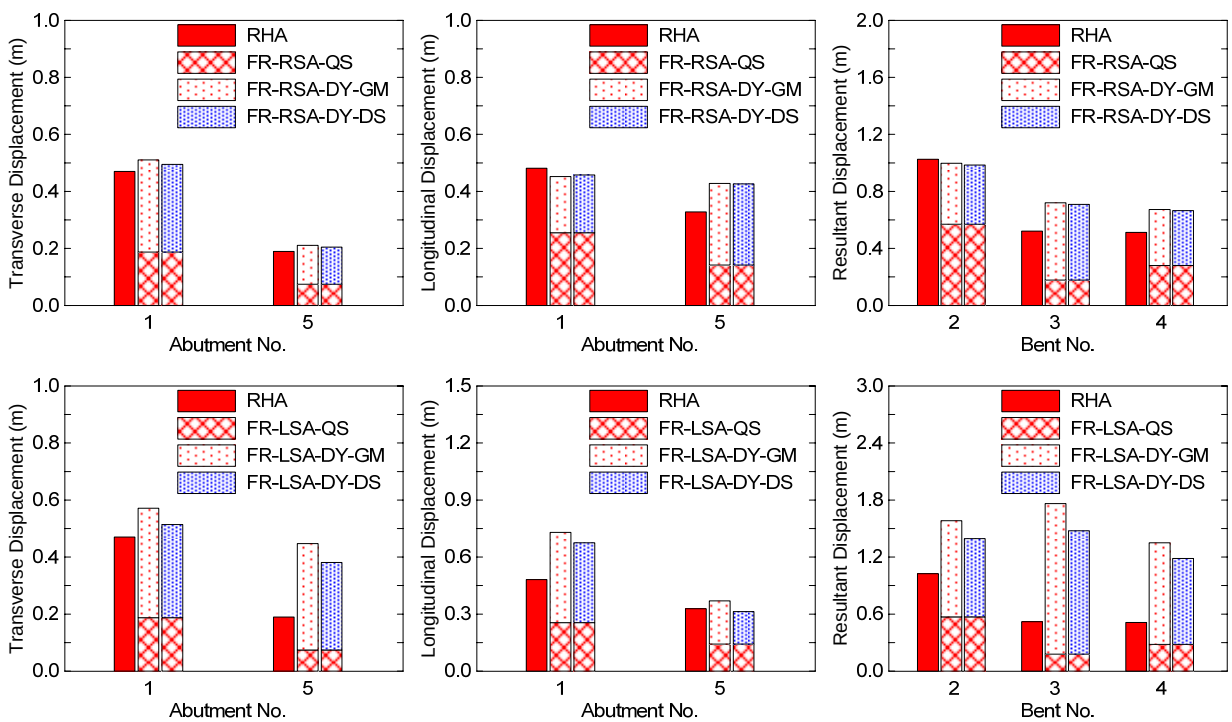

Figure B.20 Results of Bridge 55-0939G under Fault-a
when $\theta = 41^{o}$ and longitudinal abutment stiffness $= 1.0K_{eff}$.

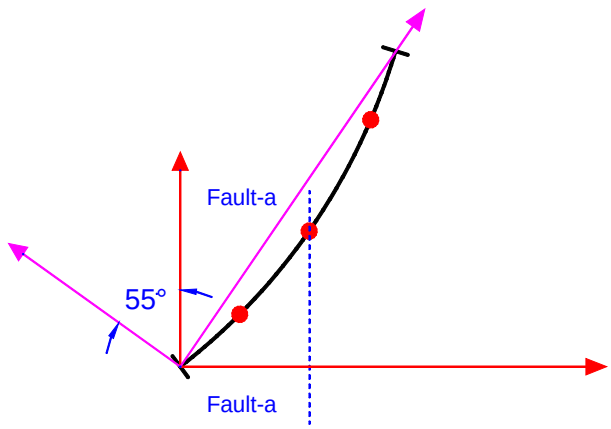

Figure B.21 Sketch of Bridge 55-0939G under Fault-a when $\theta = 55^{o}$.

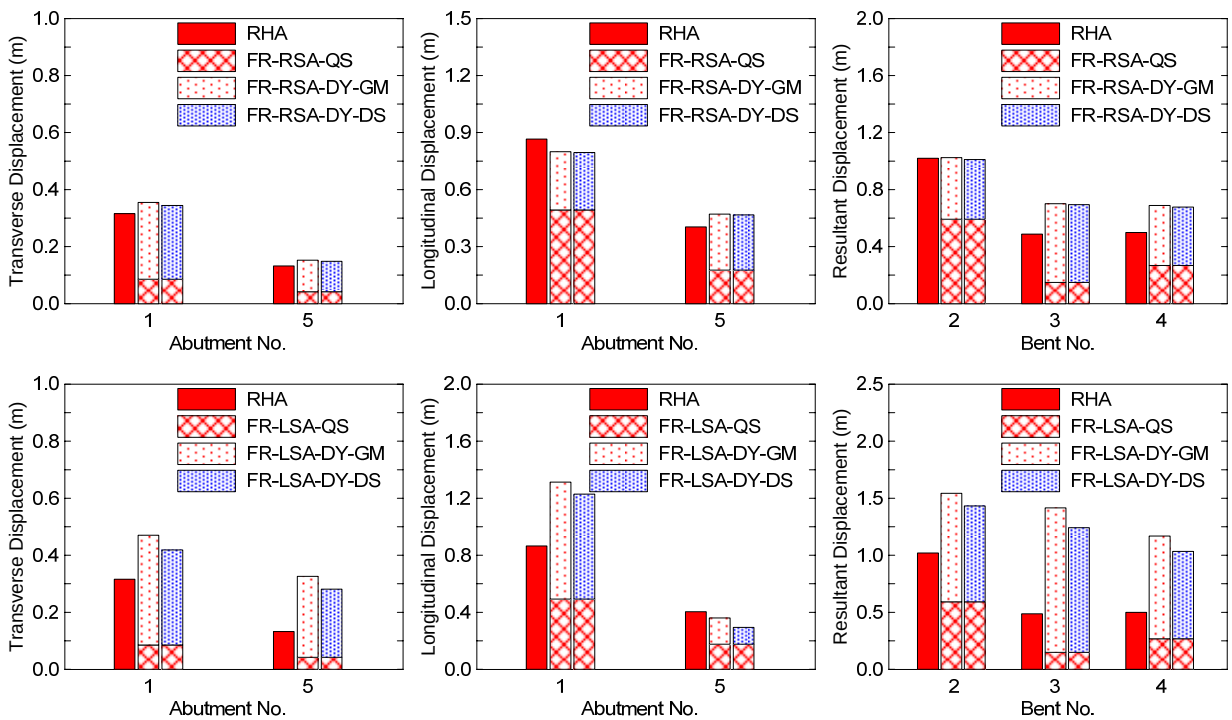

Figure B.22 Results of Bridge 55-0939G under Fault-a when $\theta = 55^{o}$ and longitudinal abutment stiffness $= 0.10K_{eff}$.

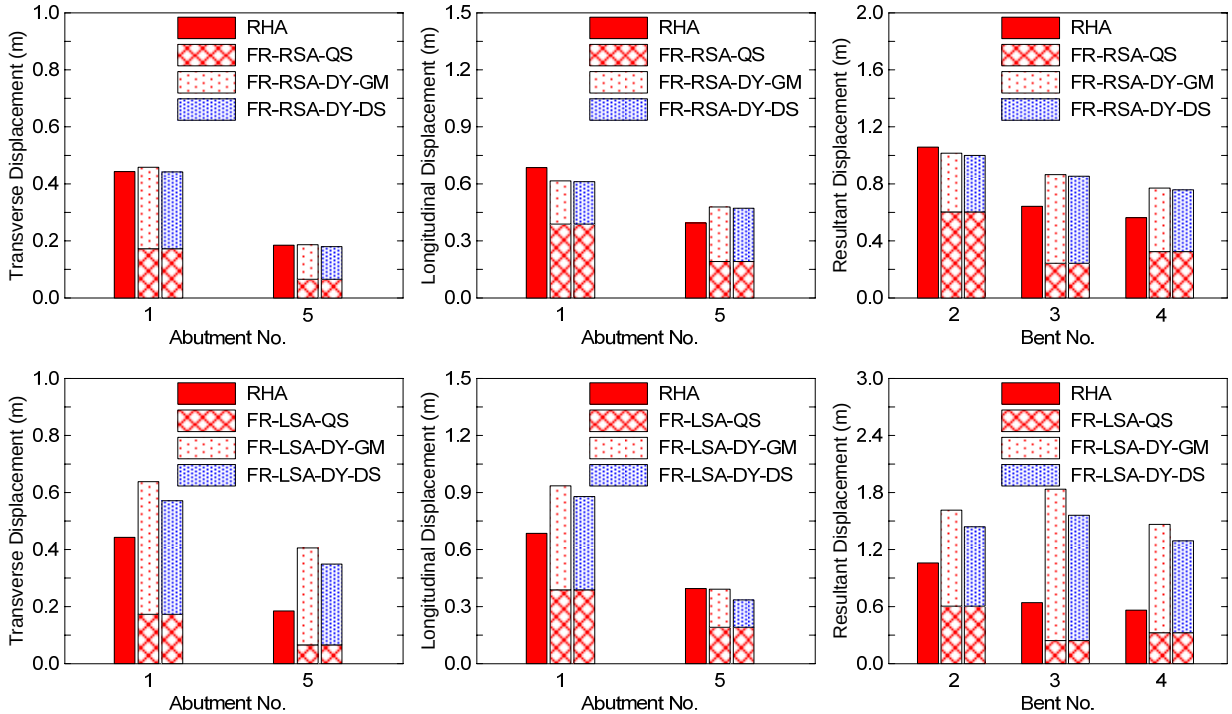

Figure B.23 Results of Bridge 55-0939G under Fault-a when $\theta = 55^{o}$ and longitudinal abutment stiffness $= 0.55K_{eff}$.

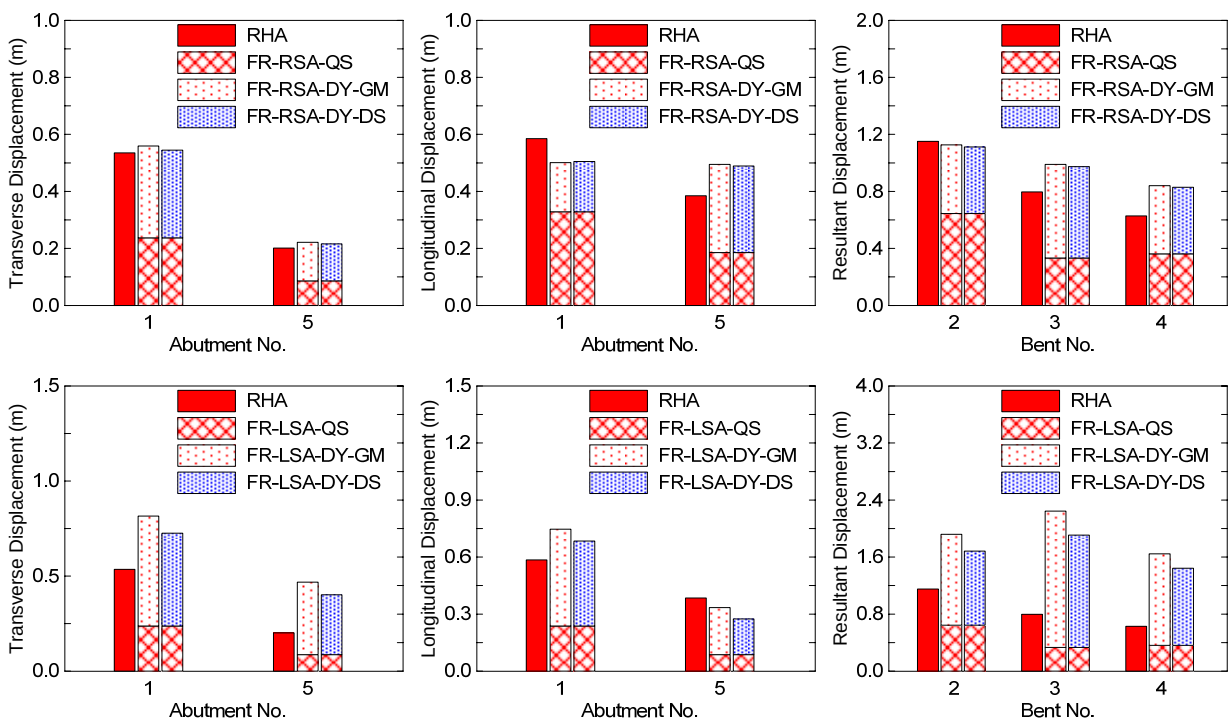

Figure B.24 Results of Bridge 55-0939G under Fault-a when $\theta = 55^{o}$ and longitudinal abutment stiffness $= 1.0K_{eff}$.

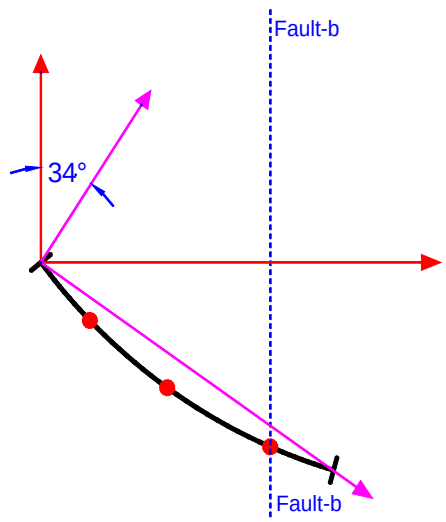

Figure B.25 Sketch of Bridge 55-0939G under Fault-b when $\theta = -34^{o}$.

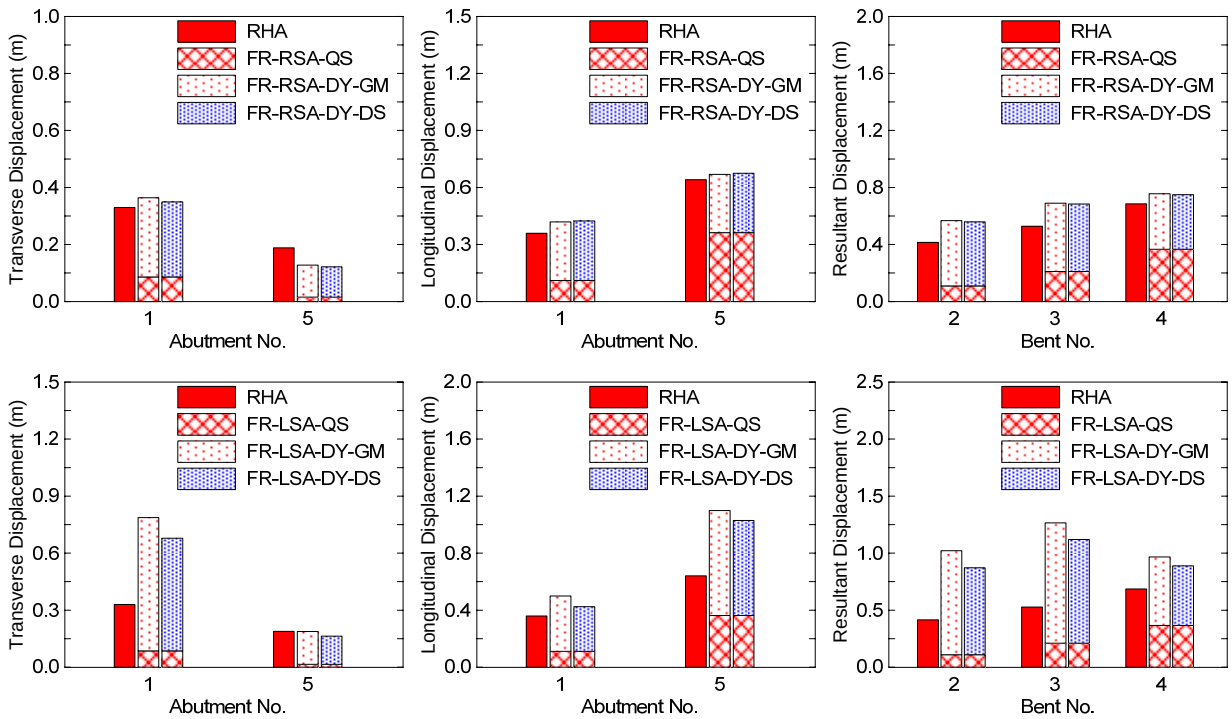

Figure B.26 Results of Bridge 55-0939G under Fault-b
when $\theta = -34^{o}$ and longitudinal abutment stiffness $= 0.10K_{eff}$.

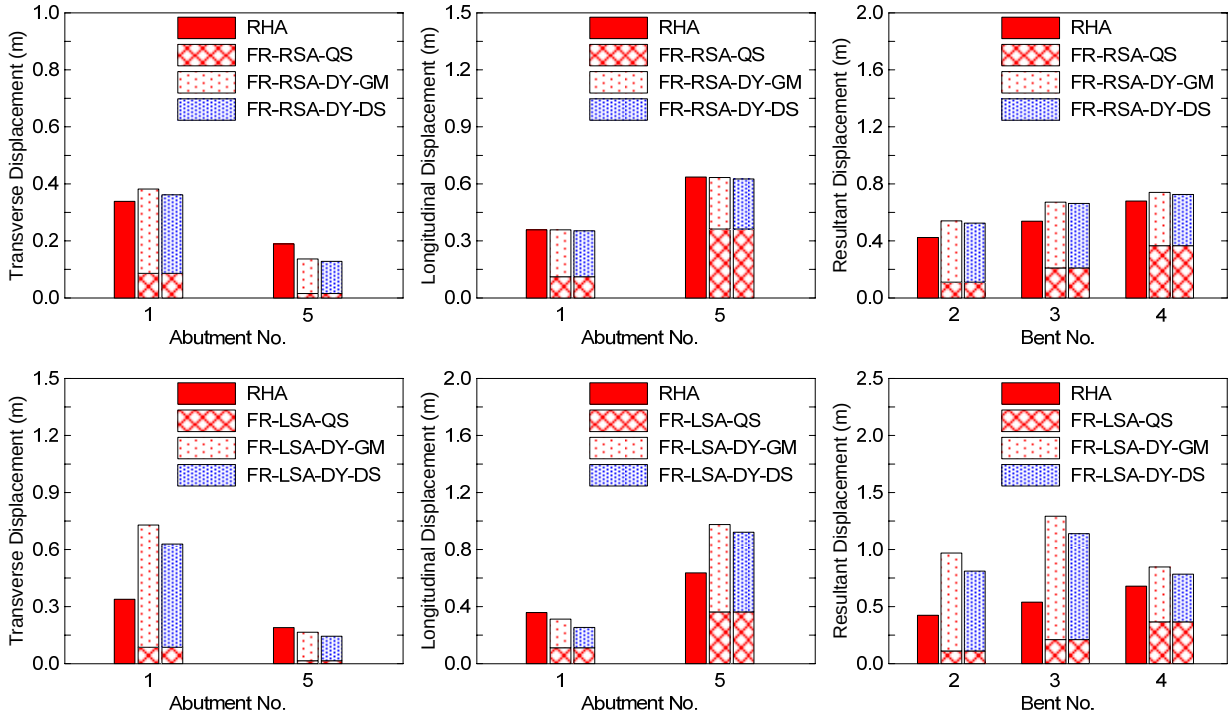

Figure B.27 Results of Bridge 55-0939G under Fault-b
when $\theta = -34^{\circ}$ and longitudinal abutment stiffness $= 0.55K_{eff}$.

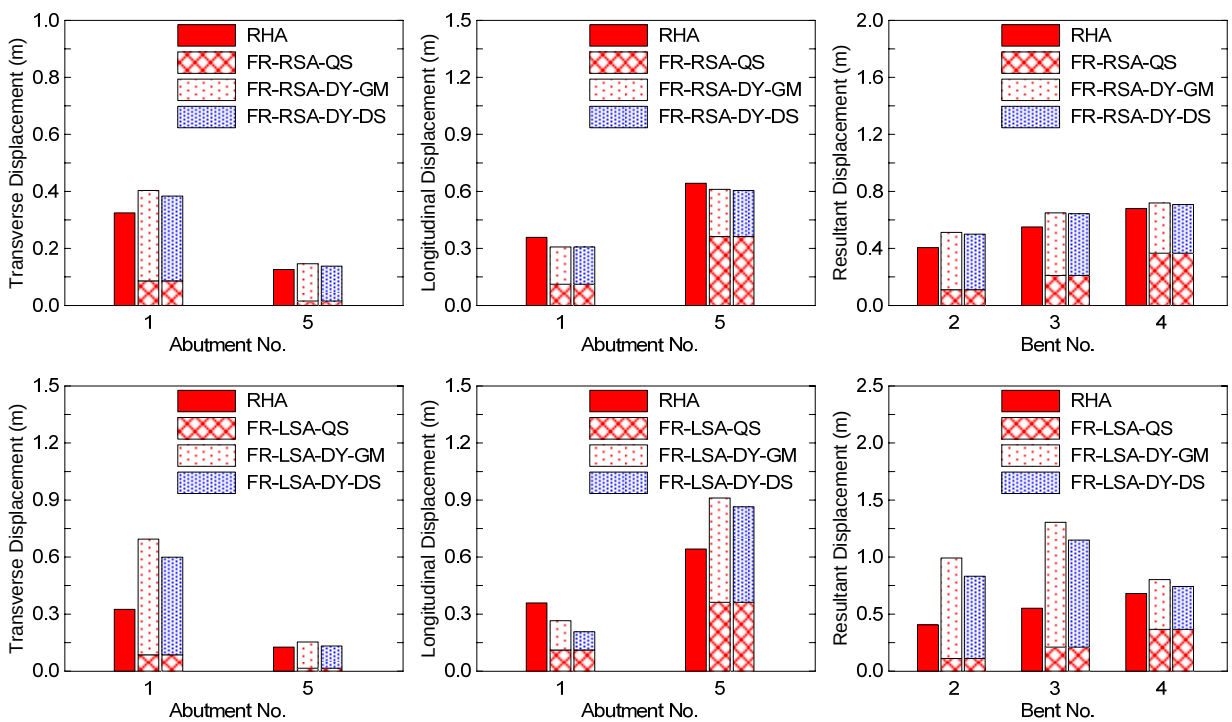

Figure B.28 Results of Bridge 55-0939G under Fault-b
when $\theta = -34^{\circ}$ and longitudinal abutment stiffness $= 1.0K_{eff}$.

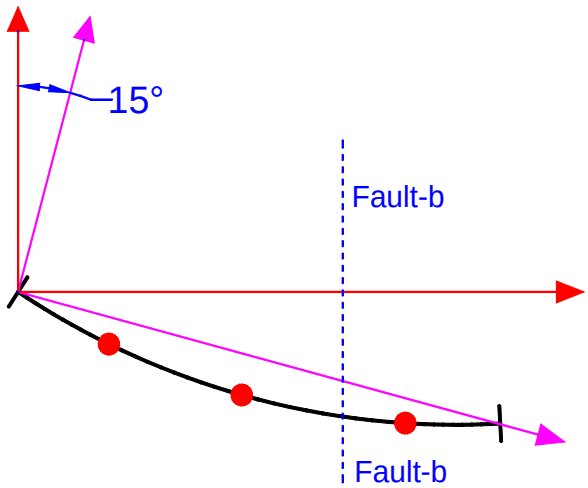

Figure B.29 Sketch of Bridge 55-0939G under Fault-b when $\theta = -15^{o}$.

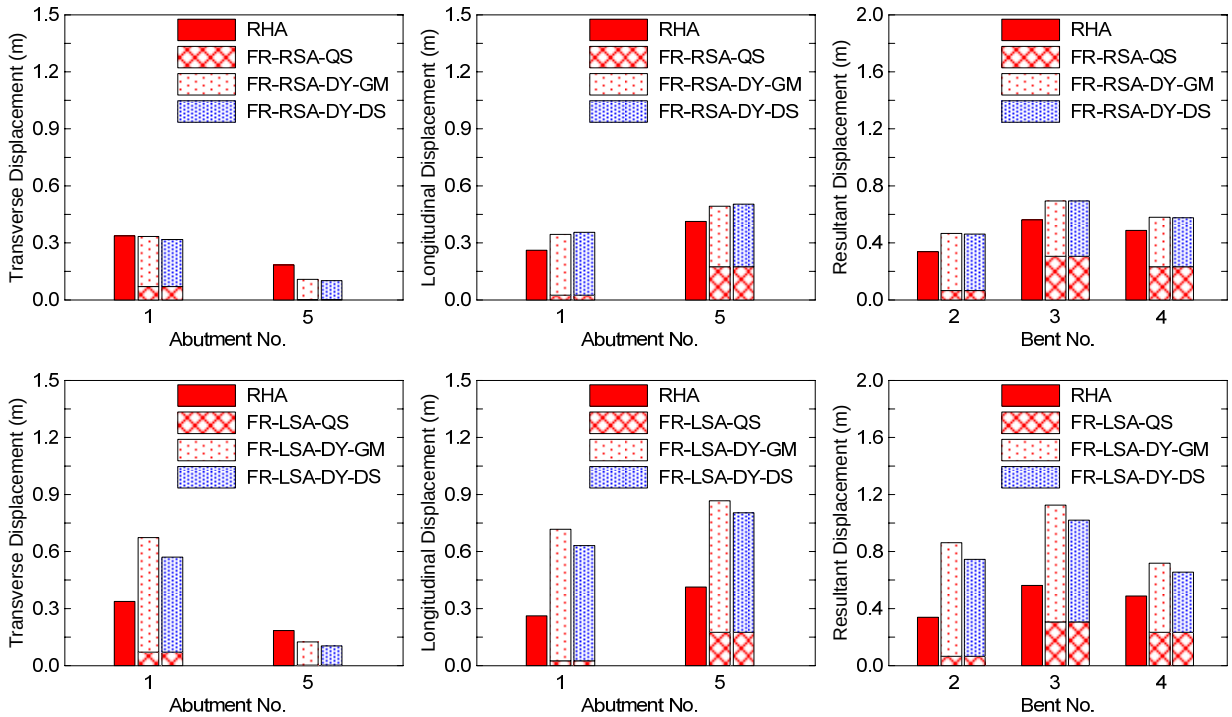

Figure B.30 Results of Bridge 55-0939G under Fault-b
when $\theta = -15^{o}$ and longitudinal abutment stiffness $= 0.10K_{eff}$.

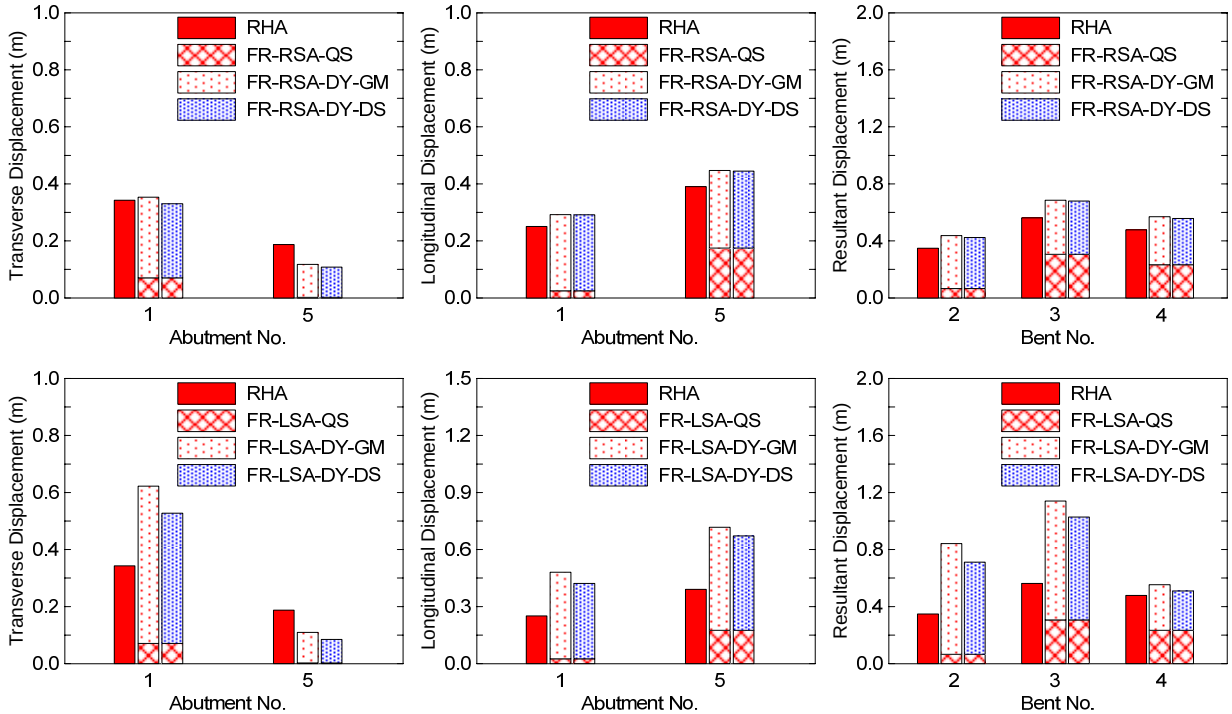

Figure B.31 Results of Bridge 55-0939G under Fault-b
when $\theta = -15^{\circ}$ and longitudinal abutment stiffness $= 0.55K_{eff}$.

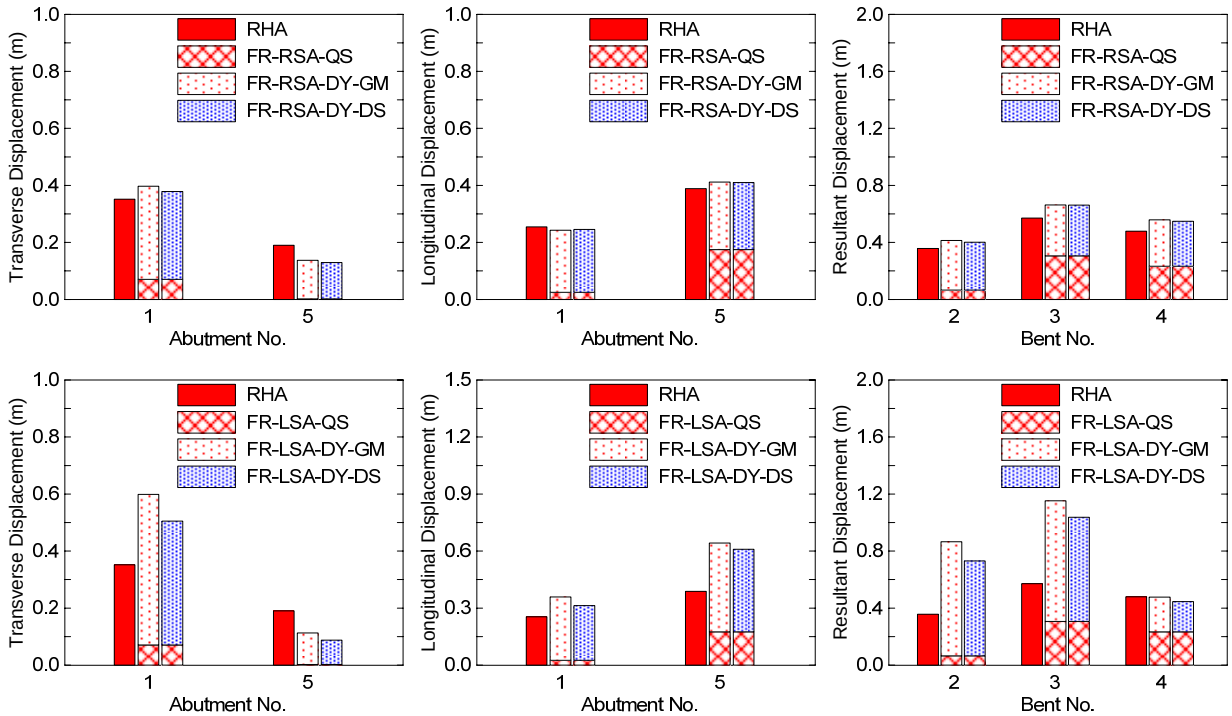

Figure B.32 Results of Bridge 55-0939G under Fault-b
when $\theta = -15^{\circ}$ and longitudinal abutment stiffness $= 1.0K_{eff}$.

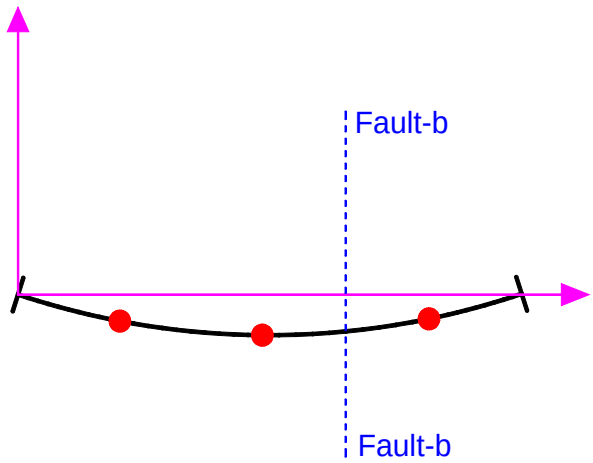

Figure B.33 Sketch of Bridge 55-0939G under Fault-b when $\theta = 0^{\circ}$.

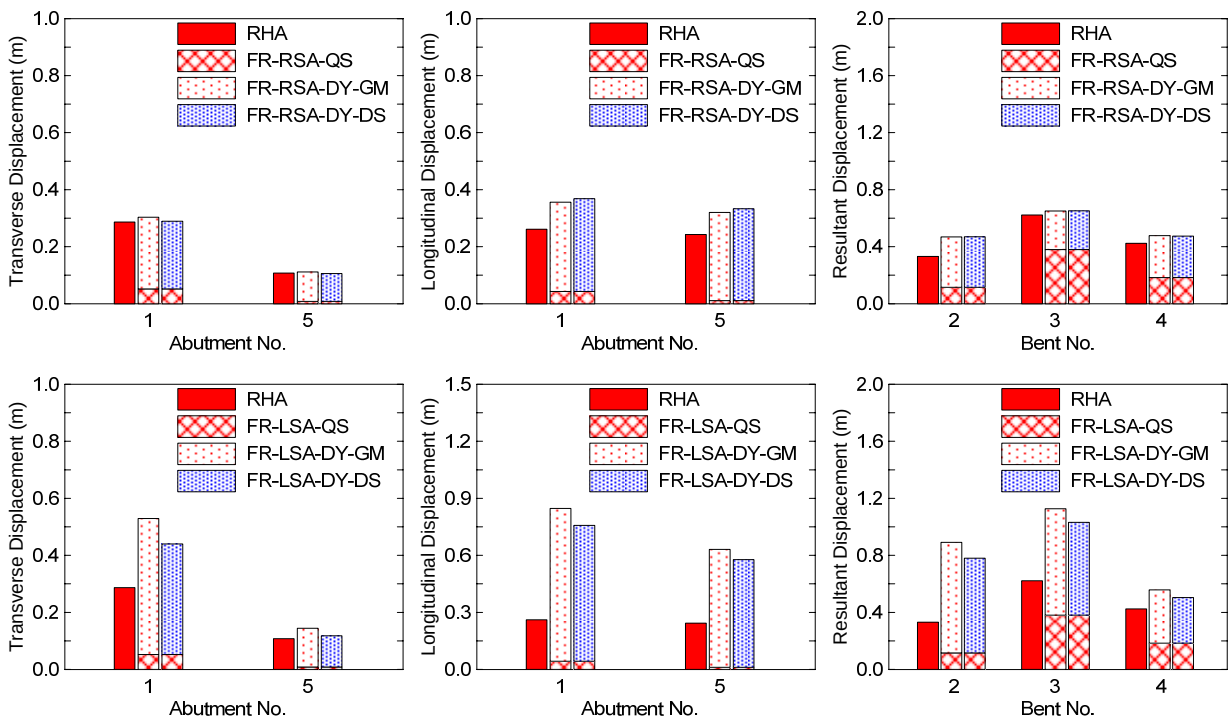

Figure B.34 Results of Bridge 55-0939G under Fault-b when $\theta = 0^{\circ}$ and longitudinal abutment stiffness $= 0.10K_{eff}$.

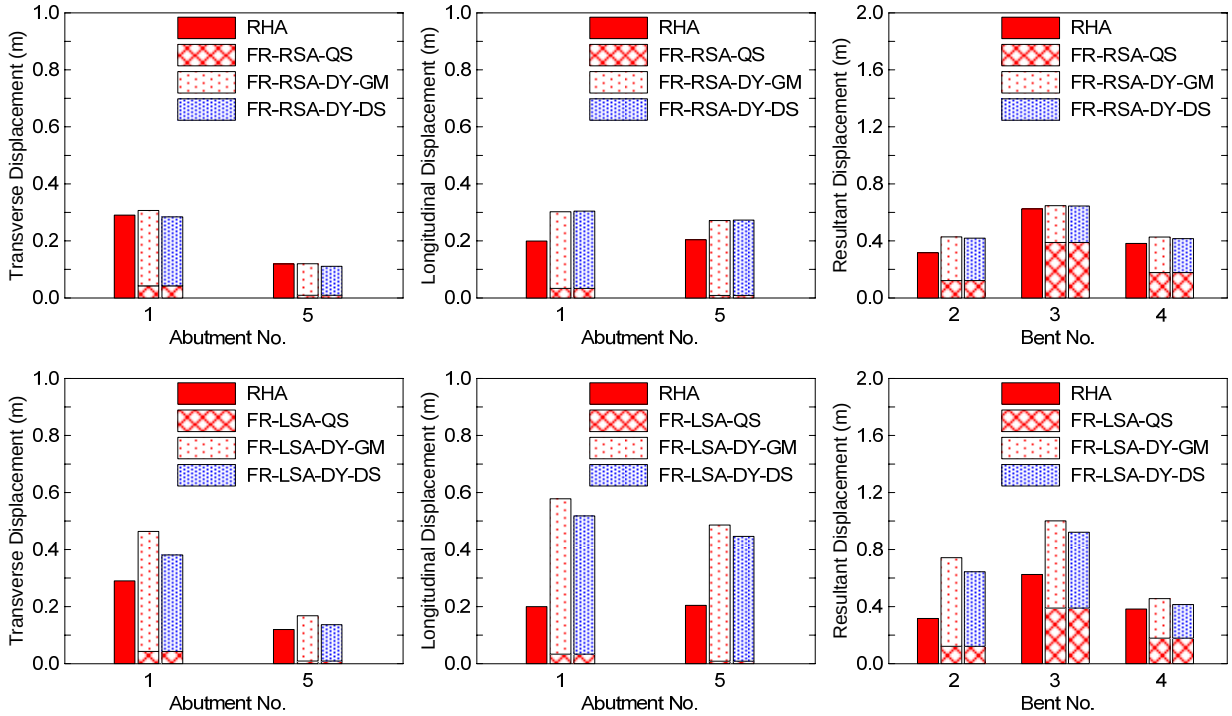

Figure B.35 Results of Bridge 55-0939G under Fault-b when $\theta = 0^{\circ}$ and longitudinal abutment stiffness $= 0.55K_{eff}$.

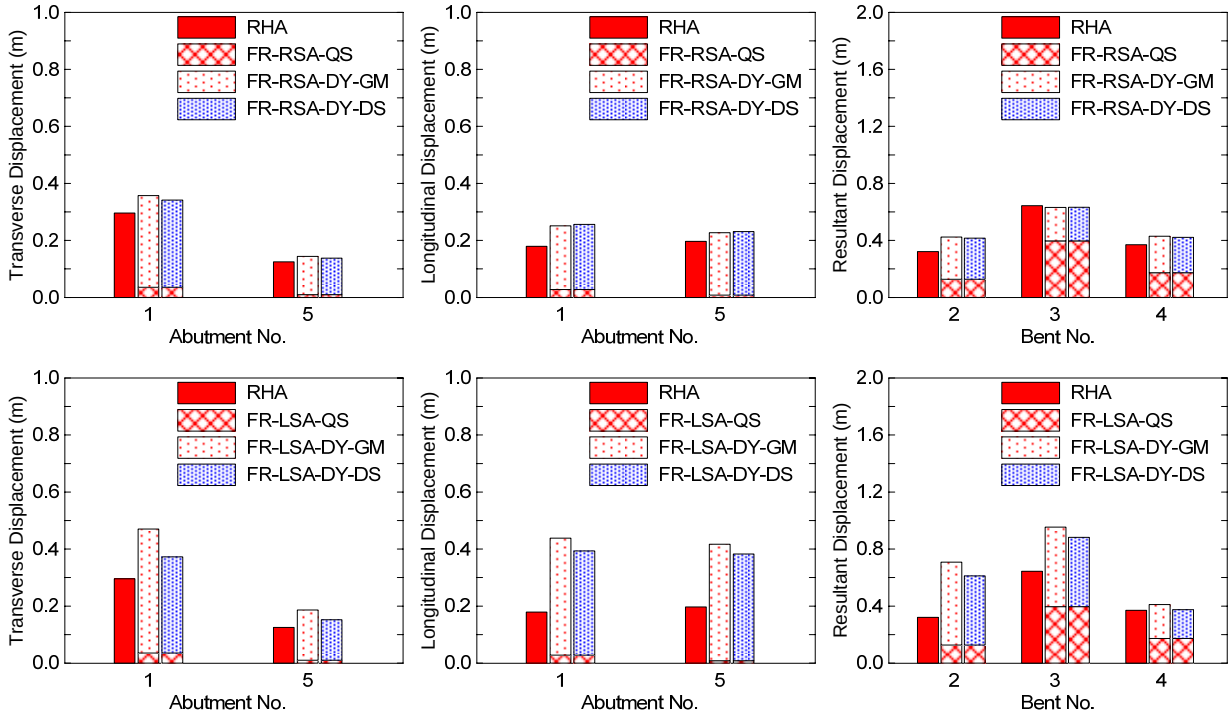

Figure B.36 Results of Bridge 55-0939G under Fault-b when $\theta = 0^{\circ}$ and longitudinal abutment stiffness $= 1.0K_{eff}$.

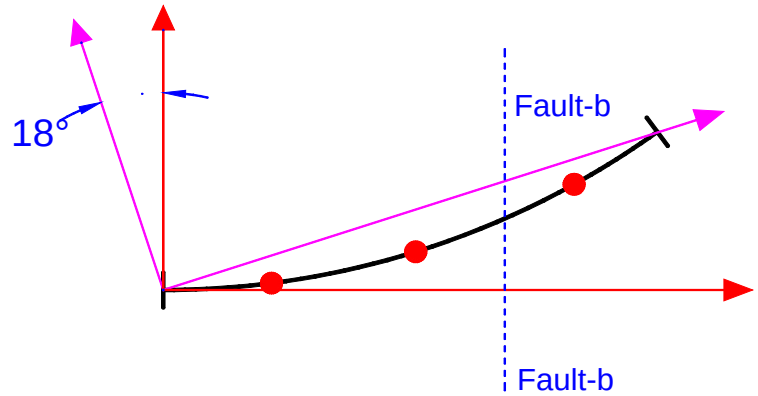

Figure B.37 Sketch of Bridge 55-0939G under Fault-b when $\theta = 18^{o}$.

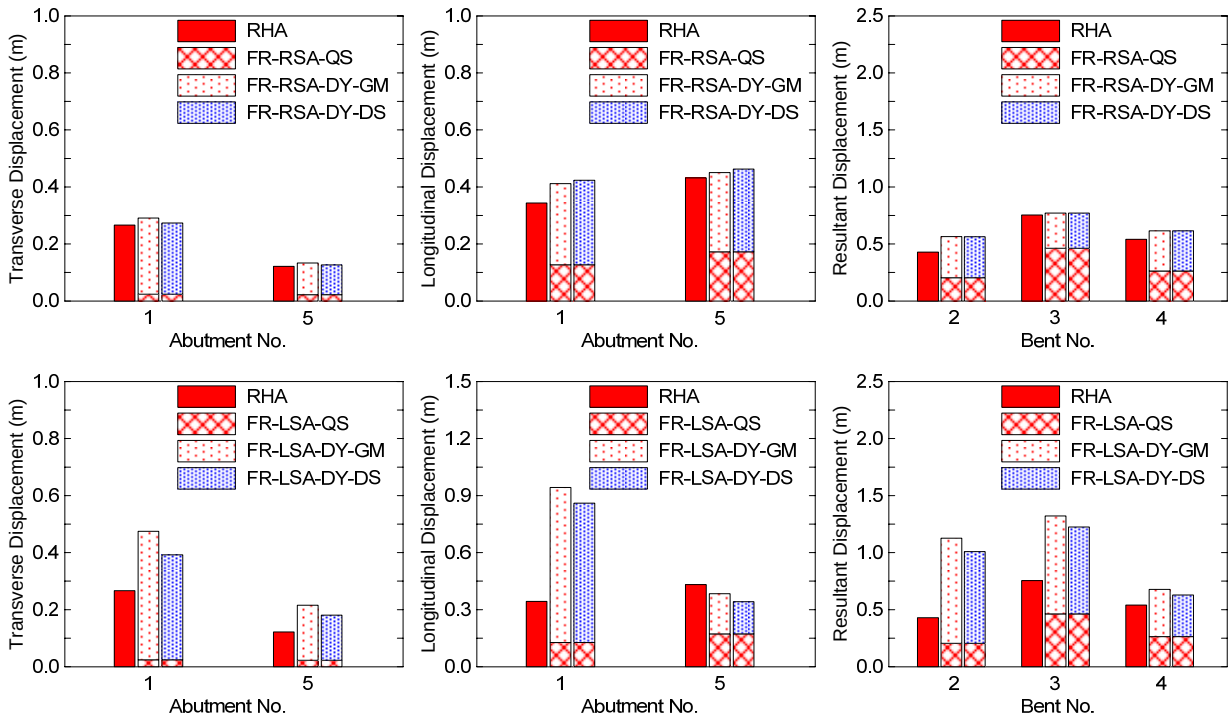

Figure B.38 Results of Bridge 55-0939G under Fault-b
when $\theta = 18^{o}$ and longitudinal abutment stiffness $= 0.10K_{eff}$.

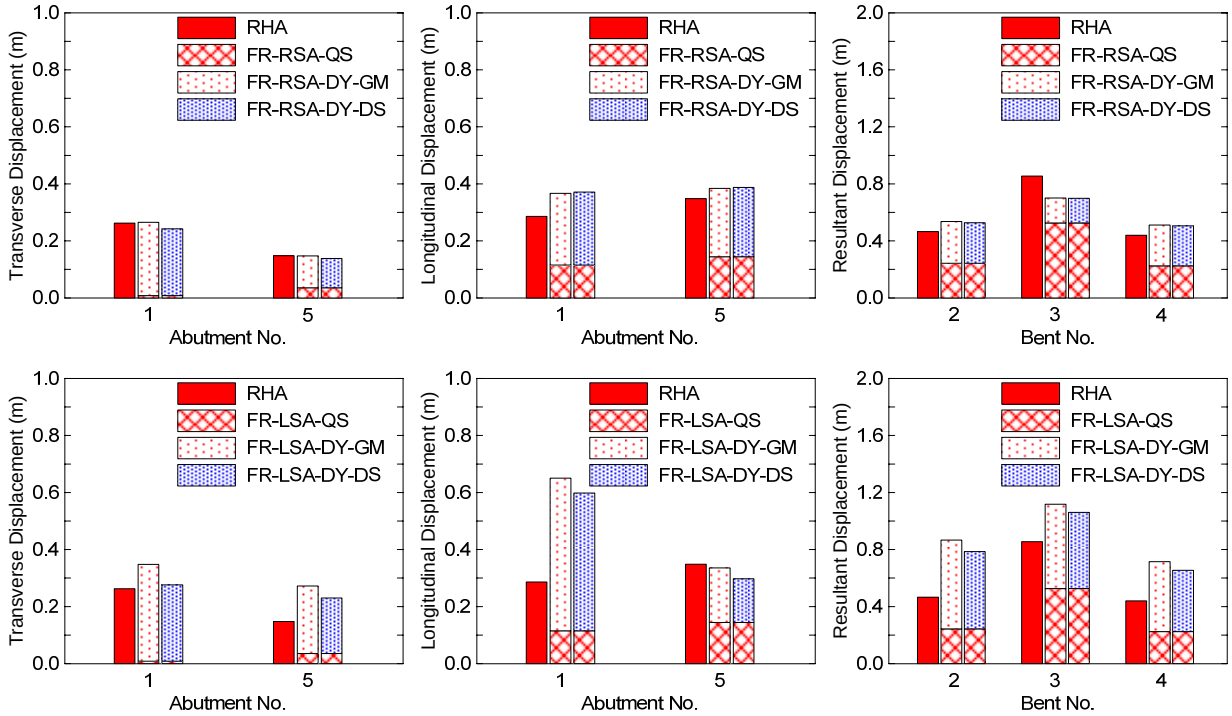

Figure B.39 Results of Bridge 55-0939G under Fault-b
when $\theta = 18^{o}$ and longitudinal abutment stiffness $= 0.55K_{eff}$.

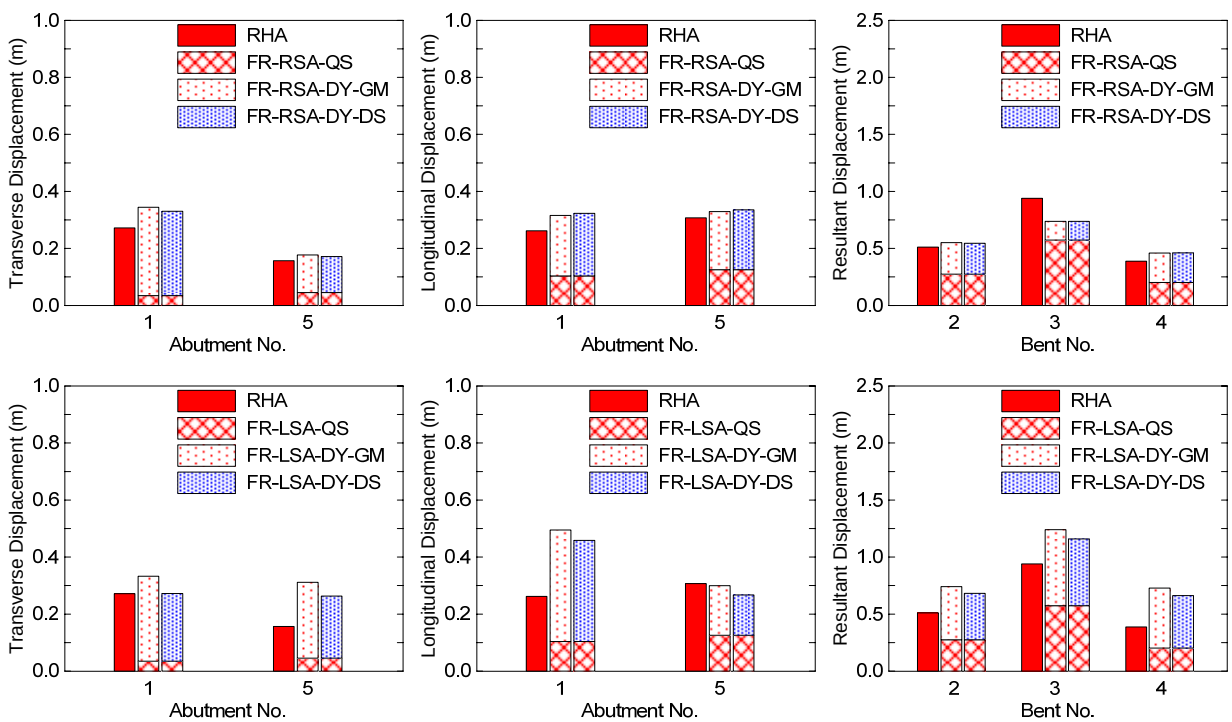

Figure B.40 Results of Bridge 55-0939G under Fault-b
when $\theta = 18^{o}$ and longitudinal abutment stiffness $= 1.0K_{eff}$.

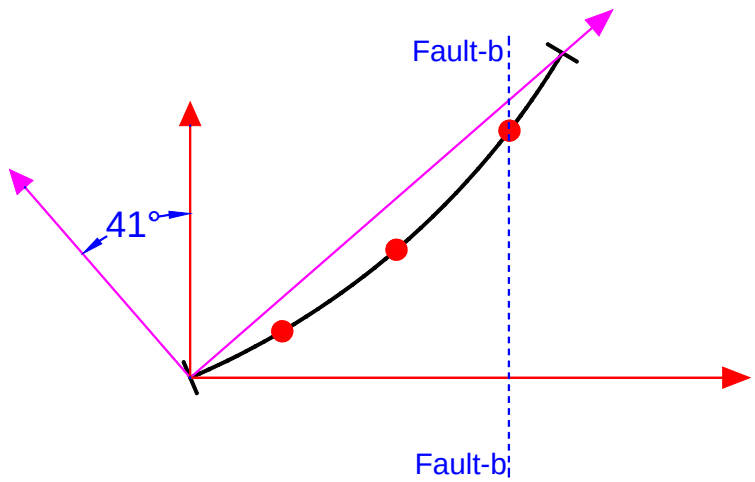

Figure B.41 Sketch of Bridge 55-0939G under Fault-b when $\theta = 41^{o}$.

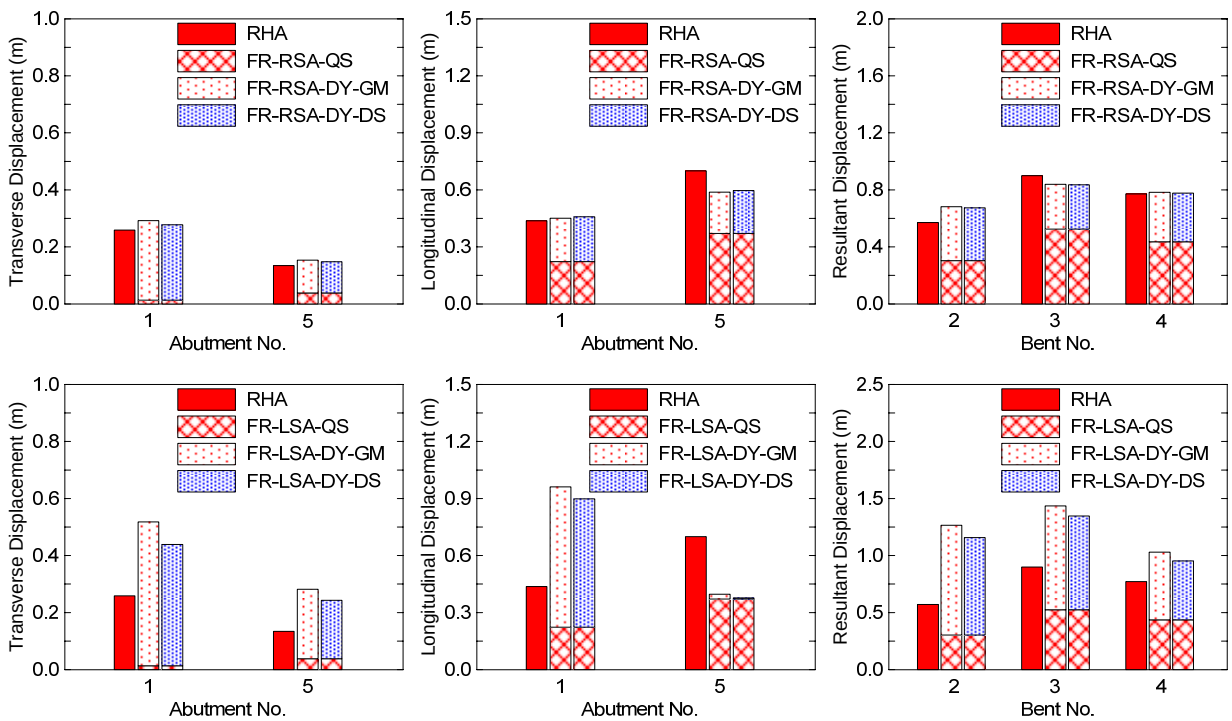

Figure B.42 Results of Bridge 55-0939G under Fault-b
when $\theta = 41^{o}$ and longitudinal abutment stiffness $= 0.10K_{eff}$.

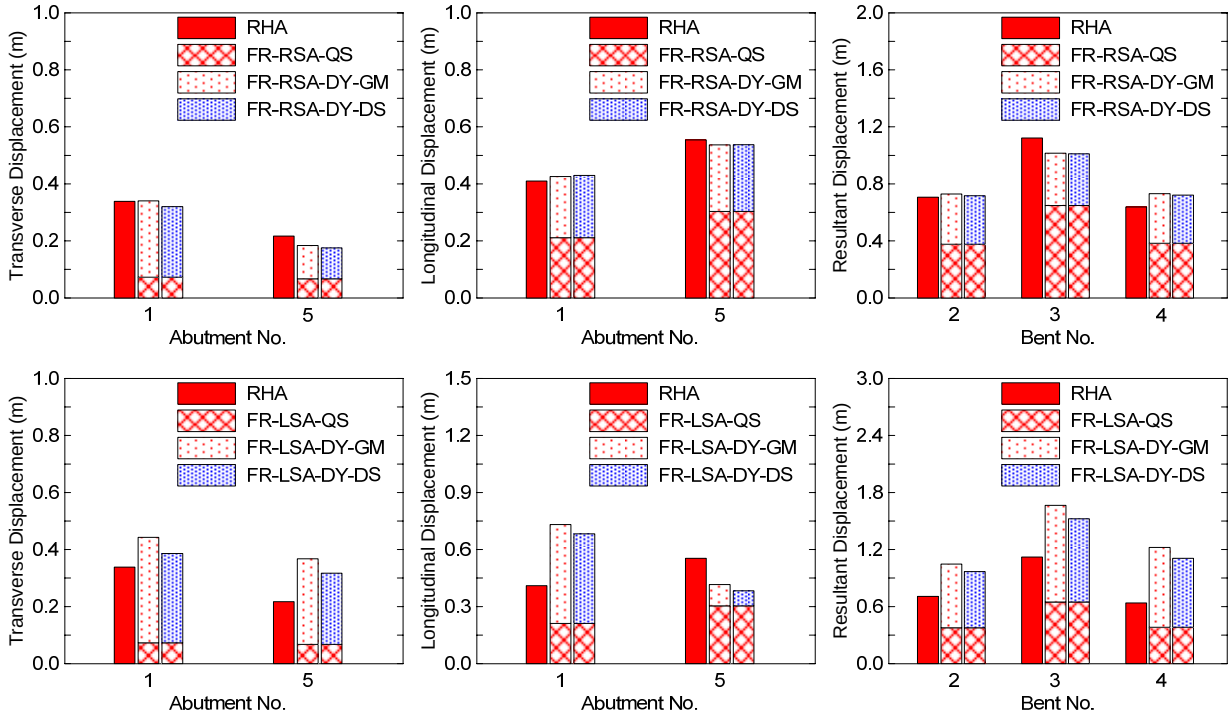

Figure B.43 Results of Bridge 55-0939G under Fault-b
when $\theta = 41^{o}$ and longitudinal abutment stiffness $= 0.55K_{eff}$.

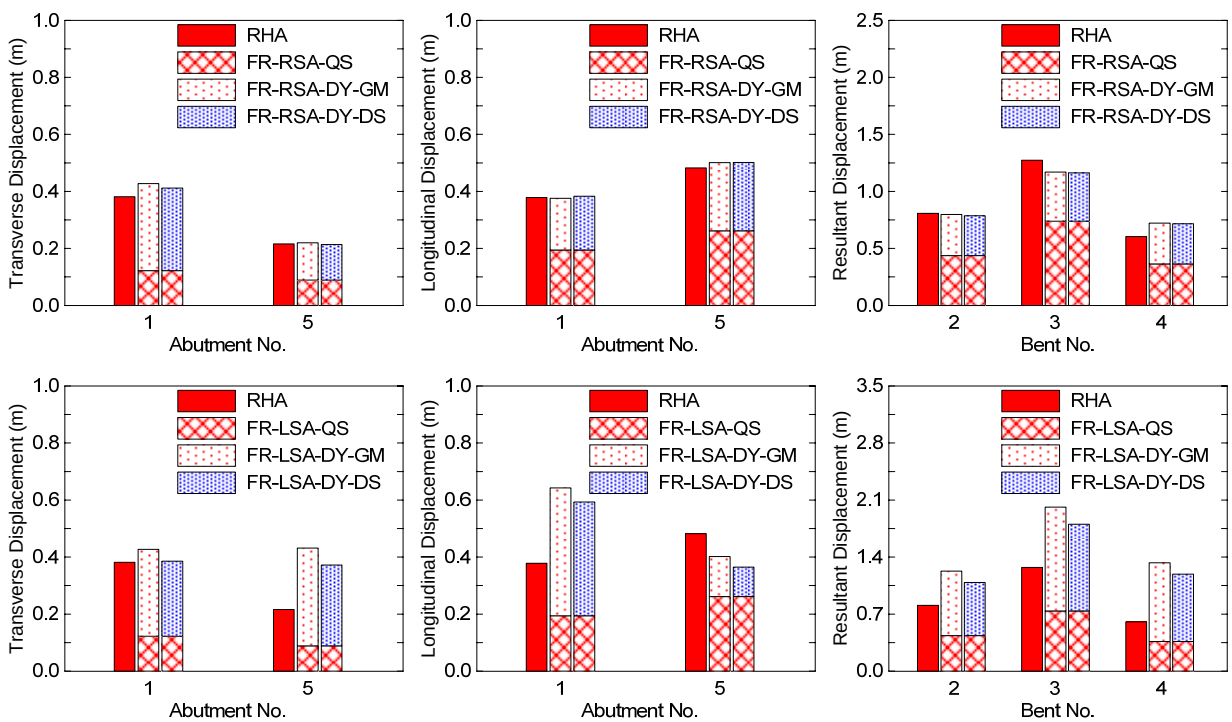

Figure B.44 Results of Bridge 55-0939G under Fault-b
when $\theta = 41^{o}$ and longitudinal abutment stiffness $= 1.0K_{eff}$.

APPENDIX C

PERIODS AND MODE SHAPE COMPARISONS OF CSI-BRIDGE™ AND OPENSEES BRIDGE MODELS

Table C.1 Comparison of Bridge 55-0837S periods

Mode Number	Periods of Vibration (sec)		
	OpenSees Fault-Normal/Parallel	CSiBridge™ Fault-Parallel	CSiBridge™ Fault-Normal
1	0.9760	0.9765	0.8866
2	0.8372	0.9028	0.8779
3	0.8055	0.8199	0.7869
4	0.6363	0.6985	0.6957
5	0.5432	0.5359	0.5339
6	0.4135	0.4137	0.4132
7	0.3627	0.3380	0.3381
8	0.2901	0.2709	0.2689
9	0.2663	0.1744	0.1742
10	0.2442	0.1542	0.1539
11	0.2315	0.1327	0.1217
12	0.2193	0.1298	0.1185

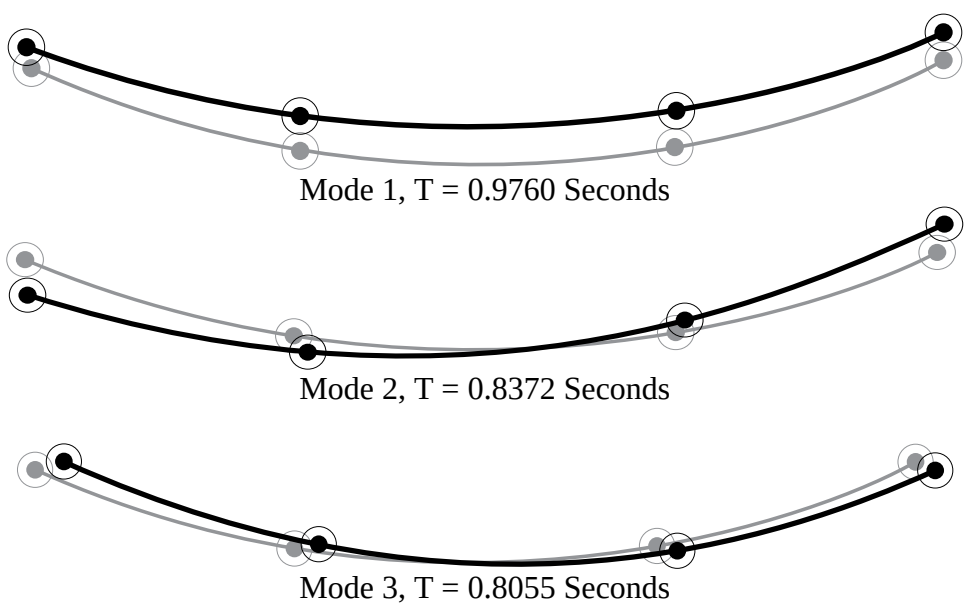

Figure C.1 OpenSees Mode Shapes determined by eigenvalue analysis

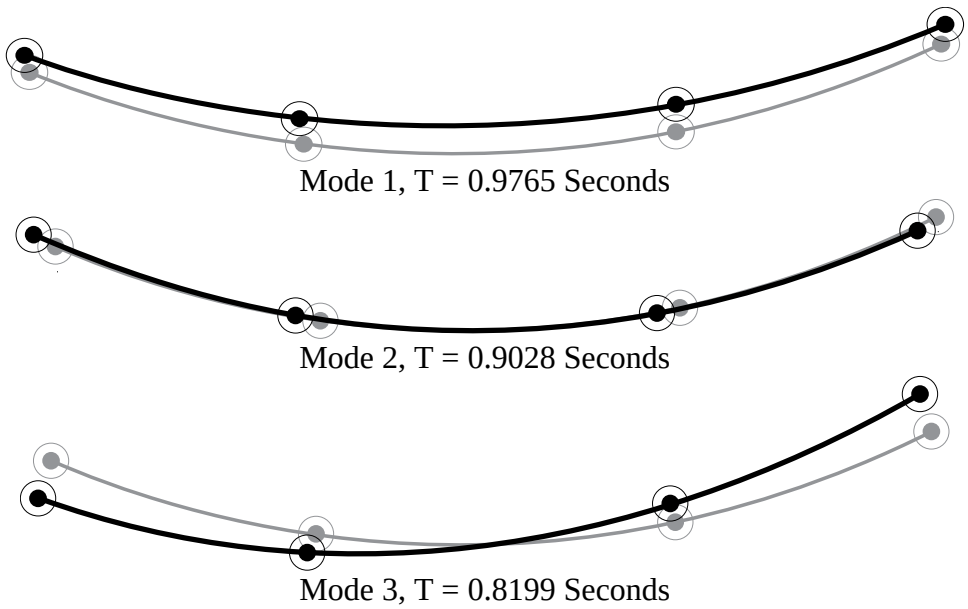

Figure C.2 CSiBridge™ Ritz vectors and corresponding bridge periods for Fault-Parallel Response Spectrum Analysis

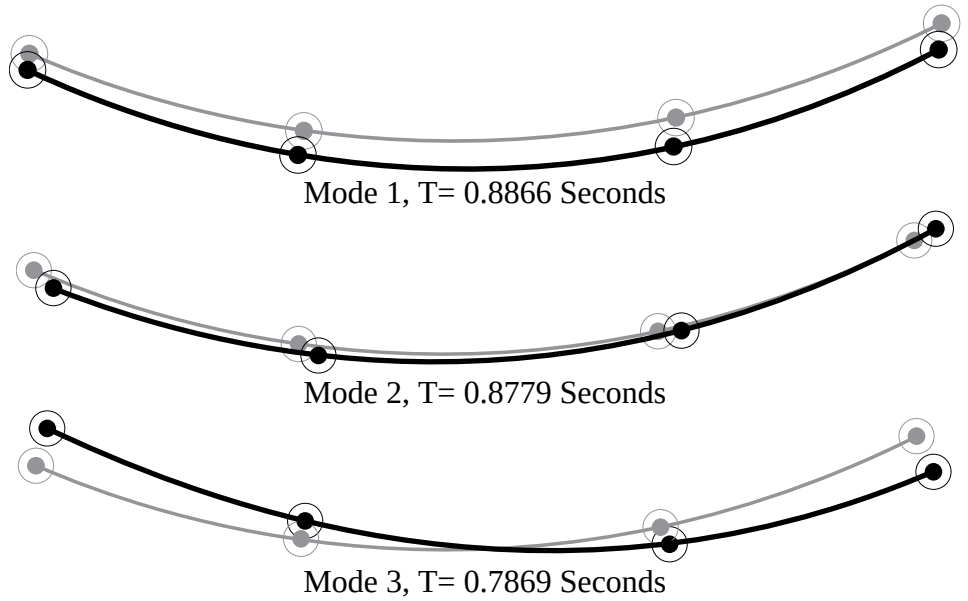

Figure C.3 CSiBridge™ Ritz vectors and the corresponding bridge periods for Fault-Normal Response Spectrum Analysis

APPENDIX D

COMPLETE RESULT COMPARISON QUANTITIES FOR VALIDATION OF CSIBRIDGE™

Table D.1 Bridge 55-0837S abutment displacement

		QS		RSA-FP		RSA-FN		Combined	
Abut	**Program**	**Trans**	**Long**	**Trans**	**Long**	**Trans**	**Long**	**Trans**	**Long**
1	OpenSees	-0.1382	-0.0128	0.2018	0.0606	0.0643	0.1370	0.4043	0.2104
	CSiBridge™	0.1307	-0.0352	0.1882	0.0572	0.0787	0.1701	0.3976	0.2625
4	OpenSees	0.1393	-0.0120	0.1931	0.0676	0.0675	0.1321	0.3999	0.2117
	CSiBridge™	0.1170	0.0031	0.1838	0.0567	0.0775	0.1644	0.3784	0.2242

Table D.2 Bridge 55-0837S bent top node displacement

		QS		RSA-FP		RSA-FN		Combined	
Bent	**Program**	**Trans**	**Long**	**Trans**	**Long**	**Trans**	**Long**	**Trans**	**Long**
2	OpenSees	-0.2986	0.1460	0.0791	0.0480	0.0517	0.1312	0.4294	0.3252
	CSiBridge™	-0.2969	0.1551	0.0769	0.0468	0.0458	0.1599	0.4196	0.3617
3	OpenSees	0.3179	-0.0920	0.0809	0.0193	0.0491	0.1317	0.4479	0.2430
	CSiBridge™	0.2966	-0.0980	0.0731	0.0450	0.0838	0.1407	0.4534	0.2838

Table D.3 Bridge 55-0837S bent bottom node displacement

		QS		RSA-FP		RSA-FN		Combined	
Bent	**Program**	**Trans**	**Long**	**Trans**	**Long**	**Trans**	**Long**	**Trans**	**Long**
2	OpenSees	-0.4171	-0.1675	0.0273	0.0251	0.0254	0.0814	0.4698	0.2740
	CSiBridge™	0.4028	0.1908	0.0274	0.0207	0.0232	0.0861	0.4534	0.2976
3	OpenSees	0.4229	-0.1522	0.0318	0.0066	0.0343	0.0746	0.4890	0.2334
	CSiBridge™	-0.4097	-0.1774	0.0264	0.0174	0.0437	0.0731	0.4798	0.2679

APPENDIX E

BRIDGE 55-0837S CSiBridge™ MODEL: DETAILED MODEL DEVELOPMENT PROCESS

The following is a step-by-step description of the actions performed in the software user interface of CSiBridge™ v16 Beta build "W" to develop a desired bridge model, exemplified here using Bridge 55-0837S. In addition, the corresponding screen-capture images are provided to aid in the understanding of the described CSiBridge™ commands and instructions.

CREATING A NEW BRIDGE MODEL

- Open CSiBridge™ v.16.
  - Select *New* under the Orb drop down window to begin a new bridge model.
  - In the New Model window, set units to *kN,m,C* and select Template *Blank.*

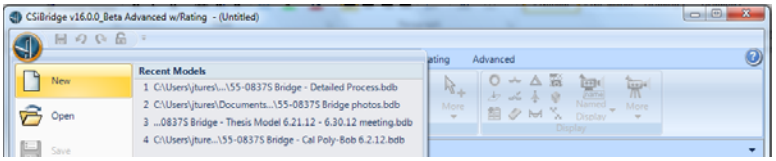

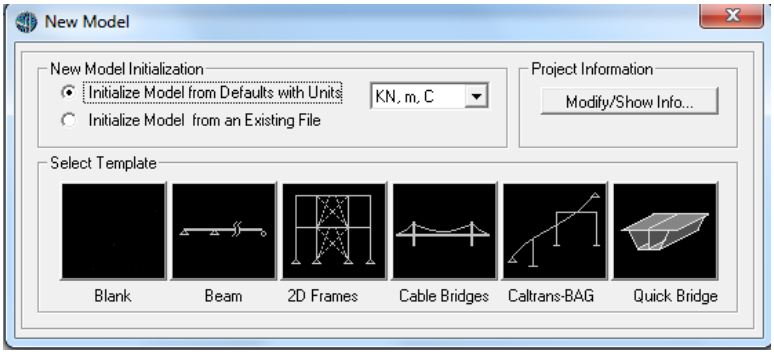

DEFINING THE BRIDGE LAYOUT LINE

- The layout line represents the centerline of the assigned deck section.

- Create a bridge layout line by selecting the *New* icon in the Layout Line section under the *Layout* tab.
  - Name the Bridge Layout Line.
  - In the Initial and End Station Data section, denoted the End Station of the 55-0837S Bridge which is 153.4066 m. (highlighted)
  - Define the curve of the Bridge 55-0837S deck by selecting *Define Horizontal Layout Data.*

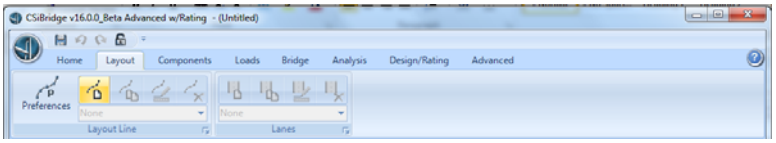

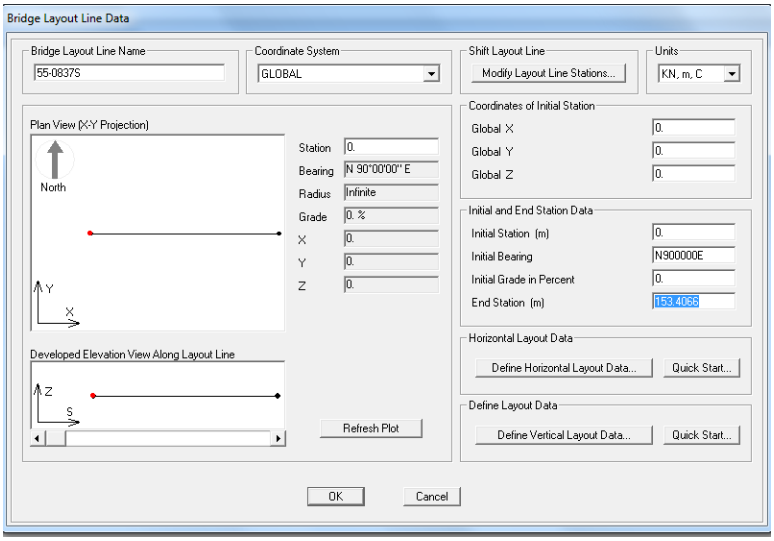

- For each direction change in the bridge deck layout, a new Layout Line Segment needs to be created. The curve of Bridge 55-0837S was modeled with 30 linear segments in OpenSees; therefore, the layout line is assigned 30 *Straight to New Bearing To Station* line layout segments oriented at increasing degrees of rotation to achieve the approximate curve.

- Add Bridge 55-0837S line layout segments, defined in Table E.1 on Page 96, in the Bridge Layout Line – Horizontal Layout Data window.
  - Select a Layout Line Segment Type from the drop down window options.
  - Specify the Station (or location) at which that segment's ending node will be located.
  - In the Bearing window, specify the rotation of the segment with respect to the initially straight deck. First, denote the direction of rotation; in this case, *S* rotates the segment clockwise and *N* rotates the segment counterclockwise. Denote the degrees of rotation in the next two numerical place holders.
  - Insert the segment between the two abutments by selecting *Insert Below*.
  - Select *OK* when all segments have been defined.

- Vertical Layout Line Data does not need to be altered for this bridge model because the elevation of the bridge deck is constant.

- Once the desired Bridge Layout Line has been created, select *OK* to return to the main window.

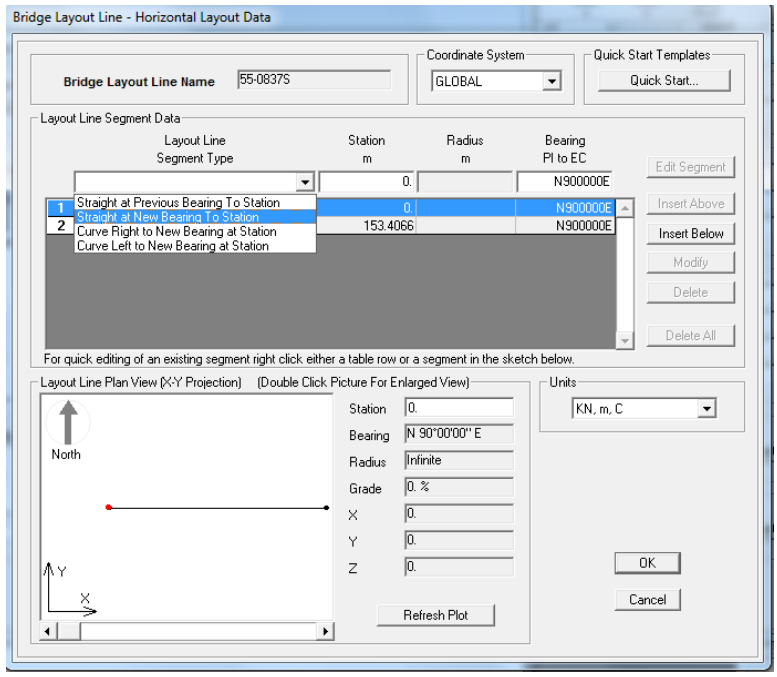

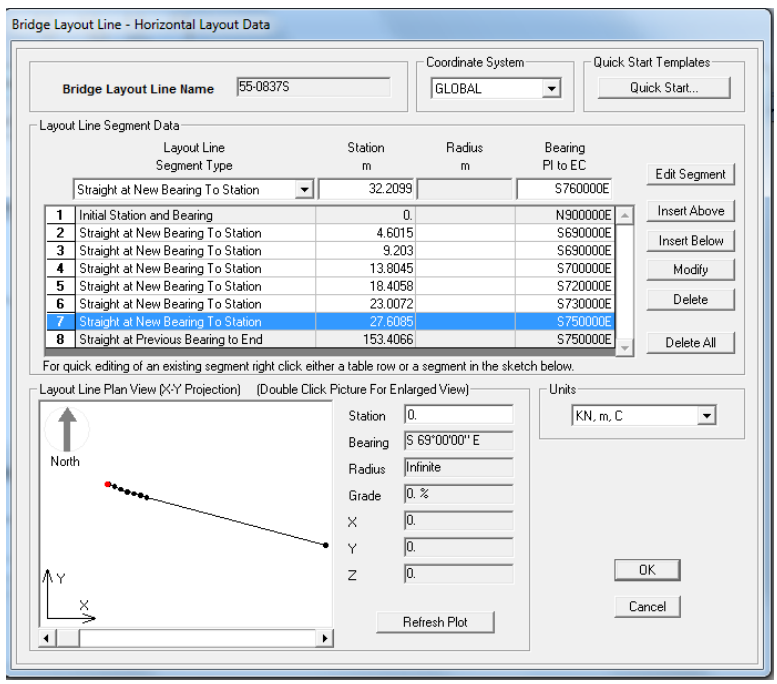

- In the View section under the *Home* tab, select *XY* to see the created bridge layout line in plan.

- The bridge layout line can be further edited by selecting the *Modify* icon in the Layout Line section under the *Layout* tab.

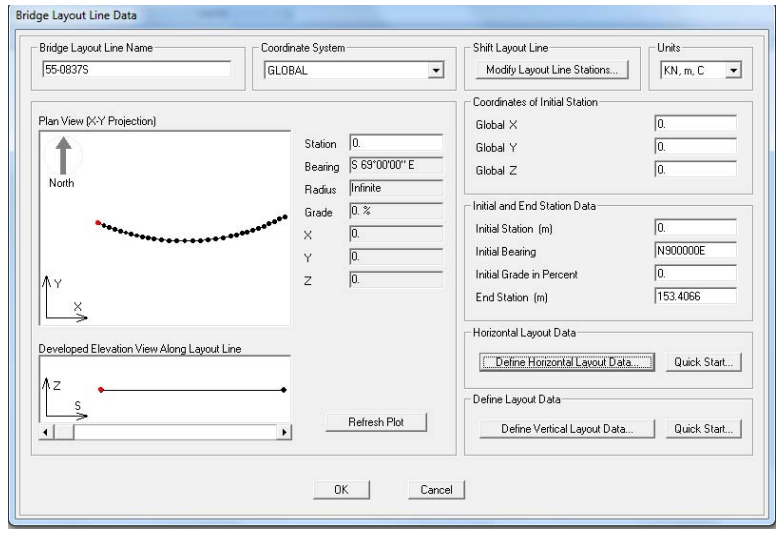

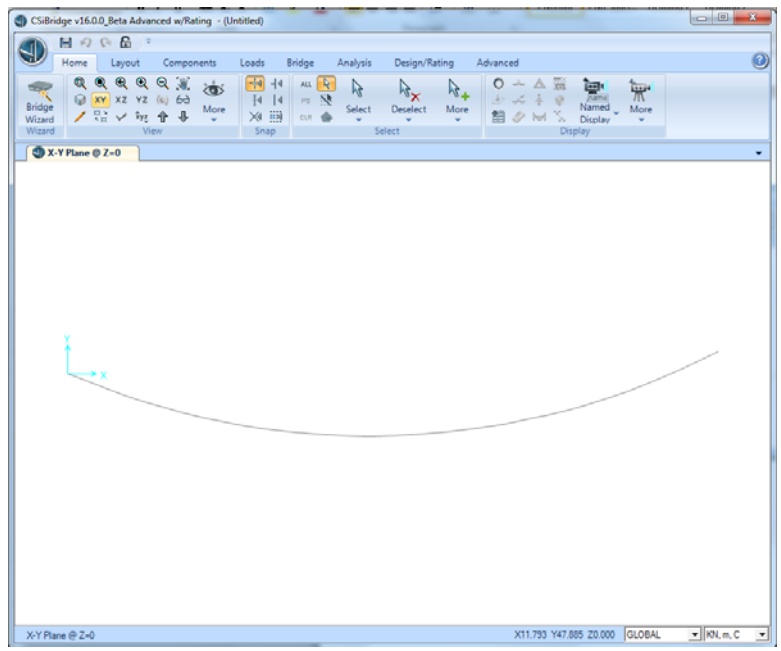

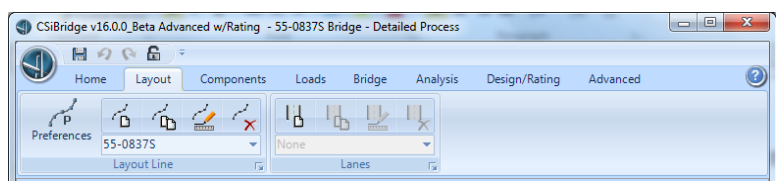

Table E.1 Bridge 55-0837S Layout Line Segment Data

	Layout Line Segment Type	Station m	Bearing PI to EC
1	Initial Station and Bearing	0	S690000E
2	Straight at New Bearing To Station	4.6015	S690000E
3	Straight at New Bearing To Station	9.2030	S690000E
4	Straight at New Bearing To Station	13.8045	S700000E
5	Straight at New Bearing To Station	18.4058	S720000E
6	Straight at New Bearing To Station	23.0072	S730000E
7	Straight at New Bearing To Station	27.6085	S750000E
8	Straight at New Bearing To Station	32.2099	S760000E
9	Straight at New Bearing To Station	36.8112	S780000E
10	Straight at New Bearing To Station	41.4126	S790000E
11	Straight at New Bearing To Station	46.0139	S810000E
12	Straight at New Bearing To Station	52.1569	S830000E
13	Straight at New Bearing To Station	58.2999	S850000E
14	Straight at New Bearing To Station	64.4430	S870000E
15	Straight at New Bearing To Station	70.5860	S890000E
16	Straight at New Bearing To Station	76.7290	N890000E
17	Straight at New Bearing To Station	82.8721	N870000E
18	Straight at New Bearing To Station	89.0151	N850000E
19	Straight at New Bearing To Station	95.1581	N830000E
20	Straight at New Bearing To Station	101.3011	N810000E
21	Straight at New Bearing To Station	107.4442	N790000E
22	Straight at New Bearing To Station	112.0404	N770000E
23	Straight at New Bearing To Station	116.6367	N760000E
24	Straight at New Bearing To Station	121.2329	N740000E
25	Straight at New Bearing To Station	125.8292	N730000E
26	Straight at New Bearing To Station	130.4254	N710000E
27	Straight at New Bearing To Station	135.0216	N690000E
28	Straight at New Bearing To Station	139.6179	N680000E
29	Straight at New Bearing To Station	144.2141	N660000E
30	Straight at New Bearing To Station	148.8104	N650000E
31	Straight at Previous Bearing to End	153.4066	N650000E

DEFINING MATERIAL PROPERTIES

- The material properties used in OpenSees to model Bridge 55-0837S are defined in Table E.2.

- Create each material model by selecting *Material Properties* from the *Type* drop down window in the Properties window under the *Components* tab.
  - Select the *New* icon to create a new material.
  - In the Quick Material Definition window select the Region *United States*, Material Type as either *Concrete* or *Rebar*, and Standard as *User* for user defined.
  - Define the Material Property Data according to Table E.2.
  - Select OK to save.
  - Repeat to create all three materials.

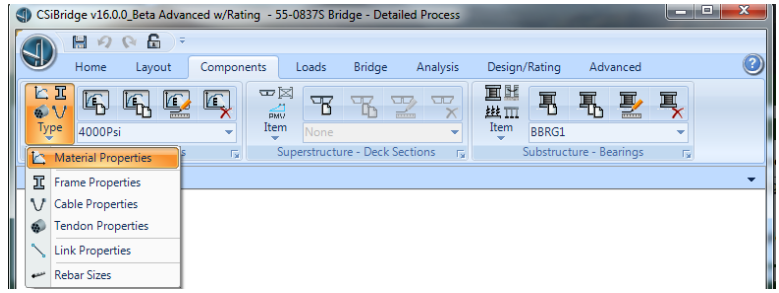

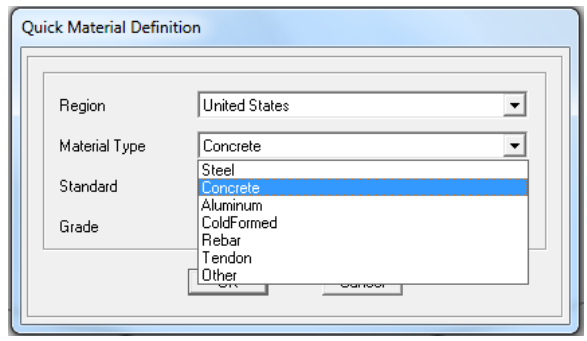

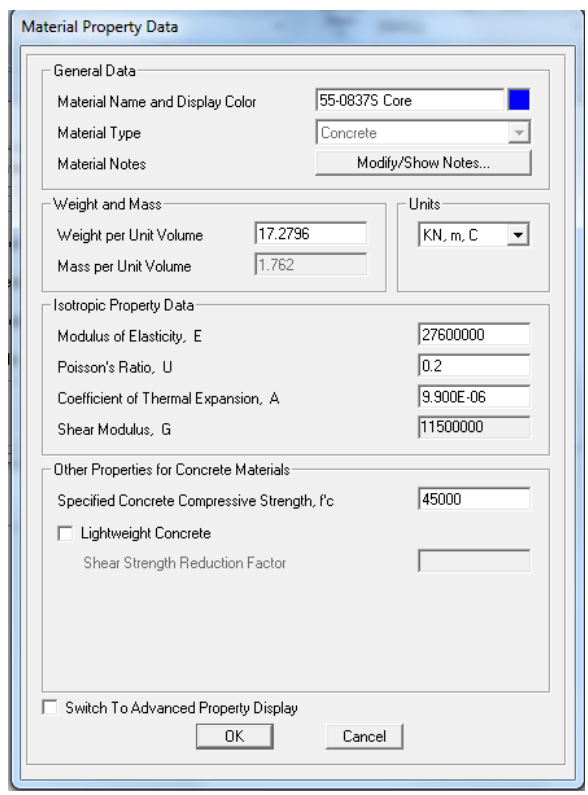

Table E.2 Material Properties (kN, m, C)

Material Name	**55-0837S Core**	**55-0837S Cover**	**55-0837S Rebar**
Material Type	Concrete	Concrete	Rebar
Weight per Unit Volume	17.2796	17.2796	76.9729
Modulus of Elasticity, E	27600000	27600000	2.00E+08
Poisson's Ratio, U	0.2	0.2	-
Coeff. of Thermal Expansion, A	9.90E-06	9.90E-06	1.17E-05
Specified Concrete Comp. Strength, f'c	45000	34500	-
Minimum Yeild Stress, Fy	-	-	475000
Minimum Tensile Stress, Fu	-	-	620528.2
Expected Yield Stress, Fye	-	-	455054
Expected Tensile Stress, Fue	-	-	682581

DEFINING FRAME SECTIONS

- A frame section is any set of cross-section parameters that may be applied to any component of the bridge object. For Bridge 55-0837S, two frame sections need to be defined; the deck section and the bent column section. Both frame sections will be manually assigned properties to match those defined in the OpenSees Model.

- Create each frame section model by selecting *Frame Properties* from the *Type* drop down window in the Properties section under the *Components* tab.
  - Select the *New* icon to begin creating a new frame section.
  - Select *Other* from the Add Frame Section Property Type window to manually define section properties.

- Create the deck frame section.
  - Select *General.*
    - Set Properties as defined in Table 5.2 on Page 37.
    - Select *OK* to continue defining the section.
  - Name the deck frame section.
  - Define the material as *55-0837S Core.*
  - The Mass will later be applied manually at each node along the deck therefore; the Mass Property Multiplier must be set equal to 0.
    - Select *Set Modifiers*
    - Change Mass from 1 to 0 in the Frame property/Stiffness Modification Factors window. Set all other multiplies equal to 1.
    - Select *OK* to save.
  - Select *OK* to create the deck frame section.

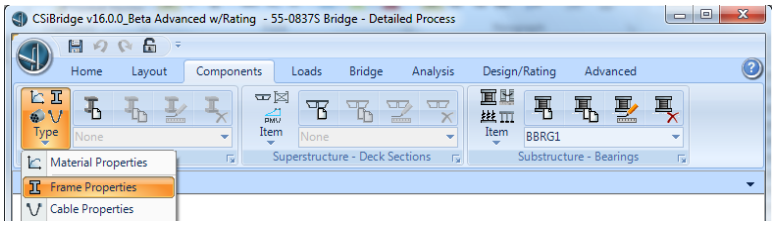

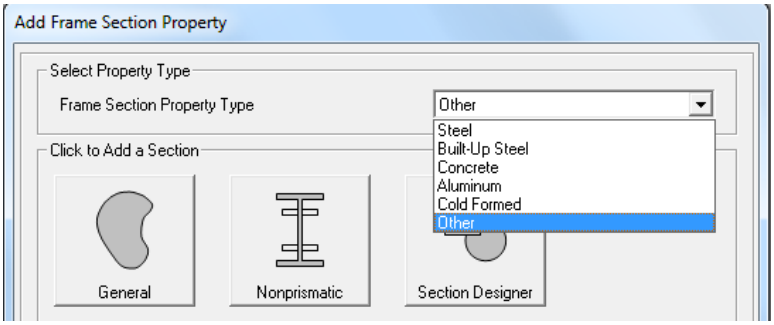

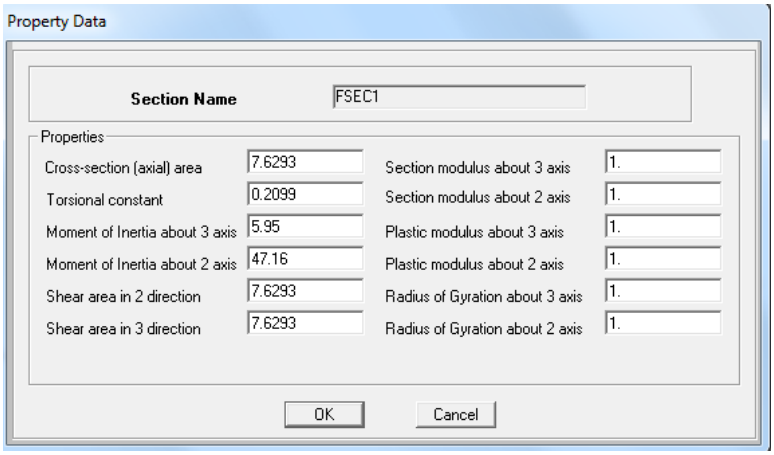

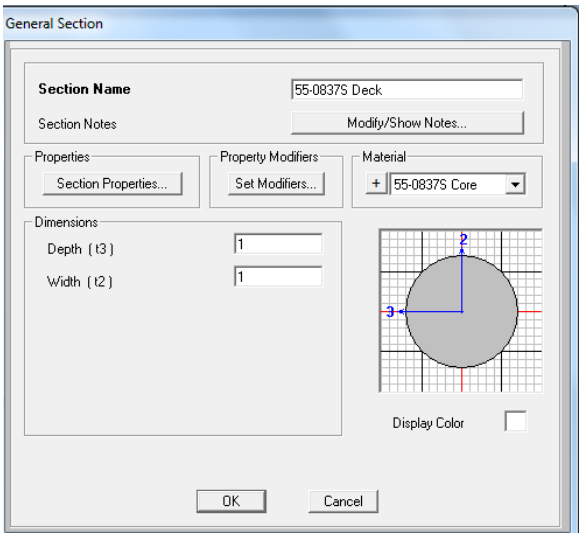

- Create the bent column frame section.
  - Select *Section Designer* to define geometry and reinforcing.
  - Name the column section
  - Set the Base Material to be *55-0837S Cover*.
  - Designate the Design Type to be *Concrete Column* with *Reinforcement to be Checked*.
  - Select *Set Modifier*.
    - Change the *Mass* modifier to 0.
    - Select *OK* to save.
  - Select Section Designer to open the Section Designer Interface and create the 55-0837S Column Section.
  - Create the section.
    - Set units to *kN, m, C*.
    - Select the *Draw* tab, then *Draw Caltrans Shape*, then *Draw Round* to create a default column cross-section.
    - Click anywhere on the grid to place the Draw Round object.
    - Select the *Arrow* icon in the left-hand toolbar and right-click on the object to edit its parameters.

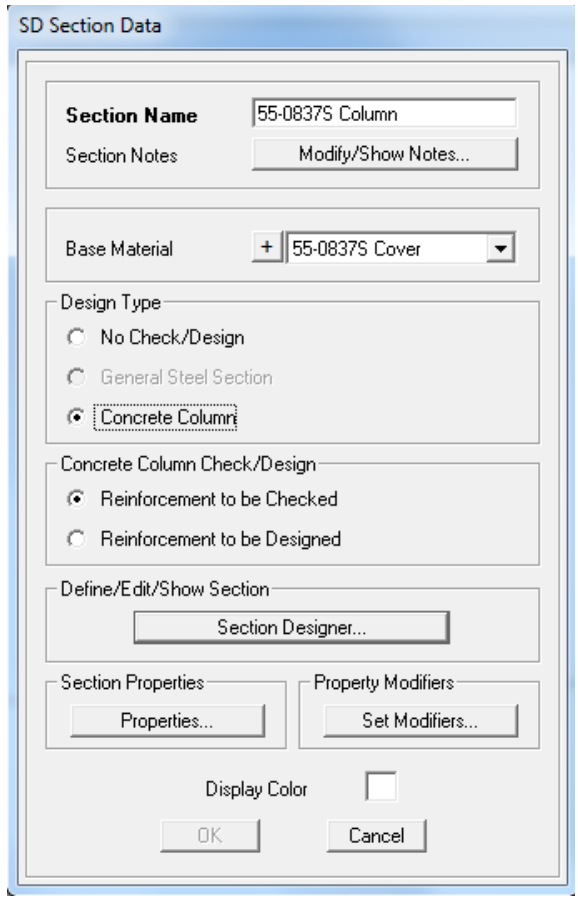

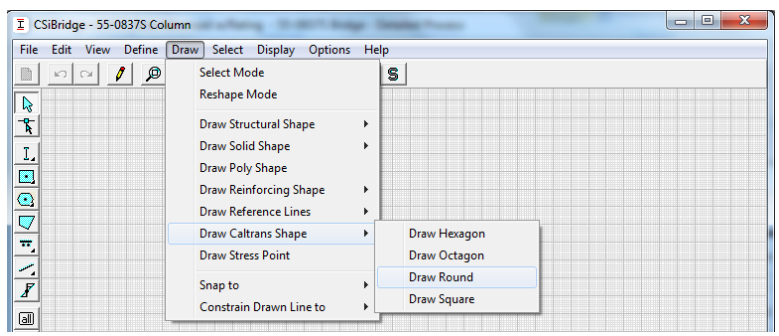

- Set parameters as defined in Table E.3 and select *OK* to save.
- Select *DONE* in the lower right-hand corner of Section Designer to save the bent column and return to the SD Section Data Window.

o Select *Properties* to ensure the bent column cross-sectional properties match those defined in Table 5.1 on Page 36.

o Select *OK* to create the bent column frame section.

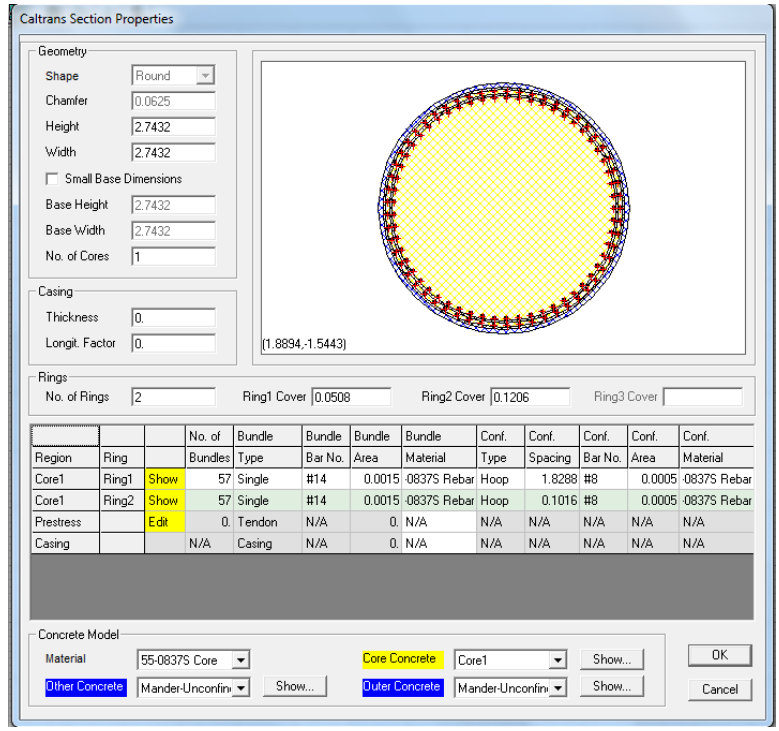

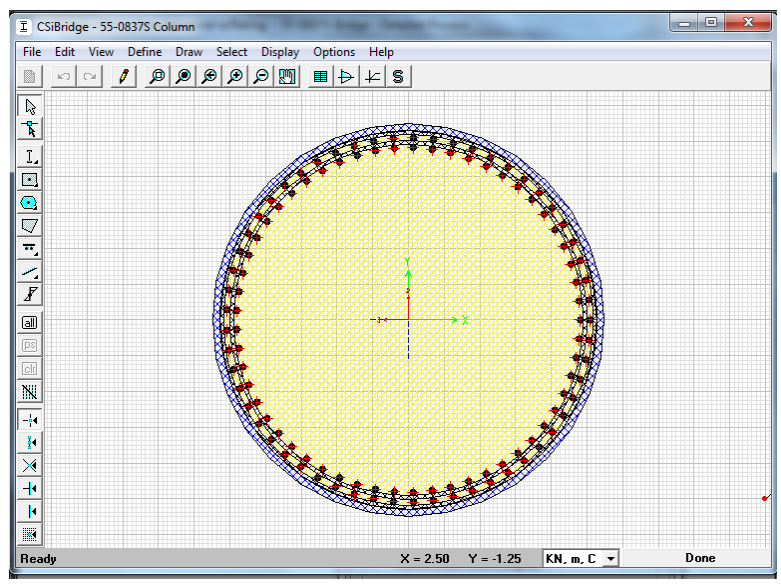

Table E.3 Bent Column Section Designer Frame Properties

Geometry		
Height (m)	2.7432	
Width (m)	2.7432	
No. of Cores	1	
No. of Rings	2	
Rings		
Core	1	2
Cover (m)	0.0508	0.1206
No. of Bundles	57	
Bundle Type	Single	Single
Bundle Bar No.	#14	#14
Bundle Material	55-0837S Rebar	55-0837S Rebar
Conf. Type	Spiral	Spiral
Conf. Spacing (m)	1.8288	0.1016
Conf. Bar No.	#8	#8
Concrete Model		
Conf. Material	55-0837S Rebar	
Material	55-0837S Core	
Core Concrete	Core1	
Other Concrete	Mander-Unconfined	
Outer Concrete	Mander-Unconfined	

DEFINING THE SUPERSTRUCTURE & SUBSTRUCTURE

- In order to create a bridge object, a deck cross-section is automatically applied to the layout line. In this model, the desired deck section is user-defined as a general frame section (55-0837S Deck). Therefore, the automatic deck cross-section needs to be created merely as a place holder to be later overwritten by the already defined deck frame section.

- Create a deck section by selecting *Deck Section* from the *Item* drop down window in the Superstructure section under the *Components* tab.
  - Select the *New* icon to begin creating a new deck section.
  - Select AASHTO-PCI-ASBI Standard.
  - Select *OK* without making any changes to the geometry because this deck section will later be overwritten and is therefore, trivial.

- Create foundation springs by selecting *Foundation Springs* from the *Item* drop down window in the Substructure section under the *Components* tab.
  - Select the *New* icon to begin creating a new foundation spring.
  - Name the foundation spring.
  - Ensure the units are kN, m, C
  - Click on the *Release Type* to select the fixity from the drop down window according to Table 5.3 on Page 40.
  - If partially fixed, specify the *Stiffness*.
  - Select *OK* to save.
  - Create both the Bent Foundation Spring and the Abutment Spring (Note: Abutment Springs are also a series of foundation springs and can be defined in the same way as the Bent Foundation Spring).

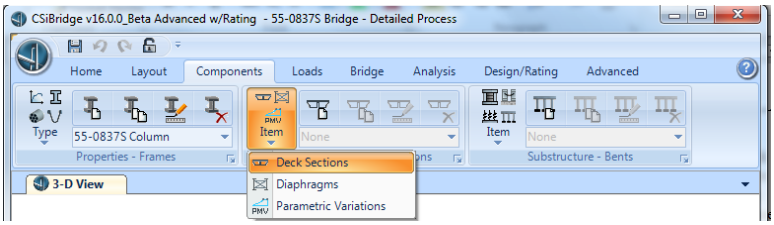

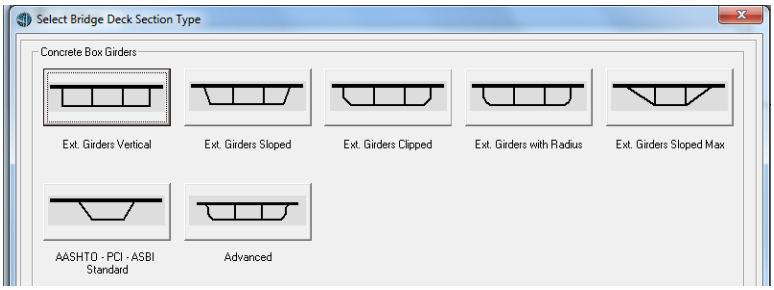

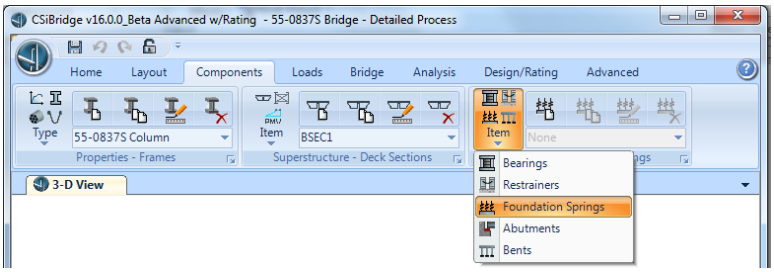

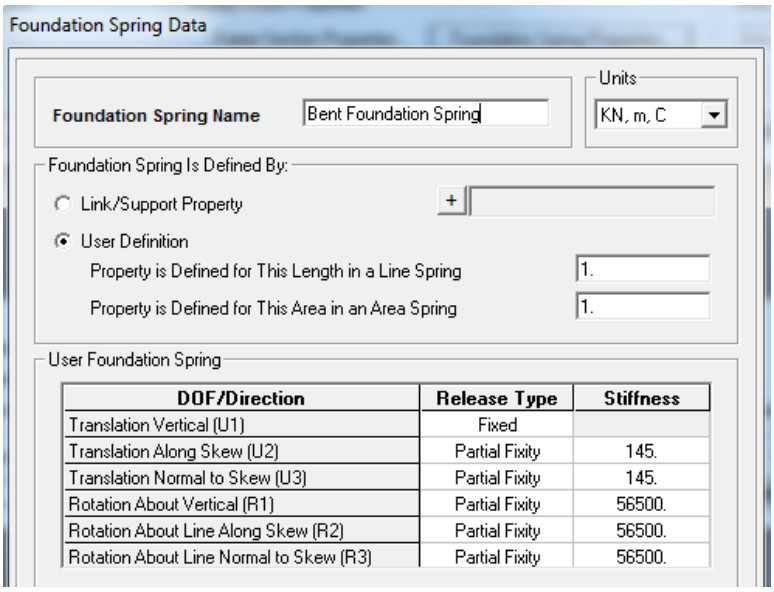

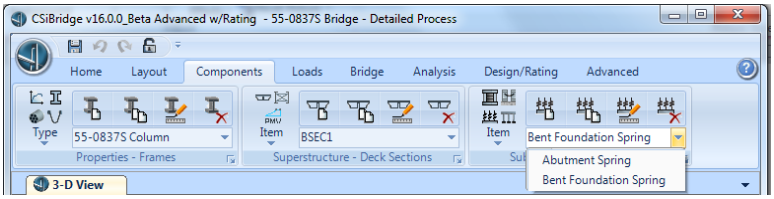

- Create each bent by selecting *Bents* from the *Item* drop down window in the Substructure section under the *Components* tab.
  - Select the *New* icon to begin creating a new bent.
  - Name the bridge bent.
  - Ensure the units are *kN, m, C.*
  - Specify Bent Data according to Table E.4.
  - Set Bent Type to *Single Bearing Line (Continuous Superstructure)* and Girder Support Condition to *Connect to Girder Bottom Only*.
  - Select *Modify/Show Column Data* to define bridge bent column properties.
    - Within the Bridge Bent Column Data window, modify properties according to Table E.4.
    - Select *OK* to save.
  - Select *OK* to save.
  - Create both Bent 2 and Bent 3.

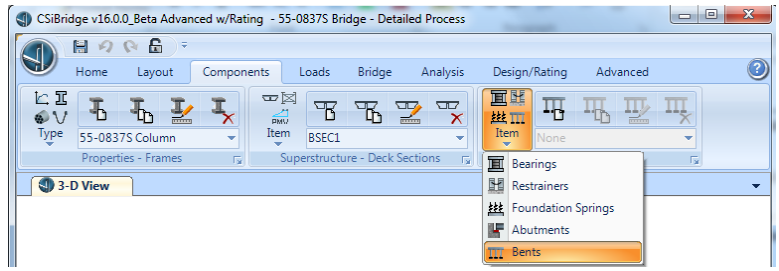

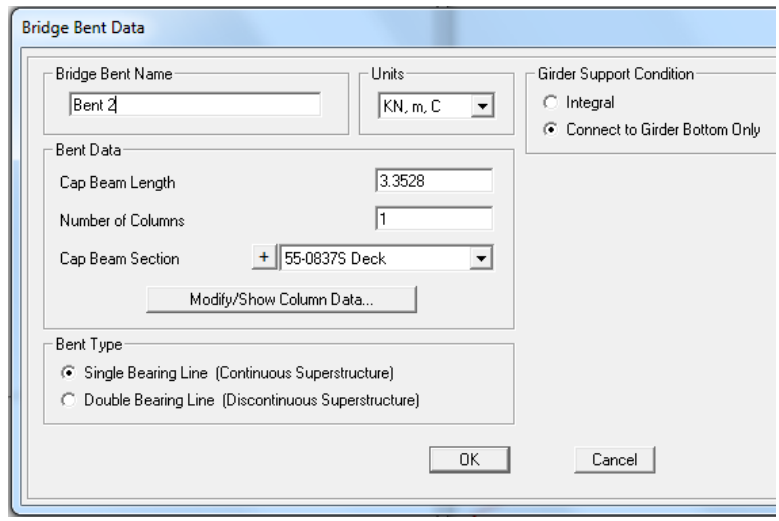

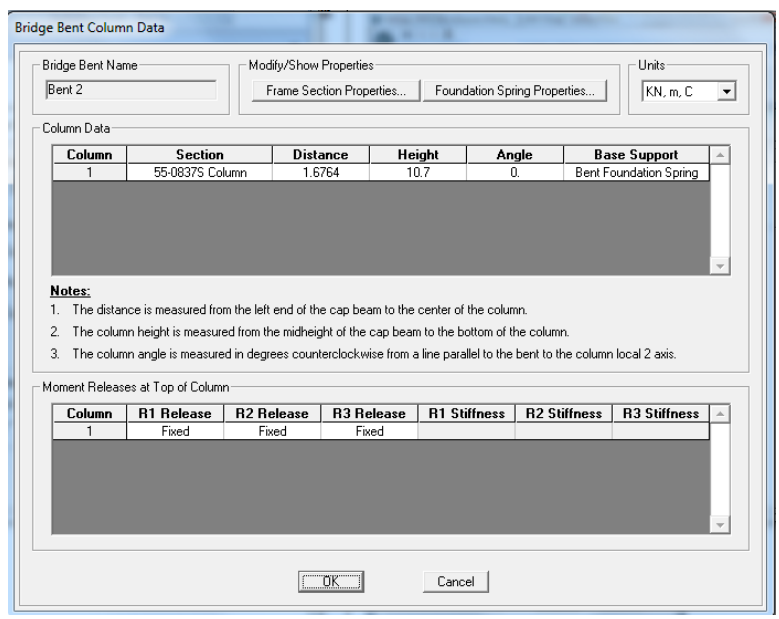

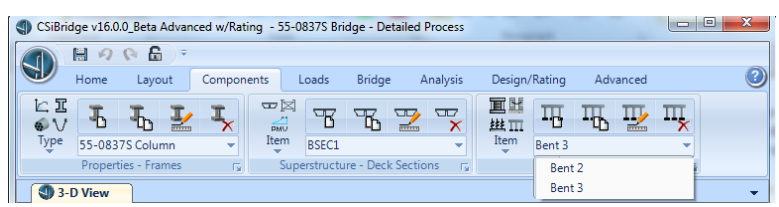

Table E.4 Bridge Bent Properties (kN, m, C)

Bridge Bent Data		
Bridge Bent Name	Bent 2	Bent 3
Cap Beam Length (m)	3.3528	3.3528
No. of Columns	1	1
Cap Beam Section	55-0837S Deck	55-0837S Deck
Bridge Bent Column Data		
Section	55-0837S Column	55-0837S Column
Distance (m)	1.6764	1.6764
Height (m)	10.7	11
Angle	0	0
Base Support	Bent Foundation Spring	Bent Foundation Spring
Moment Releases at Top of Column	All Fixed	All Fixed

- Create each abutment by selecting *Abutments* from the *Item* drop down window in the Substructure section under the *Components* tab.
  - Select the *New* icon to begin creating a new abutment. This abutment definition will be used for both Abutment 1 and Abutment 4.
  - Name the abutment.
  - Ensure the units are k*N, m, C.*
  - Set Girder Support Condition to *Connect to Girder Bottom Only* and Substructure Type to *Foundation Spring*.
  - Select *Abutment Spring* from the drop down window to define the Foundation Spring Property.
  - Select *OK* to save.

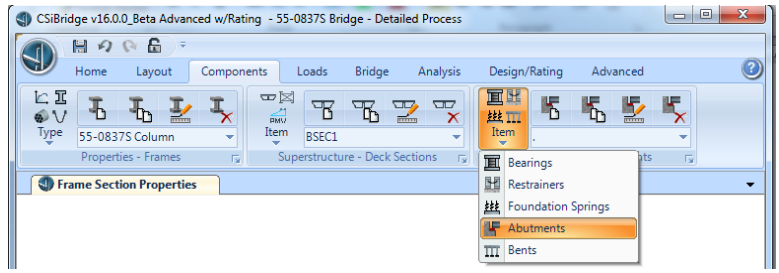

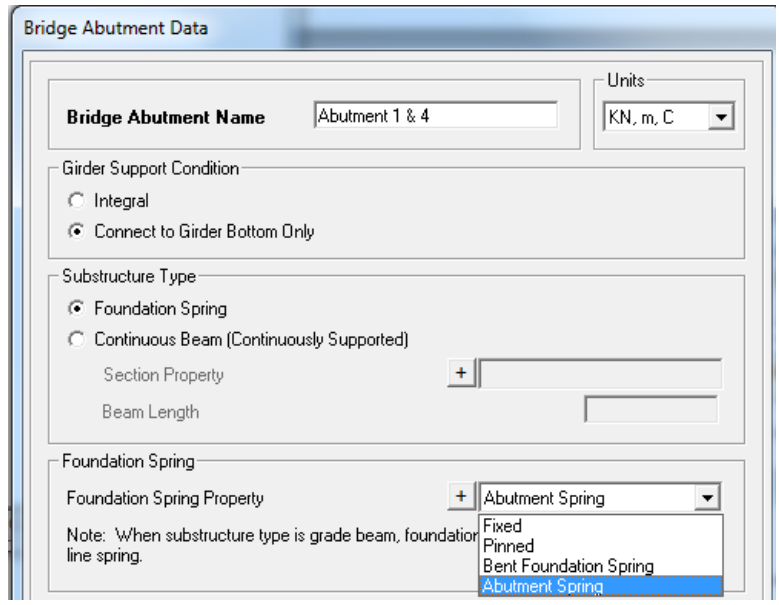

CREATING A BRIDGE OBJECT

- A bridge object assigns the superstructure and various substructure components to the layout line.

- Create a bridge object by selecting the *New* icon in the *Bridge Objects* section under the *Bridge* tab.
  - Name the bridge object.
  - Select 55-0837S as the Layout Line Name.
  - Define the Bridge Object Reference Line.
    - Add spans by entering the station location of the first bent in the Station (m) window.
    - Select *Add* (Span Label and Span Type will update automatically).
    - Bent 2 is located at 46.0139 m
    - Bent 3 is located at 107.4442 m
  - Select *OK* to create the bridge object.

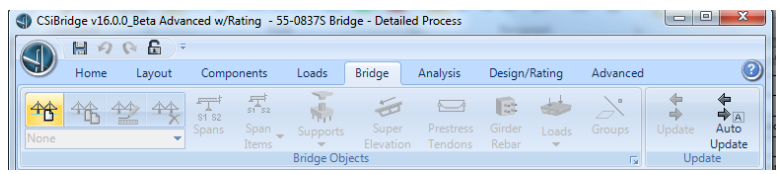

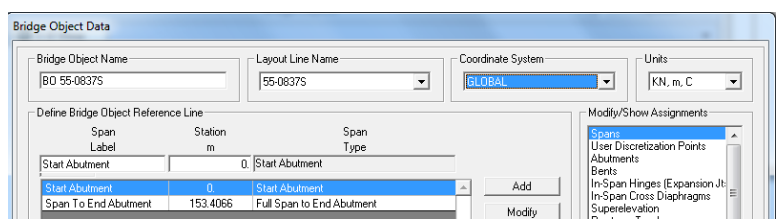

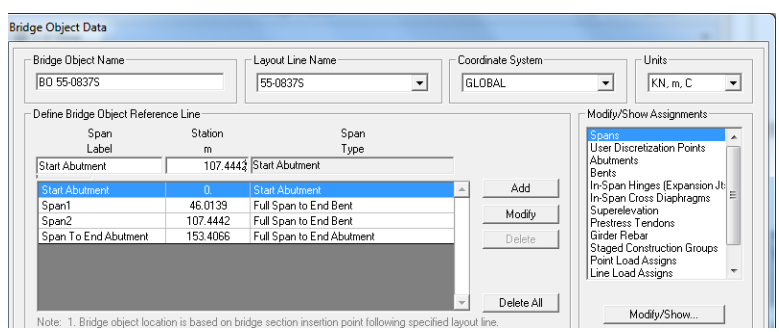

- Assign abutments to the bridge object by selecting *Abutments* from the *Supports* drop down window in the Bridge Objects section under the *Bridge* tab.
  - Set Substructure Assignment to *Abutment Property* and select *Abutment 1&4* (the abutment substructure previously defined) from the drop down window.
  - Set Substructure Location Elevation to *-1.68m* and Horizontal Offset to *0*.
  - Let Bearing Assignments remain set to the default *BBRG1* (a translationally fixed and rotationally free connection). Select the plus sign icon (+) to view the properties of this bearing link.
  - Set Elevation at Layout Line to *-1.68 m* (equal with Substructure Location Elevation to create a zero length bearing) with Rotational Angle from Bridge Default set to *0*.
  - Assign these abutment settings to both the *Start Abutment* tab and *End Abutment* tab (above).
  - Select *OK* to assign.

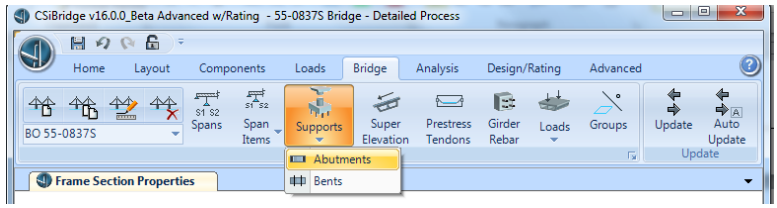

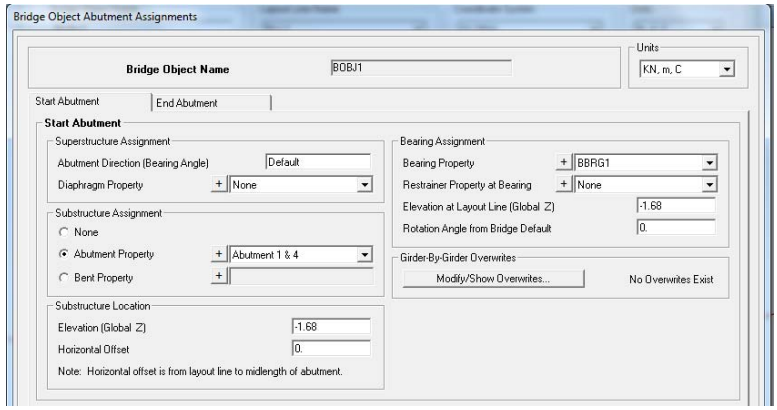

- Assign bents to the bridge object by selecting *Bents* from the *Supports* drop down window in the Bridge Objects section under the *Bridge* tab.
  - To assign Bent 2, set Specify Bent Considered to be at the end of *Span1*.
  - In the Bent Assignment section, specify the Bent Property as *Bent 2* (the bent substructure previously defined) with *Default* Bent Direction, *-1.68 m* Elevation, and *0* Horizontal Offset.
  - Let Bearing Assignments remain set to the default BBRG1.
  - Set Elevation (At Layout Line) equal to *-1.68 m* with Rotational Angle from Bridge Default set to *0*.

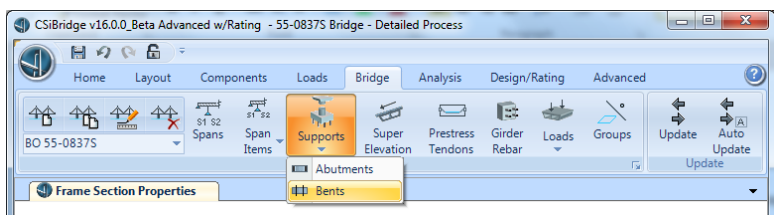

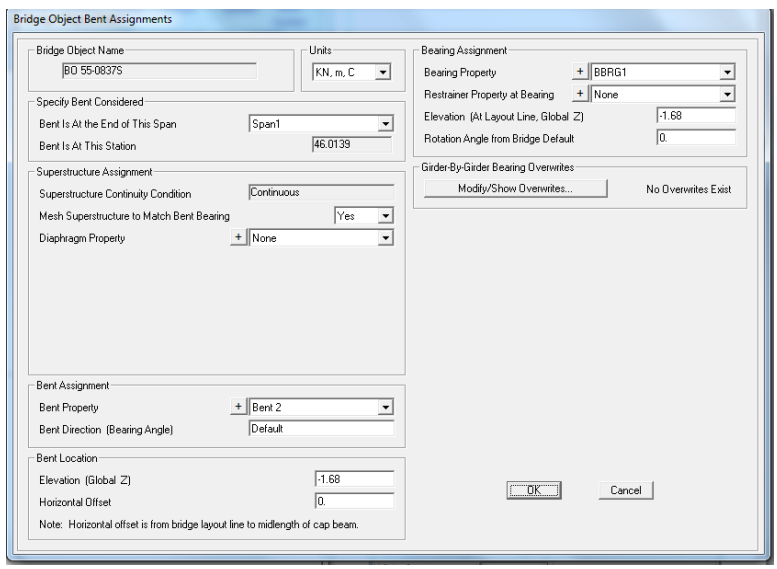

- To assign Bent 3, change the Specified Bent Considered to be at the end of *Span 2*. Change the Bent Property to *Bent 3*. All other properties are the same for both bent assignments.
- Select *OK* to assign.

- Apply the bridge object assignments to the layout line by selecting the *Update* icon in the Update section under the *Bridge* tab.
  - Do NOT select the *Auto Update* icon. This will disable the user's ability to manually override any of the automated model settings which will be imperative in the steps to come.
  - Select the Bridge Object created and choose to *Update Linked Model*.
  - Specify the Discretization Information.
  - In the Structural Model Options section, select *Update as Spine Model Using Frame Objects*.
  - Select *OK* to update.

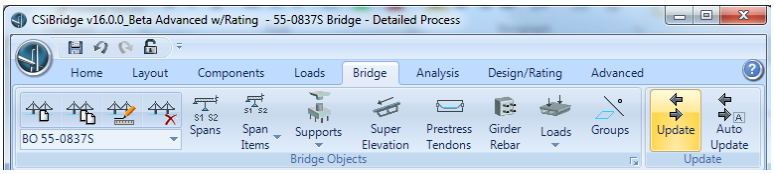

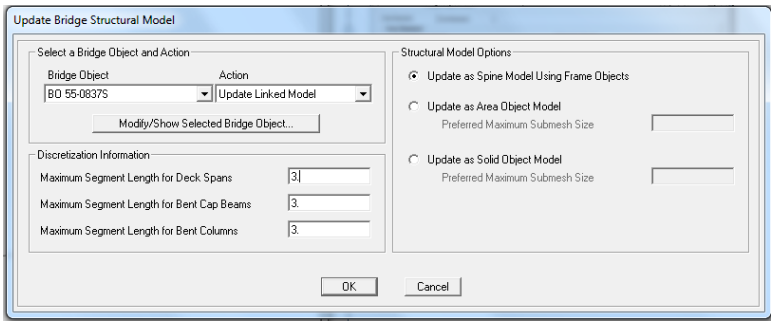

- To navigate the model, use the icons provided in the View section under the *Home* tab. To view the line model, select the icon with the check mark and uncheck *Extruded View*.

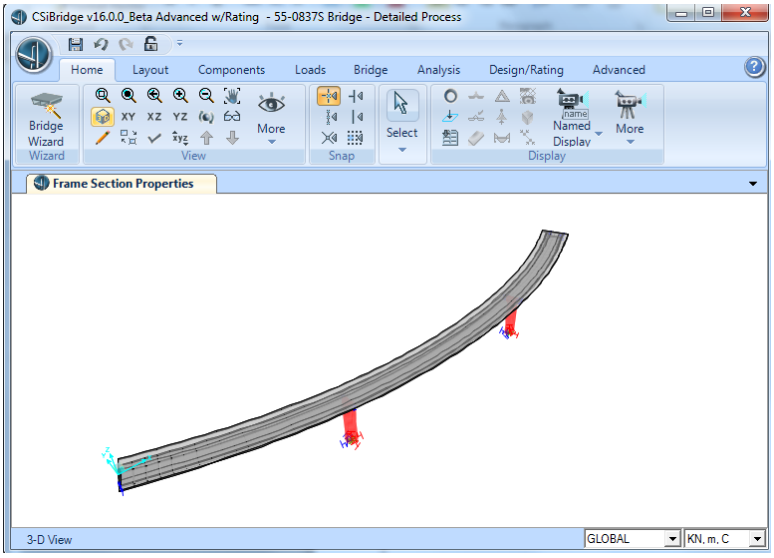

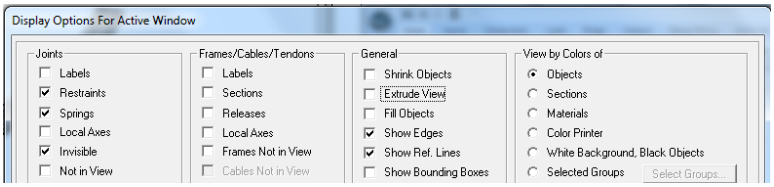

MANUALLY OVERRIDING AUTOMATED PARAMETERS

- For comparison purposes, this model of Bridge 55-0837S is designed to replicate the Finite Element model created in OpenSees. For the model to be best replicated, four default parameters need to be corrected:
  1. The deck section assigned in the bridge object needs to be overwritten with the general frame section created.
  2. Mass needs to be assigned at each joint.
  3. Local axes at the bents need to be altered.

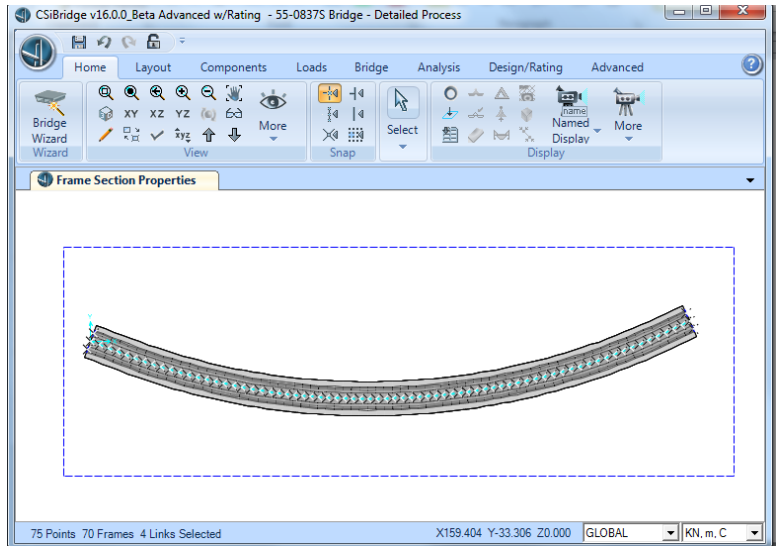

- Overwrite the deck section assigned to the bridge object by selecting the entirety of the bridge deck nodes in the *XY* viewport.
  - Under the *Advanced* tab, select the *Frames* icon in the Assign section. Select *Frame Sections* from the drop down window.
  - Select *55-0837S Deck* (the deck frame section previously defined).
  - Select *OK* to apply the new frame section to the bridge deck.

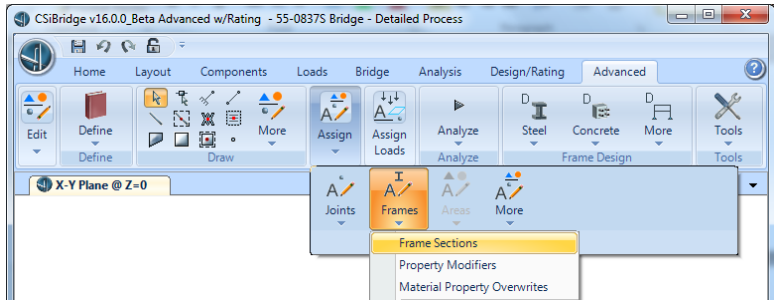

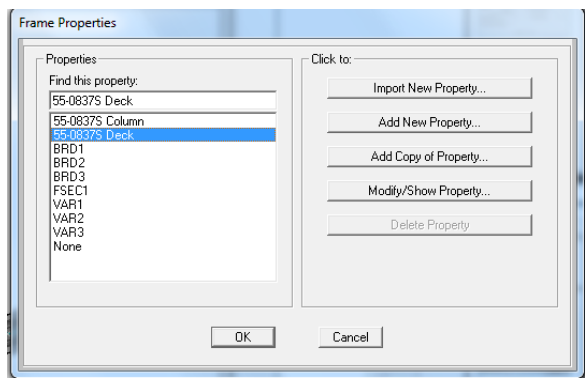

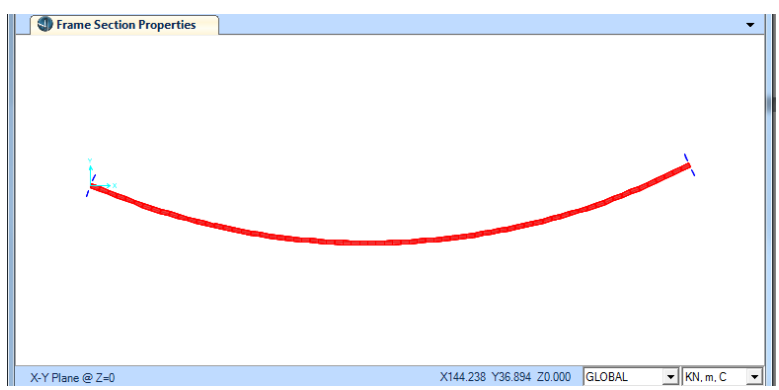

- Manually apply the masses by selecting any given joint or group of joints in either the *XY* or *3D* viewport.
  - Under the *Advanced* tab, select the *Joints* icon in the Assign section. Select *Masses* from the drop down window.
  - The mass at each joint is applied *As Mass* along the *Joint Local* Coordinate System.
  - Assign mass values corresponding to each respective joint in Table E.5.
  - No rotational mass is added.
  - Ensure the Units are *kN, m, C*.
  - Select *OK* to apply the mass.

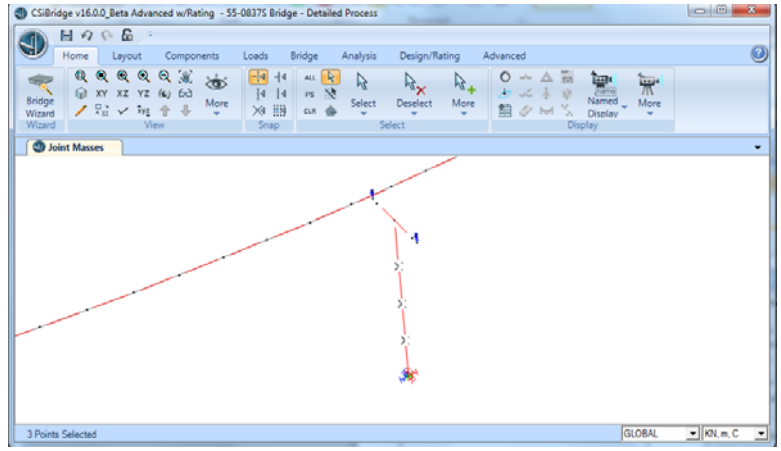

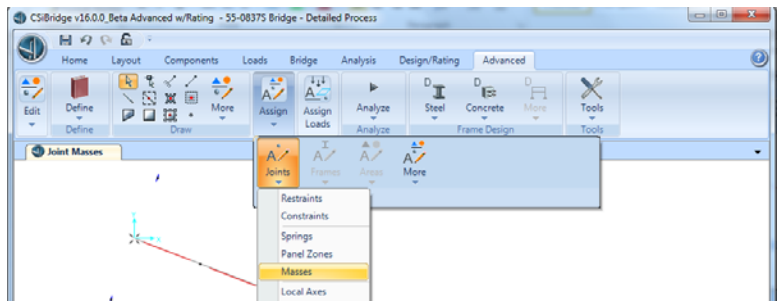

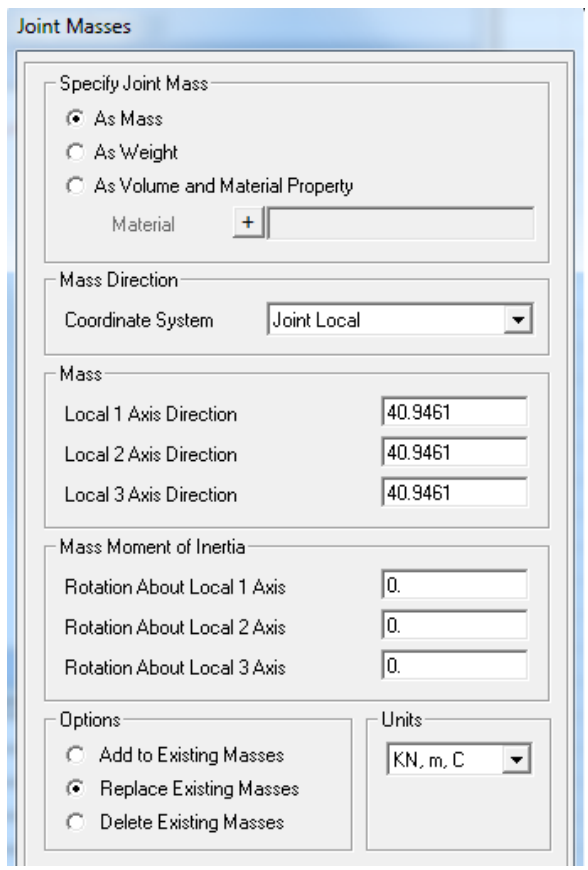

Table E.5 Masses assigned at each joint along the bridge deck and bent columns

Bridge Deck		
Joint Location	**Joint No.**	**Local 1,2,3 Axis Direction (kN)**
Abutment 1	1	40.9461
Along Span 1	2 - 10	81.8922
Bent 2	11	95.6095
Along Span 2	12 - 20	109.3268
Bent 3	21	95.5629
Along Span 3	22 - 30	81.7989
Abutment 4	31	40.8995
Bent Column 2		
Top	1	14.7025
Along Column	2 - 4	39.2067
Bottom	5	26.2447
Bent Column 3		
Top	1	15.1147
Along Column	2 - 4	40.3059
Bottom	5	26.6569

- View the local axes at each joint by selecting the check mark icon in the View section under the *Home* tab. Check *Local Axes* in the Joints section of the *Display Options for Active Window* window.

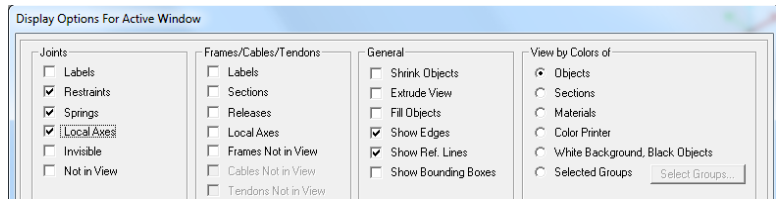

- Automatically, the abutment springs' local axes are oriented in line with the deck edge, -21° for Abutment 1 and +25° for Abutment 4 (see Figure 4.6). However, the bent foundation soil springs need to be aligned with Abutment 1 to be congruent with the OpenSees Bridge Model.

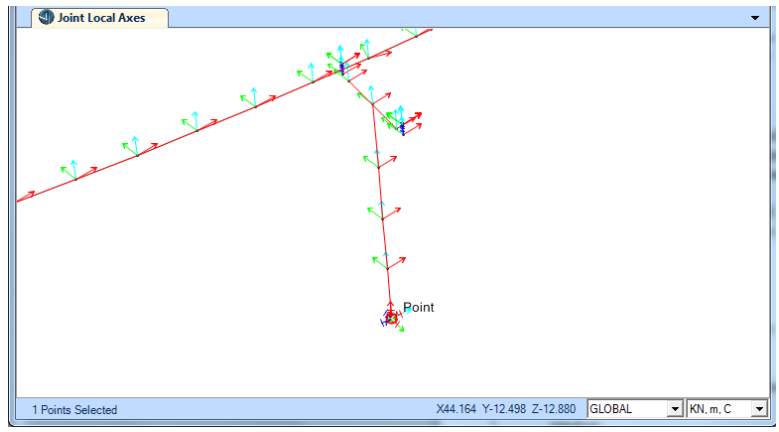

- Reorient the local axis at the bent bases according to Figure 4.6.
  - Select joint 21 (Bent 2) and joint 51 (Bent 3) in the *XY* viewport.
  - Under the *Advanced* tab, select the *Joints* icon in the Assign section. Select *Local Axes* from the drop down window.
  - Orient the selected axes according to Figure 4.6.
    - The u1, u2 and u3 DOFs are rotated by default. To keep the correct assignment of spring stiffness in the respective vertical, transverse and longitudinal directions, rotate the soil springs about the Global Y *-90°* and about the Global X *-201°*.
    - Select *OK* to apply.

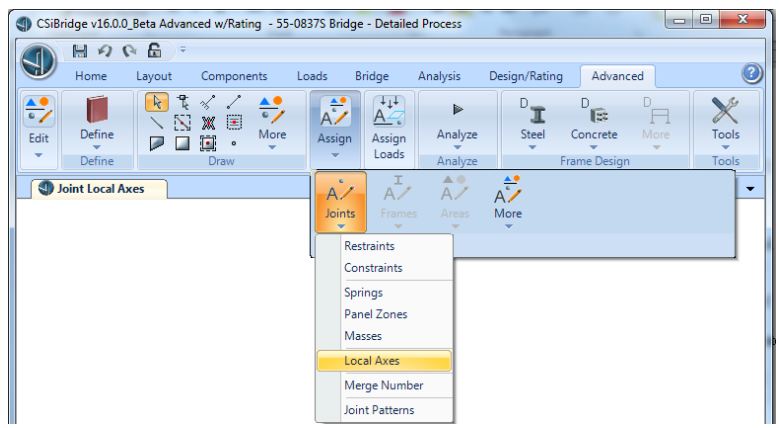

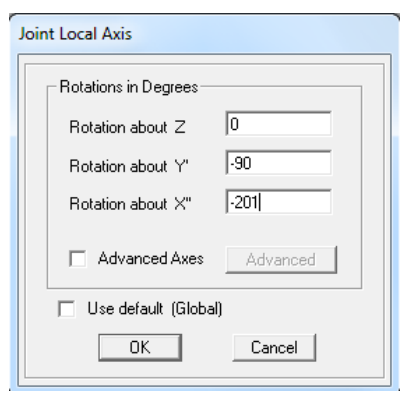

DEFINING THE RESPONSE SPECTRUM

- Define the design spectrum to be used in the fault-normal and fault-parallel response spectrum analysis.
  - Select *Response Spectrum* from the *Type* drop down window in the Functions section under the *Loads* tab.
  - Choose the Function Type *From File*.
  - Copy the values from Table E.6 into a .txt file with Periods running from 0 to 5sec with the corresponding Psa (g) in the adjacent column. Save this file.
  - Define the response function in the Response Spectrum Function Definition window.
    - Name the function.
    - Function Damping Ratio is 5%.
    - Select the .txt file using *Browse*.
    - Denote how many Header Lines to Skip.
    - Select *Display Graph*.
    - Select *Convert to User Defined* to imbed the values in the CSiBridge™ document, allowing the other .txt file to be moved or deleted.
  - Select *OK* to save.

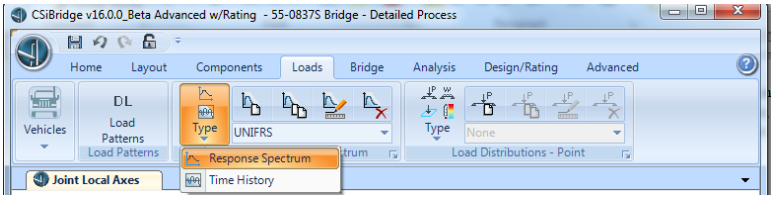

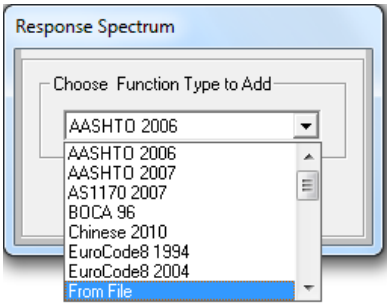

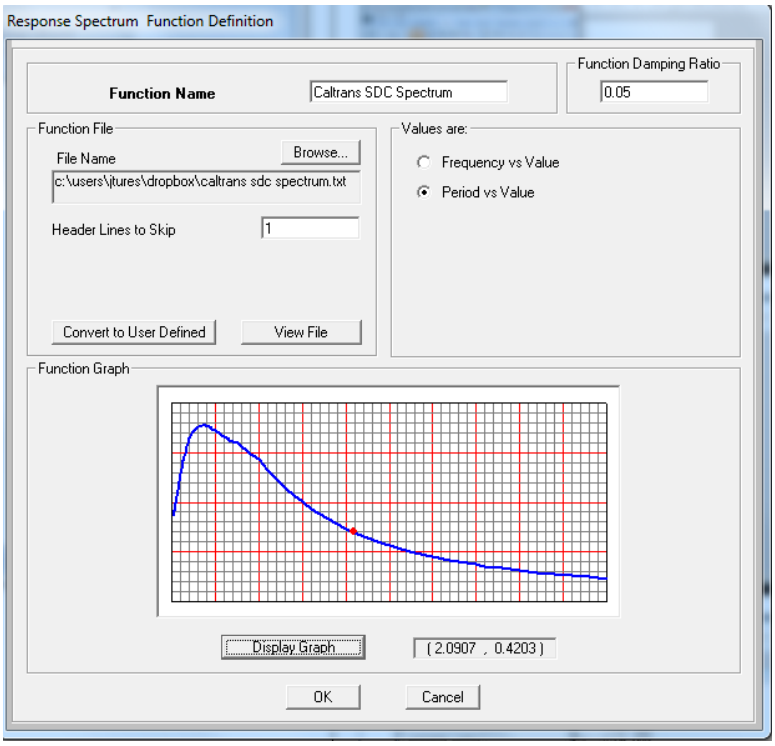

Table E.6 Caltrans SDC Design Spectrum Data

Period (sec)	Psa (g)	Period (sec)	Psa (g)	Period (sec)	Psa (g)
0.01	0.522686	0.15	0.892356	0.85	0.913194
0.02	0.531822	0.16	0.914375	0.9	0.893391
0.022	0.537514	0.17	0.934092	0.95	0.875195
0.025	0.545450	0.18	0.952711	1	0.857419
0.029	0.554750	0.19	0.969753	1.1	0.793836
0.03	0.557516	0.2	0.985467	1.2	0.737891
0.032	0.564002	0.22	1.007486	1.3	0.687659
0.035	0.573363	0.24	1.026236	1.4	0.642609
0.036	0.576447	0.25	1.034105	1.5	0.601370
0.04	0.588169	0.26	1.038831	1.6	0.562199
0.042	0.594519	0.28	1.048257	1.7	0.526867
0.044	0.600709	0.29	1.051087	1.8	0.495154
0.045	0.604071	0.3	1.053959	1.9	0.466718
0.046	0.607344	0.32	1.058716	2	0.441308
0.048	0.613574	0.34	1.061260	2.2	0.394913
0.05	0.619839	0.35	1.061657	2.4	0.356286
0.055	0.633146	0.36	1.061972	2.5	0.339213
0.06	0.646950	0.38	1.061045	2.6	0.323494
0.065	0.660695	0.4	1.059210	2.8	0.295351
0.067	0.666500	0.42	1.054312	3	0.271125
0.07	0.674891	0.44	1.048308	3.2	0.250019
0.075	0.689165	0.45	1.045620	3.4	0.231445
0.08	0.705275	0.46	1.042586	3.5	0.222997
0.085	0.721454	0.48	1.036122	3.6	0.215042
0.09	0.737416	0.5	1.030093	3.8	0.200380
0.095	0.753372	0.55	1.012006	4	0.187329
0.1	0.768957	0.6	0.996359	4.2	0.176113
0.11	0.799122	0.65	0.981859	4.4	0.165781
0.12	0.826969	0.66	0.976423	4.6	0.156388
0.13	0.851907	0.7	0.968423	4.8	0.147803
0.133	0.858486	0.75	0.955977	5	0.139894
0.14	0.873122	0.8	0.933755		

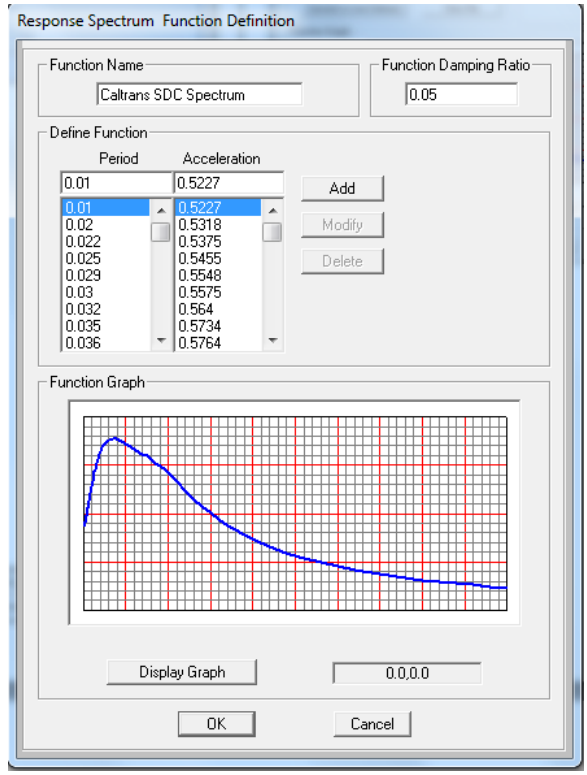

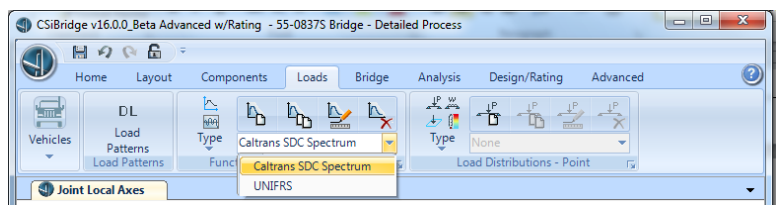

CONDUCTING CALTRANS AUTOMATED FAULT CROSSING SEISMIC DESIGN

- The Caltrans Automated Fault Crossing Seismic Design function will run both the static analysis due to fault rupture ground displacement and response spectrum analysis due to ground shaking. These responses will be combined and represented as a demand on the bents in both the transverse and longitudinal directions (see Figure 5.10).

- Create a design request by selecting the *Design Request* icon in the Seismic Design section under the *Design/Rating* tab.
  - Select *Add New Request* to begin.
  - Name the design request.
  - Select the Bridge Object created.
  - Select *Caltrans Fault Crossing* as the Check Type.
  - Select a *Planar* Fault Definition and designate the fault crossing Station as *271.89 ft*. The station must be denoted in the units of feet, regardless of selected working units.
  - Set the Orientation to *Default* which orients the fault rupture along the global Y axis (see Figure 5.9).
  - Define the Parallel Fault Displacement by setting the ground Displacement for static analysis to be the *0.5 m* used in this study, and by setting the Response Spectrum Function to the user-defined *Caltrans SDC Spectrum* to define Fault Parallel ground motion.
  - To simultaneously consider the effects due to fault normal ground motion, set the Normal Uniform Acceleration R.S. Function to the user-defined *Caltrans SDC Spectrum*, as well.
  - Select OK to create.

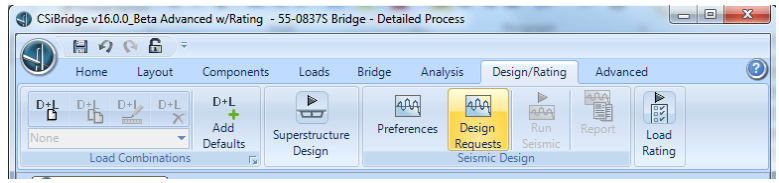

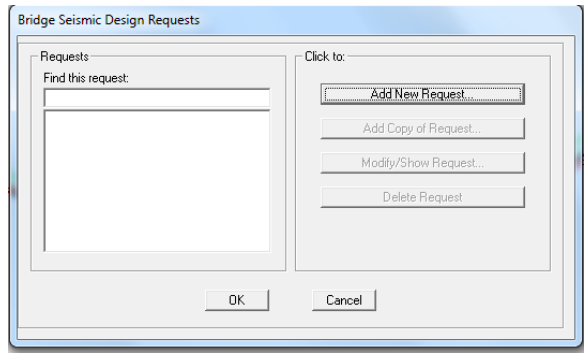

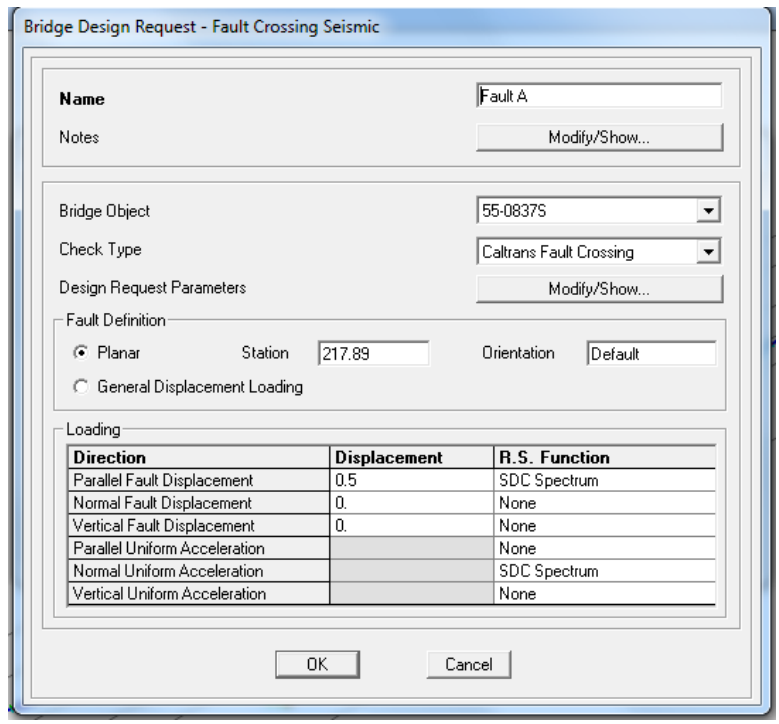

- Run Caltrans Automated Fault Crossing Seismic Design Request by selecting the *Run Seismic* icon in the Seismic Design section under the *Design/Rating* tab.
  - Set the fault crossing design request Action to *Design.*
  - Select *Design Now* to run analyses.

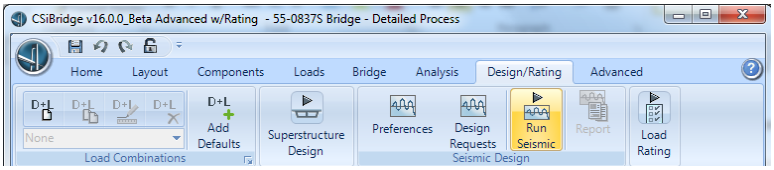

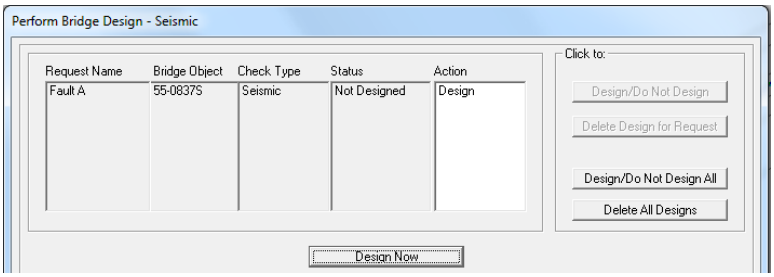

- The Bridge Seismic Design 01 – Bent D-C window will appear when the analysis is complete. Select Done, for now. This window will be discussed further in the Interpreting Results portion of this tutorial.

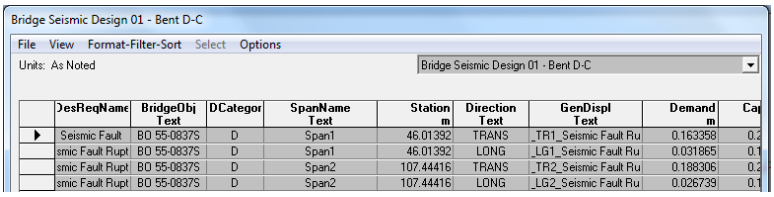

INTERPRETING RESULTS

- View the bridge displacement due to each component of fault rupture analysis by selecting the triangle icon in the Display section under the *Home* tab.
  - Select the desired response component to view in the dropdown window. Each case refers to a deformed bridge shape due to the following loads:
    - Gravity Load (GRAV)
    - Ritz Vectors (MODAL)
    - Fault Parallel Response Spectrum (RS_DIS)
    - Fault Normal Response Spectrum (RS_UNIF)
    - Fault Rupture Displacement (DIS)
    - Push Over Analysis in the respective transverse and longitudinal directions about Bent 1 (PO_TR1 and PO_LG1)
    - Push Over Analysis in the respective transverse and longitudinal directions about Bent 1 (PO_TR2 and PO_LG2)
  - Select *OK* to view.

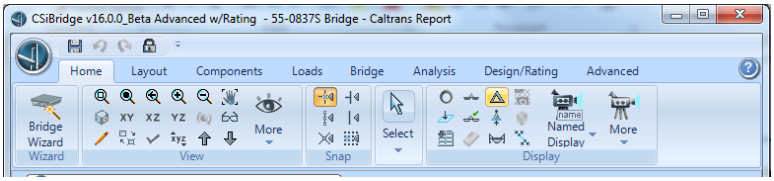

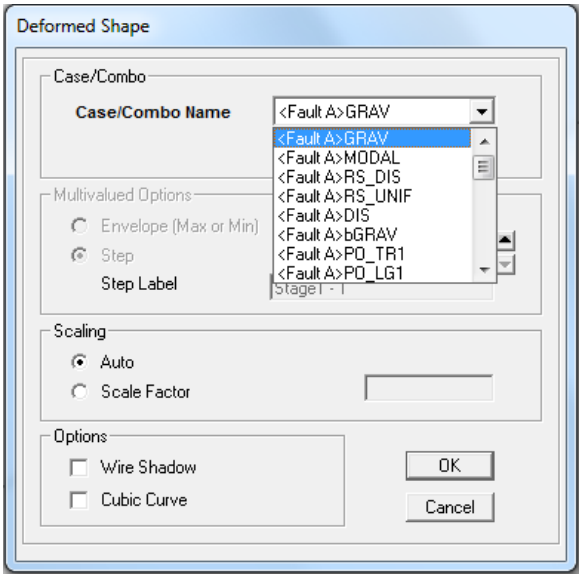
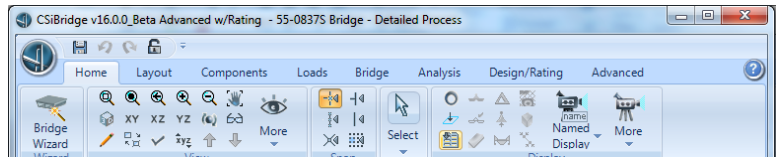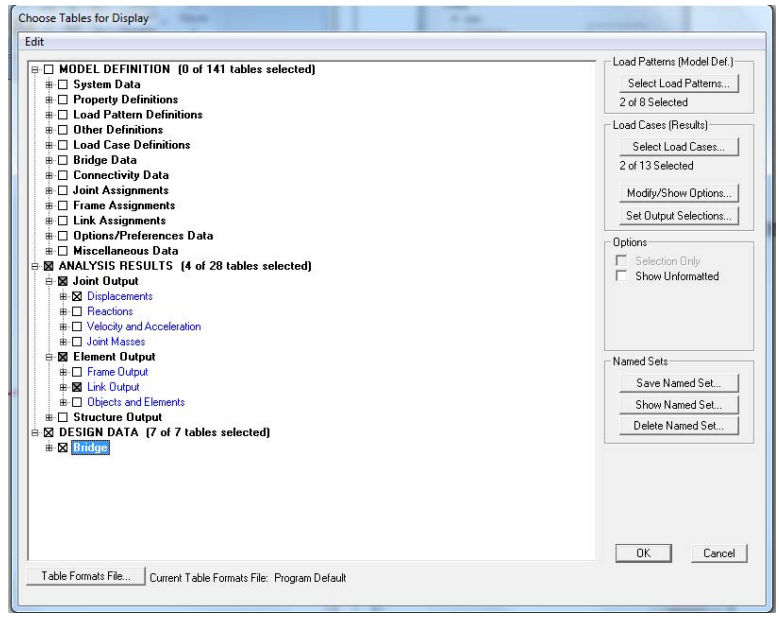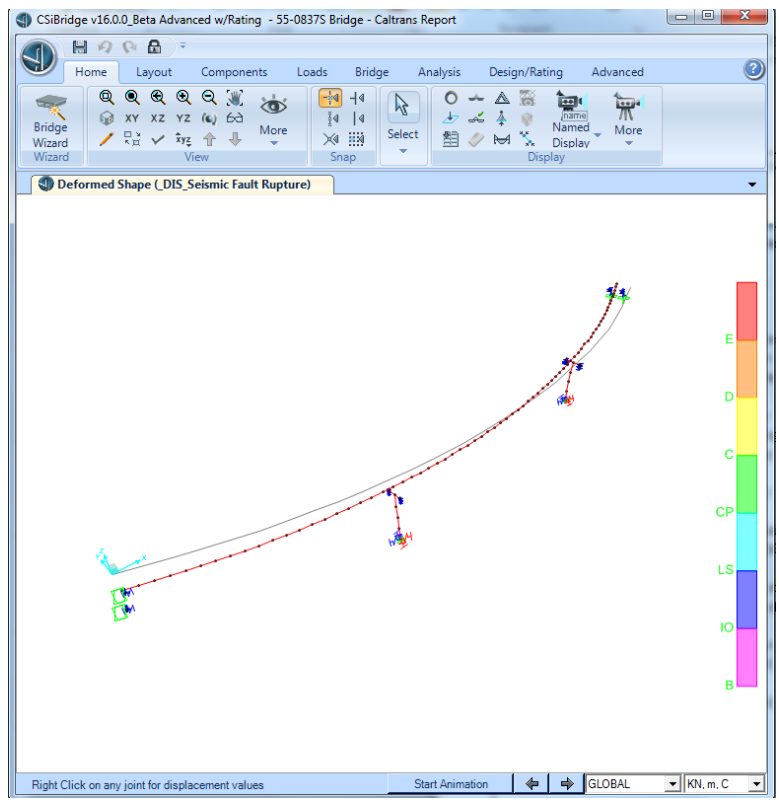
- Results from all load cases can be output by selecting *Tables* in the Display section under the *Home* tab.
  - The displacement due to all load cases at the top and bottom joints of each bent can be output by checking Displacements under Joint Output in Analysis Results.
  - The displacements at the abutments measure by the change in length in the attached abutment soil springs can be output by checking Link Output under Element Output in Analysis Results.
  - The bent demand (drift) generated by the Caltrans Automated Fault Crossing Seismic Design is output by checking Bridge in Design Data.
    - These bent drifts are calculated by combining the responses due to only quasi-static analysis from fault rupture offset and the fault-parallel response spectrum analysis.
    - Bent drift due to rotation at the top and bottom ends of the bents are also excluded in the demand calculation, i.e., the equation used by CSiBridge™ to calculate bent drift is Ut-Ub-L(Rt+Rb) where U and R respectively represent the translational and rotational displacement at the top node(t) and bottom node (b) of a given bent with length, L.
    - The lumped plasticity model and distributed plasticity model adopted in the bents of the CSiBridge™ and OpenSees models, respectively, provide different values of angle of rotation at the ends of the members. Therefore, the bent drift quantities were not used in the validation of Caltrans Automated Fault Crossing Seismic Design.